Thermodynamic Properties of Gases and Gas Mixtures at Low Temperatures and High Pressures

by

David Robert Roe, M.A.

May 1972

A thesis submitted for the degree of
Doctor of Philosophy of the University of London
and for the Diploma of Imperial College.

Department of Chemical Engineering
and Chemical Technology,
Imperial College,
London, S.W.7.

ABSTRACT

An apparatus of the "Burnett"-type has been constructed for the measurement of accurate compressibility factors of gases at pressures up to 100 bar. Results have been obtained in the temperature range 155 - 291 K for methane, nitrogen, two methane/nitrogen mixtures, one methane/nitrogen/ethane mixture and two natural gases.

A method of data treatment using non-linear least-squares analysis has been developed, which included an investigation of the effect of experimental errors on the derived virial coefficients by means of data simulated on the computer.

The compressibility factors for methane agree within .05% with those of Douslin et al. (43) above 0 ^{o}C and within 0.2% of those of Vennix et al. (52) below 0 ^{o}C. The results for nitrogen are in good agreement with those of Crain et al. (34) and Canfield et al. (67). There are no previously published results for the methane/nitrogen system at low temperatures.

Second virial coefficients of methane, nitrogen, argon and ethane were used to determine parameters of the Lennard-Jones (n-6) and Kihara intermolecular potential models and, for methane, of the potential of Barker et al. (125). The latter and the Lennard-Jones (18-6) potential gave good agreement with the coefficient of the long-range dispersion interaction and the experimental third virial coefficients when the triple-dipole non-additive contribution was included.

None of the combining rules tested were found to be

adequate for all of the systems: CH_4/N_2, CH_4/Ar, CH_4/C_2H_6 and N_2/Ar. A geometric mean correction factor, k_{12} ($= 1 - (\epsilon_{12} - (\epsilon_{11} \cdot \epsilon_{22})^{\frac{1}{2}})$) of 0.03 was necessary for CH_4/N_2.

The results for the multicomponent mixtures, including data on natural gases taken from the literature, were compared with the predictions of the extended corresponding-states principle as due to Leland et al. (158). Agreement was excellent, within experimental error, above 0 °C and fairly good below 0 °C.

CONTENTS

ACKNOWLEDGEMENTS

My sincere thanks are due to the following:

Dr. G. Saville, for his helpful supervision and invaluable guidance throughout this project.

The Gas Council, London Research Station, for enabling me to carry out this research and for financial support.

The members of the Departmental, Electronics, and Glass workshops for their skilful assistance.

Dr. A. Harlow for the sound design of parts of the apparatus; and to Dr. C.A. Pollard for his helpful advice during its construction.

Mr. R.E. Clifford and staff of The Gas Council, Watson House, for providing the gas mixtures; and to Mr. B. Juren and Dr. Angela Gunning for information on dew-points.

My parents, for their support, and my wife for her constant encouragement.

CHAPTER ONE

INTRODUCTION

1.1 The Equation of State

The equation of state of a perfect gas at pressure P, temperature T and molar volume V is,

$$PV = RT \qquad (1.1\text{-}1)$$

where R is the gas constant.

Real gases depart from perfect-gas behaviour because of the finite size of the molecules and the forces between them.

The compressibility factor, Z, of a real gas is defined by,

$$Z = \frac{PV}{RT} \qquad (1.1\text{-}2)$$

It is a function of temperature and pressure (or density) and is a convenient measure of the non-ideality of a gas because it is non-dimensional. As the pressure tends to zero and the gas becomes more ideal, Z approaches the value 1.0.

The variation of Z with reduced temperature and pressure is of the qualitative form shown in figure 1.1. This graph has been plotted in reduced form, where reduced temperature and pressure are here defined by,

$$T^R = \frac{T}{T^C} \quad . \quad P^R = \frac{P}{P^C} \qquad (1.1\text{-}3)$$

where T^C is the critical temperature and P^C is the critical pressure, as it is found that most simple gases roughly follow the same curves (the principle of corresponding states).

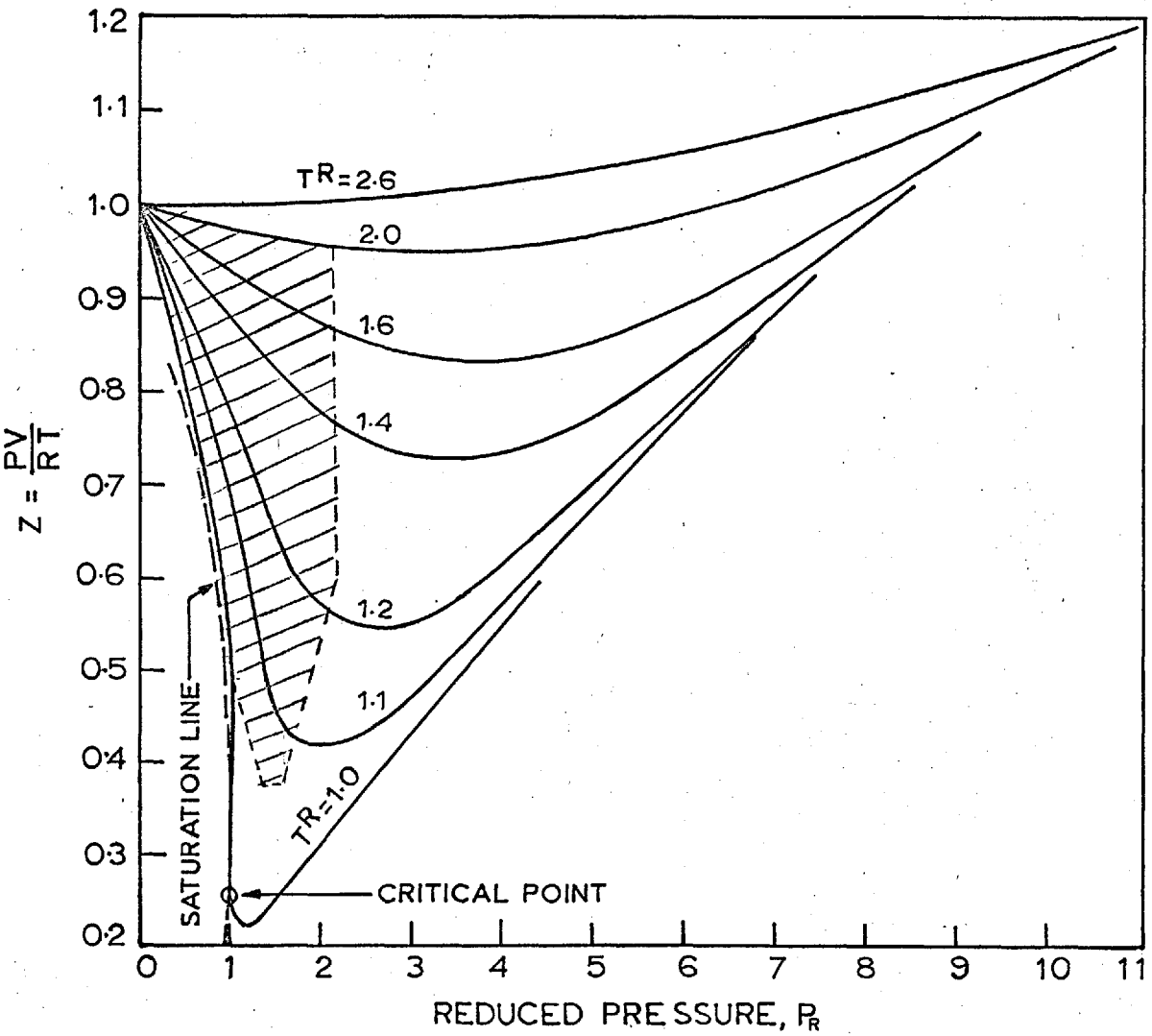

FIG 1·1. GENERALIZED COMPRESSIBILITY FACTORS (FOR PARAFFIN HYDROCARBONS OR NATURAL GAS)

Many equations of state, both theoretical and empirical, have been proposed to express quantitatively the variation of the compressibility factor with pressure and temperature, but no one simple equation has yet been completely successful over the whole range. In this work most of the interest is in the low pressure region of figure 1.1 where the virial equation of state is appropriate.

(a) The virial equation of state

The virial equation of state is an expansion of Z as an infinite series in powers of density:

$$Z = 1 + B\rho + C\rho^2 + D\rho^3 + \ldots\ldots \qquad (1.1\text{-}4)$$

An equation of this type, but in truncated form, was first suggested as an empirical representation of PVT data. The significance of the virial series is not in its usefulness in this respect, as the series appears to diverge at high densities (1) where other equations requiring fewer terms are preferable, but in the fact that it has sound theoretical foundations.

It can be shown that each of the virial coefficients, B, C, D, etc., is related to the intermolecular forces in a direct manner (2). Statistical-mechanical calculation shows that the second virial coefficient, B, is a function of the interaction between pairs of molecules, as described in Chapter 5, the third virial coefficient, C, is a function of the interaction between three molecules, and so on. The coefficients are independent of density and are functions of temperature of the general form shown in figures 1.2 and 1.3.

The second virial coefficient is one of the few macroscopic properties of a system which has a sound theoretical relationship with the intermolecular forces between a pair of molecules and which can provide quantitative information on these forces. However, very accurate experimental data are necessary.

For mixtures it can be shown by the methods of statistical mechanics (2), as described briefly in Chapter 5, that the second virial coefficient is given by,

$$B_{mix} = \sum_{i=1}^{n} \sum_{j=1}^{n} x_i \, x_j \, B_{ij} \qquad (1.1\text{-}5)$$

where x_i is the mole-fraction of the i th. component.

B_{ii} is the second virial coefficient of the i th. pure component.

B_{ij} $(i \neq j)$ is the interactional second virial coefficient which is directly related to the interaction between molecule i and molecule j.

Similarly,

$$C_{mix} = \sum_{i=1}^{n} \sum_{j=1}^{n} \sum_{k=1}^{n} x_i \, x_j \, x_k \, C_{ijk} \qquad (1.1\text{-}6)$$

where C_{ijk} is related to the interaction between the three molecules of type i, type j and type k.

Thus by measurement of the compressibility factors and hence second and third virial coefficients of mixtures, it is possible to obtain information on the intermolecular forces between unlike molecules. In a multicomponent mixture the

interactions consist of interactions between pairs of molecules plus interactions between clusters of three molecules, and so on. However, the interactions between clusters of more than two molecules can largely (but not wholly) be described as the sum of interactions between pairs (pairwise additivity). For this reason it is necessary to have experimental data on the binary mixtures of the components of a multi-component mixture of practical importance, such as a natural gas, before its compressibility factor can be predicted with high accuracy.

1.2 Compressibility factors of natural gas

In the metering of large quantities of gas in pipelines the compressibility factor (or density) is required to obtain the measured flow-rate in units of mass per second. A small error in the pre-supposed value of Z at a certain temperature and pressure could lead to errors of millions of cu. ft. in the quantity of gas transmitted. The problem is more acute for natural gases, the compressibility factor of which varies considerably with temperature and pressure in the range of interest, than for town gas, the compressibility factor of which is fortuitously close to 1.0 because of the high hydrogen content.

Ideally, it is desirable for Z to be measured or predicted as a function of composition, temperature and pressure to as high an accuracy as possible, or at least to an accuracy greater than that inherent in the actual metering.

Knowledge of the volumetric behaviour of natural gas

and its components is also important in the design and operation of compressors and gas-treatment plants, particularly in relation to the liquefaction of natural gas, when information on Z at low-temperatures is required.

The work reported here was initiated as the first part of a long-term project to measure accurately the compressibility factors of the constituents of natural gas, their binary mixtures, then ternary mixtures, leading up to multicomponent mixtures. Data of this type are sparse, particularly at low temperatures.

The gases studied in this investigation were methane (the major component of natural gas), nitrogen and their binary mixtures at temperatures from 155.9 K to 291.4 K at pressures up to 100 bar; this covers, approximately, the lighter shaded region of figure 1.1. Nitrogen is an important component in natural gas not only because it is inert to combustion but also because it is more ideal than methane and the higher hydrocarbons. The mole-fractions of the hydrocarbons tend to decrease in a regular manner along an homologous series and the compressibility factor of a natural gas consisting solely of hydrocarbons can usually be correlated with the average molecular weight or the specific gravity. The presence of only a small percentage of nitrogen upsets this correlation.

As there was an immediate requirement for a predictive method capable of high accuracy, measurements were also obtained for three multi-component mixtures: a mixture of methane, nitrogen and ethane, and two natural gases. The results could then be compared with those of various predictions. This is done in Chapter 6.

1.3 Other thermodynamic properties

An equation of state based on accurate PVT measurements is important not only in interpolation of the data and prediction of the compressibility factor (or density) but also, of course, in connection with the calculation of other thermodynamic properties. The changes in thermodynamic properties of a gas over ranges of temperature and pressure are simply related to the equation of state. For example, we have for a reversible infinitesimal change in enthalpy of a fluid of constant composition,

$$dH = TdS + VdP \tag{1.3-1}$$

$$\therefore \left(\frac{\partial H}{\partial P}\right)_T = T\left(\frac{\partial S}{\partial P}\right)_T + V \tag{1.3-2}$$

From the Maxwell relation,

$$\left(\frac{\partial S}{\partial P}\right)_T = -\left(\frac{\partial V}{\partial T}\right)_P \tag{1.3-3}$$

we have

$$\left(\frac{\partial H}{\partial P}\right)_T = -T\left(\frac{\partial V}{\partial T}\right)_P + V \tag{1.3-4}$$

Therefore, from an equation of state of the form

$$V = f(T,P) \tag{1.3-5}$$

the partial derivative $\left(\frac{\partial H}{\partial P}\right)_T$ can be calculated.

For a change in enthalpy with both temperature and pressure,

$$dH = \left(\frac{\partial H}{\partial T}\right)_P dT + \left(\frac{\partial H}{\partial P}\right)_T dP \tag{1.3-6}$$

$$= C_p\, dT + \left(V - T\left(\frac{\partial V}{\partial T}\right)_P\right) dP \tag{1.3-7}$$

where C_p is the specific heat at constant pressure.

$\therefore$ the enthalpy H of a gas at temperature T_1 and pressure P_1 is:-

$$H = H_o + \int_{T_o}^{T_1} C_p \, dT + \int_{P_o}^{P_1} (V - T(\frac{\partial V}{\partial T})_P) dP \quad (1.3\text{-}8)$$

where H_o is an integration constant and is usually set to an arbitrary value at some chosen standard state, (P_o, T_o), such as at 1 atm., 0 ^oC. The integration with respect to temperature is usually performed first, C_p taking the value at P_o, and then the integration with respect to pressure is performed at temperature T_1. Thus from a knowledge of C_p at pressure P_o and from $(\frac{\partial V}{\partial T})_P$ and V, i.e. the equation of state, $H - H_o$ may be calculated.

Similarly,

$$S - S_o = \int_{T_o}^{T_1} C_p \cdot \frac{dT}{T} - \int_{P_o}^{P_1} (\frac{\partial V}{\partial T})_P \, dP \quad (1.3\text{-}9)$$

High precision is required in the equation of state and hence in the PVT measurements, as accuracy is always lost on differentation of an equation of state. For the gas phase, thermodynamic properties derived in this manner tend to be of higher accuracy than those from direct calorimetric measurements (3). Entropy changes cannot, of course, be measured directly by experiment.

1.4 The Burnett Method of measurement of compressibility factor

Burnett (4) proposed a method of measurement of the gas

compressibility factor that did not require accurate measurement of the volume, mass or absolute temperature of the gas under study. Other methods are described briefly in section 4.4(a); they either involve the determination of the pressure of a fixed volume of gas as a function of temperature (isochoric measurements), or the determination of the pressure as a function of volume at constant temperature (isothermal measurements).

With reference to figure 1.4, a Burnett apparatus consists basically of a volume V_A, at constant temperature T_A, connected by means of an expansion valve, E, to a second volume V_B at constant temperature T_B. When T_A is equal to T_B it is known as an 'isothermal' apparatus. At the start of an experiment V_A is charged with gas and the initial pressure P_o is measured. The gas is then expanded through the valve E into the previously evacuated volume V_B and, after establishment of temperature equilibrium, the new pressure P_1 is measured. Volume V_B is then vented and evacuated, another expansion of gas from V_A into V_B is carried out, and the pressure P_2 measured. Expansions are continued until the minimum measurable pressure is attained; the sequence of pressures, P_o P_1 ... P_j ... P_n constitute the basic data of a Burnett 'run'.

The number of moles of gas, n_o, in V_A prior to the first expansion is given by

$$n_o = \frac{P_o V_A}{RTZ_o} \qquad (1.4\text{-}1)$$

where Z_o is the compressibility factor at pressure P_o.

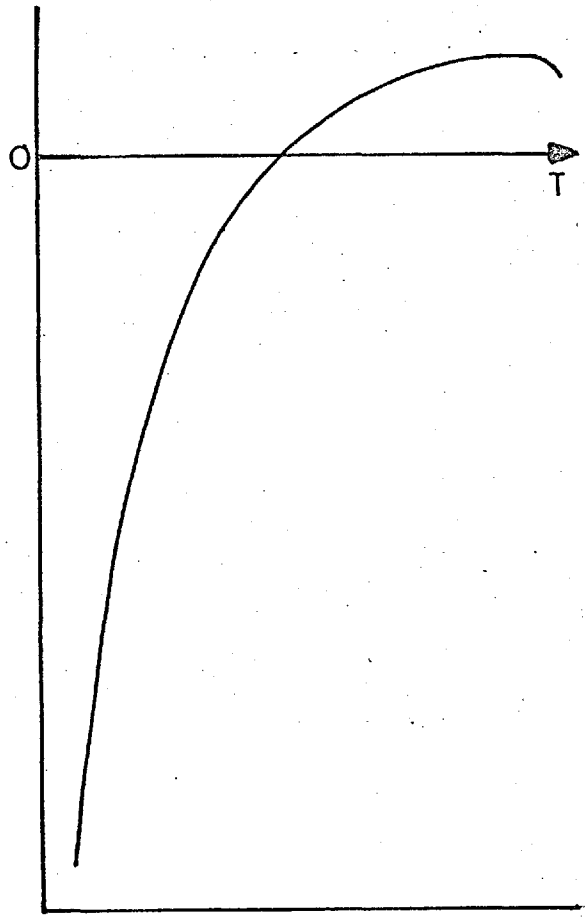

FIG.1·2. SECOND VIRIAL COEFFICIENT

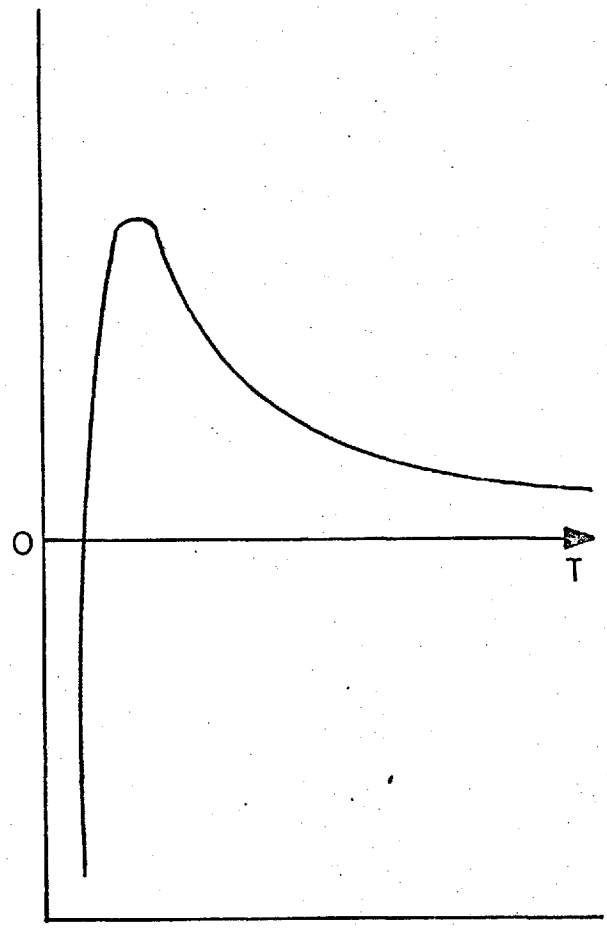

FIG.1·3. THIRD VIRIAL COEFFICIENT

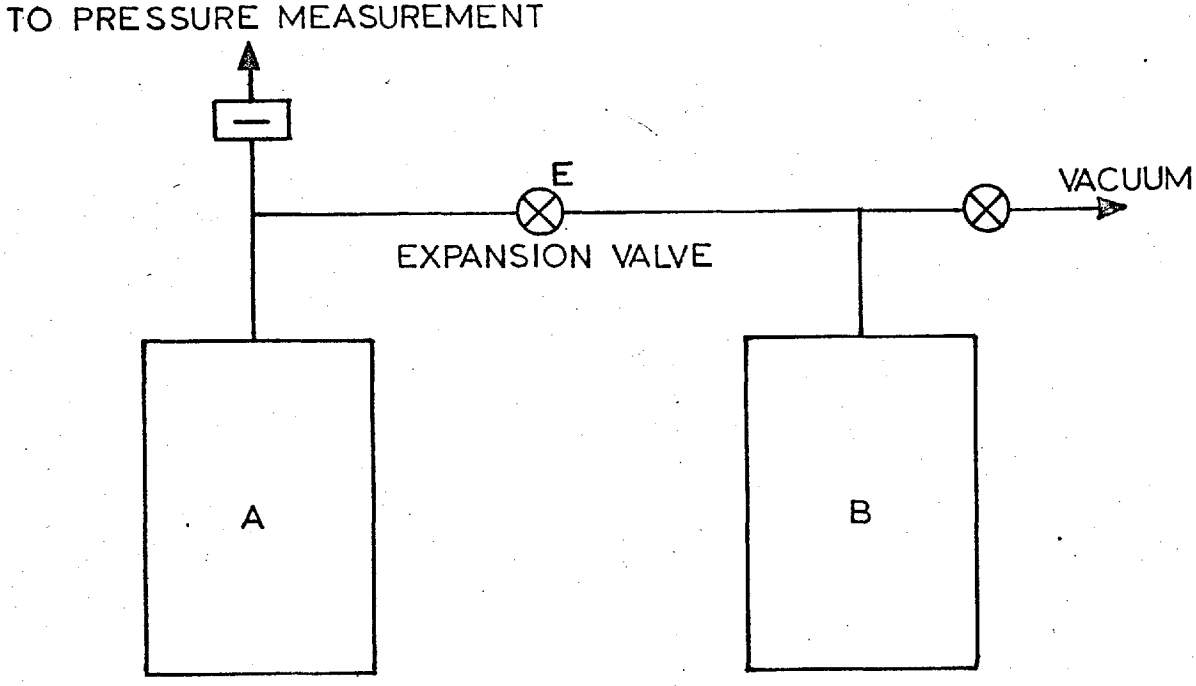

FIG 1·4. THE BURNETT APPARATUS.

After the first expansion,

$$n_o = \frac{P_1(V_A + V_B)}{RTZ_1} \qquad (1.4\text{-}2)$$

$$\text{Hence, } \frac{P_o}{P_1} = \left(\frac{V_A + V_B}{V_A}\right) \cdot \frac{Z_o}{Z_1} = N \cdot \frac{Z_o}{Z_1} \qquad (1.4\text{-}3)$$

where N is known as the 'cell constant' or 'apparatus constant'.

Similarly, after the second expansion

$$\frac{P_1}{P_2} = N \cdot \frac{Z_1}{Z_2} \qquad (1.4\text{-}4)$$

and after the jth. expansion,

$$\frac{P_{j-1}}{P_j} = N \cdot \frac{Z_{j-1}}{Z_j} \qquad (1.4\text{-}5)$$

From equations (1.4-3) and (1.4-4),

$$P_2 \cdot N^2 = \left(\frac{P_o}{Z_o}\right) \cdot Z_2 \qquad (1.4\text{-}6)$$

and similarly,

$$P_j \cdot N^j = \left(\frac{P_o}{Z_o}\right) \cdot Z_j \qquad (1.4\text{-}7)$$

It can be seen that to obtain the compressibility factors from the experimental pressures, N and (P_o/Z_o) must be determined; this is accomplished, directly or indirectly, from either a graphical or analytical method of data treatment. These procedures are described in Chapter 3.

The Burnett method requires good temperature control and precise pressure measurements. As no accurate measurements of volume, mass of gas, or absolute temperature

are necessary, the method is particularly suited to the determination of precise values of Z at low density and hence accurate second and third virial coefficients, particularly at low temperature, where other methods may lack the necessary precision at low pressures, and at very high temperatures where the accurate measurement of absolute temperature is difficult. However, as compressibility factors are not determined directly in a Burnett apparatus, their accuracy may be effected not only be experimental errors in measurement but also by such factors as the degree of curvature of the isotherm, the magnitude of N and hence the number of expansions in a run, and the method of data treatment employed: these factors are considered in detail in Chapter 3.

(a) The non-isothermal Burnett Method

In the 'isothermal' Burnett apparatus both volumes are maintained at the same temperature. At low temperatures the problem of temperature control with the conventional stirred-fluid bath can be difficult. It is much easier to ensure close temperature control and eliminate temperature gradients for each vessel separately. For these reasons a 'non-isothermal' Burnett apparatus may be employed, as in this investigation, in which, with reference to figure 1.4, volume V_B is at a temperature T_B which is easily maintained constant, such as 0 ^{o}C. Volume V_A is maintained at the temperature T_A for which experimental compressibility factors are required. The expression equating moles of gas before and after the jth. expansion is then,

$$\frac{P_{j-1} \cdot V_A}{T_A \cdot (Z_A)_{j-1}} = \frac{P_j \cdot V_A}{T_A \cdot (Z_A)_j} + \frac{P_j \cdot V_B}{T_B \cdot (Z_B)_j} \qquad (1.4\text{-}8)$$

The disadvantages of the 'non-isothermal' Burnett method are threefold. Firstly, the equation of state of the gas at temperature T_B must be known either from published results or by performing an experiment with $T_A = T_B$; however, it is fortunate that errors in the values of Z_B lead to much smaller errors in the experimental values of Z_A, as described in section 4.3. Secondly, some of the interconnecting tubing, valves, etc. constitute "dead-space volume" which is maintained at temperatures intermediate between T_A and T_B, and part of which must necessarily contain a temperature gradient. The interior volume of this dead-space must be known and corrections for the gas inside included in the calculation of Z_A. Thirdly, the whole data treatment is rendered slightly more complex.

Apart from the major advantage of easier temperature control, the non-isothermal Burnett method has the advantage that the expansion valve can usually be maintained at normal temperatures; many leakage problems occur with valves at extremes of low or high temperatures. Absolute leak-tightness of the valve is essential to the accuracy of the method. Another advantage is that if the gas under investigation adsorbs on the walls of the vessel at low temperature then the effect of adsorption on the results is much smaller when V_B is at a higher temperature where adsorption is insignificant (5). The problem of adsorption is discussed further in section 4.3(c).

CHAPTER TWO

DESCRIPTION OF APPARATUS AND EXPERIMENTAL PROCEDURE

2.1 Introduction

A general scheme of the 'non-isothermal' Burnett apparatus is shown in figure 2.1. The first vessel, A, was at the experimental temperature in the low-temperature system, described in detail in section 2.2. The second vessel, B, was situated in an ice-bath at 0 ^{o}C.

Both vessels were double-walled and pressure compensated, i.e. the same pressure existed both inside and outside of the inner vessel; this served to reduce the distortion due to pressure of the inner volume and enabled this distortion to be calculated with accuracy, as described in Section 2.9. The gas under study was confined within the inner volumes and the pressure difference between this gas and that in the outer volumes, which were directly connected to the pressure measurement system, was nulled by means of a Precision Pressure Gauge (Texas Instruments).

Pressures between 25 bar and 110 bar were measured by means of an oil piston-gauge (or pressure balance). The oil was separated from the pressure-compensating gas by a differential-pressure cell (Ruska). Pressures below about 25 bar were measured by means of a gas piston-gauge.

The whole apparatus was situated in an enclosure, the temperature of which was controlled at a few degrees C above ambient room temperature by means of a toluene regulator with a proportionating head in conjunction with two 1000 watt heating elements; the air was circulated by two 10" fans and

FIGURE 2.1

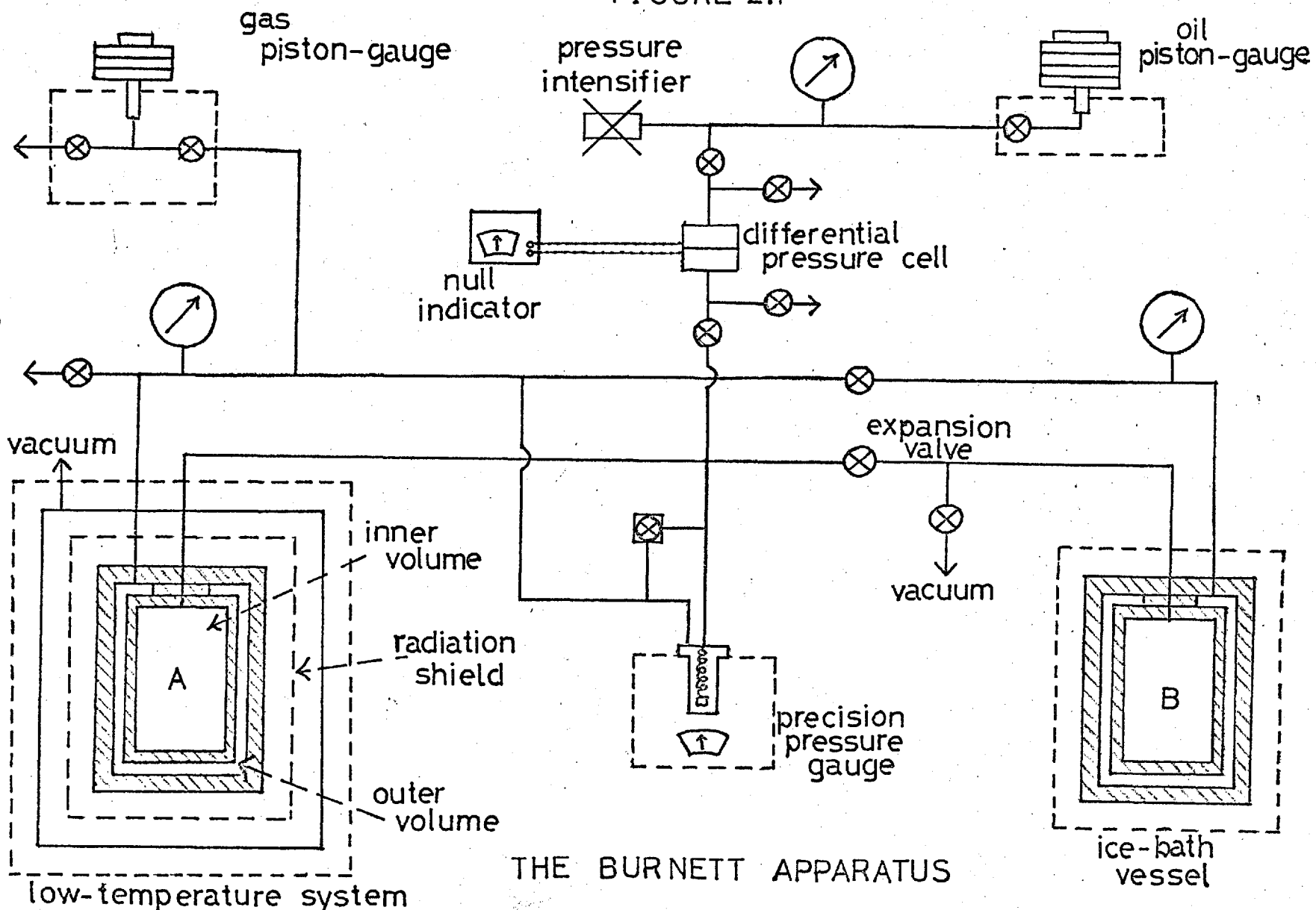

THE BURNETT APPARATUS

the temperature inside the enclosure was constant to 0.1 ^{o}C. Thus the piston-gauges, the dead-space volume and the electronic equipment were all maintained at a constant temperature.

2.2 The Low Temperature System

The low temperature system is shown in figure 2.2. The cylindrical stainless-steel pressure vessel is suspended within a copper radiation shield which is itself suspended within an evacuated outer jacket, the whole being situated in a Dewar containing refrigerant. Platinum resistance thermometers in the pressure vessel were used in conjunction with an automatic controller to govern the supply to heaters around the outside of the vessel, thus maintaining its temperature at a constant value. The temperature of the radiation shield was controlled by means of a differential thermocouple at about 1 ^{o}C. below that of the pressure vessel, which thereby was provided with a constant-temperature environment.

The system was thus designed such that the heat loss from the pressure vessel was small and radiative, giving close temperature control and small temperature gradients within the vessel.

(a) The Pressure Vessel

The pressure vessel was of EN58J stainless-steel. It consisted of an inner volume, with walls of .125" thickness, containing the gas under study, and an outer volume, with walls of 1" thickness, containing gas at the same pressure.

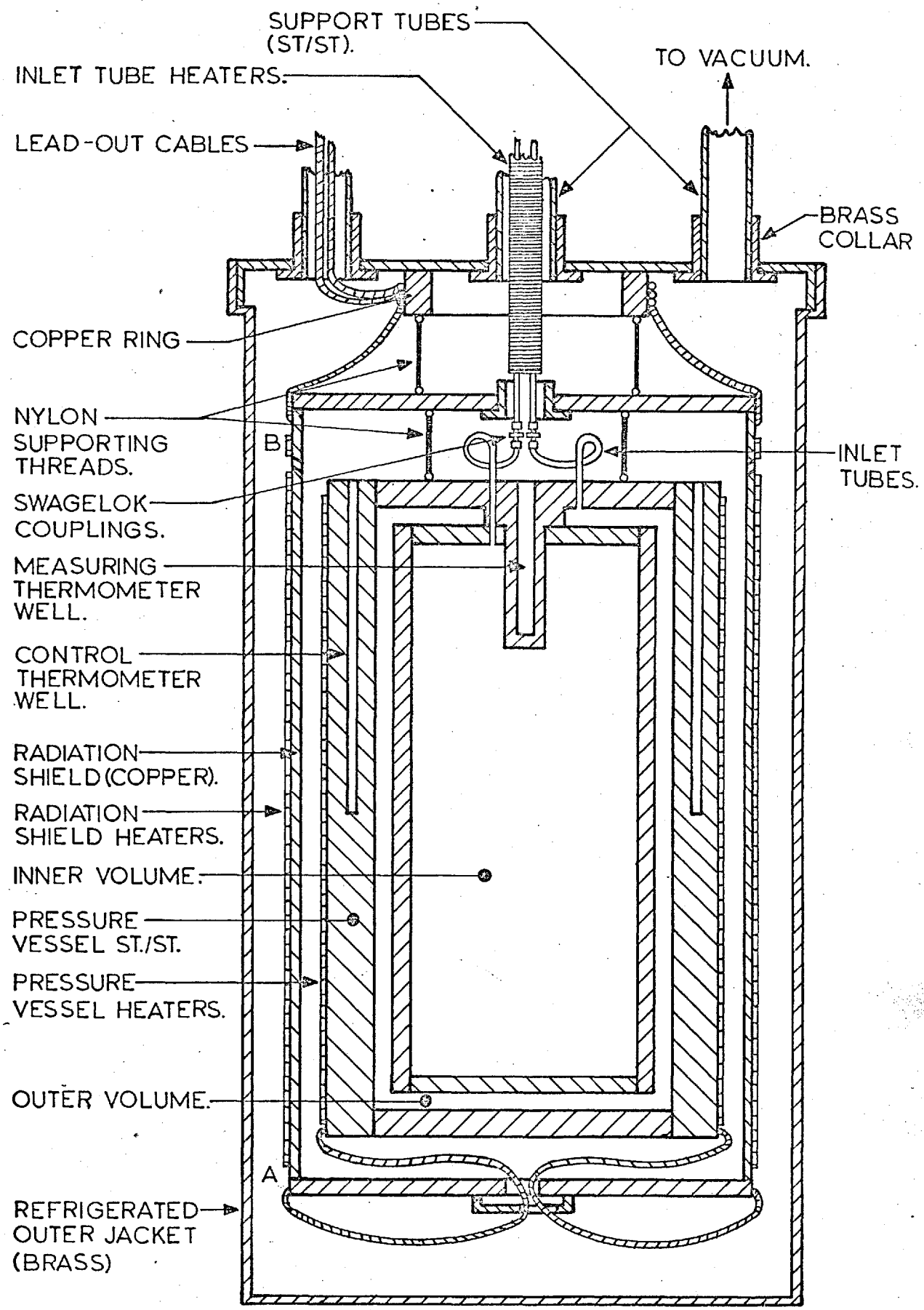

FIG. 2.2 LOW-TEMPERATURE SYSTEM

The interior surfaces of the vessel were polished to reduce adsorption and it was assembled using electron-beam welding (by courtesy of Vickers Ltd.) to prevent damage to the polished surfaces. The vessel was provided with a central well, which housed the platinum resistance thermometer used for temperature measurement, and ten $\frac{1}{8}$" diameter vertical holes drilled in the outer wall to house the controlling platinum resistance thermometers.

A copper/constantan thermocouple was soldered to the pressure vessel at its mid-point and heaters of 32 s.w.g. cotton-covered manganin wire were non-inductively wound along the length of the outer wall. The heaters were electrically insulated from the pressure vessel by a layer of nylon stocking material that was stretched over the vessel and then painted with Formvar (a solution of poly-vinyl formal in chloroform), which also served as an adhesive. The thermocouple and heater circuitry is described in section 2.4.

(b) The Radiation Shield

The copper radiation shield consisted of a 0.125" thick cylindrical side section to which were screwed top and bottom end plates. To the outside of each section were soldered the required thermocouple wires, as described in section 2.4.

The pressure vessel was suspended from hooks screwed into the top of the radiation shield by means of several strands of strong nylon thread (dental floss), which acted as both thermal and electrical insulant. The radiation shield was similarly suspended from the top of the outer brass jacket.

The side section had two spiral grooves along its length, in which were embedded two cables consisting of all the electrical leads to the radiation shield and pressure vessel. One cable carried the heater leads and the other carried all thermocouple and thermometer leads; both also contained spare leads in order to avoid re-wiring of the radiation shield heaters in the event of breakage or shorting in the cables. Along the length of the side section were non-inductively wound 32 s.w.g. manganin wire heaters, insulated from the radiation shield by formvar-painted nylon stocking that also held in place the embedded cables. The top and bottom sections each consisted of two copper discs between which was sandwiched a heater of manganin wire wound on a circular sheet of mica.

Heater and thermocouple leads from the top and side sections were passed down over the outside of the side heaters, from which they were insulated by nylon tape, and together with those from the bottom section they were soldered at point A to the appropriate leads in the embedded cables. Leads from the pressure vessel heaters, thermocouples and platinum resistance thermometers were sheathed in P.V.C. sleeving, passed through the bottom plate of the radiation shield and similarly connected to the cable leads. The hole in the bottom plate was provided with a cover to prevent heat loss by direct radiation from the pressure vessel to the refrigerated outer jacket. All the soldered junctions at point A were covered with nylon tape and fixed at about 1 cm. from the bottom of the radiation shield so that they would be at about the same temperature.

The leads at the top of the embedded cables were soldered at point B to the appropriate leads in the cables coming out of the low temperature system. The purpose of the spiral grooves was to ensure that the ends of the embedded cables at point A were reduced to the temperature of the radiation shield, thus eliminating heat transfer by conduction down the cables to the thermocouple junctions and platinum resistance thermometers.

The inside of the radiation shield was covered with bright aluminium foil to reduce the heat loss by radiation from the pressure vessel. Eight holes of 0.125" diameter in the side of the radiation shield, drilled at an angle to avoid the transmission of direct radiation, assisted the quick evacuation of the interior.

(c) The Inlet Tubes

The two inlet tubes to the inner and outer volumes of the pressure vessel were of 0.063" o.d., 0.043" i.d. stainless-steel tubing. The tubing chosen was thin-walled, to reduce the heat transfer by conduction to the pressure vessel, and of small diameter in order to reduce the quantity of gas contained within.

Before assembling the low-temperature system, eleven copper/constantan thermocouples were attached to the tubes at the positions shown in Figure 2.3. The thermocouple junctions were insulated from the tubes by a thin sheet of paper coated with formvar and then covered with a further layer of insulating paper. A heater of 32 s.w.g. manganin

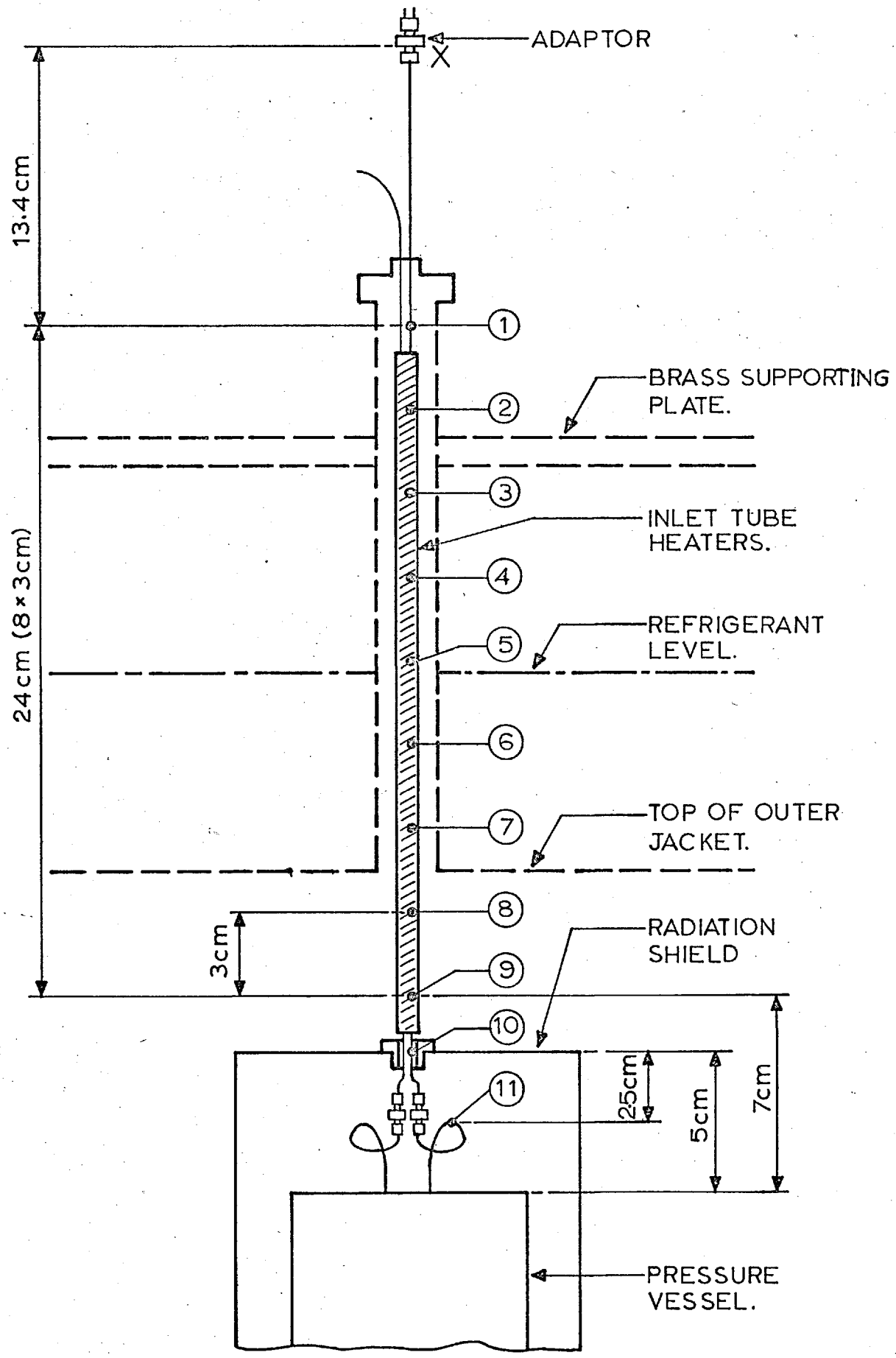

FIG. 2·3 INLET-TUBE THERMOCOUPLE POSITIONS.

wire was then non-inductively wound over the tubes between thermocouples 2 and 10.

The tubing leaving the pressure vessel was coiled to allow for thermal expansion and contraction and then connected by means of "Swagelok" couplings to the inlet tubes. These passed through a hole in the top plate of the radiation shield, from which they were separated by a teflon sleeve. The inlet tubes passed out to the atmosphere at the top of the central support tube through a brass adaptor, the seal being made by means of a soft-soldered joint.

The heater and thermocouple wires were soldered at point B to the appropriate wires in the lead-out cables.

The E.M.F. of each thermocouple was measured by a digital volt-meter ("Solartron") having a resolution of about 3 microvolts. The cold junctions were encapsulated in protecting glass tubes situated in distilled water / ice, and the terminals of the thermocouples connected into the D.V.M. through a mercury-bath switch.

(d) The Outer Brass Jacket and Supports

The cylindrical brass jacket surrounding the radiation shield was supported by means of four stainless-steel tubes, which were thin-walled to reduce heat transfer to the refrigerant from outside the cryostat. To the bottom of each support tube had been hard-soldered a brass collar, which allowed the tube to be soft-soldered readily into the top of the outer jacket. The tubes were joined in a similar

manner to a 0.25" thick brass supporting plate which was bolted to the framework of the apparatus.

The lead-out cables were sheathed in P.V.C. sleeving and wound several times around a copper ring.soldered to the underside of the top of the jacket. This served to cool the cables down,thus reducing their disturbing effect on the temperature control of the radiation shield. The central support tube contained the inlet-tubes, the second support tube contained the lead-out cables from all of the heaters and a third contained the lead-out cables from all of the thermometers and thermocouples. The fourth tube led directly to the vacuum system and contained no cables because of the possible breakdown of electrical insulation that would result from condensation of mercury from the diffusion pump.

The cables passed through a black-waxed B29 brass cone/glass socket joint at the top of the support tubes. Each group of twelve wires were led out to the atmosphere through black-waxed B29 cone: socket seals. The seal was formed by baring the wires, embedding them into the black wax of the socket and inserting the waxed cone stopper. The wires were soldered onto 16 s.w.g. pins, of the same metal, mounted in a perspex disc on each stopper cone.

The inside of the brass outer jacket was covered with bright aluminium foil to reduce heat loss by radiation from the radiation shield. The last stage of the assembly of the low temperature system was the soldering of the brass jacket to its lid. A low melting-point (115 ^{o}C) tin/indium solder

was used to avoid melting the soldered connections on the radiation shield and the other soldered joints on the outer jacket, and also to avoid damage to the inner electrical insulation.

(e) The Cryostat

The brass jacket was immersed in a refrigerating fluid contained in a large silvered Dewar flask. For temperatures of the pressure vessel below 200 K the refrigerating fluid was liquid nitrogen, the level of which was maintained to within 2 cm. by an automatic level controller.

After several experiments at low temperature a small leak appeared in the evacuated brass jacket at the point where one of the support tubes was soldered into the jacket lid. This leak, which was present only when the jacket was immersed in liquid nitrogen, was temporarily cured by repeated application of rubber-based sealant solution. When the temperature of the pressure vessel was above 200 K a slurry of solid CO_2/methanol was used as refrigerant. Although this is less convenient to use than liquid nitrogen, it avoided the problem of leakage.

(f) Low Temperature System Cables

All of the thermocouples were formed by joining 40 s.w.g. copper wire and 36 s.w.g. constantan wire using thermoelectric-free solder. Wires of the same sizes were used for all the thermocouple leads from the low-temperature system to the measuring instruments.

The lead-out cables passed through the support tubes in contact with the refrigerant fluid. As variations in the refrigerant level led to changes in lead resistance, the thermometer and heater leads were of manganin wire, which has a much lower thermal coefficient of resistivity than does copper. The heater leads were of 32 s.w.g. manganin wire, whereas the platinum resistance thermometer leads, which had to have a low resistance, were of 28 s.w.g. manganin wire. This was the largest diameter that could be manipulated easily during the wiring of the system.

In the embedded cables there were no changing temperature gradients and so 32 s.w.g. copper wire was used for both heater and thermometer leads.

From the pin-blocks at the top of the support tubes there were no restrictions on the size of leads and so 18 s.w.g. copper wire was used for the heater leads and for the control platinum resistance thermometer leads. The measuring platinum resistance thermometer leads were of coaxial cable with a 18 s.w.g. copper core and a copper sheath which served to reduce the pick-up of electrical noise by the core.

2.3 Temperature Measurement

The temperature of the pressure vessel was measured by means of a platinum resistance thermometer (Tinsley type 5187 L, No. 193958). It was of the type having a helium-filled outer platinum sheath and both resistance and potential leads, with a nominal ice-point resistance of 25 ohms.

The thermometer was calibrated at the National Physical Laboratory with respect to the International Practical Temperature Scale of 1948. The temperature was given by the Callendar van Dusen equation,

$$t = \frac{R_t - R_o}{\alpha R_o} + \delta\left(\frac{t}{100} - 1\right)\left(\frac{t}{100}\right) + \beta\left(\frac{t}{100} - 1\right)\left(\frac{t}{100}\right)^3 \qquad (2.3.1)$$

where t = temperature in degrees C (IPTS 1948)

R_t = resistance at t ^{o}C

R_o = resistance at 0 ^{o}C.

With a measuring current of 1mA the constants of the equation were calibrated as,

R_o = 24.8370 ohm

α = 0.00392617

β = 0 for T > 0 ^{o}C

β = 0.1096 for T < 0 ^{o}C

δ = 1.4936.

The differences between the IPTS 48 scale and the IPTS 68 scale (in effect the true thermodynamic temperature scale) are given by Hust (6). These differences in the range 150 - 325 K were fitted to a polynomial in temperature and the resultant equation used to change the measured values to the IPTS 68 scale.

The maximum difference between the two scales in this range is .04 K.

The thermometer resistance was measured by means of an A.C. Precision Double Bridge (Automatic Systems Laboratories Ltd., model H8). The ratio arms of the bridge were balanced by means of a 'quadrature' control and an 'in-phase' control

consisting of eight decade switches, which displayed the value of the ratio,

$$r = \frac{R_t}{R_t + R_s} \qquad (2.3\text{-}2)$$

where R_t = resistance of thermometer

R_s = resistance of a standard resistor.

The standard resistor was of nominal 50 ohm resistance (Tinsley type 1659, No. 175884), with both resistance and potential leads. Its resistance at a temperature of t_s ^{o}C was given by

$$R_s = 50.0008 + (t_s - 20).10^{-5} \text{ ohms.} \qquad (2.3\text{-}3)$$

The bridge was set such that the voltage across the thermometer was about R_t mV, giving a current of 1 mA.

Connections to the bridge were made by means of low-noise plugs with gold-plated pins, to which the leads were carefully soldered, using thermoelectric-free solder.

The bridge was equipped with a changeover switch which could change the positions of the ratio arms, thus giving a check on the accuracy of the balance position. Differences between the 'normal' and 'check' positions were usually equivalent to about .001 ^{o}C. The bridge sensitivity was equivalent to .0005 ^{o}C. The overall accuracy of the absolute temperature measurement was estimated as $\pm$ .005 K.

2.4 Temperature Control System

(a) Temperature Control of the Pressure Vessel

The principle of the temperature control system was that a series of platinum resistance thermometers in the wall of the pressure vessel comprised one arm of a Wheatstone bridge circuit, the unbalance signal from which formed the input to an electronic control unit. The output from the control unit supplied power to the heaters around the pressure vessel.

The ten controlling thermometers (De Gaussa type P5), each of nominal 100 ohm resistance at 0 ^{o}C, were housed in ten equally spaced vertical wells in the outer wall of the pressure vessel. They were provided with silver extension leads which enabled them to be connected in series, giving a total nominal 1000 ohm resistance at 0 ^{o}C and a temperature coefficient of resistance of about 4 ohm / ^{o}C. Compensating leads of the same type of wire ran alongside the leads between the thermometers and the bridge.

The bridge circuit is shown in figure 2.4. The ratio arms, R_1 and R_2, were set to 1000 ohms, a value which was close to that of the thermometer, R_4, in order to give optimum control. The variable resistance, R_3, consisted of four decade boxes, which totalled 10,000 ohms in increments of 1 ohm, in series with a 10 x 0.1 ohm wire-wound resistance. Thus the value of R_3 could be pre-set to the nearest 0.1 ohm, corresponding to 0.025 ^{o}C. At the control point,

$$\frac{R_4}{R_3} = \frac{R_2}{R_1} = 1. \qquad (2.4\text{-}1)$$

FIG. 2.4 TEMPERATURE CONTROL CIRCUIT : PRESSURE VESSEL

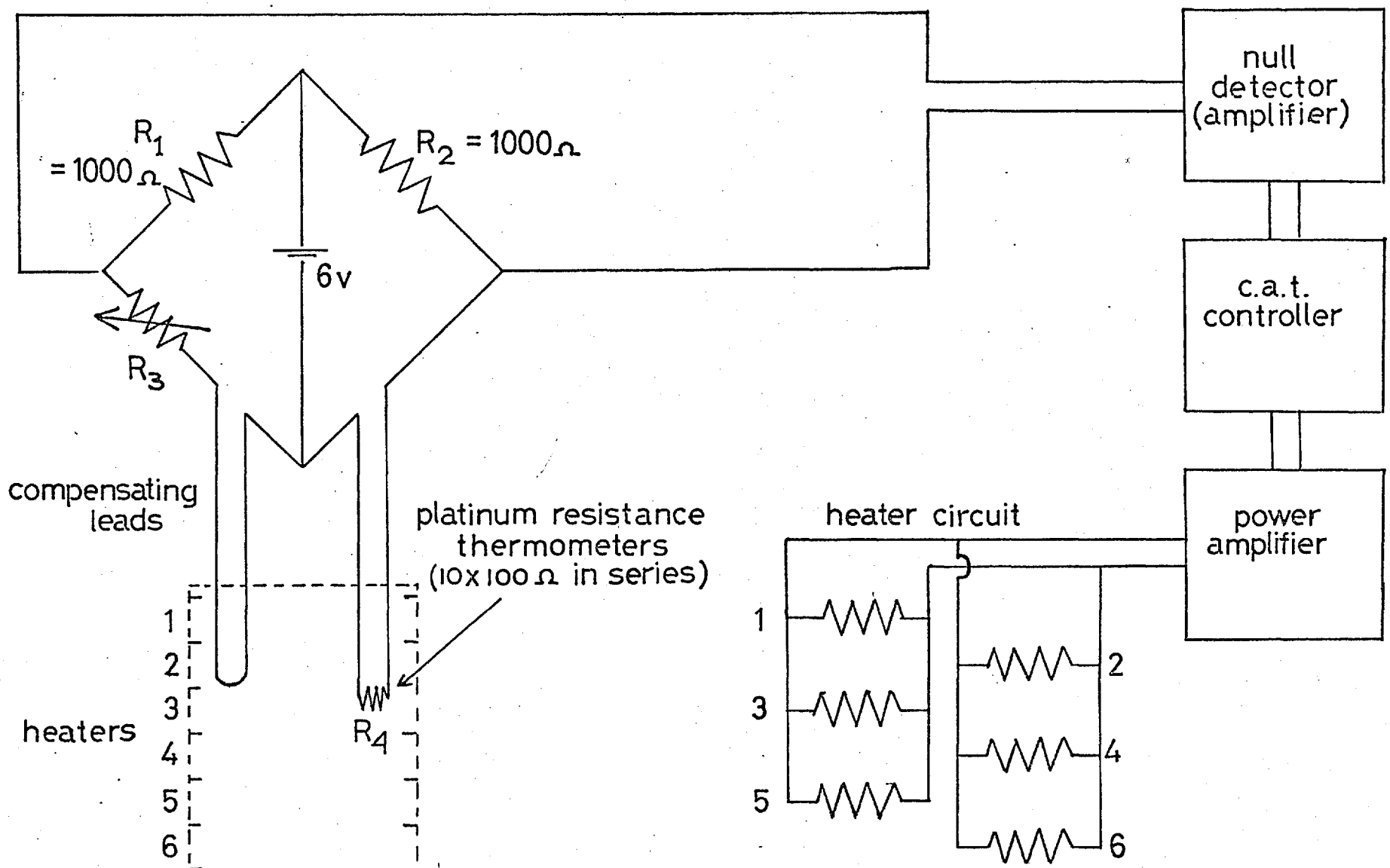

The output sensitivity of the bridge was calculated as follows:

When the bridge was just off balance, then the resistance of the thermometers changed to $R_4 + \delta R_4$

$$\therefore \quad \text{Voltage across } R_4 + \delta R_4 = \frac{V(R_4 + \delta R_4)}{(1000 + R_4 + \delta R_4)} \qquad (2.4\text{-}2)$$

$$\text{Voltage across } R_3 = \frac{V\ R_3}{(1000+R_3)} = \frac{V\ R_4}{(1000+R_4)} \qquad (2.4\text{-}3)$$

$$\therefore \quad \text{Output voltage} = \frac{V(R_4+\delta R_4)}{(1000+R_4+\delta R_4)} - \frac{V\ R_4}{(1000+R_4)} \qquad (2.4\text{-}4)$$

$$\simeq \frac{1000.V.\delta R_4}{(1000+R_4)^2} \qquad (2.4\text{-}5)$$

The battery voltage was chosen as 6 volts, giving a bridge output of 6 microvolts for a change in temperature of 0.001 ^{o}C at 0 ^{o}C (R_4 = 1000 ohms, δR_4 = 0.004 ohms). The bridge output increased at lower temperatures of the pressure vessel, e.g. 8.7 microvolts/0.001 ^{o}C at 190 K. (R_4 = 670 ohms).

The output voltage from the bridge formed the input to an electronic D.C. Null Detector (Leeds and Northrup, model 9834-2). This instrument was a high-gain, low-noise operational amplifier, giving an output voltage of from-0.5 to + 0.5 volts, displayed on a front-panel meter. The maximum drift rate was about 0.1 microvolts per hour, corresponding to an apparent temperature change of about 0.001 ^{o}C during an experiment.

The output from the Null-Detector provided the input to a Current-Adjusting-Type Control Unit (Leeds and Northrup, Series 60), which gave from 0 to 5 mA output. This instrument had 3-action control: proportional, integral and rate control.

The proportional control functioned in rapid response to the error signal by providing a restoring signal in proportion. The integral control provided an extra restoring signal to maintain the control point at the correct set position at which the error signal was zero. Rate control supplied a further restoring signal in proportion to the rate of change of temperature.

The output from the control unit was amplified by a Power Supply-Amplifier (Hewlett-Packard, model 6823 A). This provided a maximum power of 10 watts at 20 volts d.c. and 0.5 amp. It could also be used as a direct manually-controlled power supply; this was important when rapid heating of the pressure vessel was necessary.

Ideally, the pressure vessel heaters should cover as large a surface area of the pressure vessel as possible and should have the optimum total resistance of 40 ohm consistent with the Power Supply/Amplifier rating. It was possible to meet these conditions using six sections of 32 s.w.g. manganin wire heaters, each of 240 ohms, connected in parallel to give a total resistance of 40 ohm. Alternate sections were connected in parallel inside the radiation shield and these two 80 ohm units were then joined outside the low temperature system. Thus in the event of failure in one of these 80 ohm heaters, the other could be used without recourse to rewiring of the pressure vessel.

On assembly of the control system, much attention was paid to the removal of noise and feed-back interference caused by ground-loops in the Null-Detector circuit. Even so, it

was not possible to use the Null-Detector at its full sensitivity because of unstable oscillations of the null detector output. At the setting used a change in control temperature of 0.001 ^{o}C resulted in a meter deflection of 2 mm. of scale. After adjustment of the control unit settings to give optimum control, it was found that it was possible to maintain the temperature of the controlling thermometers such that the meter reading of the null detector was constant to within 1 mm., corresponding to 0.0005 ^{o}C. However, the temperature as measured by the central measuring platinum resistance thermometer exhibited slow oscillations of $\pm$ 0.001 ^{o}C. The slightly worse control at the centre of the pressure vessel was thought to be due to the time-lag involved in heat transfer across the outer wall and the layer of pressure-compensating gas.

On establishment of equilibrium after an expansion the control temperature was usually less than the value before the expansion. These increments were about 0.003 ^{o}C for an expansion from 100 bar and decreased in magnitude with the pre-expansion pressure. The overall change during an experiment was about 0.005 ^{o}C to 0.01 ^{o}C. This phenomenon was thought to be due to the effect of the layer of compensating gas on the small temperature gradient across the pressure vessel.

(b) Temperature Control of the Radiation Shield

The control system is shown in figure 2.5. Copper /constantan differential thermocouples were used to monitor the differences in temperature between the pressure vessel and the side of the radiation shield, AB; between the top and the side, CD; and between the bottom and side, EF. Electrical connection between the three sections of the radiation shield was made by means of the copper of the shield itself.

The thermocouple AB was connected in series with a microvolt source. This source consisted of the voltage taken across a variable number of small resistances in series with a 1 megohm resistor and a mercury-cadmium cell. The combined E.M.F. of the source and thermocouple provided the input to a Null Detector and C.A.T. Control Unit (Leeds and Northrup), of the same type that were used in the control system of the pressure vessel. Thus when the E.M.F. of the differential thermocouple was equal and opposed to that of the microvolt source, the radiation shield temperature was at its control point. The source could be pre-set at a value from 5 to 100 microvolts; corresponding to a temperature of the radiation shield of from .15 to 3.0 ^{o}C below that of the pressure vessel. This was set for each experiment to as small a value as possible consistent with good temperature control of the pressure vessel.

The output of the control unit was amplified by a Power Supply/Amplifier (Hewlett Packard, model 6824A), having a maximum output of 50 watt at 1 amp, which supplied the radiation shield and inlet tube heaters. The heater circuit is also shown in figure 2.5. The side section of the radiation shield

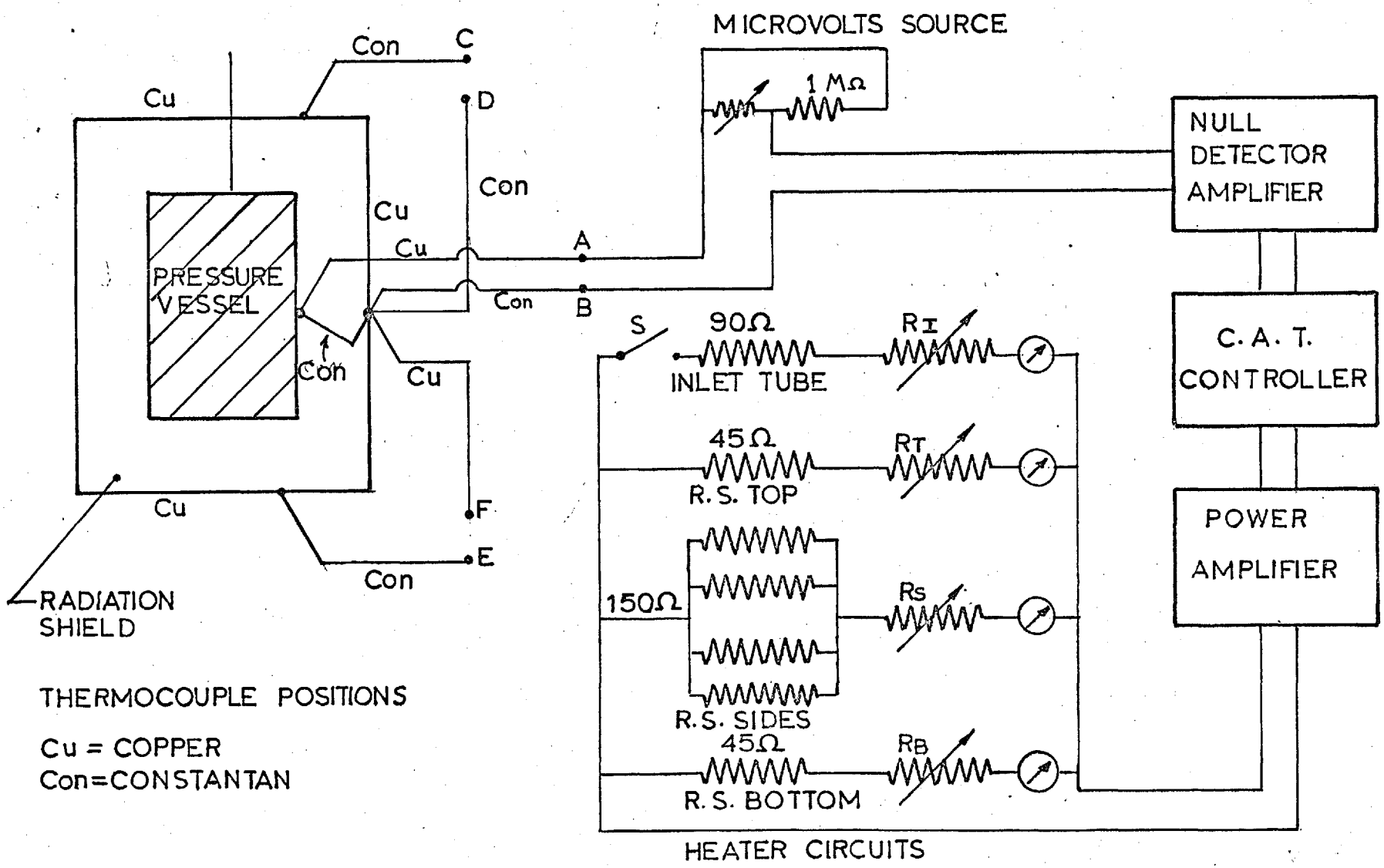

FIG. 2·5 RADIATION SHIELD : TEMPERATURE CONTROL

possessed four heaters of 32 s.w.g. manganin wire, each of 600 ohms, connected in parallel to give a combined resistance of 150 ohm. The top and bottom sections each possessed one heater of 45 ohms. The values of these heaters were approximately proportional to the mass of copper that they were required to heat.

The E.M.F.'s across thermocouples CD and EF were indicated by means of a sensitive 10 ohm suspension galvanometer (Tinsley, SR4). By manual adjustment of the three rheostats, R_S, R_T and R_B in series with the radiation shield heaters, all three sections could be maintained at the same temperature. In practice it was found that after the initial setting of these rheostats, little further adjustment was required owing to the good thermal contact between the three sections of the shield and the high thermal conductivity of the copper.

Rheostat R_I controlled the current supplied to the inlet tube heater, which was of 90 ohms resistance. The supply to this heater could be cut off by means of the switch, S, to prevent over-heating at the top of the inlet tubes if rapid warm-up of the radiation shield were required before an experiment.

In practice, the temperature of the radiation shield was controlled to within 0.1 ^{o}C, corresponding to $\pm$ 3 microvolts in the output of the differential thermocouple. It was found that with solid CO_2/methanol as refrigerant, then at 295 K the required heating level of the radiation shield was nearly 1 amp and temperature control was difficult.

2.5 The Ice-Bath Vessel

A diagram of the ice-bath vessel is shown in figure 2.6. As in the case of the low temperature pressure vessel, the ice-bath vessel was double-walled and pressure compensated, enabling the variation with pressure of the volume to be calculated with accuracy. Another feature of the design was the provision of four interchangeable inner vessels of different lengths, giving four possible ice-bath volumes of 514·9 cc, 385·7 cc, 281·3 cc, and 176·2 cc (at 20°C). The accuracy of the results is effected by the particular volume used in an experiment, as described in section 3.4(g).

The vessels were machined from EN58J stainless-steel and the interior surfaces polished to reduce adsorption. They were assembled by means of precision argon-arc welding. The inlet tube to each inner vessel was of .063" o.d., .043" i.d. stainless-steel tubing. An 'O'-ring in a groove at the top of the pressure compensating jacket formed the seal between the outer volume and the atmosphere. The inner vessel was held in place by means of the end-cap of the pressure compensating jacket and eight $\frac{3}{8}$"-whit. stainless-steel bolts which screwed through the end-cap and located on the top of the inner vessel end-plug. The tension in these bolts was adjusted to give a leak-tight seal at the 'O'-ring. The bolts also passed through a steel ring which was connected by means of four $\frac{3}{8}$" diameter steel rods to the framework of the apparatus and thus served to support the whole vessel.

The vessel was situated in a large Dewar flask containing a mixture of distilled water and finely crushed ice. Good

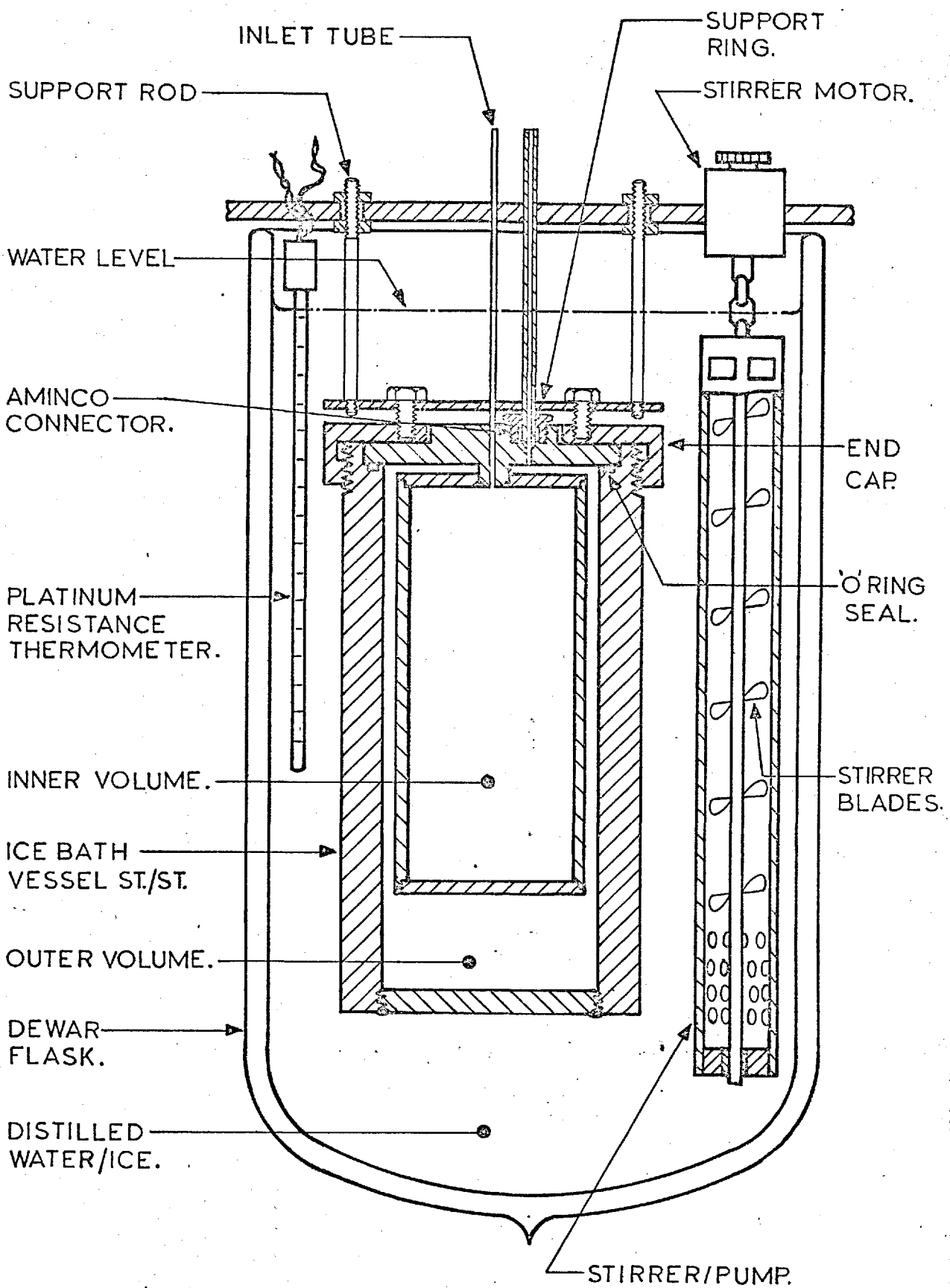

FIG. 2.6 ICE-BATH VESSEL

circulation of water in the bath was provided by a six-bladed stirrer inside a plastic tube with holes positioned as shown in figure 2.6 such that a vigorous pumping action resulted.

A platinum resistance thermometer inserted in the bath indicated whether there was sufficient circulation of water in the bath. As a preliminary check on the temperature stability of the gas in the inner vessel, it was filled to about 80 bars with nitrogen and the pressure monitored by the oil piston-gauge. It was found that, as long as there was sufficient ice in the bath and the stirring rate was reasonably high, the fluctuations in temperature were less than .002 ^{o}C during a pressure measurement. Both of the independent vacuum systems comprised an oil rotary pump, a water-cooled mercury diffusion pump and a liquid nitrogen trap. One system maintained the vacuum in the outer jacket of the low temperature system, and the other was used to evacuate the ice-bath vessel prior to an expansion and to evacuate the apparatus at the end of an experiment.

The vacuum in the pumping line was measured by means of an Ionization Gauge. Because of the small-bore inlet tubing of the ice-bath vessel, the pressure inside the vessel during its evacuation was greater than that measured by the Ionization Gauge. Therefore a few tests were carried out to determine the time of evacuation necessary.

The ice-bath vessel, containing nitrogen at 1 atmosphere pressure, was directly connected to the pressure port of the Precision Pressure Gauge, the reference side being under vacuum. It was found that an evacuation time of 40 minutes was required to reduce the residual pressure to less than 5.10^{-5} bar, the

minimum value that could be detected by the P.P.G. To be certain of complete evacuation, this time was increased to 60 minutes in the course of experiments.

2.6 Pressure Measurement

(a) The Oil Piston-Gauge

Pressures from about 25 - 110 bar were measured by means of an oil piston-gauge (Budenberg), having a piston/cylinder unit, No. K231, of .125 in^2 nominal piston area. Its characteristics are described in detail by Bett (7), who calibrated it against a standard mercury column.

The applied pressure on the piston, i.e. the excess of internal fluid pressure over atmospheric pressure, was given by the quotient of the total downward force on the piston, F, and its 'effective area', A. Prior to the present study the piston/cylinder unit was submitted to the National Physical Laboratory for calibration of the effective area against a primary standard piston-gauge. With reference to figure 2.7, showing the piston/cylinder unit, the reference level chosen by the N.P.L. for specification of the applied load was that of the lower end of the piston at the mid-point of its range of movement, level C. During calibration the piston was balanced at its midway position and rotated freely at 35-40 revs/min, in both directions. The oil used as pressure transmitting fluid, both by the N.P.L. and in the present study, was a mixture of Shell 'Diala-B' and Shell 'Talpa-30' in the ratio 3:2.

FIGURE 2.7

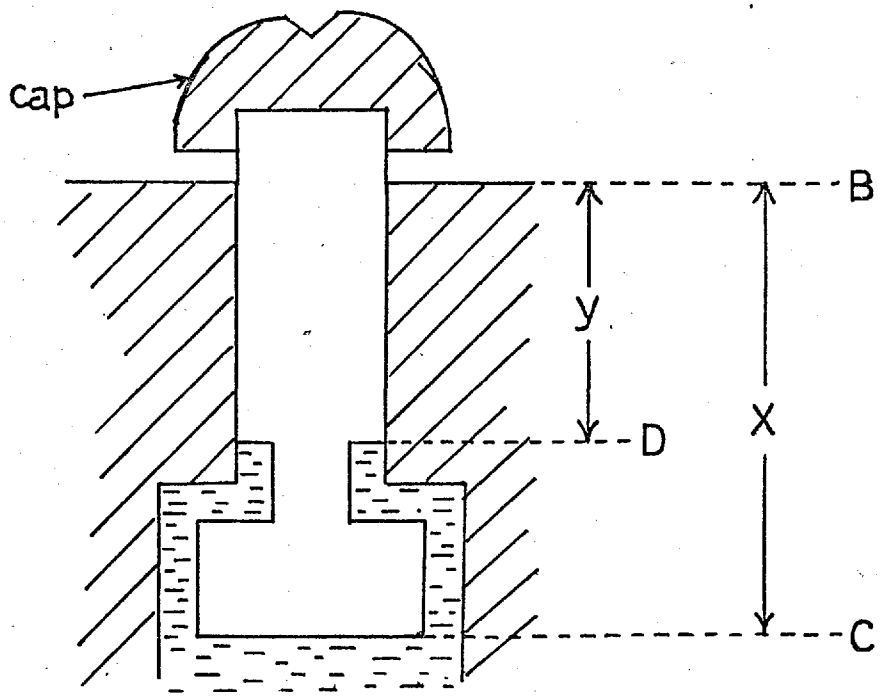

PISTON/CYLINDER UNIT

FIGURE 2.8

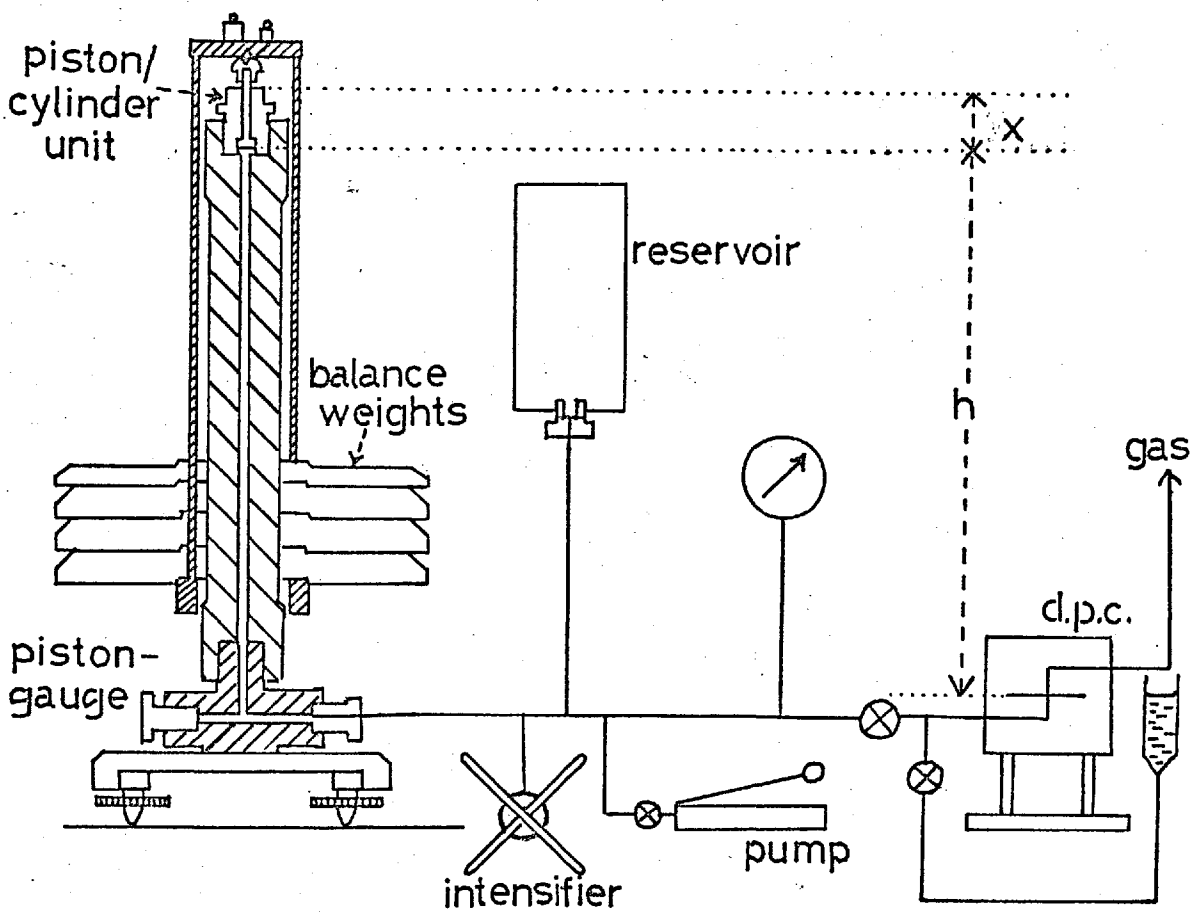

PRESSURE MEASUREMENT (OIL SYSTEM)

The effective piston area, A_p, at a pressure of P bars, was given by

$$A_p = A_o (1 + bP) \qquad (2.6\text{-}1)$$

At 20 °C the calibrated values of A_o and b were,

$$A_o = 0.806424 \pm 0.000013 \text{ cm}^2$$

$$b = 4.0 \cdot 10^{\pm 7} \text{ bar}^{-1}.$$

The N.P.L. value of A_o differed from that found by Bett, 0.806392 cm^2, but agreement was reasonably good considering the possible effects of ageing on the piston area and that in the earlier calibration a different pressure standard and a different fluid, paraffin oil, were used.

The effective area at a temperature t°C was,

$$A = A_p (1 + 2\alpha (t-20)) \qquad (2.6\text{-}2)$$

$$\alpha = 11.5\ 10^{-6}\ ^{\circ}C^{-1} \qquad (2.6\text{-}3)$$

A load was applied to the piston by means of counter-balancing disc weights supported on a stainless-steel weight carrier, as shown in figure 2.8. The carrier rested on a ball-bearing in the top of the piston-cap. If the total mass of the counterbalancing weights, carrier, ball-bearing, piston and cap is M, then the total downward force, F, on the piston at level C is,

$$F = Mg - fa - fo + fs \qquad (2.6\text{-}4)$$

g = acceleration due to gravity.

fa = upward force due to buoyancy in air of all the weights, etc., above level B.

fo = upward force due to buoyancy of that part of the piston submerged in oil.

fs = downward force due to surface tension at the oil meniscus at the top of the piston.

(i) The Acceleration due to Gravity

The absolute value of the acceleration due to gravity, g, was recently determined at the National Physical Laboratory (8).

$$g = 9{\cdot}81182 \text{ m.sec}^{-2} \qquad (2.6\text{-}5)$$

The value at the Department of Geophysics, Imperial College, was determined (1971) as equal to 9.81202 $\text{m.sec}^{-2} \pm .00006 \text{ m.sec}^{-2}$ by using a comparative gravimeter. This was the value assumed for use in this investigation.

(ii) Determination of the Mass of Counterbalancing Weights

The piston-gauge counterbalancing weights were weighed in air on a 10 Kg. balance (Stanton Instruments), against rhodium-plated brass analytical weights which had been standardised at the N.P.L. in 1951. These analytical weights were checked, prior to the weighings of the piston-gauge weights, by comparison with a primary standard of mass. This standard was a chromium-plated brass integral weight which had been used on only three occasions since its calibration. It was therefore assumed to have the mass given in the calibration, which was 6653.759 gm., to the nearest 0.001 gm.

With the standard integral weight on one scale pan, the mass of analytical weights required for balance on the other pan were found to the nearest .002 gm. by the method of oscillations using a previously determined value of the balance sensitivity. The balancing was repeated with the integral weight moved to the other scale pan, and the geometric mean of the two readings taken to compensate for inequality in the lengths of the balance arms. The total

mass of analytical weights was found to differ from that of the integral weight by less than 0.004 gm. Analytical weights used in this check were then balanced against others of the same total nominal mass. It was determined that the mass of no analytical weight differed from its nominal value by more than 0.003 gm. and so no corrections to these values were necessary.

Each of the piston-gauge disc weights, the carrier, ball and piston were then weighed in air against the analytical weights by the same method of double weighing, to the nearest 0.005 gm.

The true mass of the object being weighed was given by the mass of the balancing analytical weights corrected for the effect of buoyancy in air,

$$M = M_B \left(1 + \rho \left(\frac{1}{d} - \frac{1}{d_B}\right)\right) \qquad (2.6\text{-}6)$$

M_B = Mass of balancing brass analytical weights.

d = Density of object being weighed.

d_B = Density of brass analytical weights.

ρ = Density of air.

The densities of the relevant materials were,

Cast Iron	7.10 $gm.cm^{-3}$
Steel	7.83 "
Stainless steel	7.90 "
Brass	8.40 "

The value for the oil-blacked cast iron disc weights was that determined by Bett (7). The density of air was taken from tables of ambient air density given in Kaye and Laby (9).

TABLE 2.1

Masses of Piston-Gauge Disc Weights, Carrier and Piston

Weight No.	Mass , gm. July 1969	December 1970	December 1971
18	6668.37	6668.37	6668.39
19	6669.25	6669.25	6669.27
20	6669.38	6669.38	6669.40
21	6669.45	6669.46	6669.48
22	6670.27	6670.27	6670.27
23	6669.93	6669.93	6669.94
24	6668.77	6668.79	6668.80
25	6669.26	6669.26	6669.27
115	6469.91	6469.91	6469.94
116	6516.99	6516.98	6517.00
117	6425.84	6425.84	6425.82
60	2666.45	2666.46	2666.48
61	2666.40	2666.42	2666.43
62	2666.45	2666.46	2666.47
64	1333.01	1333.03	1333.04
65	1333.03	1333.05	1333.06
66	666.18	666.19	666.20
67	666.49	666.51	666.52
69 (steel)	266.709	266.707	266.708
71 (")	266.731	266.735	266.741
141 (")	266.499	266.503	266.506
72 (")	133.333	133.335	133.344
73 (")	133.192	133.198	133.196
Piston Unit (steel)	45.273	-	-
Carrier (s.steel)	1130.879	1130.880	1130.881
Ball (s.steel)	2.039	2.039	2.037

Each object was reweighed on the same day and the results were reproducible to within 0.005 gm. The maximum buoyancy correction amounted to 0.17 gm. for the largest weights and the error in this correction was estimated as less than 0.005 gm. Hence the mass of each weight was taken as having a maximum error of $\pm$ 0.01 gm., for the largest weights, and $\pm$ 0.005 gm. for the smaller weights. Table 2.1 shows the values obtained on three separate occasions during the present study. It can be seen that most of the cast-iron disc weights exhibited a small increase in mass over this period, possibly due to an increase in adsorption of water vapour or to the effects of slight corrosion.

A set of stainless steel analytical weights, ranging from 0.01 gm. to 100 gm., was used to supplement the set of disc weights. The true mass of each of these weights was found to be within 0.002 gm. of its nominal value.

(iii) Buoyancy and Other Corrections to the Load on the Piston

The upward force, f_a, due to air buoyancy is given by

$$f_a = g. \sum_w m_w \rho / d_w \qquad (2.6\text{-}7)$$

where d_w is the density of a weight of mass m_w and ρ is the density of air. Air buoyancy corrections had to be made to all weights above point B (figure 2.7). The mass of piston and cap above level B was calculated from the dimensions of the piston and its total mass.

The tables of ambient air density (9) in the ranges of 25 - 32 ^{o}C. and 730 - 780 mmHg atmospheric pressure

were represented for computational purposes by the following equation,

$$\rho = (1.180 - 0.0045\ (t - 27) + 0.0016\ (h - 767)).10^{-3} \qquad (2.6\text{-}8)$$

ρ is the air density, in $g.cm^{-3}$.

t is temperature, ^{o}C.

h is atmospheric pressure, mmHg.

The error resulting from use of this equation was estimated as less than .5%. The maximum error in the value of the density of the disc weights was estimated as 1.5%, giving a total maximum error in the buoyancy correction of 2%. This corresponded to an error in pressure of 3 parts in 10^6.

The upward force, f_o, due to oil buoyancy was,

$$f_o = g.\ V_{BC}.\ \rho_o \qquad (2.6\text{-}9)$$

where V_{BC} is the volume of the piston between B and C, and ρ_o is the density of the oil.

However, the N.P.L. calibration included the additional pressure at C, caused by the hydraulic head of oil between B and C, with the oil buoyancy correction to the total load,

i.e. $f_o = g.V_{BC}\rho_o - g.\ \rho_o.x.A \qquad (2.6\text{-}10)$

$$= g\rho_o\ (A.y + V_{CD}') - g\rho_o.xA \qquad (2.6\text{-}11)$$

$$= g\rho_o\ (V_{CD}' - A(x - y)) \qquad (2.6\text{-}12)$$

$x - y = 0.992$ cm. $\quad V_{CD}' = 0.947\ cm^3 \qquad (2.6\text{-}13)$

V_{CD}' is the volume of that part of the piston between D and C, calculated from its dimensions.

At 20 ^{o}C, f_o = 0.013 N, from equation (2.6-12); this value agrees well with the figure given by the N.P.L. of 0.014 N. The major error in the calculation of f_o from equation (2.6-12) arose from the uncertainty in V'_{CD}, estimated as $\pm$ 0.015 cm^3, leading to a maximum error in f_o of about 0.0013 N. This corresponded to an error in pressure of $1.5.10^{-4}$ bar.

The effect of surface tension was calculated by the N.P.L. as,

$$f_s = 0.0096 \text{ N} \qquad (2.6\text{-}14)$$

The oil-system is shown in figure 2.8. The hydraulic pump (Blackhawk) was employed for quick pressurization of the oil and the oil-injection pump provided fine changes in pressure. All valves were Autoclave 2-way needle valves with ¼" o.d., .07" i.d. stainless-steel interconnecting tubing.

Before the first pressure measurement, the base of the piston-gauge was levelled. During each measurement the carrier was rotated freely at about 40 revs. min^{-1} in such a way that there was no eccentricity in rotation. Oil leaking past the piston was periodically removed with paper tissue to maintain the correct shape of the meniscus. It was found that the gauge was capable of high sensitivity, its resolution being better than 5.10^{-5} bar, The short-term reproducibility on measurement of a constant pressure was better than 10^{-4} bar, the direction of rotation of the piston being immaterial. Just after each measurement, the temperature of the piston was measured with a mercury-in-glass thermometer. This was felt to give a truer indication of the piston temperature than a thermometer permanently set into

the base of the gauge.

(iv) Hydraulic Head of Oil

With reference to figure 2.8, the pressure of the oil at the diaphragm of the Differential Pressure Cell was greater than that at level C by δP, where

$$\delta P = g. \rho_p .h. \qquad (2.6\text{-}15)$$

ρ_p is the density of oil at pressure P bars.

The distance h+x was measured with an accurate cathetometer; the mean of several readings gave

$$h+x = 34.597 \text{ cm.} \qquad (2.6\text{-}16)$$

Hence,

$$h = (34.597 - 3.716) \text{ cm.}$$

$$h = 30.881 \text{ cm.}$$

The major errors in this figure were due to the uncertainty in the exact diaphragm position, which was given by a mark on the outside of the D.P.C., and to deviations from the true mid-point floating position. The maximum error in h was estimated as 0.05 cm, or 0.15%.

The oil density was determined by means of a 25 ml. glass density bottle at temperatures from 25 ^{o}C to 32 ^{o}C. At each temperature the bottle was first filled with mercury to determine its volume and then with oil; the bottle was maintained in a water bath inside the temperature-controlled enclosure to ensure a steady, known temperature. The estimated maximum error in each of the measured values of the oil density given below is 0.0005 g cc^{-1} (Table 2.2)

The density of the oil increased with pressure. A value for the compressibility, β, was calculated on the basis of measured values for mineral oils of similar constitution

to the mixture used (10).

$$\rho_P = \rho_o(1 + \beta P) \qquad (2.6\text{-}17)$$
$$\beta = 9.\,10^{-5}\ \text{bar}^{-1}$$

This leads to a total maximum possible error in ρ_P of 0.0015 g.cc^{-1} at 100 bar, or 0.2%. Combined with the errors in h, the maximum possible error in δP was about 0.35% at 100 bar, i.e. 0.35% of 0.028 bar.

$$\simeq 0.0001 \text{ bar}$$

(b) The Differential Pressure Cell

The differential pressure cell (Ruska), or D.P.C., served both to isolate the gas from the oil of the high-pressure piston-gauge and to accurately null the pressure difference between the two media.

It consisted of two stainless-steel pressure chambers separated by a thin, circular stainless-steel diaphragm. Attached to the upper surface of the diaphragm was the movable core of a differential transformer. A pressure difference between the two chambers caused a deflection of the diaphragm and thereby a change in the inductance of the transformer. The resultant signal was amplified and displayed on a Null Indicator adjacent to the pressure cell. The instrument had a maximum sensitivity of 0.0003 bar pressure difference for full scale deflection.

With reference to figure 2.9, each chamber opening had been threaded to take a 3/8", 24 t.p.i. double male fitting (Ruska). One half of each fitting was machined to ¼" o.d. so that it could be connected to the ¼" o.d. pressure tubing by means of standard "Ermeto" couplings.

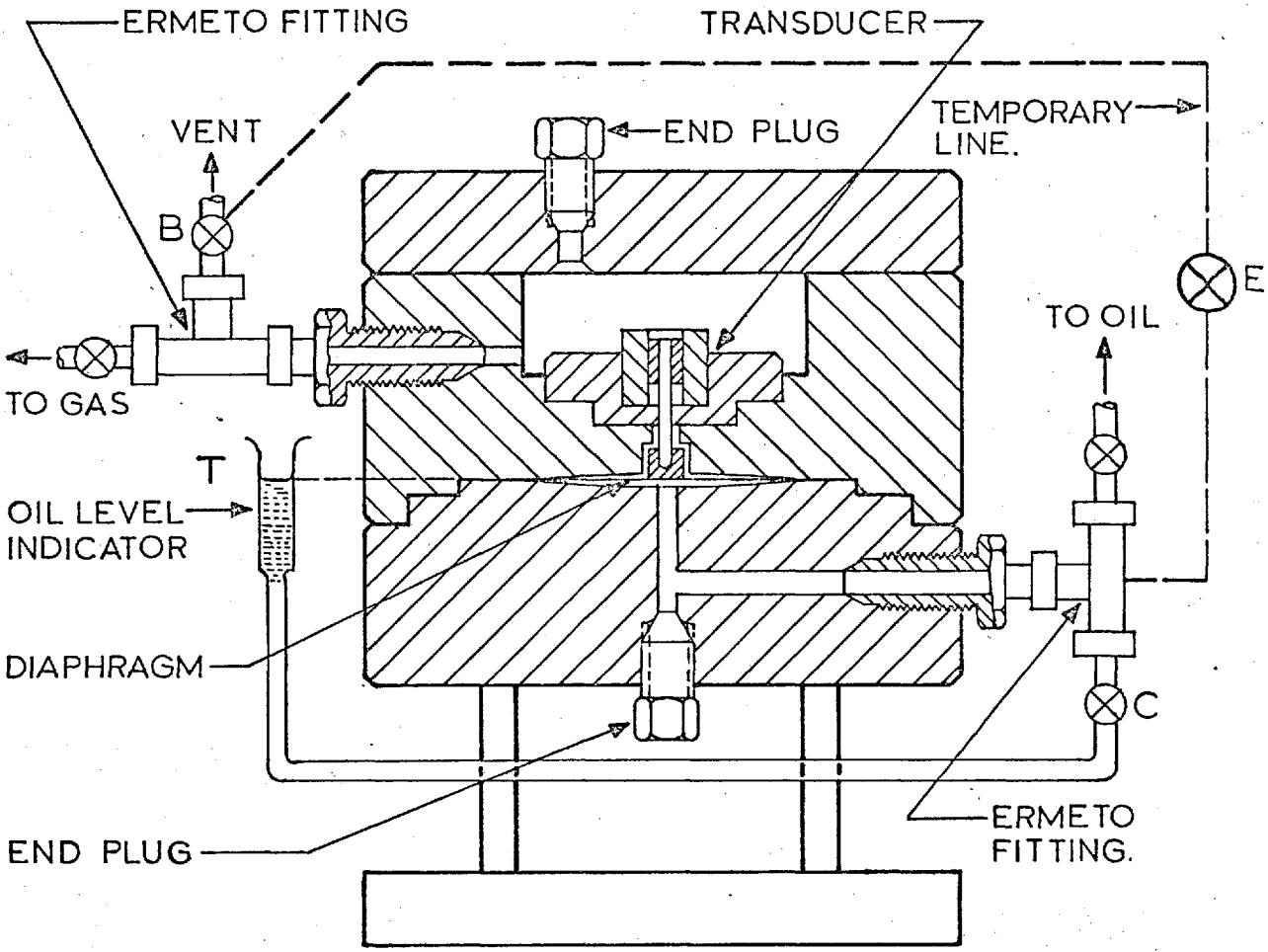

FIG. 2·9 DIFFERENTIAL PRESSURE CELL (RUSKA)

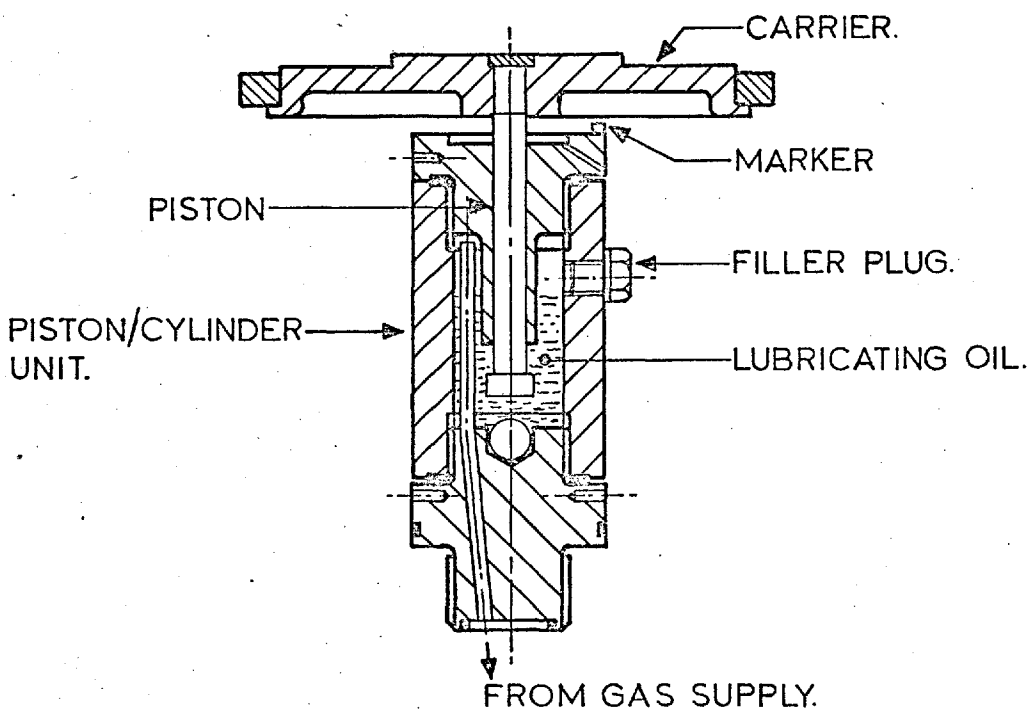

FIG. 2·10 GAS PISTION GAUGE (BUDENBERG)

Before the introduction of oil into the lower chamber a temporary line of pressure tubing and a valve, E, were inserted so that the two chambers might be connected directly and the shift with pressure of the D.P.C. null position investigated.

This null-shift was estimated from the calibration curve supplied by Ruska as being proportional to pressure below 110 bar and as having the value

$$\Delta P/P = 2.10^{-6} \qquad (2.6\text{-}17)$$

After nulling the indicator with both chambers open to atmosphere, on filling the cell with dry nitrogen at 100 bar a null shift of almost full scale deflection on maximum sensitivity was observed, corresponding to a ΔP of 3.10^{-4} bar. This shift was very small and the difference between it and the value predicted by the calibration was negligible; throughout this work the Ruska calibration was used, therefore, to estimate the null-shift with pressure.

After this preliminary check on the null-shift, the lower chamber was filled with the oil mixture,which had previously been filtered to prevent the introduction of metallic particles that might puncture the diaphragm. Before a pressure measurement, valves B and C were opened and the side-tube, T, raised or lowered until the oil meniscus was level with the position of the diaphragm. The null indicator was then set on the null position at maximum sensitivity. The lower chamber was then alternately pressurised to 130 bar and then depressurised until a stable null was achieved. After each depressurization several minutes were allowed to elapse to give a steady cell temperature. During each pressure

measurement care was taken to ensure that the pressure in the upper chamber never greatly exceeded that in the lower chamber as this could have lead to a permanent shift in null-position. After a measurement the null-position at 1 atmosphere was redetermined; usually a shift corresponding to a ΔP of up to 10^{-4} bar was noted. Whenever the change represented a ΔP of greater than 10^{-4} bar, the pressure measurement was immediately repeated.

Throughout this study no deterioration in performance of the D.P.C. was apparent and the only servicing necessary involved the replacement of a faulty capacitor in the null-indicator.

(c) The Gas-Operated Piston Gauge

The lowest pressure that could be measured accurately with the oil piston-gauge was about 10 bar owing to an increase in friction between piston and cylinder at low pressure. The instrument used at lower pressures was a gas-operated, oil-lubricated piston-gauge (Budenberg) with a working range of about 2-28 bar and a nominal piston area of 0.125 in^2. A diagram is shown in figure 2.10.

The nylon tubing connecting the various sections of the gauge was replaced by copper tubing with brass 'Simplifix' couplings to eliminate leaks. Mineral oil, grade S.A.E. 10 (Castrol), was used to lubricate the piston/cylinder unit.

The masses of the counterbalancing piston-gauge weights were determined on the 10 Kg. balance, using the same procedure as that described in section 2.6(a). The values obtained are shown in Table 2.3. Weights Nos. 1-10 were of oil-blackened steel, density 7.8 $g.cc^{-1}$, and weights Nos. 11 and 12 were of stainless-steel, density 7.90 $g.cc^{-1}$.

TABLE 2.2

Density of 3:2 Mixture of Shell "Diala B" and "Talpa 30" Oil

Temp. ^{o}C	Density g/cc at 1 atmos.
20.0 (N.P.L.)	0.8840
25.1	0.8792
26.6	0.8779
27.5	0.8772
28.6	0.8765
29.8	0.8757
32.0	0.8744

TABLE 2.3

Masses of Gas-Operated Piston-Gauge Weights

Mass, g.

Weight No.	July 1969	December 1970
1 (steel)	5671.06	5671.08
2 "	5671.08	5671.09
3 "	5671.00	5671.02
4 "	2835.54	2835.56
5 "	2835.56	2835.59
6 "	2268.22	2268.24
7 "	1133.99	1134.01
8 "	1134.04	1134.06
9 "	567.220	567.220
10 "	283.494	283.496
11 (stainless steel)	113.465	113.469
12 "	113.453	113.455

The oil piston-gauge was used to calibrate the gas piston-gauge in the range from 7 to 28 bar (100 - 400 $lb.in^{-2}$). The pressure of nitrogen in the ice-bath vessel was monitored by both gauges. It was found that the gas piston-gauge was sensitive to pressure changes as low as 10^{-4} bar, providing that the carrier was rotated at about 30 - 50 revs. min^{-1}, the direction of rotation being immaterial. Reproducibility to 2.10^{-4} bar was attained as long as the vertical floating position of the piston was constant, owing to the large effect of the buoyancy in oil of the submerged section of the piston. A marker of adhesive tape was attached to the outside of the piston/cylinder unit and the under surface of the rotating carrier was always aligned with the top of the marker. In use, the gas pressure caused oil to leak slowly past the piston and the reservoir level to fall, decreasing the buoyancy effect. It was necessary to replenish the oil before each measurement, topping up to the level of the filler plug, and to clear excess oil from the well at the top of the cylinder/piston unit.

The total mass in grammes, m, of the counterbalancing weights, excluding the carrier and piston, were recorded at intervals of 25 lb. in^{-2} from 100 to 450 $lb.in^{-2}$. It was found that the variation of the pressure, P, with m was very linear between 150 - 375 $lb.in^{-2}$,

$$P = \alpha + \lambda m \quad \text{bar} \qquad (2.6\text{-}18)$$

α and λ were determined by a least-squares curve fit,

α = 0.68848 bar, standard deviation = 2.10^{-5} bar.

λ = 0.00121606 $bar.g^{-1}$, standard deviation ; 4.10^{-8}.

Below 150 lb.in^{-2} the apparent pressure measured by the oil piston-gauge was systematically higher than the true pressure because of the high friction between piston and cylinder.

In normal use of the gas-operated gauge, the pressure as given by (2.6-18) was corrected for the differences between the air density, ρ, and piston temperature, t, and the values at the time of the calibration, 0.00118 g.cc^{-1} and 27.5 ^{o}C respectively.

$$P = \frac{a\left(1 - \frac{(\rho - 0.00118)}{\rho_c} + m\lambda\left(1 - \frac{(\rho - 0.00118)}{\rho_w}\right)\right)}{(1 + 2.3.10^{-5}\ (t - 27.5))} \qquad (2.6\text{-}19)$$

ρ_c is the average density of the carrier and piston = 4 g.cc^{-1}.

ρ_w is the density of the weights = 7.8 g.cc^{-1}.

The gas-operated piston gauge was not used to measure pressures below about 2.5 bar as at these low pressures the frictional force on the piston increased and the calibration, i.e. (2.6-18), was probably invalid.

(d) Atmospheric Pressure Measurement

The atmospheric pressure was measured by means of a standard Fortin barometer of 13 mm. bore.

The pressure is given by

$$P = g\rho_t h + \Delta P \qquad (2.6\text{-}20)$$

g = acceleration due to gravity at barometer.

ρ_t = density of mercury at barometer temperature, t ^{o}C.

h = corrected height of mercury column at t ^{o}C.

ΔP = small correction for the difference in levels between the barometer and the piston gauges.

As a check that the barometer was sound, it was compared with a similar, but new, barometer in a nearby laboratory. Their heights as measured with a metre cathetometer agreed to within 0.2 mm; this was taken as the maximum possible "intrinsic error" of the barometer.

The measured height of the mercury column was corrected for capillary depression, according to values given by Gould and Vickers (11), and for the scale expansion. The reading was multiplied by $(1 + \alpha t)$, where α is the linear thermal expansion coefficient of brass.

$$\alpha = 1.84.10^{-5}.\ ^{o}C^{-1} \qquad (2.6\text{-}21)$$

The density of mercury at 1 atmosphere was obtained from tables given by Bigg (12). Errors in atmospheric pressure measurement are discussed in Section 6(f) of this chapter.

(e) The Precision Pressure Gauge (P.P.G.)

This instrument was a Model 145 Precision Pressure Gauge (Texas Instruments) with a Type 4 stainless-steel capsule having a quartz spiral Bourdon tube, rated at a maximum differential pressure of 8.5 bar (125 $lb.in^{-2}$) at total pressures up to 136 bar (2000 $lb.in^{-2}$). This type of nulling device was chosen mainly because of the very low change in volume with pressure exhibited by the quartz spiral (less than 1 part in 10^{10} up to the maximum pressure). A Texas Instruments low-pressure capsule had also been found to have high sensitivity and null stability (13).

A diagram of the capsule and a scheme of the associated optical system are shown in figure 2.11. A light beam from the source passed through the sapphire window of the capsule and was reflected from the mirror attached to the quartz

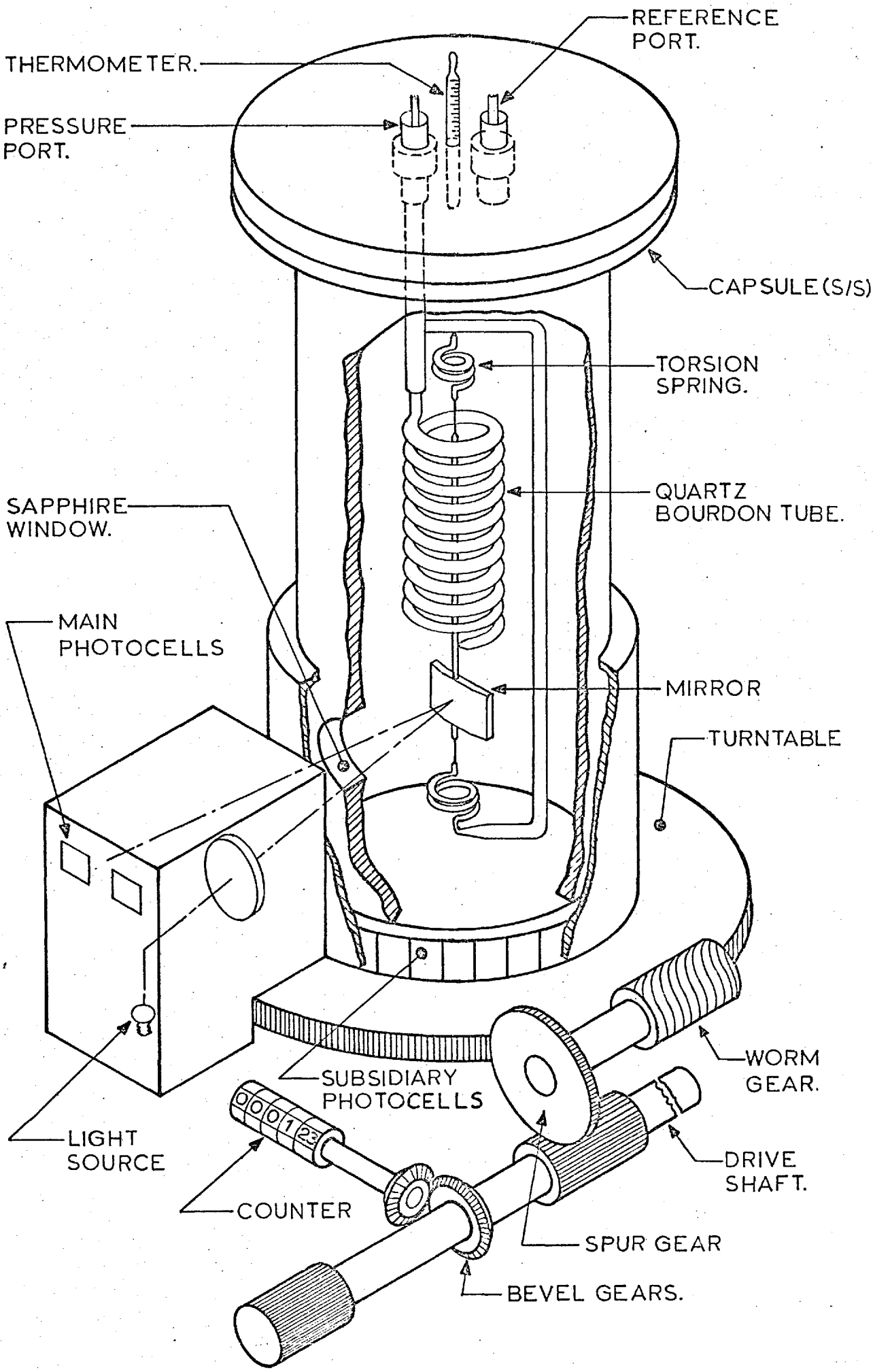

FIG. 2.11 PRECISION PRESSURE GAUGE (TEXAS INSTRUMENTS)

spiral. The image was focussed onto two silicon photo-cells. When the image was divided equally between the two cells, the output from each cell was equal and opposed and no net current flowed through the associated ammeter circuit. A pressure difference across the spiral caused the mirror to deflect and the reflected light beam to move from its central position, giving rise to a deflection on the meter: the sensitivity was of the order of 1 mm. of scale deflection for 10^{-4} bar pressure differential.

The optical system, including photocells, was mounted on a worm-gear turntable that rotated about a central vertical axis. When the pressure and reference ports were directly connected the P.P.G. could be nulled by rotation of the turntable until there was no meter deflection.

A digital counter was operated through a system of gearing from the turntable rotation, giving a reading of 300.000 for the full-scale 100 ^{o} rotation. When the operational mode of the P.P.G. was changed from 'METER' to 'SERVO', the output from the photo-cells actuated an electric motor which automatically drove the turntable around the capsule until the reflected light-beam was at the centre of the photo-cells. The digital counter reading, when multiplied by an appropriate calibration factor, indicated the pressure difference across the gauge. Supplementary photo-cells provided the restoring signal for the servo-system when the light-beam moved off the central photo-cells.

The capsule was maintained in anenvironment at a constant temperature of 45 ^{o}C.

(i) Modifications to the P.P.G.

The original pressure port of the capsule was modified in order to reduce the dead-space volume above the quartz spiral. With reference to figure 2,12, .125" o.d., .030" i.d. stainless-steel tubing was hard-soldered through the centre of the brass filler which was then machined to fit the lower part of the pressure port. An 'O'-ring, .063" diameter, seating in a groove in the filler, formed the seal between the wall of the port and the filler. The whole unit was held in place by the original fitting, as shown. This modified fitting reduced the volume of the port from about $2cm^3$ to less than $0.1cm^3$.

The second modification required the incorporation of an automatic device to protect the quartz spiral in the event of an excessive pressure differential across the gauge (> 8.5 bar). A general scheme of the automatic safeguard is shown in figure 2.13. The lines to the two ports of the P.P.G. were connected by a pneumatically-operated two-way needle valve (Autoclave). The supply of nitrogen (at 4 bar) to the valve chamber was controlled by means of a 24 volt d.c., 3-way solenoid valve (ASCO). When the solenoid was energised, the pneumatic valve was in the closed position.

An electronic switching device was designed and constructed by the Electronics Workshop. It amplified the output from the four most central photocells and, through an electronic gate, operated a bi-stable switch when the output from each of the photocells fell to a very small value, i.e. when there was essentially no light beam on any of the photocells. The switch cut off the 24 volts d.c. supply to the solenoid, thus causing the pneumatic

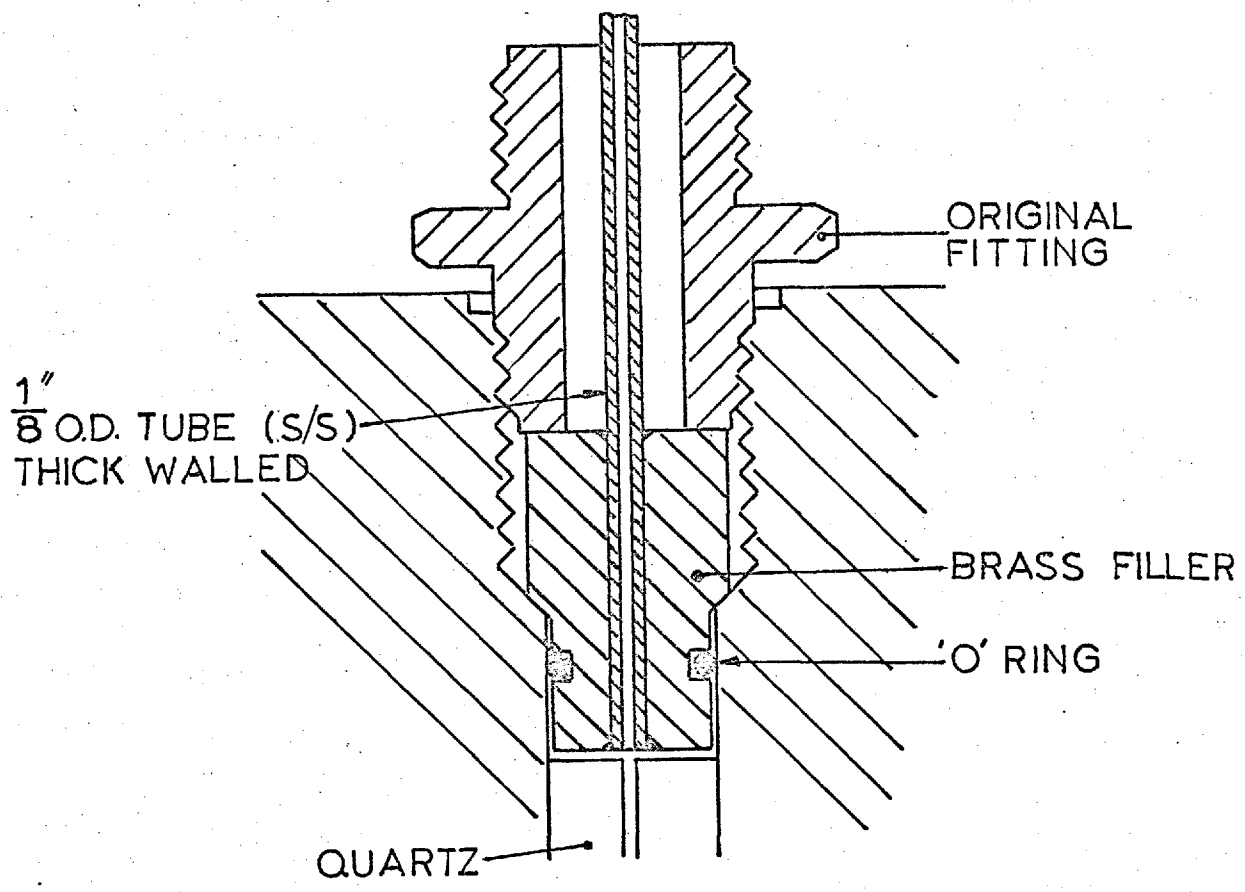

FIG 2·12 P.P.G. MODIFICATION TO ENTRANCE PORT

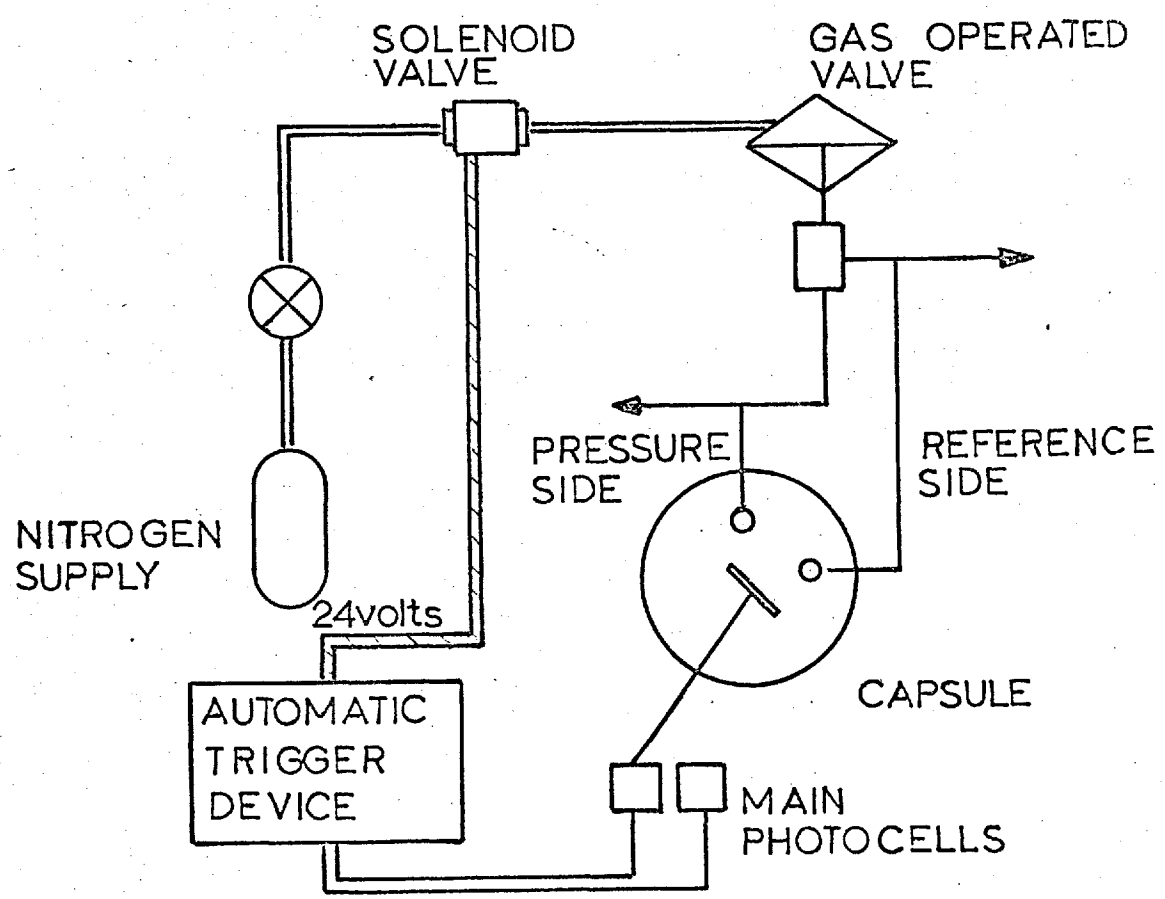

FIG. 2·13 P.P.G. AUTOMATIC SAFEGUARD

valve to open, connecting the pressure and reference ports of the gauge.

It was found that when pressure was slowly applied to the reference port the switching mechanism operated satisfactorily at a pressure differential of about 4 bars. This corresponded to the point where the light beam was cut off by the steel capsule at the edge of the sapphire window. When pressure was applied to the pressure port, however, it was found necessary to reduce the size of the window with black photographic paper in order to obtain a sufficiently low triggering point, 7 bar.

At first the electronic switch was occasionally triggered by spurious external electrical noise. This problem was solved by supplying both the P.P.G. and the electronic switching device from a different mains fuse box to that which supplied the rest of the laboratory.

(ii) The Effect of Pressure on the P.P.G. Null Position

After initial testing of the P.P.G. and adjustment of the light source to give a sharp, rectangular image on the photocells, the pressure and reference ports were connected and evacuated. It was found that the null position, 000.000, was stable to within .002 divisions, corresponding to about 2.10^{-4} bar, over a period of one week.

However, on filling both sides of the capsule to about 100 bar, it was observed that the null position had changed to about 999.050, corresponding to an apparent pressure differential of 0.1 bar. The magnitude of this null-shift was not expected, neither from the published specifications of the P.P.G. nor from the known behaviour of a low-pressure glass capsule (13). It was established that,

FIGURE 2.14

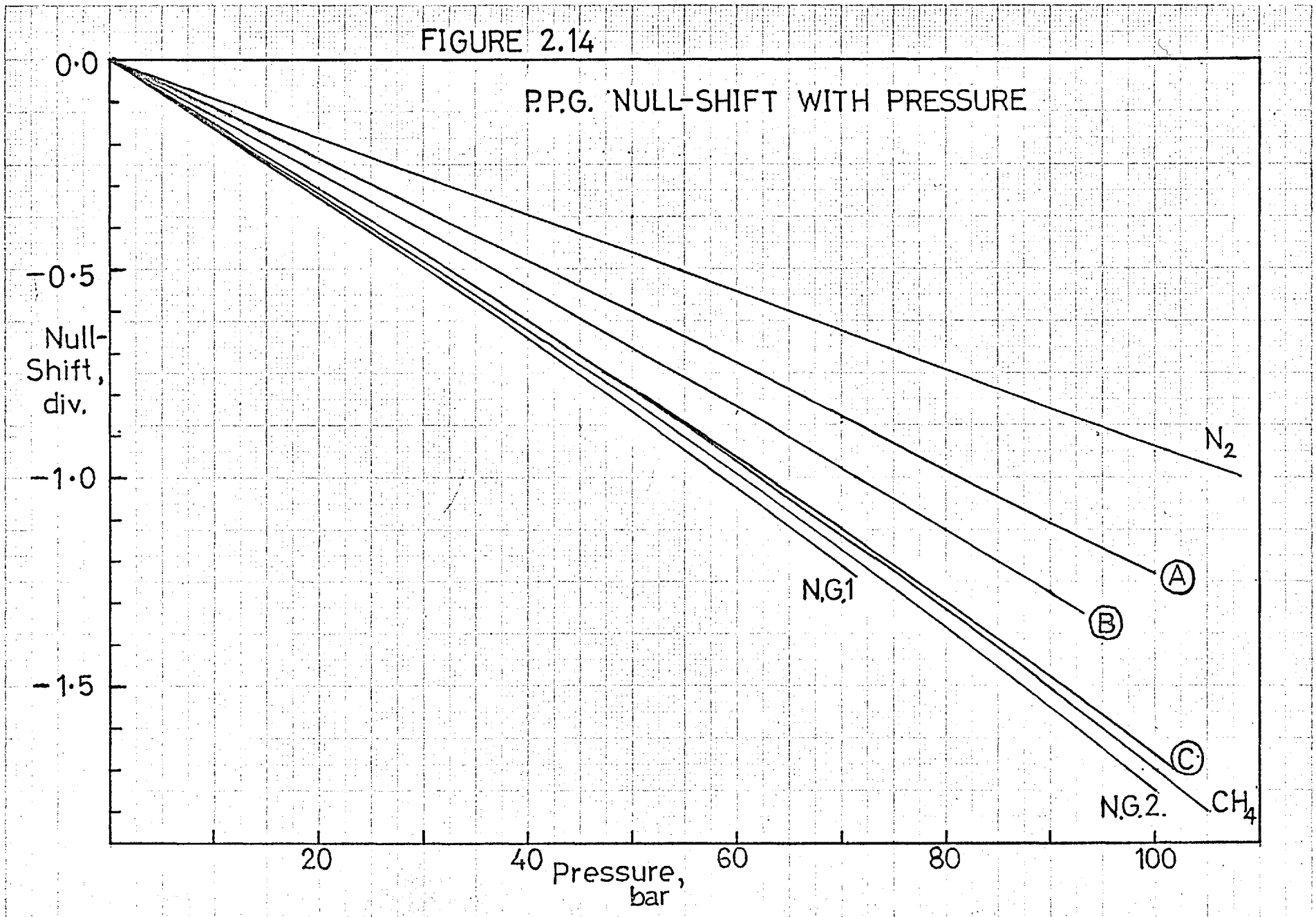
P.P.G. NULL-SHIFT WITH PRESSURE
0·0
−0·5
−1·0
−1·5
Null-Shift, div.
20
40
60
80
100
Pressure, bar
N2
A
B
C
N.G.1
N.G.2.
CH4

1) The shift was very nearly proportional to the total pressure.

2) At constant pressure, the shift was constant within .001 divisions over 24 hours: it was a real change in null position and not a hysteris effect.

3) The magnitude of the shift depended on the particular gas in the capsule, being larger for methane than for nitrogen.

The null-shifts for each of the gases studied were measured at intervals of about 3 bar up to 100 bar using the piston-gauges to measure the pressure. These calibrations are shown in Figure 2.14. Each was found to be reproducible to about .003 divisions, or 3.10^{-4} bar, at 100 bar. At the beginning of a new series of runs with a particular gas, the calibration was repeated.

The null-shifts for each gas were fitted to a polynomial in pressure, usually a quadratic, which was used in the main data treatment computer program to calculate the true null position, to the nearest .001 divisions, from the true experimental pressure. Before a pressure measurement the approximate null position was estimated, to the nearest .005 divisions, from the appropriate calibration curve and the approximate pressure as shown on a standard Bourdon gauge. The pressure difference between this set null position and the true null position was calculated using the gauge sensitivity as determined in section 2.6(e)(iii).

The characteristics of the null-shift with pressure suggested that this phenomenon was due to the variation with pressure of the refractive index of the gas in the reference side of the capsule. With reference to figure 2.15, consider

FIGURE 2.15.
REFRACTIVE INDEX EFFECT

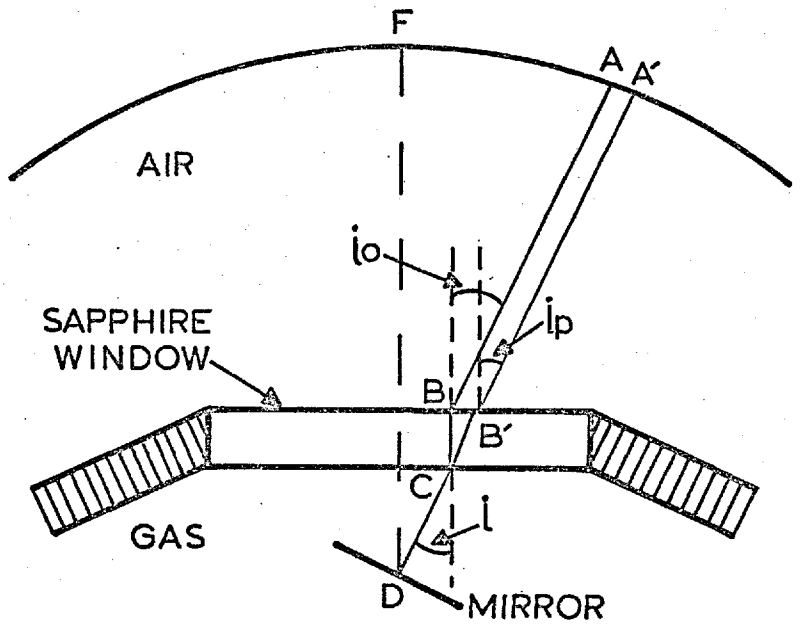

FIGURE 2.16.
P.P.G. SENSITIVITY

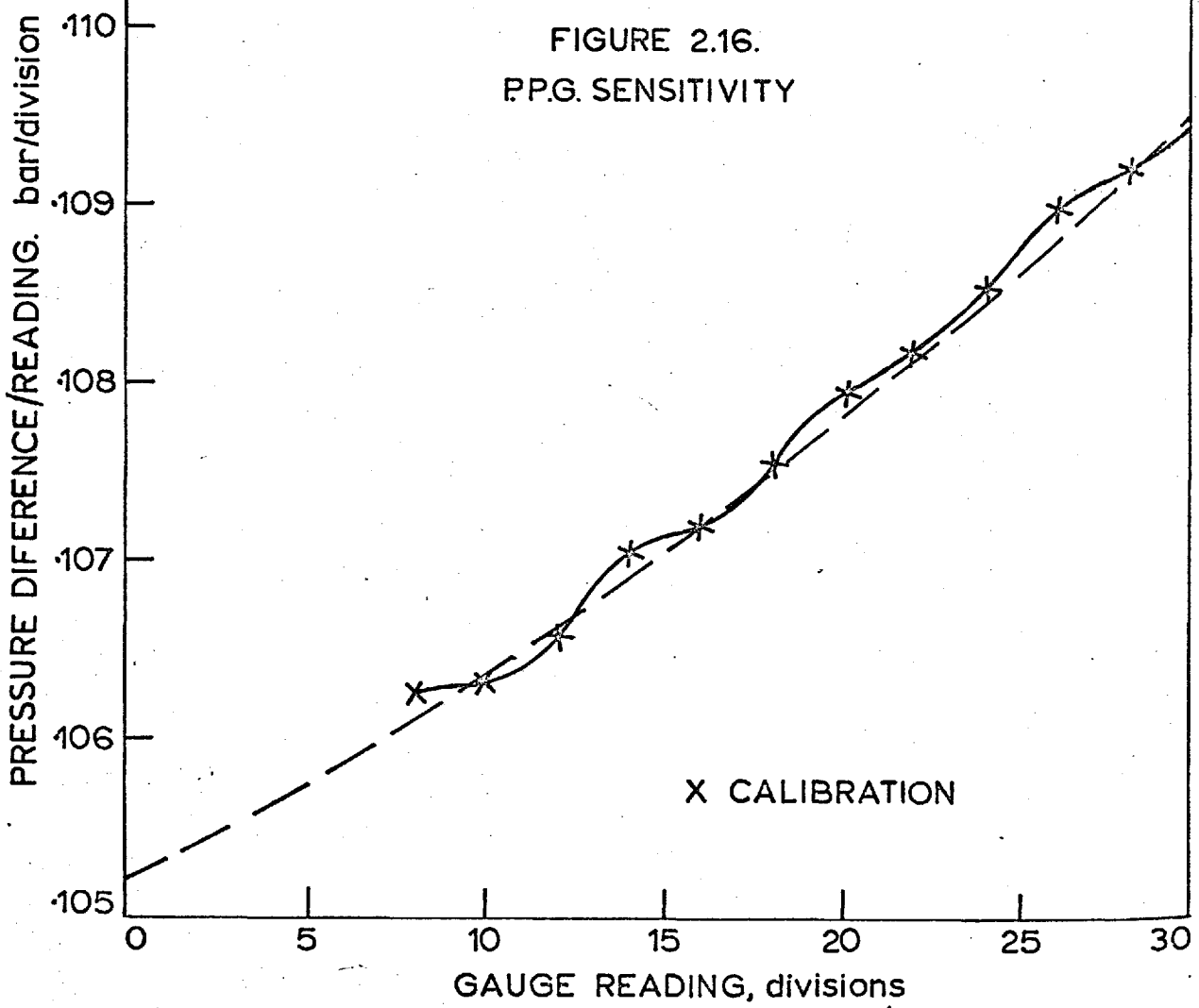

the relative positions of the mirror, sapphire window and light source. When both the spiral and its surroundings are under vacuum, the light path is ABCDCBA. If μ_a is the refractive index of the air outside the capsule then,

$$\mu_a \sin i_o = \sin i \qquad (2.6\text{-}22)$$

When there is the same pressure p in both sides of the gauge, it is assumed that the mirror remains at the same position (i.e. there are no strain effects on the spiral), and the light path is now A'B'CDCB'A'; if μ_p is the refractive index of the gas in the capsule at pressure p,

$$\mu_a \sin i_p = \mu_p \sin i \qquad (2.6\text{-}23)$$

$$\therefore \quad \sin i_p = \mu_p \sin i_o \qquad (2.6\text{-}24)$$

Now as the dimensions of the gauge are such that AB $\gg$ BD and AA' $\gg$ BB'

$$\sin i_p - \sin i_o \simeq \frac{\widehat{AA'}}{AB} \qquad (2.6\text{-}25)$$

$$\therefore \quad \widehat{AA'} = AB \sin i_o \, (\mu_p - 1) \qquad (2.6\text{-}26)$$

The null-shift, ΔR_p, is proportional to the angular deflection of the light beam from A, i.e. $\widehat{AA'}$

$$\therefore \quad \Delta R_p = \zeta (\mu_p - 1) \qquad (2.6\text{-}27)$$

where ζ is a constant depending solely on the dimensions of the gauge.

The refractive index of a gas at pressure p is given, to a good approximation, by the Lorenz-Lorentz equation,

$$\frac{\mu_p^2 - 1}{\mu_p^2 + 2} \cdot V = \psi \qquad (2.6\text{-}28)$$

where ψ is a constant, its value depending on the gas, and V is the molar volume,

$$V = \frac{RTZ}{p} \qquad (2.6\text{-}29)$$

For the gases under consideration and up to 100 bar, $\mu_p - 1$ is small and

$$\frac{\mu_p^2 - 1}{\mu_p^2 + 2} \cdot V = (\mu_p - 1) \cdot \frac{2}{3} V = \psi \qquad (2.6\text{-}30)$$

$$\therefore \quad (\mu_p - 1) \cdot \frac{Z}{p} = \frac{3\psi}{2RT} = \chi \qquad (2.6\text{-}31)$$

$$\therefore \quad \Delta R_p = \zeta \chi \frac{p}{Z} \qquad (2.6\text{-}32)$$

The variations of null-shift with pressure shown in figure 2.14 are certainly of a form consistent with equation (2.6-32). An approximate quantitative test can be performed: for example, when the gauge contains nitrogen at 1 atmosphere (at 45 °C).

$\mu_p - 1 = .000297$ and $Z \simeq 1$

$\therefore$ from (2.6-31),

$$\chi_{N_2} = .000297 \qquad (2.6\text{-}33)$$

At 100 atmospheres, $Z \simeq 1.01$,

$$\therefore \quad (\Delta R_p)_{N_2} \simeq \frac{\zeta .0297}{1.01} \simeq .0294\,\zeta \qquad (2.6\text{-}34)$$

For methane (at 1 atmosphere, $\mu_p - 1 = .000443$, $Z \simeq .998$, at 100 atmospheres $Z \simeq 0.90$) the corresponding null shift at 100 atmospheres is ,

$$(\Delta R_p)_{CH4} \simeq .0492\,\zeta \qquad (2.6\text{-}35)$$

$$\therefore \quad \frac{(\Delta R_p)_{CH_4}}{(\Delta R_p)_{N_2}} \simeq 1.64 \qquad (2.6\text{-}36)$$

It can be seen from figure 2.14 that at 100 atmospheres (101·3 bar) the appropriate ratio is actually equal to 1.75. This agreement is good considering the approximations inherent in the development of equation (2.6-32), and tends to show that the cause of the null-shift is indeed that suggested. Further evidence comes from the relative sizes of the null

shifts for the mixtures, which are consistent with the preceding treatment.

It can be seen that the magnitudes of these null-shifts were due to a design-fault in this capsule; at the null position the mirror was inclined at an angle to the flat sapphire window giving rise to a large angle of incidence at the window. This null-shift effect has been considered here in detail because it was one of the largest sources of error in pressure measurement.

(iii) Calibration of the P.P.G. Sensitivity

As the P.P.G. was to be used as a means of absolute pressure measurement during the calibration of the dead-space volumes (secton 2.8), it was calibrated against the gas piston-gauge in the range from 10 to 25 $lb.in^{-2}$ (.68 to 1.7 bar) at intervals of 1 $lb.in^{-2}$ (0.69 bar). The P.P.G. was nulled before each measurement with both ports open to the atmosphere; the reference port was left open to the atmosphere throughout each measurement.

Figure 2.16 shows the variation with gauge reading of the gauge sensitivity, i.e. pressure/gauge-reading. It can be seen that there was a definite periodic variation in sensitivity, the maxima recurring at intervals of 3.000 in the P.P.G. reading which corresponded to 1 ^{o} of turntable rotation or one turn of the worm gear. It was therefore thought to be due to eccentricity in the worm gear.

The gauge sensitivity at very low pressure differentials (less than .001 bar) was also required to correct for the difference between the set null position during a measurement and the true null position. This sensitivity was determined both for methane and for nitrogen by using the piston gauges

to measure small pressure changes about the null-position while the system was pressurized and under temperature control. It was found that the gauge sensitivity at the null position was equal to 0.105 bar/division with a standard deviation of .005 bar/division. This value agrees within experimental error with the extrapolation of figure 2.16 to zero reading.

It can be shown by a treatment similar to that describing the null-shift variation that the gauge sensitivity about the null position also depends on the refractive index of the gas in the pressure port; it also depends on the exact angular position of the turntable, owing to the worm gear eccentricity. As the maximum difference encountered between the 'set' and the 'true' null positions was only .010 divisions these effects on the pressure correction were negligible.

However, if the P.P.G. were to be used not as a nulling device, as in this study, but for the measurement of absolute pressure differences at high pressure then close attention would have to be paid to the aforementioned effects on gauge sensitivity and null position before high sensitivity could be attained.

It is believed that the ideal differential-pressure null indicator for use in a Burnett apparatus of this type, where the indicator can be maintained at room temperature, would be a Texas Instruments P.P.G. designed such that the mirror was parallel to the sapphire window at the null position, thus reducing the null-shift effect, and having a more sensitive spiral. Use of a more sensitive spiral would not only increase the gauge sensitivity but would also decrease the refractive-index effects: the pressure shift would be smaller for the same angular deflection.

(f) Errors in Pressure Measurement

There were three basic types of experimental error inherent in each series of pressure measurements which constitute a run,

Type 1: Systematic errors proportional to the pressure.

Type 2: Systematic errors independent of pressure.

Type 3: Random errors.

As the accuracy of the derived compressibility factors depends essentially on the accuracy of pressure ratios as opposed to that of absolute pressures, Type 1 errors are much less important than Type 2 and Type 3 errors of similar magnitude. Detailed investigation of the dependence of the derived results on the errors in pressure is given in Chapter 3.

Type 1 errors arise from the uncertainty in the calibrated effective area of the piston of the oil piston-gauge (2 parts in 10^5 max.) and of the gas piston-gauge (4 parts in 10^5 max.); others arise from uncertainties in the value of the acceleration due to gravity, in the buoyancy corrections, in the masses of the weights and in the null-shift calibration of the P.P.G., totalling in all about 2 parts in 10^5 max. Thus Type 1 errors have a total maximum of about 6 parts in 10^5, although the probable errors are much less than this.

The more important Type 2 and Type 3 errors will be discussed in more detail, as an estimate of their magnitude is necessary, or at least helpful, in the data treatment.

Random errors introduced by the piston-gauges were caused mainly by fluctuations in the control temperature, but these were small ($\pm$ 5 parts in 10^6 maximum). For the gas

piston-gauge there were the further random, Type 3, errors caused by uncertainties in the correct floating position of the piston ($\pm$ 2.10^{-4} bar max.). Others were caused by uncertainties in nulling the D.P.C. and by the D.P.C. null-shift ($\pm$ 3.10^{-4} bar max.); uncertainties in barometric reading ($\pm$ 3.10^{-4} bar max.); and errors in the P.P.G. null-shift calibrations ($\pm$ 2 part in 10^{5}).

Thus the total random errors were estimated as having a maximum of about $\pm$ 3.10^{-3} bar at 100 bar, decreasing to $\pm$ 8.10^{-4} bar at low pressure. The probable random errors were estimated as about $\pm$ 2.10^{-4} to 8.10^{-4} bar.

Systematic errors in pressure, Type 2, are difficult to estimate. The intrinsic error in the scale of the barometer gives rise to a maximum Type 2 error of 0.2 mm. (3.10^{-4} bar). Incorrect initial null-setting and zero-drift of the P.P.G. cause Type 2 errors, estimated as having a value of about 2.10^{-4} bar. Errors in the correction for the hydraulic head of oil gives rise to a small Type 2 error. An unknown systematic error must also arise from the extrapolation of the gas piston-gauge calibration to low pressure; it is probably only significant at pressures below about 3 bar. Total Type 2 errors in pressure measurement were therefore estimated as about 5.10^{-4} bar. These systematic errors which are not proportional to pressure are probably the most important: as will be shown in Chapter 3, their magnitude is not readily apparent from the actual experimental data.

2.7 Pressure and Density Gradients due to Gravity

The gravitational pressure difference between two points separated by a small vertical distance, δx, in a column of gas at temperature T is,

$$\delta P = g.d.\delta x \qquad (2.7\text{-}1)$$

$$\therefore \quad \delta P = g.\frac{P.M.}{RT.Z}\ \delta x \qquad (2.7\text{-}2)$$

Figure 2.17 shows the various heads of gas that were present in the apparatus. For computational purposes the reference level was taken to be that of the topmost thermocouple in the inlet-tubes.

A preliminary calculation shows the expected order of magnitude of these gravitational efects.

e.g. For methane at 218.8 K, 96.9 bar, $Z \simeq 0.46$, $M = 16$, we have from (2.7-2),

$$\frac{\delta P}{\delta x} \simeq 2.10^{-4} \text{ bar cm}^{-1} \qquad (2.7\text{-}3)$$

This value is certainly large enough to warrant correction of the measured pressure for gravitational effects. However it is sufficiently small that, to a very good approximation, P and Z in equation (2.7-2) could be regarded as constant,

$$\text{i.e.} \quad \Delta P = \frac{g.PM}{RT.Z} \div x \qquad (2.7\text{-}4)$$

Equation (2.7-4) was used to calculate the pressure gradients for all of the heights shown in figure 2.17 except along h_2, h_5 and h_7, where there were temperature gradients.

Assuming a linear temperature gradient between one point (T_1, Z_1) and another (T_2, Z_2) separated by a distance h, then at height x above T_1,

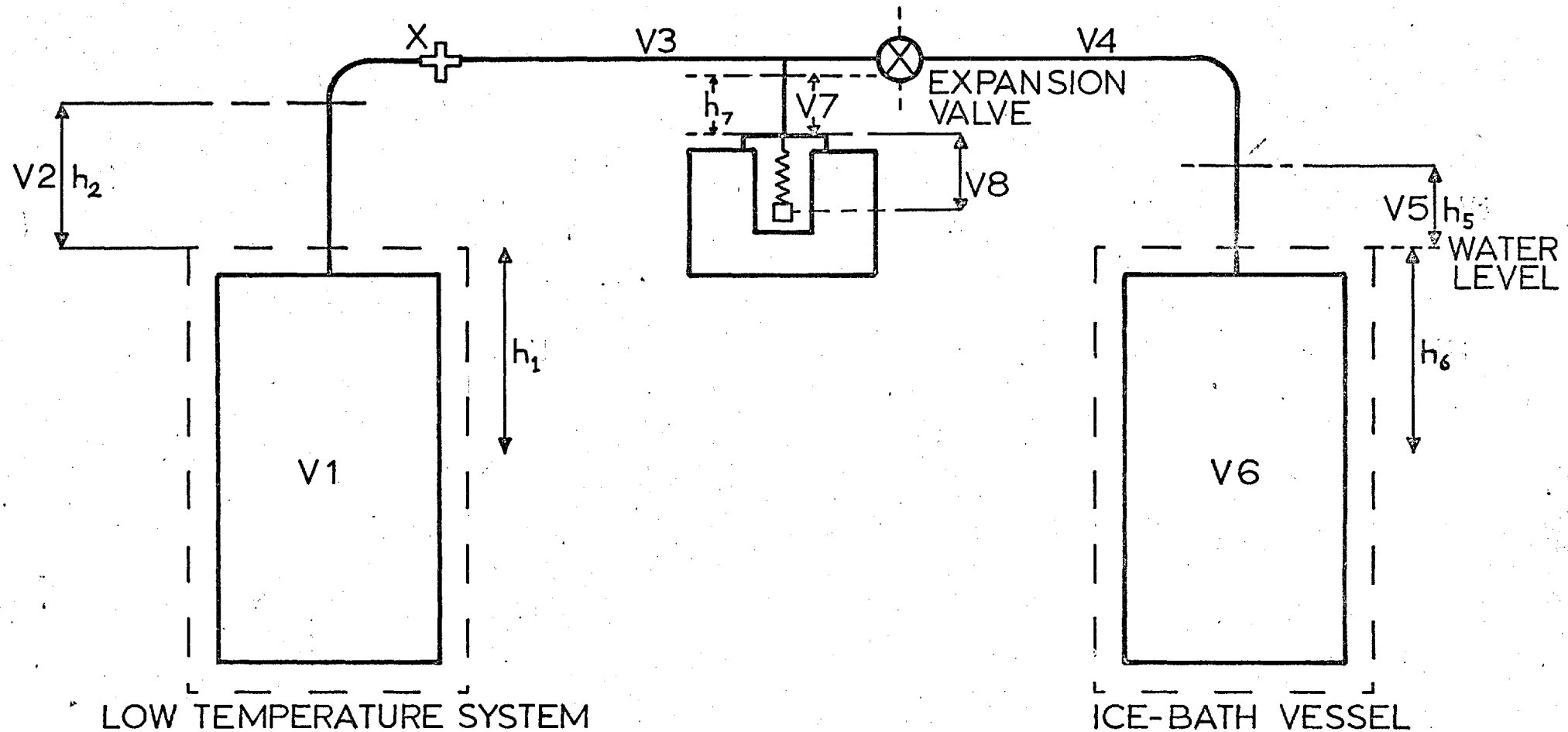

FIG. 2·17. APPARATUS VOLUMES AND PRESSURE-HEADS

$$T = T_1 + x/h\ (T_2 - T_1) \qquad (2.7\text{-}5)$$

$$Z = Z_1 + x/h\ (Z_2 - Z_1) \qquad (2.7\text{-}6)$$

$$\therefore\ \delta P = \frac{gPM}{R}\ \frac{\delta x}{(T_1 + x/h\ (T_2 - T_1))(Z_1 + \frac{x}{h}\ (Z_2 - Z_1))} \qquad (2.7\text{-}7)$$

$$\int_P^{P+\Delta P} \frac{\delta P}{P} = \frac{gM}{R} \int_0^h \frac{\delta x}{(T_1 + x/h\ (T_2 - T_1))(Z_1 + x/h(Z_2 - Z_1))} \qquad (2.7\text{-}8)$$

$$\therefore\ \ln\left(\frac{1 + P + \Delta P}{1 + P}\right) \simeq \frac{\Delta P}{P} = \frac{gMh}{R}\ \frac{\ln\left(\frac{T_1 Z_2}{Z_1 T_2}\right)}{(T_1 Z_2 - Z_1 T_2)} \qquad (2.7\text{-}9)$$

Equation (2.7-9) was used to calculated the pressure gradient along h_5 and h_7, and between each pair of thermocouples down the inlet-tubes.

It is to be noted that corrections for gravitational effects were not applied to the P.P.G. null as there was the same pressure gradient down both the reference and pressure sides and hence the null position was unaffected.

It was believed that errors introduced by the use of equation (2.7-9) were negligible as the total corrections were small and all temperature gradients were nearly linear. When $|T_1 - T_2| < 1\ ^{o}C$, equation (2.7-4) was used.

2.8 Calibration of Volumes

For the purpose of calculating the quantity of gas in the inner volumes of the two vessels and their interconnecting tubing, they were considered as divided into eight sections as shown in figure 2.17.

The volume of the pressure vessel, V1, included the inlet tubing up to the top of the radiation shield. The volume of the ice-bath vessel, V6, included the tubing up to the level of water in the ice-bath.

As the ratio V1/V6 was determined with accuracy in the treatment of the Burnett data, both V1 and V6 were estimated from the measured dimensions of the vessels and the values used as first approximations in the computer program,

$$V1 = 360.9 \text{ cc at } 0\ ^{\circ}C \qquad (2.8\text{-}1)$$

$$V6 = 281.1 \text{ cc at } 0\ ^{\circ}C \qquad (2.8\text{-}2)$$

All the other sections constituted dead-space volume. The vessels were connected in such a way as to minimise as far as possible the length of the interconnecting, small-bore tubing. The Aminco-type fittings into the valves required coned and threaded ¼" o.d. tubing. Short lengths of ¼" o.d., 0.070" i.d. stainless-steel tube were employed containing lengths of 0.063" o.d. steel rod to reduce their internal volume and that of the valves. Apart from the 0.063" o.d. inlet tubes, all other tubing consisted of $\frac{1}{8}$" o.d., 0.027" i.d. stainless-steel tube. 'Swagelok' couplings were used throughout, containing steel rod to reduce their internal volume where necessary.

The volume per unit length of the inlet tubes was determined from the weight of mercury required to fill a measured length,

$$\text{Volume/cm} = 0.00870 \text{ cc.} \qquad (2.8\text{-}3)$$

The volumes of the other dead-spaces were calibrated gas volumetrically using a small gas burette in conjunction with the P.P.G. as a pressure measuring instrument. First of all the gas burette, which had been calibrated previously by filling with mercury, was connected directly into the pressure port of the P.P.G. After nulling the P.P.G. with both sides open to the atmosphere the pneumatic safety valve was closed, and the air expanded from the P.P.G. into the burette. The pressures before and after the expansion were obtained by using the P.P.G. readings in conjunction with the appropriate gauge sensitity shown in figure 2.16. Hence the internal volume, V8, of the P.P.G. could be calculated.

The other dead-space volumes were calibrated in a similar manner, the gas burette being connected into the tubing at point X.

The final results were,

V3 = 1.972 cc (metering-valve fully open)

V4 = 0.882 cc (with expansion valve shut)

V5 = 0.026 cc

V7 = 0.107 cc

V8 = 0.592 cc

The estimated maximum errors were

For V3, $\pm$ 0.015 cc

For V4 + V5, $\pm$ 0.015 cc

For V7 + V8, $\pm$ 0.008 cc.

2.9 Pressure distortion of the vessels

It can be shown (14) that the pressure distortion of an infinitely-long thick-walled cylinder, in which the walls are not constrained by the ends in a radial direction, is given by,

$$\frac{\delta V}{V} = \left(\frac{1}{E(r_o^2 - r_i^2)}\right) \left(P_i \left(3(1-2\nu)\, r_i^2 + 2\,(1+\nu)\, r_o^2\right) - (5 - 4\nu)\, r_o^2\, P_o\right) \qquad (2.9\text{-}1)$$

where δV = increase in volume

V = volume at zero pressure

r_i = internal radius

r_o = external radius

P_i = internal pressure

P_o = external pressure

ν = Poisson's ratio,

E = Young's modulus of elasticity

For a real cylindrical pressure vessel of finite length, equation (2.9-1) is an approximation, as there are end-effects; the walls tend to 'bulge' outwards when the internal pressure is greater than the external pressure and the ends are constrained.

When $P_i = P_o$, equation (2.9-1) reduces to

$$\frac{\delta V}{V} = \frac{-3(1-2\nu)}{E} \cdot P_i = - K P_i \qquad (2.9\text{-}2)$$

where K is the bulk compressibility of the material of the vessel. Equation (2.9-2) is exact and independent of the shape of the pressure vessel; thus the pressure compensation of both vessels of the apparatus not only reduces the pressure distortion but also enables it to be calculated with accuracy. Only about 1% of the surface area of each inner vessel, where it was supported, was not pressure compensated.

For EN58J stainless-steel (15),

$E = 1954$ kbar at 20 °C

$\nu = 0.255$ at 20 °C

$$\therefore \quad \frac{\delta V}{V} = - 0.7626 \cdot 10^{-6} P \quad (P \text{ in bar}) \qquad (2.9\text{-}3)$$

The effect of temperature on this distortion is small.

For the inlet-tubes and interconnecting tubing in the other dead-spaces, the external pressure is effectively zero, and equation (2.9-1) reduces to

$$\frac{\delta V}{V} = \left(\frac{1}{E(r_o^2 - r_i^2)}\right) \left(3(1-2\nu) r_i^2 + 2(1+\nu) r_o^2\right) P_i \qquad (2.9\text{-}4)$$

For the inlet-tubes, $\frac{\delta V}{V} = 1.51 \cdot 10^{-6} P$ (2.9-5)

For the narrow-bore .0625" o.d. tubing,

$$\frac{\delta V}{V} = 1.38 \cdot 10^{-6} P . \qquad (2.9\text{-}6)$$

Equation (2.9-6) was used to calculate the pressure distortion of all other dead-spaces, which included the interiors of valves, 'Swagelok' couplings, etc.; the errors in this approximation are negligible compared with the uncertainty in the dead-space compressibility factors.

2.10 Preparation of Gas Mixtures and Gas Analyses

The methane used was Matheson ultra-high-purity (99.99%). The analysis provided by the suppliers is shown in Table 2.4. An analysis performed on a mass spectrometer (MAT Varian, GD150) confirmed that the total impurities were not more than 100 p.p.m. Nitrogen was supplied by Air Products (99.999%); the quoted maximum limits of impurities are shown in Table 2.4. Mass spectrometric analysis showed that the impurities totalled less than 20 p.p.m. Both methane and nitrogen were used without further purification.

The three synthetic gas mixtures, A, B, and C were prepared by the Gas Quality Division of the Gas Council at Watson House. The constituent gases were mixed at about 2 atmospheres pressure in a 500 m^3 balloon for 24 hours before being compressed into cylinders. This technique avoided the problem of incomplete mixing that accompanies the mixing of gases at high pressures. The mass spectrometric analyses, together with the estimated limits of error, are presented in Table 2.4.

The composition of Mixture C agrees well with the results of an analysis by gas chromatography (Watson House); the mass-spectrometric analysis was used in all subsequent calculations.

Of the two natural gases studied, Mixture 1 was a Phillips North Sea gas collected at a pressure of 76 bar (1100 $lb.in^{-2}$), and Mixture 2 was a sample of natural gas originating from the No. 4 feeder main and compressed by Air Products Ltd. to full cylinder pressure. For complex hydrocarbon mixtures, analysis by mass-spectrometry is inaccurate and so both natural gases were analysed by gas-

TABLE 2.4 Analyses of Gases

	Methane (Matheson) Mol.%	Nitrogen (Air Products) Mol.%	Mixture A (Mass Spec.) Mol.%	Mixture B (Mass Spec.) Mol.%	Mixture C (Mass Spec.) Mol.%	Natural Gas 1 (Gas Chrom.) Vol.%	Natural Gas 2 (Gas Chrom.) Vol.%
Methane	>99.99		48.4 ± .1	71.9 ± .1	76.8 ± .1	92.35 ± .5	93.09 ± .5
Nitrogen	.0016	>99.995	51.6	28.1	15.6 ± .1	2.3 ± .05	2.4 ± .05
Oxygen	<.0005	<.0005			0.4	–	0.24
Ethane	.0038				7.2 ± .1	3.7 ± .05	3.1 ± .05
Propane	<.0005					0.90 ± .04	0.63 ± .04
i-Butane						0.18	0.13
n-Butane						0.24	0.14
Pentanes						0.13	0.08
Hexanes						0.06	0.04
Heptanes						0.01	0.02
Octanes						0.01	0.01
Nonanes +						0.01	0.01
Benzene						0.01	0.03
Helium						0.06	0.04
Carbon Dioxide	<.001	<.0001				0.04	0.04
Others		<.0003	<.01	<.01		<.01	<.01

chromatography in the Analytical Research Group at the Gas Council's London Research Station. The results of the analyses, together with estimated maximum limits of error, are shown in Table 2.4.

2.11 Experimental Procedure

On the day preceding the start of a series of expansions the following operations were carried out

(1) The ice bath was prepared in order to ensure that the ice bath vessel was at the temperature of the bath at the start of the experiment the following day.

(2) Both vessels, the interconnecting tubing and the P.P.G. were fully evacuated.

(3) The outer jacket was surrounded by refrigerant and the temperature of the pressure vessel controlled at a few ^{o}C below the required experimental temperature. Then on subsequently filling the pressure vessel with gas the temperature would rise to about the required value.

(4) The toluene regulator was adjusted to ensure that the cabinet temperature was controlled at a few deg. C above that of the surroundings.

At the start of the run the ice bath was re-made with freshly crushed ice and distilled water, and the refrigerant around the outer jacket was replaced. The vacuums in the outer jacket and the vessels were checked. With the safety valve connecting 'pressure' and 'reference' ports open, the P.P.G. was nulled at 000,000 and the null position tested for stability. The whole system was then flushed through twice with the gas under investigation and re-evacuated. Both expansion valves were then shut and

while the evacuation of the ice bath vessel was continued, both volumes of the pressure vessel were slowly filled with gas to the desired pressure. Meanwhile the null-shift with pressure of the P.P.G. was either fully calibrated or measured at one or two pressures as a check on the previous calibration.

After filling, the temperature of the pressure vessel was adjusted until it was close to the required control temperature. When rapid cooling was necessary a small quantity of helium, as a heat-transfer medium, was admitted to the outer jacket for a short period. As it usually led to a large temperature drop along the inlet tubes, this method of cooling was not used when the pressure vessel held a gas mixture at low temperature in order to avoid any condensation of liquid in the tubes and hence separation of the mixture. As the required experimental temperature was approached the controllers were set to 'automatic' and the system allowed to come to equilibrium. When a steady temperature was attained, the null position of the P.P.G. was recorded and this value subsequently used as the null-position for the first pressure measurement. The safety-valve was then closed, isolating the volume of gas under study.

Before the first pressure measurement the oil piston-gauge carrier was loaded with sufficient weights to balance the piston at a pressure just above the first experimental pressure. The D.P.C. was then nulled (as described in section 2.6(b)) and its lower chamber and the piston-gauge pressurized with oil, using the hand-pump, until the piston was floating. The upper chamber of the D.P.C. was flushed

through with the gas under study to remove air and then filled to the first experimental pressure. The valve connecting it to the P.P.G. and the outer volume of the pressure vessel was then opened. By means of small adjustments to the compensating gas pressure and the weights on the piston-gauge, the piston was made to float at the correct height, with the D.P.C. at null at full sensitivity and the P.P.G. at the correct null position.

The following were then recorded: the A.C. bridge reading and the temperature of the standard resistor; the barometer height and temperature; the temperatures of the cabinet and piston as measured with mercury-in-glass thermometers; the E.M.F.'s of the inlet-tube thermocouples; the weights on the piston-gauge carrier.

Measurements were repeated at intervals of about fifteen minutes until full temperature equilibrium was attained and the pressure was constant.

Before an expansion, the ice-bath vessel was isolated from the vacuum system. Both fine metering valves were closed right down and both expansion valves opened. The fine-metering valves were slowly opened so that gas flowed into the two volumes of the ice-bath vessel and the P.P.G. reading stayed close to the null position.

During an expansion the temperature of the pressure vessel fell owing to the Joule effect. Therefore during and after an expansion the supply to the pressure vessel heaters was increased manually to bring the temperature back to the control point. Temperature equilibrium was regained after a length of time varying from 1 to 2½ hours,

depending on the particular gas under study, its temperature and pressure. When a gas mixture at a low temperature was expanded, the pressure vessel was heated before an expansion to prevent possible cooling below the dew point and hence condensation of liquid.

When the A.C. bridge reading was steady once again, the new pressure was measured. The expansion valve was left about ½ turn open until just before the measurement, when it was closed very slowly to prevent disproportionation of gas between the two vessels.

After the new pressure measurement, the inner volume of the ice bath vessel was vented and then evacuated for about one hour. Expansions were continued until a pressure of 2.5 bar or less was attained. Pressures below 25 bar were measured by means of the gas-operated piston-gauge (as described in Section 2.6(c)), which was vented between measurements to prevent undue loss of its lubricating oil.

Each experiment extended over a period of from 2 to 3 days. During this time the ice bath was re-made at ½ day intervals and the refrigerating CO_2/methanol mixture was replaced at intervals of about 1 day.

After the last pressure measurement the safety-valve was opened and the P.P.G. null position measured; this enabled the shift in P.P.G. null throughout the run to be evaluated.

CHAPTER THREE

TREATMENT OF EXPERIMENTAL DATA

3.1 Introduction

In order to simplify the description of methods of data treatment the case will first be considered of an 'isothermal' Burnett apparatus in which both vessels are at the same temperature, T, and in which it is assumed that the cell volumes are independent of pressure. The treatment for a 'non-isothermal' Burnett apparatus will be deferred until section 3.2(b).

Reiterating the two basic equations pertaining to the isothermal Burnett apparatus, as given in section 1.4,

$$\frac{P_{j-1}}{P_j} = N \cdot \frac{Z_{j-1}}{Z_j} \qquad (3.1\text{-}1)$$

$$P_j N^j = \left(\frac{P_o}{Z_o}\right) \cdot Z_j \qquad (3.1\text{-}2)$$

where $N = \dfrac{V_A + V_B}{V_A}$, the apparatus constant

(P_o/Z_o) is the run constant.

There are essentially two types of methods of data reduction to obtain Z_o .... Z_n from the pressure sequence P_o .... P_n; the graphical and the analytical methods.

In the original graphical method proposed by Burnett (4), N is obtained from an extrapolation of a plot of P_{j-1}/P_j against P_j. As $Z \rightarrow 1$ as $P \rightarrow 0$, it may be seen from (3.1-1) that $P_{j-1}/P_j \rightarrow N$ at zero pressure.

A second graphical plot of $P_j N^j$ is then extrapolated to zero pressure to give (P_o/Z_o), as may be seen from (3.1-2). By back substitution in (3.1-2) Z_j may be found.

As N appears to the jth. power in (3.1-2) small errors in N accumulate and lead to large errors in the compressibility factors. Unless the gas under study is near-ideal the first extrapolation does not give the required precision in N. An improvement due to Canfield (16) involves the adjustment of N, within the error of the first extrapolation, to give final values of Z_j such that Z_j has the correct limiting behaviour at low density, i.e. $(Z_{j-1})/\rho_j$ is linear with ρ_j at low density.

An alternative is to obtain N from a calibration run with helium, which is very nearly ideal at normal temperatures and for which P_{j-1}/P_j is essentially linear with pressure, enabling the extrapolation to be performed with accuracy. However, apart from the inconvenience of a separate calibration run, there is the possibility of real changes in N between runs, particularly if the apparatus is subjected to temperature cycling (13).

Before describing the analytical method of data reduction it must be mentioned why these methods have in general surpassed the graphical method. The main reason is that the graphical method requires very precise measurements at low pressure, i.e. in the region where the second graphical plot is nearly linear. In a Burnett run the most precise values of P_{j-1}/P_j occur usually in the mid-range of the data: these points are hardly utilized at all in the second graphical plot. With an analytical method

it is not necessary to have any low pressure points to obtain a result. Another disadvantage is that it is impossible to treat runs at the same temperature simultaneously with the graphical method. In fact the only major advantage of the graphical method is that no equation of state need be assumed, unlike all analytical methods.

3.2 Analytical Methods of Data Reduction

In a non-graphical method of data reduction it must be assumed that the data can be adequately represented by an equation of state,

$$Z_j = Z(\rho_j, a_1, a_2 \cdots a_k \cdots a_m)$$
$$\text{or} \quad Z_j = Z(P_j, a_1, a_2 \cdots a_k \cdots a_m) \qquad (3.2\text{-}1)$$

The m parameters of the equation of state together with N and sometimes P_o/Z_o are then determined by means of a non-linear regression analysis that is usually based on the principle of least-squares.

The principle requires that the sum of the weighted squares of the residuals, called the objective function, S, shall be a minimum with respect to the M least squares parameters,

$$S = \sum_{j=1}^{n} w_j R_j^2 \qquad (3.2\text{-}1)$$

where w_j is a weighting factor equal to the reciprocal of the expected variance in the jth. residual, and n is the number of data points.

Each residual is the difference between an observed

dependent variable, Y_j, and its adjusted value, Y_j'.

$$R_j = Y_j - Y_j' \qquad (3.2\text{-}3)$$

The adjusted values, Y_j', are related to the least-squares parameters, a_k, by the equations of condition,

$$F_i(Y_j', X_j, a_1, a_2 \cdots a_k \cdots a_m) = 0 \qquad (3.2\text{-}4)$$

where X_j represents one or more independent variables. This is the general formulation of the least-squares problem as described by Deming (17). It requires that experimental errors occur only in the observed dependent variables, Y_j, and that these errors are randomly distributed.

The particular objective function and equations of condition for application to Burnett data are partly a matter of choice. Weir et al (18), Hall and Canfield (19), and Barieau and Dalton (20) took as their objective function,

$$S = \sum_{j=1}^{n} \omega_j \, (P_j - P_j')^2 \qquad (3.2\text{-}5)$$

The adjusted pressures are related by the equations of condition, from (3.1-2),

$$P_j' N^j = \left(\frac{P_o}{Z_o}\right) Z_j \qquad (3.2\text{-}6)$$

and

$$Z_j = \frac{P_j'}{RT\rho_j'} = Z(\rho_j', a_1, a_2 \cdots a_k \cdots a_m) \qquad (3.2\text{-}7)$$

P_j' is determined by an iterative solution of equations (3.2-6) and (3.2-7). The M least-squares parameters are a_1, $a_2 \cdots a_k \cdots a_m$, N, and P_o/Z_o. This formulation of the

objective function is termed here 'Method B'.

Method B is based on the assumption that errors occur only in the observed pressures and that they are random. However, there are normally present systematic errors in the observed pressures and errors in other variables, such as the temperature and the corrections to N for the effect of pressure. In the 'non-isothermal' Burnett apparatus errors in other variables are also introduced. Because of the presence of these additional errors, mostly non-random, other forms of the objective function were considered that might offer practical advantages over (3.2-5). One that was suggested from the form of equation (3.1-1) is

$$S = \sum_{j=1}^{n} \omega_j \left(\frac{P_{j-1}}{P_j} - N. \frac{Z_{j-1}}{Z_j}\right)^2 \qquad (3.2\text{-}8)$$

where it is emphasised that the pressures, P_j, are the experimental values and not adjusted ones. The equation of condition is the equation of state,

$$Z_j = \frac{P_j}{RT\rho_j} = Z(\rho_j, a_1 \cdots a_k \cdots a_m) \qquad (3.2\text{-}9)$$

The least-squares parameters are $a_1 \cdots a_k \cdots a_m$, and N. This formulation of the objective function is termed 'Method A'.

An objective function of this type has been criticized by Barieau and Dalton (21) on the grounds that it involves the sum of squares of a function of pressure rather than a true pressure residual, and because it introduces correlation between the residuals. These objections are based on the erroneous assumption that all systematic errors are absent.

Method A has two possible advantages. Firstly, as it involves the ratio of experimental pressure, P_{j-1}/P_j, any systematic error proportional to the pressure will tend to cancel out. Secondly, a saving in computational time results through the elimination of the need for the iterative solution of (3.2-6) to find adjusted pressures. This is especially so in the case of the 'non-isothermal' Burnett apparatus.

Method A was compared with Method B (see section 3.4(b)) and, for the reasons given in that section, Method A was preferred and was adopted for use in the treatment of the experimental data of this work. The non-linear least-squares procedure is described in section 3.2(a) and the extension of the method to the non-isothermal Burnett apparatus and the resultant computer program are described in sections 3.2(b) and 3.2(c).

It can be seen that, by eliminating N between the expressions for successive expansions, equation (3.1-1),

$$\frac{P_{j-1} \cdot P_{j+1}}{P_j^2} = \frac{Z_{j-1} \cdot Z_{j+1}}{Z_j^2} \qquad (3.2\text{-}10)$$

This suggests a further form of the objective function,

$$S = \sum_{j=1}^{n-1} w_j \left(\frac{P_{j-1} \cdot P_{j+1}}{P_j^2} - \frac{Z_{j-1} \cdot Z_{j+1}}{Z_j^2} \right)^2 \qquad (3.2\text{-}11)$$

N is now eliminated as a least-squares parameter at the expense of one data point. A few preliminary tests using this objective function showed that if offered no advantages over Method A; the results were very similar.

All analytical methods of data treatment suffer from one disadvantage; no matter what form of objective function or least-squares procedure is employed, a form of the equation of state must be assumed. Ideally the equation must be capable of representing the experimental compressibility factors with an accuracy greater than that inherent in the basic pressure measurements. At low or moderate pressures the equation chosen is usually the Leiden expansion,

$$Z = 1 + a_1\rho + a_2\rho^2 + \ldots a_k\rho^k \ldots + a_m\rho^m \qquad (3.2\text{-}12)$$

The coefficients of this truncated polynomial are not identical to the corresponding virial coefficients, B, C, etc., which are coefficients in an infinite series. The value of m that gives the 'best-fit', in a least-squares sense, to the data does not necessarily provide the best estimates of the second and third virial coefficients. Also, a least-squares fit to <u>all</u> the data points in a Burnett run will not necessarily provide the best estimates of <u>all</u> the compressibility factors. The problems of obtaining accurate estimates of the second and third virial coefficients and the compressibility factors will be discussed in detail in sections 3.3 and 3.4.

(a) <u>The non-linear least-squares procedure for Method A.</u>

First trial values are assigned to the least-squares parameters $a_1 \ldots a_m$, which are the coefficients in the model equation of state,

$$P_j/RT\rho_j = Z_j = 1 + a_1\rho_j + a_2\rho_j^2 + \ldots a_k\rho_j^k \ldots + a_m\rho_j^m \qquad (3.2\text{-}13)$$

Equation (3.2-13) was solved by an iterative procedure. The Mth. least-squares parameter (M = m+1) was taken as V_A, the value of V_B being calculated from the measured dimensions of the vessel. This is equivalent to taking $(V_A + V_B)/V_A$, or N, as the Mth. parameter.

The objective function, S, is given by

$$S = \sum_{j=1}^{n} w_j \, R_j^2 \qquad (3.2\text{-}14)$$

In the general formulation of Method A the residuals are functions of the observed dependent and independent variables and the least-squares parameters,

$$R_j = f(Y_j, X_j, a_1, a_2 \ldots a_m) \qquad (3.2\text{-}15)$$

For the isothermal Burnett apparatus,

$$R_j = \frac{P_{j-1}}{P_j} - N \cdot \frac{Z_{j-1}}{Z_j} \qquad (3.2\text{-}16)$$

For the non-isothermal Burnett apparatus R_j is more complex, as described in section 3.2(b).

S is to be minimized with respect to each of the parameters,

$$\frac{\partial S}{\partial a_k} = 0 \quad \text{for } k = 1, 2 \ldots M. \qquad (3.2\text{-}17)$$

$\therefore$ from (3.2-14)

$$\sum_{j=1}^{n} w_j \left(\frac{\partial R_j}{\partial a_k}\right) \cdot R_j = 0 \quad \text{for } k = 1, 2 \ldots M \qquad (3.2\text{-}18)$$

This set of M equations are known as the normal equations and are non-linear in the parameters: they must

be linearized before a solution can be obtained.

Assuming that approximate values of a_k' exist such that

$$a_k' = a_k + \Delta a_k \quad \text{for } k = 1 \ldots M \tag{3.2-19}$$

Rj may be expanded as a Taylor series about its value when S is a minimum,

$$R_j'(a_1', a_2' \ldots a_m') = R_j(a_1, a_2 \ldots a_m) + \Delta a_1 \cdot \frac{\partial R_j}{\partial a_1} + \Delta a_2 \cdot \frac{\partial R_j}{\partial a_2} + \ldots \Delta a_m \cdot \frac{\partial R_j}{\partial a_m} + \ldots \tag{3.2-20}$$

This procedure is known as the Gauss-Newton method of linearization. Terms higher than the second are neglected.

It follows from equation (3.2-18),

$$\Delta a_1 \sum_{j=1}^{n} \omega_j \left(\frac{\partial R_j}{\partial a_k}\right)\left(\frac{\partial R_j}{\partial a_1}\right) + \Delta a_2 \sum_{j=1}^{n} \omega_j \left(\frac{\partial R_j}{\partial a_k}\right)\left(\frac{\partial R_j}{\partial a_2}\right) \ldots + \Delta a_M \sum_{j=1}^{n} \omega_j \left(\frac{\partial R_j}{\partial a_k}\right)\left(\frac{\partial R_j}{\partial a_M}\right)$$

$$= \sum_{j=1}^{n} \omega_j \left(\frac{\partial R_j}{\partial a_k}\right) \cdot R_j'(a_1', a_2' \ldots a_M') \quad \text{for } k = 1, 2 \ldots M \tag{3.2-21}$$

These are the linearized normal equations. The residuals, R_j', are evaluated from the first trial values of the parameters, a_k'. The derivatives $\left(\frac{\partial R_j'}{\partial a_k'}\right)$ are calculated and used as approximations to $\left(\frac{\partial R_j}{\partial a_k}\right)$ in the equations. (At the convergence point, i.e. when $\Delta a_k = 0$, this approximation is exact).

In matrix notation, equations (3.2-21) are

$$\underline{X}\ \underline{\Delta a} = \underline{Y} \tag{3.2-22}$$

where $\underline{X}$ is a M by M matrix and $\underline{Y}$ and $\underline{\Delta a}$ are column matrices.

The solution to (3.2-22) is

$$\underline{\Delta}a = \underline{X}^{-1}\,\underline{Y} \qquad (3.2\text{-}23)$$

where $\underline{X}^{-1}$ is the inverse of the symmetrical matrix $\underline{X}$.

After solution of equation (3.2-23) the new approximation to a_k is given by,

$$a_k = a_k' - \Delta a_k \qquad (3.2\text{-}24)$$

These new values of a_k are used in the recalculation of R_j' and the solution of the normal equations, the iterations being continued until all the Δa_k have converged to very small values.

The variances and covariances of the parameters are given, approximately, by

$$\sigma_{k,l}^2 = \sigma^2 \cdot x_{k,l} \qquad (3.2\text{-}25)$$

where $x_{k,l}$ is the element of the kth. row and lth. column of the inverse matrix, $\underline{X}^{-1}$, and σ^2 is the variance of the data, an estimate of which is

$$\sigma^2 = \frac{\sum_{j=1}^{n} w_j \cdot R_j^2}{n - M} \qquad (3.2\text{-}26)$$

Thus the variance of the kth. parameter is

$$\sigma_k^2 = \frac{\sum_{j=1}^{n} w_j \cdot R_j^2}{n - M} \cdot x_{k,k} \qquad (3.2\text{-}27)$$

It has been shown by Barieau and Dalton (20) that equation (3.2-27) is only an approximation to σ_k^2, albeit

a very good approximation except for models with a high degree of non-linearity in the parameters. However, even the rigorously derived expression for σ_k^2 given by these authors is only exact in the absence of any systematic error in the data. The presence of systematic error can lead to misleadingly small values of σ_k^2, as will be shown in section 3.4.

(b) Treatment of experimental data for the non-isothermal Burnett apparatus.

The formulation of the objective function for Method A, as described by equations (3.2-8) and (3.2-9), is further complicated in the case of a real non-isothermal apparatus by the following,

(i) Volume V_B is at temperature T^o (0^oC) with compressibility factors Z_j^o.

(ii) The gas in the dead-space volumes must be included.

(iii) The volumes of the vessels vary with pressure.

(iv) The pressures are not identical in each part of the apparatus because of gravitational effects; in particular the pressure in V_B, P_j^o, will be slightly different from that in V_A, P_j.

For the purpose of calculating the quantity of gas in the apparatus, it was considered as divided into eight sections of volumes V1 to V8, as shown in figure 2.17, containing n_2 to n_8 moles. (V1 $\equiv$ V_A and V6 $\equiv$ V_B in previous notation).

Equating no. of moles before and after the jth. expansion,

$$\frac{P_{j-1}\ V1_{j-1}}{RT_{j-1}\ Z_{j-1}} + (n_2 + n_3 + n_7 + n_8)_{j-1} =$$

$$\frac{P_j\ V1_j}{RT_j\ Z_j} + \frac{P^o_j\ V6_j}{RT^o\ Z^o_j} + (n_2 + n_3 + n_4 + n_5 + n_7 + n_8)_j \qquad (3.2\text{-}28)$$

On re-arrangement, the jth. residual is obtained,

$$R_j = \frac{P_{j-1}}{P_j} - \left(\frac{T_{j-1} \cdot Z_{j-1} \cdot V1_j}{T_j \cdot Z_j \cdot V1_{j-1}} + \frac{P^o_j \cdot Z_{j-1} \cdot V6_j \cdot T_{j-1}}{P^o_{j-1}\ Z^o_j \cdot V1_{j-1}\ T^o}\right)$$

$$+ \frac{R \cdot T_{j-1} \cdot Z_{j-1}}{V1_{j-1}} \cdot \{(n_2 + n_3 + n_7 + n_8)_{j-1}$$

$$- (n_2 + n_3 + n_4 + n_5 + n_7 + n_8)_j\} \qquad (3.2\text{-}29)$$

where $Z_j = \frac{P_j}{RT_j\rho_j} = 1 + a_1\rho_j + a_2\rho_j^2 + \ldots a_m\rho^m{}_j \qquad (3.2\text{-}30)$

and similarly for Z^o_j, $Z3_j$, etc.

No 'adjusted pressures' are employed in Method A, and $n_2 - n_8$ are calculated before the iterative least-squares procedure commences and remain unchanged throughout the program.

In volumes V3, V4 and V8 the temperature was constant and the no. of moles were given by, for example,

$$n_3 = \frac{P_j\ V3_j}{RT3_j\ Z3_j} \qquad (3.2\text{-}31)$$

In volumes V5 and V7, which were both very small, there was a temperature gradient that was assumed linear and 'effective' temperatures, T5 and T7, were calculated for use in the equation corresponding to (3.2-31).

In the inlet-tubing, volume V2, there existed a temperature gradient for which a special calculation was necessary. The E.M.F.s of the inlet tube thermocouples were first converted to temperatures by means of a polynomial fitted to the relevant calibration curve. Consider two adjacent thermocouples, T_k and T_{k+1}, separated by a distance l. The no. of moles of gas in a narrow section of tubing, thickness δx, at a distance x from thermocouple T_k is given by

$$\delta n = \frac{P_k \cdot A \cdot \delta x}{RTx\ Zx} \qquad (3.2\text{-}32)$$

where A is the cross-sectional area of the tubing

Zx is the compressibility factor at temperature Tx.

Assuming a linear temperature gradient and a linear gradient in compressibility factor between thermocouples,

$$n_k = \int dn = \int_0^l \frac{P_k \cdot A \cdot dx}{R(T_k + x/l(T_k - T_{k+1}))(Z_k + x/l(Z_k - Z_{k+1}))} \qquad (3.2\text{-}33)$$

Integrating,

$$n_k = \frac{P_k \cdot A \cdot l}{R(T_k Z_{k+1} - Z_k T_{k+1})} \ln\left(\frac{T_k \cdot Z_{k+1}}{T_{k+1} \cdot Z_k}\right) \qquad (3.2\text{-}34)$$

The equivalent expression for the pressure gradient between T_k and T_{k+1} is, from (2.7-9),

$$\Delta P_k = \frac{P_k\ g \cdot M \cdot l}{(T_k Z_{k+1} - Z_k T_{k+1})} \ln\left(\frac{T_k \cdot Z_{k+1}}{T_{k+1} \cdot Z_k}\right) \qquad (3.2\text{-}35)$$

(c) Description of computer program.

The computer program was written in the Fortran IV language for use on the University of London CDC 6600 computer (or the Imperial College 6400 computer).

Before the start of the actual least-squares procedure in the main program, the following subroutines were called

1) TEMTEM. From the platinum resistance thermometer readings the temperatures, T_j, were calculated from a solution of the Callendar-van-Dusen equation by means of a Newton-Raphson iteration. These values were then converted to the IPTS 68 scale as described in section 2.3.

2) PROIL. The experimental pressures were calculated as described in section 2.6. Allowance was made for the pressure-heads of gas between the D.P.C. (or the gas piston-gauge) and the reference level, as described in section 2.7, and for the pressure head between this level and the ice-bath.

3) VIRCO. For the gas under study and a given temperature, the appropriate polynomial coefficients $a_1 \ldots a_m$ were calculated for use in computation of the compressibility factors, $(Z2)_j - (Z8)_j$, for the dead spaces and ice-bath vessel, and for use as first trial values of the least-squares parameters at temperature T (see section 4.3(a)).

4) ZEST. The compressibility factor at temperature T and pressure P is calculated by solution of

$$Z = \frac{P}{RT\rho} = 1 + a_1\rho + a_2\rho^2 = \ldots\ a_m\rho^m \quad (3.2\text{-}36)$$

The iterative solution of this equation is obtained by a modification of the "Regula Falsi" method (22), which was found to converge more quickly to the right solution at

high density than a Newton-Raphson iteration.

5) MSSTUB. This subroutine has two functions: it calculates the no. of moles of gas, n_2, in the inlet-tubes by means of equation (3.2-34), and simultaneously it calculates the pressure gradient down the tubes by means of equation (3.2-35). Each value of Z_k was calculated by first calling VIRCO for temperature T_k and then calling ZEST for temperature T_k and pressure P_k.

The non-linear least-squares procedure, as described in section 3.2(a) was then commenced, the parameters being the polynomial coefficients a_1, a_2 ... a_k ... a_m and the volume of the pressure-vessel at zero pressure, V1. In subroutine PRAT the least-squares residuals were calculated, first determining the change in volume with pressure of V1 and V6. For the first call of PRAT only, the weighting factors were calculated according to equations (3.4-8) - (3.4-10), setting $\gamma = 10^{-5}$ and $\epsilon = 7.10^{-5}$ bar. The derivatives $\partial R_j/\partial P_j$, etc., were determined analytically.

In setting up the normal equations in the main program, the partial derivatives $\partial R_j/\partial a_k$, etc., were determined numerically by changing each value of a_k by 1% in turn and recalling ZEST and then PRAT. The normal equations were solved by means of subroutine MATRIX, which solves a set of simultaneous linear equations by means of Gauss-Jordan double-pivotal elimination. Subroutines ZEST and PRAT were recalled, using the new values of a_1 ... a_m and V1, and the iteration continued until $\Delta a_1 < 10^{-5}$ cm^3 mole^{-1} and $\Delta a_2 < 10^{-3}$ cm^6 mole^{-2}. Usually less than ten iterations were required; if the above convergence criteria were not

satisfied after fifty iterations then convergence was assumed only if $\Delta a_1 < 10^{-3}$ and $\Delta a_2 < 10^{-1}$.

The whole least-squares procedure was contained within two repeat loops (DO loops). In the first the value of m was varied from m = 2 to m = 4, 5 or 6, and in the second the initial pressure considered in the fit, P_r, was varied, e.g. from P_o to P_4 when m = 2.

The total computing-time per run was about four seconds.

3.3 Determination of Accurate Virial Coefficients from the Least-Squares Analysis of Conventional PVT Data.

The compressibility factor of a gas is given by an infinite series expansion in powers of density, the virial series,

$$Z = 1 + \alpha_1\rho + \alpha_2\rho^2 + \ldots \alpha_k\rho^k \ldots + \ldots \qquad (3.3\text{-}1)$$

The series is convergent except in the vicinity of the critical point, in the liquid state, and at very high densities. The coefficient α_k is the k + 1 th. virial coefficient.

If one considers a set of experimental PVT measurements consisting of n data points (Z', ρ), then a least-squares curve fit to these points can be carried out, giving the n points (Z_m', ρ). The least-squares residuals are,

$$R_j = (Z_m' - Z')_j \qquad (3.3\text{-}2)$$

and Z_m' is the truncated polynomial,

$$Z_m' = 1 + a_1'\rho + a_2'\rho^2 + a_k'\rho^k + \ldots a_m'\rho^m \qquad (3.3\text{-}3)$$

The problem is to relate the coefficients of this truncated series to the corresponding virial coefficients. It is a problem that has been considered by Michels, de Graaff and ten Seldam (23), Hall and Canfield (19) and Van Doren (24). In all of these treatments, in order to simplify the statistical analysis it is normally assumed that the experimental values of Z are subject to random errors but that the values of the density, ρ, are known exactly.

Another polynomial can be considered, that of a least-squares curve fit to the hypothetical error-free points (Z, ρ),

$$Z_m = 1 + a_1\rho + a_2\rho^2 + \ldots a_k\rho^k + \ldots a_m\rho^m \qquad (3.3\text{-}4)$$

The mean square error involved in using a_k' to represent the true virial coefficient, α_k, can be shown to be (24),

$$\langle(a_k' - \alpha_k)^2\rangle = \langle(a_k' - a_k)^2\rangle + (a_k - \alpha_k)^2 \qquad (3.3\text{-}5)$$

The first term on the right of equation (3.3-5) is the variance of the kth. polynomial coefficient, σ_k^2, and can be estimated from the experimental data, as shown in section 3.2(a), equation (3.2-27),

$$\text{i.e. } \sigma_k^2 = \frac{\sum_{j=1}^{n} \omega_j R_j^2}{n - m} \cdot x_{k,k} \qquad (3.3\text{-}6)$$

where R_j in this case is given by equation (3.3-2).

The second term on the right-hand side of equation (3.3-5) is termed the bias in a_k, and is introduced through the truncation of the infinite virial series.

Hall and Canfield present a criterion for estimation of the value of m that gives the "best-fit" to the data,

i.e. when $\sum_{j=1}^{n} (Z_m' - Z)_j^2$ is a minimum with respect to m.

This criterion is, subject to several simplifying assumptions,

$$m \cdot \frac{\sum_{j=1}^{n} \omega_j (Z_m' - Z')_j^2}{n - m} = \text{minimum} \qquad (3.3\text{-}6)$$

This enables m to be chosen such that the least-squares values, Z_m', provide the best-fit to the true compressibility factors, Z. Hall and Canfield also present a criterion for the 'best-fit' to the virial coefficients, i.e. when equation (3.3-5) is a minimum with respect to m. This criterion is also subject to several assumptions: it contains, for instance, an expression involving the unknown true virial coefficients, α_k, which must be approximated by the series coefficients, a_k', from the 'best-fit' to the data. However, Van Doren (24) questions the validity of the Hall and Canfield criterion for the 'best-fit' to the virial coefficients. The statistical analysis presented by Van Doren shows that, from the experimental data alone, no estimate is possible of the second term on the right-hand side of equation (3.3-5), the bias in a_k. Therefore no reliable estimate can be made of the errors involved in approximating the virial coefficients, α_k, by the least-squares coefficients, a_k'.

In view of this disagreement and the over-simplifications

inherent in the statistical analysis of this problem, especially with regard to the neglect of systematic error in the data, it was deemed necessary to adopt a more empirical approach to the problem. An investigation of the results from non-linear least-squares fitting of simulated Burnett data was therefore instigated.

3.4 Simulation of Burnett Data

In a second computer program a model virial series was used to generate the 'exact' pressures and compressibility factors of a hypothetical Burnett run. Various error distributions, both random and systematic, could be superimposed on the exact data to give simulated experimental pressures, which were then submitted to the non-linear least-squares treatment of either Method A or Method B. Simulated runs were investigated for both methane and nitrogen, choosing the volumes and temperatures of the 'apparatus' such that the results of the program could be compared with those of the actual experimental runs.

The objectives of the program were

1) To compare Method A and Method B, and to choose a method of data treatment that was capable of high accuracy.

2) To examine the effect of various factors on the closeness of the derived virial coefficients and compressibility factors to those of the exact model. These factors are,

   i) The errors superimposed on the simulated data.

   ii) The degree, m, of the truncated virial series used in the least-squares fit and the maximum pressure, P_r, considered in that fit.

iii) The temperature and maximum density of the run, particularly in relation to the critical point.

iv) The distribution of weighting factors.

v) The magnitude of the apparatus constant, which determines the number of expansions in each run.

In the simulated apparatus no dead-space volumes were assumed and the volumes of the vessels, V_A and V_B, were independent of pressure.

Thus, for Method A, the objective function is,

$$S = \sum_{j=r}^{n} \omega_j \left(\frac{P_{j-1}}{P_j} - \frac{\left(\frac{V_A}{TZ_j} + \frac{V_B}{T^oZ^o_j}\right)}{\frac{V_A}{TZ_{j-1}}} \right)^2 \qquad (3.4\text{-}1)$$

where

$$Z_j = \frac{P_j}{RT\rho_j} = 1 + a_1\rho_j + a_2\rho_j{}^2 \cdots a_k\rho_j{}^k \cdots a_m\rho_j{}^m \qquad (3.4\text{-}2)$$

For Method B the objective function is,

$$S = \sum_{j=r}^{n} \omega_j \, (P_j' - P_j)^2 \qquad (3.4\text{-}3)$$

where the adjusted pressures P_j' are found such that

$$\frac{P'_{j-1}}{P_j'} - \frac{\left(\frac{V_A}{TZ'_j} + \frac{V_B}{T^oZ^o_j}\right)}{\frac{V_A}{TZ'_{j-1}}} = 0 \qquad (3.4\text{-}4)$$

$$\text{and } Z_j' = \frac{P_j'}{RT\rho_j'} = 1 + a_1\rho_j' + a_2(\rho'_j)^2 \cdots a_k(\rho'_j)^k \cdots a_m(\rho'_j)^m \qquad (3.4\text{-}5)$$

Exact values of V_A, V_B, T, T^o (273.15K), the initial pressure P_o, and the coefficients $a_1 \ldots a_m$ and $a_1^o \ldots a_m^o$ are the parameters required to generate the values of P_j, Z_j and Z_j^o for $j = o \ldots n$ that constitute the simulated exact data. The last pressure, P_n, was such that $P_n \geqslant 2$ bar.

Then, using these exact pressures, the non-linear least-squares analysis was applied to all the data using first m = 2 (B and C only), then m = 3, etc. This was repeated without considering the first pressure, i.e. in the range $P_1 - P_n$ (r = 1), then in the range $P_2 - P_n$ (r = 2), etc. The maximum value of m used in a particular range was such that the least-squares degrees of freedom were never less than one,

$$\text{i.e. } (n - r) - (m + 1) \geqslant 1 \qquad (3.4\text{-}6)$$

These same curve-fits were then repeated after various error distributions had been superimposed on the exact pressures. For a random error distribution,

$$P_j \text{ (experimental)} = P_j \text{ (exact)} + \epsilon_j + \gamma_j P_j \qquad (3.4\text{-}7)$$

where ϵ_j and γ_j were independent of pressure and randomly distributed about a zero mean with standard deviations ϵ_r and γ_r respectively. These were chosen to cover the range of random errors expected in the actual experimental measurements:

ϵ_r = 0, .00015 and .00035 bar

γ_r = 0, 10^{-5} and 2.10^{-5} .

The expected variance in P_j is given by

$$\sigma_{P_j}^2 = \epsilon_r^2 + \gamma_r^2 P_j^2 \qquad (3.4\text{-}8)$$

The weighting factor for each residual, assigned on the prior assumption of the form of the error distribution, is given by the reciprocal of its expected variance,

$$\omega_j = 1/\sigma_{R_j}^2 \qquad (3.4\text{-}9)$$

For Method A:

$$\sigma_{R_j}^2 = \left(\frac{\partial R_j}{\partial P_j}\right)^2 \sigma_{P_j}^2 + \left(\frac{\partial R_j}{\partial P_{j-1}}\right)^2 \sigma_{P_{j-1}}^2 \qquad (3.4\text{-}10)$$

For Method B:

$$\sigma_{R_j}^2 = \left(\frac{\partial R_j}{\partial P_j}\right)^2 \sigma_{P_j}^2 = \sigma_{P_j}^2 \qquad (3.4\text{-}11)$$

The partial derivatives in (3.4-10) were determined by straightforward partial differentiation.

Systematic errors could also be assigned,

$$P_j \text{ (experimental)} = P_j \text{ (exact)} + \epsilon_s + \gamma_s P_j \qquad (3.4\text{-}12)$$

where $\epsilon_s = 0$, .00035 or .0007 bar

and $\gamma_s = 0$, 2.10^{-5} or 4.10^{-5} .

Before describing the results of this program, mention should be made of an investigation by Levelt Sengers (25) into the least-squares analysis of PVT data. It was difficult to utilize the general results of Levelt Sengers, however, because only conventional PVT data were considered, not Burnett data. It was shown that a m = 2 fit to a

certain number of measurements gave higher accuracy than a fit with larger m to the same number of measurements spread over a wider pressure range. In a Burnett experiment, increasing the range gives more measurements which might be expected to compensate to an unknown extent for the necessity of using a higher value of m. Furthermore, Levelt Sengers did not consider systematic errors: these are difficult to include in a statistical treatment and are best included in the specific set of simulated data under study and their effect investigated empirically.

(a) The model virial series.

It has been claimed by van Doren (24) that because the true virial coefficients are unknown, no information can be obtained from tests using simulated data obtained with an approximation to the virial series as the 'exact' model. This is true if there is no available prior information on any of the virial coefficients, but as only order of magnitude values are all that are really required in this application excellent approximations to B and C can be taken from the literature. Estimates of the magnitudes of higher virial coefficients may usually be obtained either from experimental PVT data or from theoretical calculations such as those based on the Lennard-Jones (12-6) intermolecular potential (26).

If all theoretical virial coefficients are used in the model large discrepancies could arise between the compressibility factors so calculated and the experimental values: a simulated Burnett run might have a different number of

expansions than the corresponding experimental run. For the model series used here, experimental estimates of B, C, and D were obtained from the literature. With reference to figures 3.1 and 3.2, it can be seen that the experimental values of the fourth virial coefficient from different sources are in reasonable order of magnitude agreement with the theoretical values. For nitrogen, the four-coefficient equation of Wood et al (27) was employed in one set of tests on simulated data, and in another set the same series was extended to α_6 (seven virial coefficients).

The last coefficient, α_6, was such that it contributed .0001 to Z at the maximum density encountered.

For methane the higher coefficients were such that the ratio of successive coefficients was constant along the series and equal to the ratio of the earlier theoretical coefficients; this ensured a realistic convergence rate to the series and gave the required large increase in absolute magnitude of the higher coefficients at low temperatures. Coefficients up to α_8 (the ninth virial coefficient) were used; the last contributed .0001 to Z at the maximum density encountered.

In retrospect, perhaps an empirical equation of state would be simpler to use as the model provided, of course, that it could be reduced to virial form and that it gave realistic estimates of the lower virial coefficients.

(b) Comparison of Method A and Method B.

It was found that Method A and Method B both gave virtually identical sets of least-squares coefficients,

FIG. 3.1

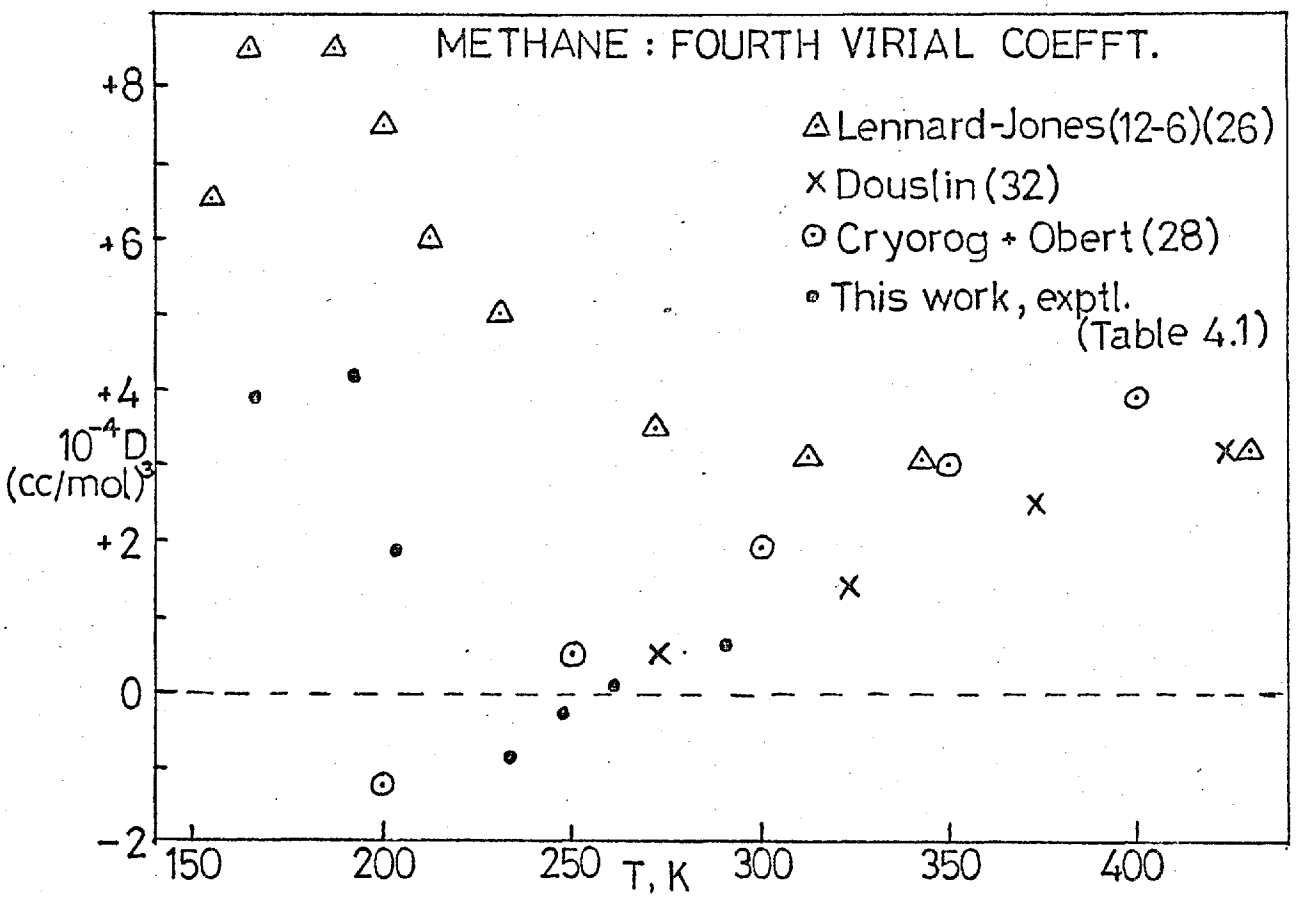
METHANE : FOURTH VIRIAL COEFFT.
Lennard-Jones(12-6)(26)
Douslin (32)
Cryorog + Obert (28)
This work, exptl.
(Table 4.1)
+8
+6
+4
+2
0
−2
10^{-4} D
(cc/mol)^3
150
200
250
T, K
300
350
400

FIG. 3.2

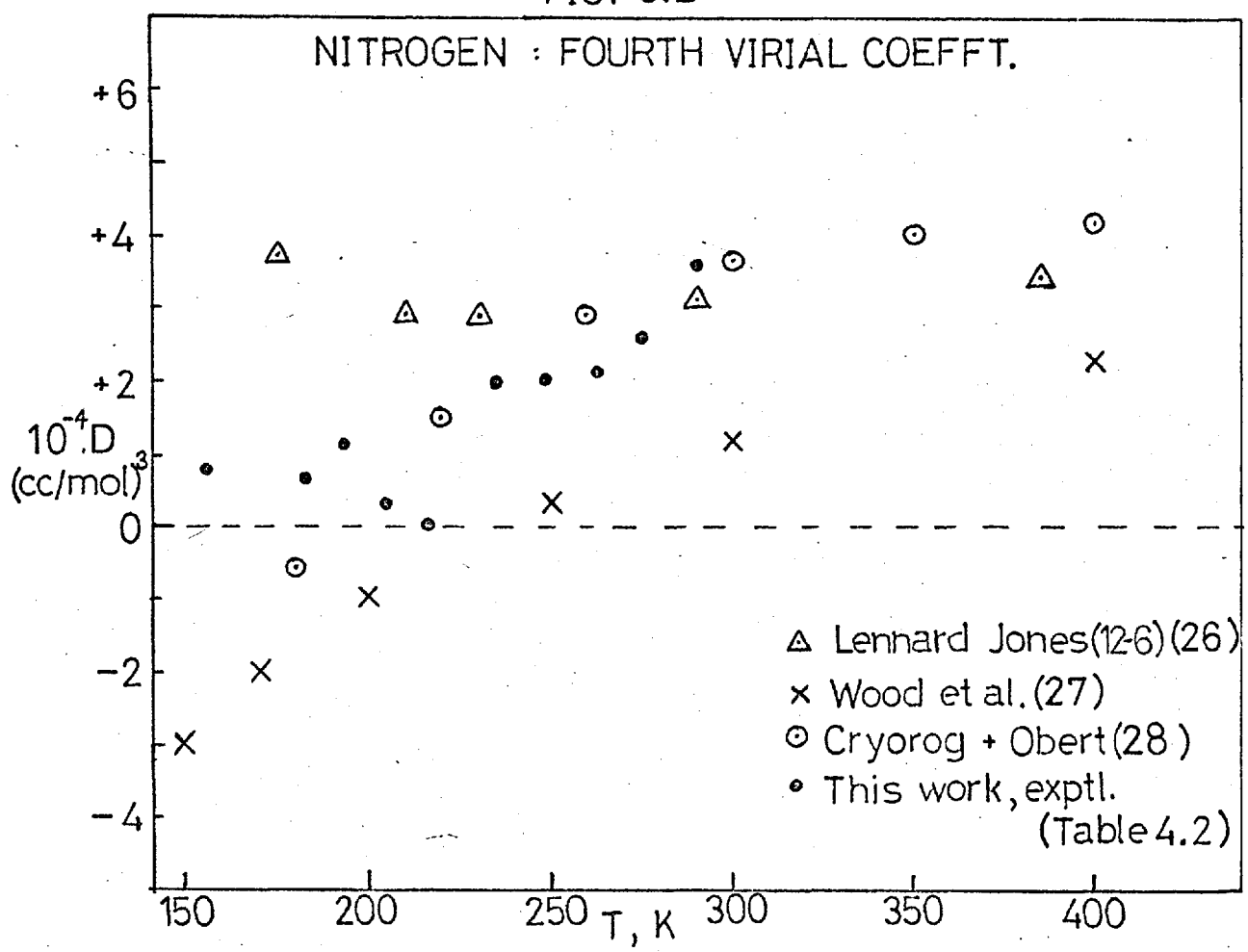
NITROGEN : FOURTH VIRIAL COEFFT.
Lennard Jones(12-6)(26)
Wood et al.(27)
Cryorog + Obert(28)
This work, exptl.
(Table 4.2)
+6
+4
+2
0
−2
−4
10^{-4}.D
(cc/mol)^3
150
200
250
T, K
300
350
400

$a_1 \ldots a_m$ and compressibility factors $Z_o \ldots . Z_n$ when simulated Burnett runs were treated. For a given convergence criterion, such as $\Delta a_1 < 10^{-5}$ cm^{-3} mole^{-1}, Method B required about twice as many iterations. Also, because of its slower convergence and the extra iterative computation inherent in the calculation of the adjusted pressures, Method B required about ten times more computing time than Method A. It was therefore felt that Method A, as described in section 3.2(a) and (b) should be adopted for further use both in this program and for treatment of the actual experimental data. Subsequently, all results given are from the use of Method A.

(c) Isotherms of Low Curvature

The nitrogen runs cover the range from 155.9 to 291.4K (T^R = 1.24 to 2.31) at densities up to a maximum of .007 mole cm^{-3} (ρ^R = 0.63) and pressures up to 103 bar. All of these isotherms, except possibly the one at 155.9K, are of low curvature (on a Z - ρ plot) in a region where the virial series converges relatively quickly and the general results from simulated data are similar. As an example, the results for the simulated 218.9K isotherm are presented in Table 3.1; the maximum pressure is 97 bar, with a corresponding Z_o of .903759, and a four-coefficient model virial series was used to generate the simulated data.

The results are characterized by the average absolute deviation in compressibility factor,

$$|\overline{\Delta Z}| = \frac{1}{(n + 1 - r)} \sum_{j=r}^{n} |Z_j(\text{calc.}) - Z_j(\text{exact})| \qquad (3.4\text{-}13)$$

TABLE 3.1

Simulated Data: Nitrogen 218.9K. P_o = 96.7 bar

No errors	$\gamma = 0$ $\varepsilon = 0$								
	m = 4		m = 3			m = 2				
	P_o	P_1	P_o	P_1	P_2	P_o	P_1	P_2	P_3	P_4
ΔB	$<10^{-3}$	$<10^{-3}$	.119	.034	.010	-.354	-.079	-.014	-.001	+.001
σ_B	$<10^{-4}$	6.10^{-4}	.025	.007	.002	.078	.019	.004	6.10^{-4}	$<10^{-4}$
$\lvert\overline{\Delta Z}\rvert\ 10^{-4}$	<.01	<.01	.4	.08	.02	2.0	.3	.04	<.01	<.01
Random errors	$\gamma_r = 10^{-5}$ $\varepsilon_r = 0.00015$									
	m = 4		m = 3			m = 2				
	P_o	P_1	P_o	P_1	P_2	P_o	P_1	P_2	P_3	P_4
ΔB	.075	.416	.107	.042	.332	-.339	-.081	-.028	+.189	.100
σ_B	.194	.431	.067	.147	.311	.077	.047	.088	.179	.585
$\lvert\overline{\Delta Z}\rvert.10^{-4}$	.32	1.0	.75	.15	.86	1.9	.48	.10	.57	.40
Systematic errors	$\gamma_s = 2.10^{-5}$ $\varepsilon = 0$									
	m = 4		m = 3			m = 2				
	P_o	P_1	P_o	P_1	P_2	P_o	P_1	P_2	P_3	P_4
ΔB	.001	$<10^{-3}$	.120	.034	.010	-.356	-.080	-.014	-.001	$<10^{-3}$
σ_B	$<10^{-4}$	$<10^{-4}$	.025	.007	.002	.078	.019	.004	5.10^{-4}	$<10^{-4}$
$\lvert\overline{\Delta Z}\rvert.10^{-4}$	<.01	<.01	.4	.08	.02	2.0	.3	.04	<.01	<.01
Systematic errors	$\gamma_s = 2.10^{-5}$ $\varepsilon_s = .00015$									
	m = 4		m = 3			m = 2				
	P_o	P_1	P_o	P_1	P_2	P_o	P_1	P_2	P_3	P_4
ΔB	.122	.228	.212	.143	.207	-.465	-.079	.046	.134	.274
σ_B	.033	.058	.018	.022	.048	.091	.031	.025	.038	.066
$\lvert\overline{\Delta Z}\rvert.10^{-4}$	.7	.9	1.0	.7	1.0	3.2	.4	.3	.6	.8
Systematic errors	$\gamma_s = 2.10^{-5}$ $\varepsilon_s = .0004$									
	m = 4		m = 3			m = 2				
	P_o	P_1	P_o	P_1	P_2	P_o	P_1	P_2	P_3	P_4
ΔB	.225	.461	.264	.229	.391	-.516	-.067	.101	.262	.541
σ_B	.062	.111	.017	.046	.094	.094	.039	.042	.074	.131
$\lvert\overline{\Delta Z}\rvert.10^{-4}$	1.3	1.9	1.4	1.3	1.6	3.8	.2	.6	1.1	1.6

and by the deviation in the second virial coefficient,

$$\Delta B = B(\text{calc.}) - B(\text{exact}) = a_1' - \alpha_1 \qquad (3.4\text{-}14)$$

and the calculated standard deviation of B, $\sigma_B (=\sigma_1)$.

Because of the well-known high correlation between least-squares parameters, it was found that ΔB, ΔC and $|\overline{\Delta Z}|$ were closely inter-linked: whenever ΔB was negative, ΔC was positive. A curve-fit that gave a good estimate of B also gave good estimates of C and the compressibility factors; therefore, to simplify the following discussion it will be confined largely to the variation in ΔB.

When there were no errors in the pressures ($\gamma = 0$, $\epsilon = 0$) the agreement between the least-squares parameters and the exact values was perfect for m = 4, i.e. when the number of coefficients in the fitting polynomial was equal to the number in the model. This was to be expected if the least-squares method was used correctly. For m = 3 and m = 2 agreement was excellent over the lower pressure ranges but became systematically worse as P_r increased. When m was obviously too small, e.g. m = 2 in the range $P_o - P_n$, ΔB was much greater than the calculated value of σ_B because of the large 'bias', $(a_1 - \alpha_1)^2$, appearing in equation (3.3-5), that was unaccounted for in the calculation of σ_B.

When random errors only were superimposed on the pressures the values of ΔB and $|\overline{\Delta Z}|$ increased as the range $P_r - P_n$ became too narrow and the number of measurements decreased. When the six-coefficient model was used to generate the simulated data the results were virtually the

same except that the m = 4 fit in the $P_o - P_n$ range was slightly worse. With m = 5 and m = 6 the fits were poor in the presence of even very small errors.

For example, in figure 3.3 is shown the variation in ΔB with P_r; the random error distribution is characterized by $\gamma_r = 10^{-5}$, $\epsilon_r = .00015$ bar. The 'error-bars' represent the values of σ_B. For each value of m there is a particular pressure range, $P_r - P_n$, for which ΔB is a minimum, e.g. for m = 2 the optimum P_r is P_2. This optimum range does not necessarily correspond to the minimum σ_B. Only in smaller ranges for each m, where the fitting model is a good approximation to the exact model, does the value of σ_B represent a true standard deviation and it approximates the value of ΔB.

As the random errors decrease the relative shapes of these curves remain much the same but the minima are shifted slightly to smaller values of P_r and, of course, are at much smaller values of ΔB. For quite a wide spread of random errors the optimum $P_r - P_n$ ranges remain the same.

When a systematic error proportional to the pressure was superimposed on the data (Table 3.1, $\gamma_s = 10^{-5}$, $\epsilon = 0$), the results were virtually identical to those for the exact pressures. This is because the objective function involves the ratio of experimental pressures, P_{j-1}/P_j, and this systematic error cancels out. As there are errors of this type in the actual experimental pressures, owing primarily to the uncertainty in the piston-area of the piston-gauge, this is an important feature of the method.

No such cancellation occurred when a systematic error, ϵ_s,

FIGURE 3.3

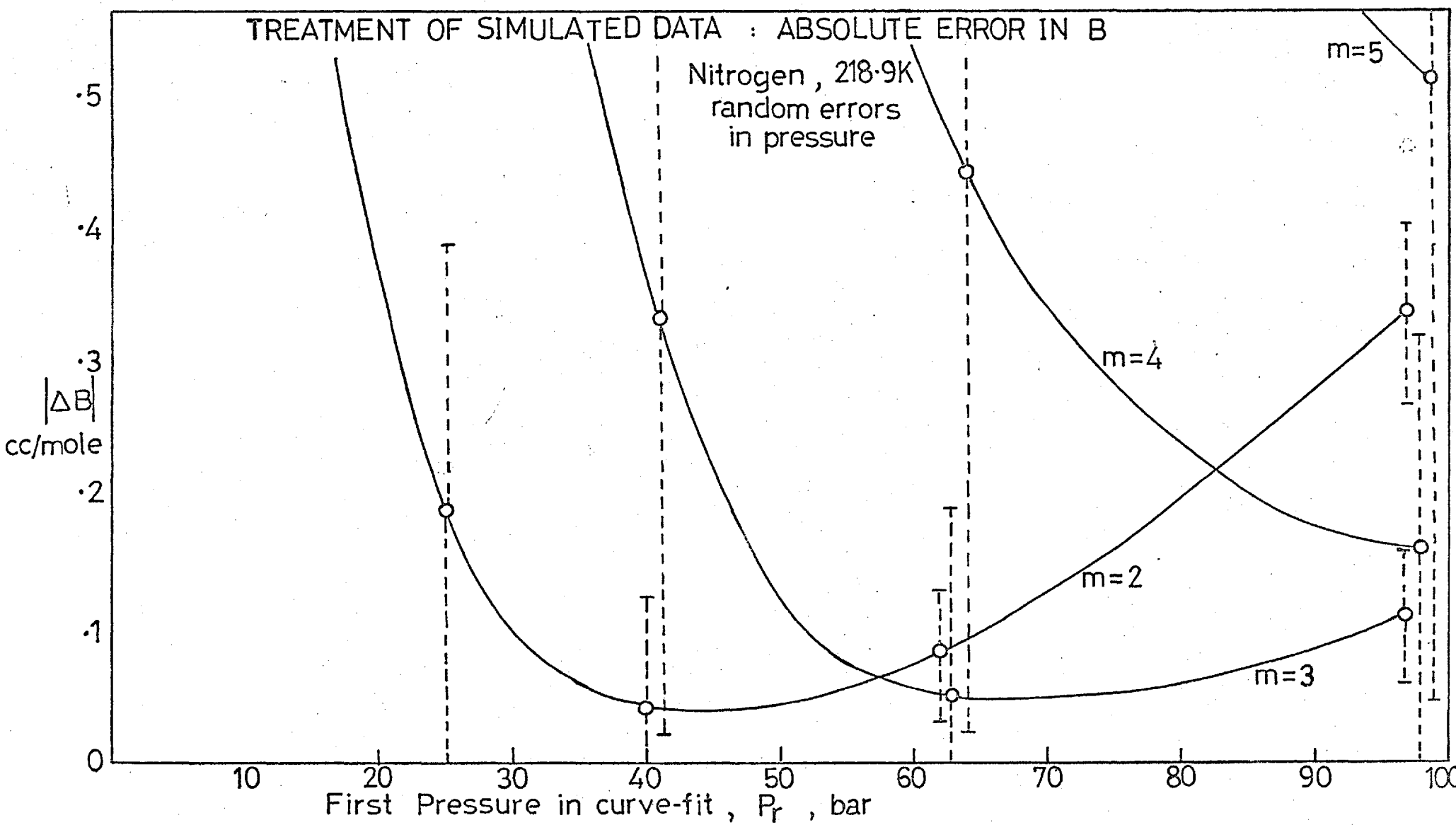
TREATMENT OF SIMULATED DATA : ABSOLUTE ERROR IN B
Nitrogen , 218·9K
random errors
in pressure
m=5
m=4
m=2
m=3
·5
·4
·3
·2
·1
0
|ΔB|
cc/mole
10
20
30
40
50
60
70
80
90
100
First Pressure in curve-fit , P_r , bar

independent of pressure, was superimposed on the exact data. In figure 3.4 is shown the variation in ΔB , with the systematic error distribution characterised by $\gamma_s = 2.10^{-5}$, ϵ_s = .00015 bar. It can be seen that the general results are similar to those for random errors. However, the standard deviations, σ_B, now underestimate ΔB no matter what the pressure range. The presence of systematic errors is indicated in these results by relatively large changes in B and Z from curve-fit to curve-fit; a random error distribution which would produce the same small standard deviations would lead to good estimates of B and C which were changed little from curve-fit to curve-fit, provided, of course, that m was not too small for the range considered.

Thus it can be seen that for this simulated run the best overall estimates of B and of C, are given by the m = 2 fit in the P_2 - P_n range. This fit also gives the best estimates of the compressibility factors Z_2 .... Z_n. The best estimate of Z_1 is given by either the m = 3 fit in the P_1 - P_n range, or by the m = 4 fit in the P_o - P_n range, the latter giving also the best estimate of Z_o. When the systematic error is larger, e.g. ϵ_s = .0004 bar (Table 3.1), the best m = 3 and m = 4 fits (P_1 - P_n and P_o - P_n respectively) give very similar values of B and of the compressibility factors but these are subject to relatively large errors, i.e. ΔB = .23 cm^3 $mole^{-1}$, $|\overline{\Delta Z}|$ = .00013. The m = 2 fit in the P_2 - P_n range is definitely superior in this instance. This is because the more the parameters in the fitting equation, which is constrained to pass through Z = 1.0 at zero pressure, the more flexible is the curve-fit, enabling it to 'follow'

FIGURE 3.4

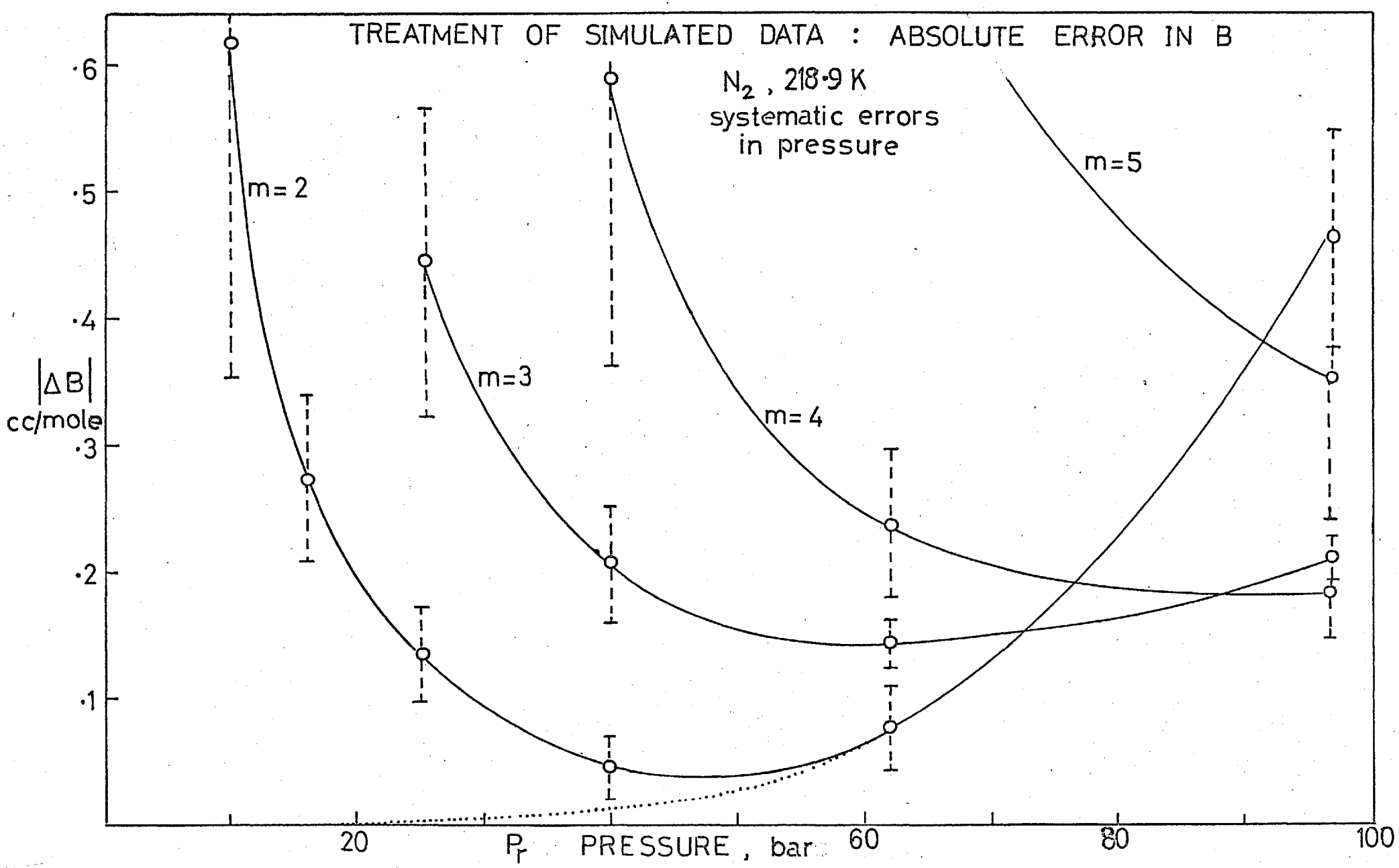
TREATMENT OF SIMULATED DATA : ABSOLUTE ERROR IN B
N_2 , 218·9 K
systematic errors
in pressure
m=2
m=3
m=4
m=5
|ΔB|
cc/mole
·6
·5
·4
·3
·2
·1
20
60
80
100
P_r PRESSURE , bar

the systematic deviation at low pressure: in the simulated data Z does not tend to 1.0 at zero pressure because of the systematic error. This would give the wrong limiting behaviour at low pressure and hence the wrong estimate of B.

Similar behaviour was found for the other simulated runs. For each Z_j there was a particular number of fitting coefficients, m, and pressure range $P_r - P_n$ which provided the best estimate of Z_j. In general a m = 2 fit was best for the estimation of B and C, especially in the presence of relatively large systematic errors that are independent of pressure. Another reason for the choice of a m = 2 fit is that the uncertainties in the magnitudes of the model virial coefficients increase along the series and hence the uncertainties in the results from this program increase with the value of m. The general conclusion can be drawn that if the 'true' B were unknown, it would be dangerous to assume that the value of σ_B represented a realistic estimate of ΔB because of the possible presence of systematic errors, especially when a large value of m is used.

(d) Isotherms of High Curvature

The results for those simulated isotherms of methane above 234 K ($T^R > 1.21$ and $\rho^R < .7$) were basically similar to those for nitrogen, with the same conclusions being applicable. As the temperature approaches the critical temperature, 190.5 K, the isotherms extend to higher densities ($\rho^R = 1.14$), where the virial series is more slowly convergent, and exhibit greater curvature on a $Z - \rho$ plot.

The optimum $P_r - P_n$ range for the m = 2 fit is shifted

to smaller values of P_r as the temperature decreases. In figure 3.5 are shown the resultant values of $|\Delta B|$ for the simulated 248.5 K, 218.9 K, and 181.9 K Burnett runs, with a random error distribution characterised by $\gamma_r = 10^{-5}$, $\epsilon_r = .00015$ bar. The overall increase in $|\Delta B|$ at low temperatures is apparent. For the low temperature runs, unless the random errors were very small, the optimum range was such that the systematic difference between the fitting polynomial and the model virial series contributed significantly to $|\Delta B|$.

For the 218.9 K, 204.6 K, and 192.6 K simulated runs it was found that $m \geq 5$ was necessary to obtain a good estimate of Z_o and Z_1. These fits produced relatively poor estimates of B and C, however, (e.g. $\Delta B = 0.5$ cm^3 mole^{-1}) and of the lower compressibility factors. For these runs it is not usually possible to treat <u>all</u> of the data with one value of m and obtain good estimates of B and C and <u>all</u> of the compressibility factors. This conclusion pertains to most Burnett runs at low reduced temperature which extend to high pressure, and has not always been realised by previous experimentalists (for example (83), (29)). It is a consequence of the wide spacing of high pressure Burnett measurements in a highly-curved region of the isotherm where the virial series is slowly convergent, or possibly even divergent.

When the reduced densities, $\rho^R = \rho/\rho^C$, corresponding to the maximum pressure of each optimum range, P_r, are plotted against reduced temperature T^R the results are as shown in figure 3.6. It can be seen that for $T_R > 0.9$ the optimum densities are only slowly changing functions of

FIGURE 3.5

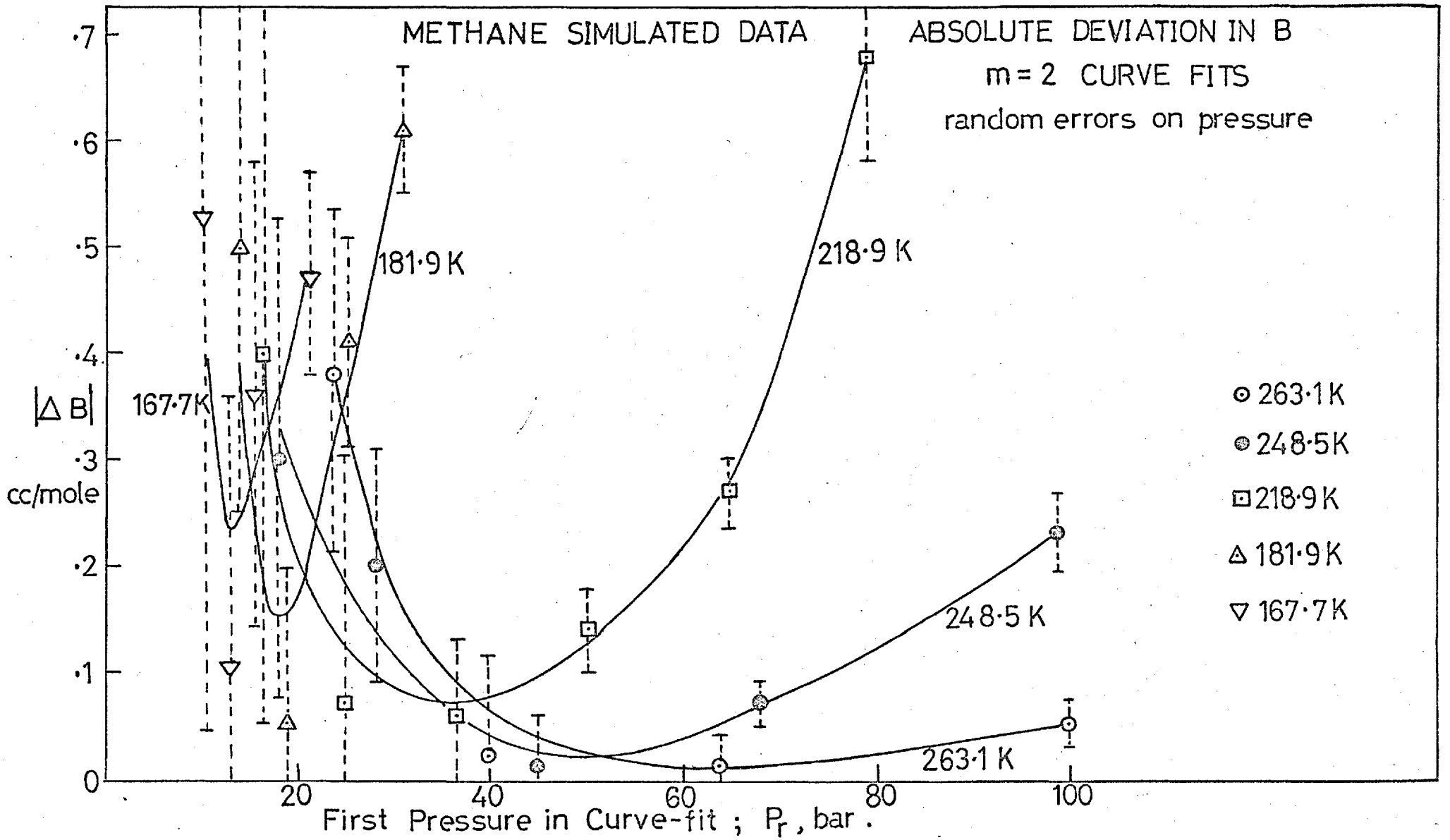
METHANE SIMULATED DATA
ABSOLUTE DEVIATION IN B
m = 2 CURVE FITS
random errors on pressure
|Δ B|
cc/mole
·7
·6
·5
·4
·3
·2
·1
0
20
40
60
80
100
First Pressure in Curve-fit ; P_f, bar .
167·7K
181·9 K
218·9 K
248·5 K
263·1 K
263·1 K
248·5K
218·9 K
181·9 K
167·7 K

FIGURE 3.6

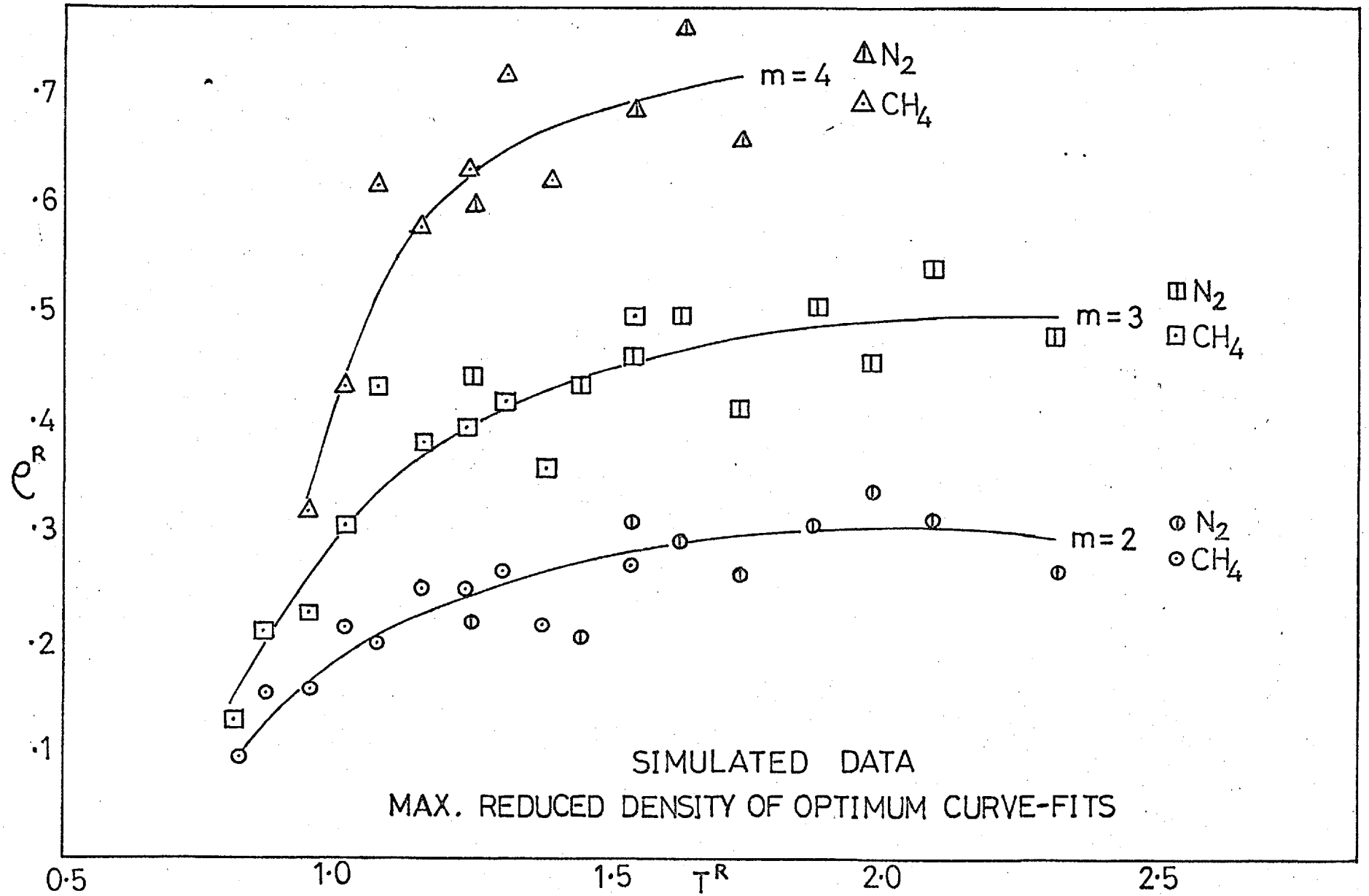
m = 4
N2
CH4
m = 3
N2
CH4
m = 2
N2
CH4
·7
·6
·5
·4
·3
·2
·1
ρR
0·5
1·0
1·5
TR
2·0
2·5
SIMULATED DATA
MAX. REDUCED DENSITY OF OPTIMUM CURVE-FITS

temperature. This offers a convenient means of interpolating the results of this program to other temperatures in this region and of extrapolation of the results to methane/ nitrogen mixtures.

(e) Weighting Factors

Several simulated runs were retreated using weighting factors that were inconsistent with the known applied error distribution. It was found that for a given set of simulated 'experimental' pressures, the results of curve-fitting were very similar when weighting factors were calculated according to equations (3.4-8) - (3.4-10) with $\gamma = 10^{-5}$ and $\epsilon = 0.0$ to .0004 bar. Only when the higher pressures were weighted much too highly (e.g. $\gamma = 0$, $\epsilon = .0004$ bar) were the results significantly worse than those in which correct weighting factors were employed.

(f) Comparison with the experimental data

In Chapter 4, Tables 4.1 - 4.7, the results are presented of the treatment of the experimental data from this investigation; the lay-out of the Tables is explained in section 4.1. By comparing the results from the various curve-fits with those from the simulated data, the optimum curve-fits were selected. In nearly all runs the results showed a pattern that was reproduced by the simulated runs, and in enabling the optimum B, C and compressibility factors to be determined the use of simulated data proved invaluable.

For some of the experimental runs at the higher reduced temperatures the maximum density was less than the optimum for m = 4; for these runs only m = 2 and m = 3 curve-fits

need be considered. This is probably also true for those runs well below the critical temperature, such as the 167.7 K (run 35) and 155.9 K (run 36) isotherms for methane, where the saturation vapour pressure limited the maximum density and hence the number of expansions.

Some of the runs at $T^R > 1.3$ show the absence of any substantial random or systematic errors, such as run 13 (nitrogen 218.9 K) and run 19 (methane 263.1 K). In these runs excellent agreement is shown between the optimum curve-fits and those in pressure ranges narrower than the optimum ranges. Many other runs show clearly the increase in the standard deviations as the range $P_r - P_n$ is narrowed, owing to random experimental errors, e.g. run 14 (nitrogen 218.9 K) and run 24 (methane 234.1 K).

Other runs show the presence of systematic errors. An example is run 30 (nitrogen 192.6 K). For the m = 2 fits as the range is decreased below the optimum (P2 - P8), the change in B (A(1)) is large compared with the standard deviation and is much larger than that due to isotherm curvature.

It has been suggested (23) that a simple method of determining the correct value of m for a given pressure range would be to increase m until the residuals were distributed in a random manner. Further increase in m would result in larger parameter standard deviations. However, it is very difficult to disentangle the two separate effects on the residuals of systematic experimental error on the one hand and an insufficient value of m on the other. Furthermore, if the pressure-range were large this procedure, although

leading possibly to the correct m for that range, would not necessarily provide the best estimates of B and C.

In a recent publication, Waxman, Hastings and Chen (30) compared various rigorously defined methods of non-linear analysis (not including Method A), testing them on experimental argon data. As these authors realised, the results were model dependent, and a comparison of this sort does not give any real information on the accuracy of the methods as the 'right' answer was unknown: simulated data must be used. The investigation of simulated data presented here goes some way towards answering some of the questions posed by Waxman et al.

(g) The Magnitude of the Apparatus Constant

This program was developed mainly for the study of the specific set of simulated data relevant to the experimental data, i.e. methane, nitrogen and their mixtures in a non-isothermal Burnett apparatus with a particular fixed apparatus constant, $(V_A + V_B)/V_A$. The program has also been modified easily into a more general form, in which it can be used to study a range of gases in any Burnett apparatus, 'isothermal' or 'non-isothermal', with a variable apparatus constant, over a wide range of temperature and pressure. In this form it is more suitable for design applications, particularly with regard to the selection of the magnitude of the apparatus constant and pressure range for a set of proposed experiments.

Weir (31) has shown that for a low-pressure (< 1 atmosphere) non-isothermal Burnett apparatus, the error expected in B

depends on the magnitude of the non-isothermal apparatus constant,

$$N' = \frac{V_A + V_B \cdot \frac{T_A}{T_B}}{V_A} \qquad (3.4\text{-}15)$$

For a fixed initial pressure, σ_B^2 exhibits a minimum as N' varies. This behaviour can be explained qualitatively: when N' is too large, there are insufficient points on the isotherm and σ_B^2 increases because of the $(n - m)^{-1}$ term in the equation for σ_B^2 (equation (3.2-27)); when N' is too small, $P_j/P_{j-1} \longrightarrow 1$ and $Z_j/Z_{j-1} \longrightarrow 1$, and obviously in the limit when N' = 1, i.e. $V_B = 0$, no information is gained. The best value of N' changes according to the temperature T_A and the maximum pressure, P_o.

For these reasons the expansion vessel of the present apparatus was supplied with four interchangeable inner volumes, of sizes selected on the basis of the calculations of Weir. However, the analysis in the case of a high-pressure Burnett apparatus is further complicated by the necessity of including the higher virial coefficients and by the fact that the maximum pressure for a fixed value of m varies with temperature.

Several simulated runs for methane were therefore investigated in order to determine the variation of the experimental results with N'. The value of ΔB for the optimum curve-fit passed through a shallow minimum at $N' \simeq 1.6$ when $T > 210$ K. As long as $1.4 < N' < 1.7$ the results were satisfactory; this is in agreement with the calculations of Weir. Below T^c the value of N' required to

give maximum accuracy decreased: more expansions were required because the first pressure of each run was limited by the saturation vapour pressure.

The volumes used for all the experimental runs were,

$V_A \simeq 360$ cc

$V_B \simeq 280$ cc.

These gave the following values of N':

273 K : N' = 1.78

210 K : N' = 1.6

155.9 K : N' = 1.4

These values are such that N' was the best from the choice available except perhaps at 291.4 K and below 170 K for methane, where N' was just too large. A smaller expansion volume leading to more measurements would have provided marginally improved accuracy for these few runs. On purely practical grounds the size of the expansion vessel was not changed, as it would probably have led to a new set of leakage problems that would have to be overcome.

CHAPTER FOUR

EXPERIMENTAL DATA

4.1 Experimental results of this investigation

Compressibility factors and second and third virial coefficients of methane, nitrogen, two methane/nitrogen mixtures and three multi-component mixtures have been measured at temperatures from 291.4 K to 155.9 K. The results are presented in Tables 4.1 to 4.7. Compositions of the mixtures have already been given in Table 2.4.

On the bottom half of each page are shown the results for several of the least-squares curve fits; at the top of each column is the number of coefficients used in the density polynomial series, m, and the pressure range included in the fit, $P_r - P_n$. Each coefficient A(K) is given together with its standard deviation, SD, in units of $(cc/mole)^k$. Thus A(1) refers to the least-squares estimate of the second virial coefficient, B, and A(2) refers to the third virial coefficient, C. V(A) refers to the estimate of the volume of the pressure vessel, which was the (m+1) th. least-squares parameter.

At the top of the page the overall optimum compressibility factors are given, selected by comparing the results with the results of treatment of the simulated data as described in Chapter 3. The densities shown were obtained from the experimental compressibility factors by using the experimental absolute temperature, T,

$$\rho = \frac{P}{RTZ} \qquad (4.1\text{-}1)$$

where $R = 83.147$ bar.cc.mole^{-1}.K^{-1}.

The compressibility factors are, to the first order of accuracy, independent of the value assumed for R and T.

The estimated maximum errors include those due to experimental errors in pressure, both random and systematic, and the uncertainties introduced by the truncation of the virial series. These are necessarily larger than is superficially apparent from the standard deviations in the optimum curve-fit, for the reasons given in Chapter 3.

In addition, the total errors in the results must also take into account the effect of various systematic uncertainties introduced by the use of a 'non-isothermal' Burnett apparatus, which are discussed in section 4.3.

4.2 Experimental virial coefficients of this investigation

The experimental second and third virial coefficients of methane, nitrogen and the two methane/nitrogen mixtures are reproduced in Tables 4.8 and 4.9 together with the errors given in Tables 4.1 - 4.4. The total limits of error must also include those systematic errors discussed in section 4.3.

The interactional second virial coefficient of a binary mixture, B_{12}, is given by

$$B_{mix} = x_1^2 B_{11} + 2x_1x_2B_{12} + x_2^2 B_{22} \qquad (4.2\text{-}1)$$

where B_{mix} is the second virial coefficient of the mixture with mole fraction x_1 of methane and x_2 of nitrogen. In Table 4.9 are shown the values of B_{12} calculated from (4.2-1) for each mixture, with their associated errors, using the pure component second virial coefficients of Table 4.8. It can be seen that there are no systematic differences between

the two sets of values; the mean was adopted for use later in this study, in Chapter 5.

The interactional third virial coefficients C_{112} and C_{221} are similarly given by

$$C_{mix} = x_1^3 C_{111} + 3x_1^2 x_2 C_{112} + 3x_2^2 x_1 C_{221} + x_2^3 C_{222} \quad (4.2\text{-}2)$$

From the results for the two mixtures at each temperature the two equations of the above form were solved to obtain estimates of C_{112} (methane-methane-nitrogen) and C_{221} (nitrogen-nitrogen-methane). These are shown in Table 4.9 together with their associated errors.

4.3 Total Error Analysis

(a) The Equation of State at 0 °C.

The largest systematic errors present are usually caused by the uncertainties in the equation of state assumed for the gas in the ice-bath.

For each gas studied a four-coefficient polynomial in density was assumed,

$$P/RT\rho = Z^o = (1 + a_1^o\rho + a_2^o\rho^2 + a_3^o\rho^3 + a_4^o\rho^4) \quad (4.3\text{-}1)$$

a_1^o is the second virial coefficient at 0 °C

a_2^o is the third virial coefficient at 0 °C, etc.

The values used are given in Table 4.10. For methane they are the coefficients of Douslin et al (32) (see section 4.4(c)), which reproduce Z^o to within 0.0001 up to 100 bar. The error in B^o is estimated as $\pm .1$ $cm^3.mole^{-1}$ and in C^o as $\pm$ 75 $cm^6.mole^{-2}$. For nitrogen, the coefficients are those

obtained by re-treating graphically the data of Michels et al (33) (see section 4.4(d)). They reproduce both the Michels compressibility factors and those of Crain and Sonntag (34) to within .0002 up to 100 bar. The error in B^o is estimated as $\pm$ .2 $cm^3.mole^{-1}$ and in C as $\pm$ 150 $cm^6.mole^{-2}$.

For methane/nitrogen mixtures the second and third virial coefficients at 0 °C were obtained from an interpolation of the results of this investigation. Each set of mixture raw data was re-treated two or three times, each time re-adjusting the 0 °C equation of state, until the virial coefficients at 0 °C were consistent with the interpolated values. B^o is estimated as accurate to $\pm$ 0.4 $cm^3.mole^{-1}$, about half of which is due to the errors in interpolation, and C^o is estimated as accurate to $\pm$ 200 $cm^3.mole^{-1}$. In retrospect, additional accuracy could have been gained by carrying out runs at, or close to, 0 °C. The higher coefficients were chosen such that Z^o at the higher pressures agreed well with the values interpolated from the results at other temperatures. A double interpolation in both temperature and pressure was necessary. Z^o at 96 bars was estimated as accurate to $\pm$ .0007.

For the multicomponent mixtures runs were carried out either at or very near to 0 °C and any interpolation necessary was small. Z^o at 100 bar was estimated as accurate to $\pm$ .001.

To determine the effect of errors in the 0 °C equation of state on the experimental results, several runs were re-processed (methane and nitrogen at 291.4, 248.5, 218.9, 181.9 and 155.9 K). Both B^o and C^o were subjected in turn

to a 1% increment, resulting in small changes in the experimental B(T) and C(T) values. In Table 4.11 are presented the resultant derivatives, $\partial B(T)/\partial B^{o}$, $\partial C(T)/\partial B^{o}$, $\partial B(T)/\partial C^{o}$ and $\partial C(T)/\partial C^{o}$. These values were very similar for both methane and nitrogen. Also shown are the maximum uncertainties, $\delta B(T)$ and $\delta C(T)$, in B(T) and C(T) arising from the estimated maximum errors in B^{o} and C^{o} for methane, nitrogen and both binary mixtures.

The derivatives $\partial Z(T,P)/\partial B^{o}$ and $\partial Z(T,P)/\partial C^{o}$, shown in figure 4.1, were found to be virtually independent of temperature and were smooth functions of pressure. If different, more accurate values of B^{o} and C^{o} become accepted figure 4.1 may be used to apply the necessary small corrections to Z(T,P); it is emphasized that both curves of figure 4.1 must be used in conjunction with one another. Any small change in $Z^{o}(P_j)$ leads to a small change in all Z(T) values, but it was found that the quantity $\delta Z(T,P_j)/\delta Z^{o}(P_j)$ was approximately constant for each isotherm, the values ranging from 0.15 to about 0.3. For example, an uncertainty in Z^{o} at 0 °C, 100 bars of .0005 leads to an error in Z(T) at 100 bars of between .00008 and .00015. In Table 4.12 are listed the maximum errors in Z for each run arising from the estimated uncertainties in Z^{o}.

(b) Other Systematic Errors

Errors in other variables which are independent of pressure, such as the volumes and temperatures of the dead-spaces, will tend to have an effect on the experimental second virial coefficients. Those errors which increase with

pressure, however, such as those in the dead-space compressibility factors, tend to have a small effect on B(T) but can lead to relatively larger errors in the high-pressure compressibility factors. The equations for use in calculating Z in the inlet-tubes and other dead-spaces were found by fitting four-coefficient polynomials in density to the data of Tables 4.1 - 4.7. The errors in these equations were found to have an insignificant effect on the results.

Only two errors could lead to a maximum error in B(T) of more than .005 $cm^3.mole^{-1}$ or to a maximum error in Z(T,P) of more than .00005; firstly, uncertainties in V3, the largest section of the dead-space volume; secondly, uncertainties in T6, the ice-bath vessel temperature. The maximum value of $\partial B(T)/\partial V3$ is 0.7: therefore the estimated uncertainty in V3 of .015 cc leads to an error in B(T) of .01 cc/mole. The maximum value of $\partial B(T)/\partial T6$ is 0.25: therefore the estimated uncertainty in T6 of .02 K leads to an error in B(T) of less than .01 cc/mole. These are both negligible.

(c) Adsorption

It is known that adsorption of gas on the walls of the containing vessel can be a serious problem in Burnett measurements at temperatures below the critical temperature. In the design of the vessel, an effort was made to ensure that the interior surfaces were clean and highly polished in order to reduce the possibility of adsorption.

There are two reasons for the belief that the effect of

adsorption was insignificant in this investigation. Firstly, the results of the curve-fitting to each low-temperature run, particularly the magnitudes of the standard deviations, were consistent with the errors expected in experimental pressure. Serious adsorption could be expected to result in much larger standard deviations and also much larger apparent curvature on the isotherms. Secondly, the effect of adsorption would tend to manifest itself as a change in the expected value of V1, the volume of the low-temperature pressure vessel (35). In figure 4.2 these volumes are plotted against temperature. There are no systematic differences between the values obtained for different gases: they all deviate from a smooth, nearly linear function of temperature by less than .1 cm^3 (.03%). The differences at low temperature are within the expected errors inherent in the curve-fitting procedure. In treatment of simulated data it was found that if the derived least-squares value of V1 was in error by 0.1 cm^3 then it was usually accompanied by errors in B of about 0.2 to 0.3 $cm^3.mole^{-1}$, in C of about 100 - 150 $cm^6.mole^{-2}$ and in $Z(T,P_o)$ of from .0002 to .0003.

As already mentioned in Chapter 1, the design of the 'non-isothermal' apparatus is such that errors due to adsorption are less than in the standard 'isothermal' apparatus. In the latter it can be shown that as the gas adsorbs in both V_A and V_B at low temperature the errors due to adsorption are accumulative (35).

TABLE 4.1
EXPERIMENTAL DATA FOR METHANE

RUN 23 291.41 K

PRESSURE LB./SQ.IN.	PRESSURE BAR	Z = PV/RT (OPTIMUM)	DENSITY MOLE/CC.10^3	LEAST-SQUARES FIT
1448.752	99.8880	.8364	4.9284	M=3 , P0-P6
837.073	57.7141	.89670	2.6563	
476.307	32.8402	.93954	1.4426	
266.916	18.4032	.96576	0.78647	M=2 , P1-P6
148.105	10.2115	.98091	0.42966	
81.698	5.6329	.98945	0.23496	
44.917	3.0969	.99419	0.12857	

OPTIMUM COEFFICIENTS		ESTIMATED ERRORS (MAX.)	OPTIMUM FIT
B, CC/MOLE =	-45.50	.15	M=2
C, CC/MOLE^2 =	2489	100	P1-P6
V(A), CC =	361.18	.05	
		Z .0002	

RESULTS OF NON-LINEAR LEAST-SQUARES ANALYSIS

	M=2 P0-P6	M=2 P1-P6	M=2 P2-P6	M=3 P0-P6	M=3 P1-P6	M=4 P0-P6
V(A)	361.158	361.182	361.148	361.186	361.140	361.134
SD	.016	.015	.010	.024	.017	.030
A(1)	-45.579	-45.500	-45.674	-45.471	-45.755	-45.816
SD	.024	.040	.043	.079	.094	.179
A(2)	2512.4	2489.3	2574.0	2464.2	2679.4	2773.1
SD	3.9	11.1	20.2	33.8	68.5	156.2
A(3)				.58 $\cdot 10^4$	-4.0 $\cdot 10^4$	-9.6 $\cdot 10^4$
SD				.40 $\cdot 10^4$	1.4 $\cdot 10^4$	5.1 $\cdot 10^4$
A(4)						10.6 $\cdot 10^6$
SD						5.3 $\cdot 10^6$
Z(0)	.83638			.83645		.83633
Z(1)	.89665	.89670		.89671	.89660	.89659
Z(2)	.93947	.93954	.93946	.93955	.93944	.93943
Z(3)	.96571	.96576	.96567	.96577	.96565	.96564
Z(4)	.98088	.98091	.98085	.98092	.98083	.98082
Z(5)	.98943	.98945	.98941	.98945	.98940	.98939
Z(6)	.99418	.99419	.99417	.99419	.99416	.99416

TABLE 4.1
EXPERIMENTAL DATA FOR METHANE

RUN 19 263.08 K

PRESSURE LB./SQ.IN.	PRESSURE BAR	Z = PV/RT (OPTIMUM)	DENSITY MOLE/CC.10^3	LEAST-SQUARES FIT
1448.325	99.8586	.74800	6.1029	M=4 , P0-P6
- 928.850	64.0420	.82871	3.5328	M=3 , P1-P6
576.275	39.7328	.89286	2.03437	
346.771	23.9090	.93565	1.16819	
204.455	14.0967	.96218	0.66978	M=2 , P2-P6
119.055	8.2086	.97803	0.38370	
68.818	4.7448	.98732	0.21970	

OPTIMUM COEFFICIENTS		ESTIMATED ERRORS (MAX.)	OPTIMUM FIT
B, CC/MOLE =	-58.34	.07	M=2
C, CC/MOLE^2 =	2788	50	P2-P6
V(A), CC =	360.74	.04	
		Z .0001	

RESULTS OF NON-LINEAR LEAST-SQUARES ANALYSIS

	M=2 P0-P6	M=2 P1-P6	M=2 P2-P6	M=3 P0-P6	M=3 P1-P6	M=4 P0-P6
V(A)	360.719	360.737	360.740	360.743	360.739	360.737
SD	.010	.005	.009	.008	.014	.022
A(1)	-58.390	-58.350	-58.339	-58.324	-58.339	-58.349
SD	.011	.010	.026	.019	.051	.091
A(2)	2800.8	2791.6	2787.8	2777.6	2785.9	2794.4
SD	1.5	2.1	8.9	6.4	27.7	59.6
A(3)				.22 $.10^4$	.09 $.10^4$	-0.2 $.10^4$
SD				.06 $.10^4$	.43 $.10^4$	1.5 $.10^4$
A(4)						0.3 $.10^6$
SD						1.2 $.10^6$
Z(0)	.74796			.74801		.74800
Z(1)	.82867	.82870		.82872	.82871	.82870
Z(2)	.89280	.89285	.89286	.89286	.89285	.89285
Z(3)	.93561	.93565	.93565	.93566	.93565	.93565
Z(4)	.96215	.96217	.96218	.96218	.96218	.96217
Z(5)	.97801	.97802	.97803	.97803	.97803	.97802
Z(6)	.98731	.98732	.98732	.98732	.98732	.98732

TABLE 4.1
EXPERIMENTAL DATA FOR METHANE

RUN 20 248.54 K

PRESSURE LB./SQ.IN.	PRESSURE BAR	Z = PV/RT (OPTIMUM)	DENSITY MOLE/CC.10^3	LEAST-SQUARES FIT
1439.944	99.2807	.68035	7.0612	M=4 , P0-P7
990.015	68.2592	.77032	4.2879	M=3 , P1-P7
652.848	45.0123	.84934	2.5645	
412.765	28.4592	.90591	1.5202	
253.367	17.4690	.94282	0.89660	M=2 , P2-P7
152.638	10.5240	.96578	0.52731	
90.915	6.2683	.97971	0.30962	
53.783	3.7082	.98803	0.18162	

OPTIMUM COEFFICIENTS		ESTIMATED ERRORS (MAX.)	OPTIMUM FIT
B, CC/MOLE =	-66.48	.10	M=2
C, CC/MOLE^2 =	3015	75	P2-P7
V(A), CC =	360.46	.04	
		Z .0001	

RESULTS OF NON-LINEAR LEAST-SQUARES ANALYSIS

	M=2 P1-P7	M=2 P2-P7	M=2 P3-P7	M=3 P0-P7	M=3 P1-P7	M=4 P0-P7
V(A)	360.473	360.463	360.452	360.456	360.458	360.460
SD	.006	.005	.005	.004	.005	.008
A(1)	-66.448	-66.479	-66.525	-66.510	-66.504	-66.505
SD	.008	.011	.018	.007	.017	.027
A(2)	3005.9	3015.2	3036.4	3035.2	3032.4	3032.2
SD	1.6	3.3	8.1	2.1	7.8	15.3
A(3)				$-0.38 \cdot 10^4$	$-0.35 \cdot 10^4$	$-0.3 \cdot 10^4$
SD				$.02 \cdot 10^4$	$.10 \cdot 10^4$	$.3 \cdot 10^4$
A(4)						$-0.0 \cdot 10^6$
SD						$.2 \cdot 10^6$
Z(0)				.68035		.68035
Z(1)	.77035			.77032	.77032	.77032
Z(2)	.84936	.84934		.84933	.84933	.84933
Z(3)	.90593	.90591	.90588	.90589	.90590	.90589
Z(4)	.94284	.94282	.94279	.94280	.94281	.94281
Z(5)	.96580	.96578	.96576	.96577	.96577	.96577
Z(6)	.97971	.97971	.97969	.97970	.97970	.97970
Z(7)	.98803	.98803	.98802	.98802	.98802	.98802

TABLE 4.1

EXPERIMENTAL DATA FOR METHANE

RUN 24 234.05 K

PRESSURE LB./SQ.IN.	PRESSURE BAR	Z = PV/RT (OPTIMUM)	DENSITY MOLE/CC.10^3	LEAST-SQUARES FIT
1144.975	78.9432	.65574	6.1862	M=4 , P0-P7
832.275	57.3834	.75334	3.9142	M=3 , P1-P7
571.661	39.4146	.83539	2.4245	
374.357	25.8110	.89475	1.4824	
237.212	16.3552	.93441	0.89945	M=2 , P2-P7
147.166	10.1467	.95974	0.54328	
90.115	6.2132	.97551	0.32730	
54.739	3.7741	.98519	0.19686	

OPTIMUM COEFFICIENTS		ESTIMATED ERRORS (MAX.)	OPTIMUM FIT
B, CC/MOLE =	-75.89	.15	M=2
C, CC/MOLE^2 =	3299	100	P2-P7
V(A), CC =	360.20	.05	
		Z .0001	

RESULTS OF NON-LINEAR LEAST-SQUARES ANALYSIS

	M=2 P1-P7	M=2 P2-P7	M=2 P3-P7	M=3 P0-P7	M=3 P1-P7	M=4 P0-P7
V(A)	360.230	360.202	360.224	360.192	360.193	360.195
SD	.018	.020	.032	.019	.030	.043
A(1)	-75.811	-75.894	-75.799	-75.951	-75.949	-75.941
SD	.029	.049	.120	.041	.098	.161
A(2)	3272.0	3298.5	3254.2	3343.1	3341.8	3336.2
SD	5.9	14.9	54.4	13.7	48.0	98.7
A(3)				-0.99×10^4	-1.0×10^4	-0.8×10^4
SD				$.12 \times 10^4$	$.7 \times 10^4$	2.2×10^4
A(4)						-0.1×10^6
SD						1.7×10^6
Z(0)				.65574		.65574
Z(1)	.75341			.75333	.75334	.75334
Z(2)	.83544	.83539		.83536	.83536	.83537
Z(3)	.89482	.89475	.89479	.89472	.89473	.89473
Z(4)	.93445	.93441	.93446	.93438	.93438	.93439
Z(5)	.95978	.95974	.95978	.95972	.95972	.95972
Z(6)	.97554	.97551	.97554	.97550	.97550	.97550
Z(7)	.98520	.98519	.98520	.98518	.98518	.98518

TABLE 4.1
EXPERIMENTAL DATA FOR METHANE

RUN 21 218.87 K

PRESSURE LB./SQ.IN.	PRESSURE BAR	Z = PV/RT (OPTIMUM)	DENSITY MOLE/CC.10^3	LEAST-SQUARES FIT
1406.197	96.9539	.4610	11.555	M=6 , P0-P9
1139.705	78.5799	.5220	8.271	M=5 , P1-P9
930.215	64.1361	.6201	5.6837	M=4 , P2-P9
717.510	49.4706	.7226	3.7622	M=3 , P3-P9
517.933	35.7102	.8096	2.4238	
354.220	24.4226	.8746	1.5344	
233.244	16.0816	.9195	0.96103	
149.806	10.3287	.9492	0.59797	M=2 , P4-P9
94.705	6.5297	.96818	0.37060	
59.278	4.0871	.98022	0.22912	

OPTIMUM COEFFICIENTS		ESTIMATED ERRORS (MAX.)	OPTIMUM FIT
B, CC/MOLE^2 =	-87.16	.30	M=2
C, CC/MOLE^2 =	3551	200	P4-P9
V(A), CC =	360.03	.08	
		Z .0005	

RESULTS OF NON-LINEAR LEAST-SQUARES ANALYSIS

	M=2 P3-P9	M=2 P4-P9	M=2 P5-P9	M=3 P2-P9	M=3 P3-P9	M=3 P4-P9
V(A)	359.974	360.029	360.063	359.976	360.060	360.077
SD	.021	.011	.009	.031	.010	.016
A(1)	-87.315	-87.161	-87.027	-87.321	-87.014	-86.927
SD	.033	.026	.029	.066	.031	.072
A(2)	3600.6	3551.2	3490.4	3607.8	3446.2	3381.8
SD	7.1	7.8	12.9	23.1	15.6	51.2
A(3)				$-.15 \cdot 10^4$	$2.2 \cdot 10^4$	$3.6 \cdot 10^4$
SD				$.21 \cdot 10^4$	$0.2 \cdot 10^4$	$1.1 \cdot 10^4$
Z(0)						
Z(1)						
Z(2)				.61989		
Z(3)	.72242			.72242	.72258	
Z(4)	.80950	.80960		.80950	.80966	.80970
Z(5)	.87448	.87462	.87469	.87448	.87468	.87472
Z(6)	.91940	.91951	.91959	.91940	.91958	.91962
Z(7)	.94907	.94915	.94921	.94907	.94921	.94924
Z(8)	.96813	.96818	.96823	.96813	.96823	.96825
Z(9)	.98018	.98022	.98024	.98018	.98024	.98026

TABLE 4.1

RUN 21 218.87 K (CONTINUED)

RESULTS OF NON-LINEAR LEAST-SQUARES ANALYSIS

	M=4 P1-P9	M=4 P2-P9	M=4 P3-P9	M=5 P1-P9	M=5 P2-P9	M=6 P0-P9
V(A)	360.046	360.086	360.079	360.093	360.075	360.104
SD		30 2	.023	.017	.030	.038
A(1)	-87.034	-86.867	-86.905	-86.821	-86.933	-86.770
SD	.043	.045	.120	.072	.171	.201
A(2)	3422.8	3311.9	3347.6	3263.7	3379.9	3224.7
SD	19.3	28.5	106.3	53.8	171.8	226.9
A(3)	$4.2\ .10^{4}$	$6.9\ .10^{4}$	$5.6\ .10^{4}$	$9.1\ .10^{4}$	$3.8\ .10^{4}$	$10.\ .10^{4}$
SD	$.3\ .10^{4}$	$.7\ .10^{4}$	$3.7\ .10^{4}$	$1.7\ .10^{4}$	$7.5\ .10^{4}$	$7.\ .10^{4}$
A(4)	$-3.4\ .10^{6}$	$-5.6\ .10^{6}$	$-4.1\ .10^{6}$	$-9.9\ .10^{6}$	$.3\ .10^{6}$	$-11.6.10^{6}$
SD	$.2\ .10^{6}$	$.6\ .10^{6}$	$4.4\ .10^{6}$	$.2\ .10^{6}$	$15\ .10^{6}$	$3.5\ .10^{6}$
A(5)				$3.1\ .10^{8}$	$-4\ .10^{8}$	$4.3\ .10^{8}$
SD				$1.3\ .10^{8}$	$-10.\ 10^{8}$	$3.9\ .10^{8}$
A(6)						$-5\ .10^{10}$
SD						$10\ .10^{10}$
Z(0)						.46106
Z(1)	.52198			.52205		.52207
Z(2)	.62001	.62008		.62009	.62006	.62011
Z(3)	.72255	.72263	.72262	.72265	.72261	.72267
Z(4)	.80964	.80972	.80971	.80974	.80970	.80976
Z(5)	.87465	.87474	.87472	.87475	.87472	.87478
Z(6)	.91955	.91964	.91963	.91966	.91962	.91968
Z(7)	.94919	.94926	.94924	.94927	.94924	.94929
Z(8)	.96822	.96827	.96826	.96828	.96825	.96829
Z(9)	.98024	.98027	.98026	.98028	.98028	.98029

TABLE 4.1
EXPERIMENTAL DATA FOR METHANE

RUN 22 204.60 K

PRESSURE LB./SQ.IN.	PRESSURE BAR	Z = PV/RT (OPTIMUM)	DENSITY MOLE/CC.10^3	LEAST-SQUARES FIT
993.587	68.5054	.3728	10.801	M=5 , P0-P10
904.313	62.3502	.4419	8.2937	
807.900	55.7027	.5377	6.0890	M=4 , P2-P10
679.785	46.8695	.6441	4.2772	
531.259	36.6290	.7429	2.8985	M=3 , P3-P10
388.711	26.8007	.8226	1.9151	
270.648	18.6605	.8815	1.2444	
182.093	12.5549	.9224	0.80012	M=2 , P5-P10
119.751	8.2566	.9499	0.51097	
77.601	5.3504	.9679	0.32496	
49.813	3.4345	.9795	0.20611	

OPTIMUM COEFFICIENTS		ESTIMATED ERRORS (MAX.)	OPTIMUM FIT
B, CC/MOLE =	-100.14	.25	M=2
C, CC/MOLE^2 =	3928	150	P5-P10
V(A), CC =	359.72	.07	
		Z .0005	

RESULTS OF NON-LINEAR LEAST-SQUARES ANALYSIS

	M=2 P3-P10	M=2 P4-P10	M=2 P5-P10	M=3 P2-P10	M=3 P3-P10	M=3 P4-P10
V(A)	359.624	359.687	359.723	359.649	359.729	359.756
SD	.031	.024	.031	.035	.027	.040
A(1)	-100.41	-100.26	-100.14	-100.34	-100.09	- 99.97
SD	.04	.05	.09	.06	.07	.15
A(2)	4018	3975	3928	3990	3866	3790
SD	8	12	33	20	31	95
A(3)				$.32 .10^4$	$1.9 .10^4$	$3.3 .10^4$
SD				$.15 .10^4$	$.4 .10^4$	$1.6 .10^4$
Z(0)						
Z(1)						
Z(2)				.53756		
Z(3)	.64396			.64400	.64414	
Z(4)	.74266	.74277		.74272	.74285	.74290
Z(5)	.82239	.82256	.82263	.82245	.82264	.82270
Z(6)	.88124	.88138	.88146	.88129	.88148	.88154
Z(7)	.92222	.92232	.92239	.92226	.92241	.92246
Z(8)	.94974	.94981	.94986	.94977	.94987	.94992
Z(9)	.96779	.96784	.96787	.96781	.96789	.96792
Z(0)	.97947	.97950	.97953	.97949	.97954	.97956

TABLE 4.1

RUN 22 204.60 K (CONTINUED)

RESULTS OF NON-LINEAR LEAST-SQUARES ANALYSIS

	M=4 P1-P10	M=4 P2-P10	M=5 P0-P10	M=5 P1-P10
V(A)	359.814	359.761	359.751	359.787
SD	.029	.033	.045	.067
A(1)	-99.73	-99.93	-99.99	-99.78
SD	.06	.11	.17	.34
A(2)	3618	3740	3800	3605
SD	26	64	118	316
A(3)	$8.3 \cdot 10^4$	$5.7 \cdot 10^4$	$3.2 \cdot 10^4$	$11 \cdot 10^4$
SD	$.4 \cdot 10^4$	$1.4 \cdot 10^4$	$.3 \cdot 10^4$	$12 \cdot 10^4$
A(4)	$-5.8 \cdot 10^6$	$-3.9 \cdot 10^6$	$0.6 \cdot 10^6$	$-13 \cdot 10^6$
SD	$.2 \cdot 10^6$	$1.1 \cdot 10^6$	$4.4 \cdot 10^6$	$23 \cdot 10^6$
A(5)			$-2.9 \cdot 10^8$	$6 \cdot 10^8$
SD			$1.9 \cdot 10^8$	$15 \cdot 10^8$
Z(0)			.37277	
Z(1)	.44198		.44191	.44195
Z(2)	.53780	.53773	.53771	.53776
Z(3)	.64429	.64420	.64418	.64424
Z(4)	.74300	.74291	.74289	.74296
Z(5)	.82283	.82271	.82269	.82276
Z(6)	.88167	.88155	.88153	.88161
Z(7)	.92258	.92248	.92245	.92253
Z(8)	.95000	.94993	.94991	.94997
Z(9)	.96798	.96793	.96791	.96796
Z(0)	.97960	.97956	.97955	.97959

TABLE 4.1
EXPERIMENTAL DATA FOR METHANE

RUN 33 192.64 K

PRESSURE LB./SQ.IN.	PRESSURE BAR	Z = PV/RT (OPTIMUM)	DENSITY MOLE/CC.10^3	LEAST-SQUARES FIT
662.282	45.6627	.4909	5.8064	M=5 , P0-P9
590.581	40.7192	.5976	4.2539	M=4 , P1-P9
487.367	33.6028	.7000	2.9967	M=3 , P2-P9
374.587	25.8269	.7864	2.0502	
272.320	18.7758	.8529	1.3743	
190.233	13.1161	.9009	0.9089	
129.316	8.9160	.9343	0.59580	M=2 , P3-P9
86.320	5.9515	.9568	0.38833	
56.936	3.9256	.9718	0.25219	
37.257	2.5688	.9817	0.16337	

OPTIMUM COEFFICIENTS		ESTIMATED ERRORS (MAX.)	OPTIMUM FIT
B, CC/MOLE =	-112.83	.25	M=2
C, CC/MOLE^2 =	4227	150	P3-P9
V(A), CC =	359.43	.07	
		Z .0003	

RESULTS OF NON-LINEAR LEAST-SQUARES ANALYSIS

	M=2 P2-P9	M=2 P3-P9	M=2 P4-P9	M=3 P1-P9	M=3 P2-P9	M=3 P3-P9
V(A)	359.371	359.433	359.430	359.473	359.464	359.416
SD	.026	.034	.053	.035	.052	.049
A(1)	-113.03	-112.83	-112.85	-112.60	-112.64	-112.92
SD	.07	.09	.20	.09	.19	.30
A(2)	4305	4227	4235	4034	4059	4306
SD	18	33	101	39	114	236
A(3)				4.7 $.10^4$	4.2 $.10^4$	-1.9 $.10^4$
SD				.4 $.10^4$	1.9 $.10^4$	5.0 $.10^4$
Z(0)						
Z(1)				.59763		
Z(2)	.69987			.70006	.70004	
Z(3)	.78633	.78644		.78652	.78650	.78641
Z(4)	.85276	.85292	.85291	.85300	.85298	.85288
Z(5)	.90081	.90094	.90093	.90103	.90102	.90090
Z(6)	.93418	.93428	.93427	.93436	.93434	.93424
Z(7)	.95675	.95682	.95682	.95689	.95688	.95680
Z(8)	.97177	.97181	.97181	.97186	.97185	.97180
Z(9)	.98165	.98168	.98168	.98171	.98171	.98167

TABLE 4.1

RUN 33 192.64 K (CONTINUED)

RESULTS OF NON-LINEAR LEAST-SQUARES ANALYSIS

	M=4 P1-P9	M=5 P0-P9
V(A)	359.453	359.438
SD	.065	.082
A(1)	-112.70	-112.82
SD	.24	.38
A(2)	4117	4258
SD	162	321
A(3)	$2.2 \cdot 10^4$	$-5.3 \cdot 10^4$
SD	$4.1 \cdot 10^4$	$11. \cdot 10^4$
A(4)	$2.5 \cdot 10^6$	$20.9 \cdot 10^6$
SD	$3.9 \cdot 10^6$	$14.4 \cdot 10^6$
A(5)		$-16. \cdot 10^8$
SD		$5. \cdot 10^8$
Z(0)		.49094
Z(1)	.59760	.59758
Z(2)	.70002	.70000
Z(3)	.78648	.78645
Z(4)	.85296	.85292
Z(5)	.90099	.90095
Z(6)	.93432	.93429
Z(7)	.95686	.95683
Z(8)	.97184	.97182
Z(9)	.98170	.98168

TABLE 4.1
EXPERIMENTAL DATA FOR METHANE

RUN 34 181.86 K

PRESSURE LB./SQ.IN.	PRESSURE BAR	Z = PV/RT (OPTIMUM)	DENSITY MOLE/CC.10^3	LEAST-SQUARES FIT
443.593	30.5847	.6518	3.1033	M=4 , P0-P7
358.884	24.7442	.7445	2.1981	M=3 , P1-P7
272.983	18.8215	.8187	1.5203	
198.338	13.6749	.8746	1.0341	
139.513	9.6191	.9146	0.69551	M=2 , P2-P7
95.982	6.6177	.9426	0.46432	
65.054	4.4853	.9616	0.30846	
43.653	3.0098	.9745	0.20425	

OPTIMUM COEFFICIENTS		ESTIMATED ERRORS (MAX.)	OPTIMUM FIT
B, CC/MOLE	= -125.71	.30	M=2
C, CC/MOLE^2	= 4256	200	P2-P7
V(A), CC	= 359.39	.07	
		Z .0003	

RESULTS OF NON-LINEAR LEAST-SQUARES ANALYSIS

	M=2 P1-P7	M=2 P2-P7	M=2 P3-P7	M=3 P0-P7	M=3 P1-P7	M=4 P0-P7
V(A)	359.314	359.386	359.419	359.426	359.437	359.442
SD	.032	.014	.014	.011	.016	.028
A(1)	-125.98	-125.71	-125.54	-125.43	-125.38	-125.34
SD	.08	.05	.07	.04	.07	.14
A(2)	4390	4256	4149	3959	3912	3867
SD	26	21	40	20	53	137
A(3)				$9.6 \cdot 10^4$	$10.7 \cdot 10^4$	$13.2 \cdot 10^4$
SD				$.3 \cdot 10^4$	$1.2 \cdot 10^4$	$5.3 \cdot 10^4$
A(4)						$-4.8 \cdot 10^6$
SD						$7.3 \cdot 10^6$
Z(0)				.65174		.65176
Z(1)	.74421			.74442	.74445	.74445
Z(2)	.81858	.81872		.81881	.81883	.81884
Z(3)	.87440	.87456	.87463	.87464	.87467	.87468
Z(4)	.91449	.91463	.91470	.91471	.91474	.91475
Z(5)	.94244	.94255	.94261	.94263	.94264	.94265
Z(6)	.96155	.96163	.96167	.96169	.96170	.96171
Z(7)	.97445	.97450	.97453	.97455	.97456	.97456

TABLE 4.1
EXPERIMENTAL DATA FOR METHANE

RUN 35 167.67 K

PRESSURE LB./SQ.IN.	PRESSURE BAR	Z = PV/RT (OPTIMUM)	DENSITY MOLE/CC.10^3	LEAST-SQUARES FIT
298.822	20.6031	.7151	2.0667	M=3 , P0-P6
237.158	16.3515	.7922	1.4805	
179.424	12.3709	.8519	1.0417	
131.116	9.0401	.8962	0.7236	M=2 , P1-P6
93.504	6.4469	.9280	0.4983	
65.555	4.5199	.9505	0.34112	
45.425	3.1319	.9662	0.23250	

OPTIMUM COEFFICIENTS		ESTIMATED ERRORS (MAX.)	OPTIMUM FIT
B, CC/MOLE =	-146.54	.40	M=2
C, CC/MOLE^2 =	4187	300	P1-P6
V(A), CC =	359.24	.10	
		Z .0004	

RESULTS OF NON-LINEAR LEAST-SQUARES ANALYSIS

	M=2 P0-P6	M=2 P1-P6	M=3 P0-P6	M=0 P0-P6	M=0 P0-P6	M=0 P0-P6
V(A)	359.19	359.24	359.23			
SD	.06	.08	.16			
A(1)	-146.71	-146.54	-146.51			
SD	.13	.25	.69			
A(2)	4272	4187	4105			
SD	51	123	551			
A(3)			3.9 .10^4			
SD			12. .10^4			
Z(0)	.71501		.71509			
Z(1)	.79213	.79222	.79221			
Z(2)	.85180	.85190	.85189			
Z(3)	.89607	.89615	.89615			
Z(4)	.92795	.92802	.92802			
Z(5)	.95045	.95050	.95051			
Z(6)	.96611	.96615	.96616			

TABLE 4.1
EXPERIMENTAL DATA FOR METHANE

RUN 36 155.89 K

PRESSURE LB./SQ.IN.	PRESSURE BAR	Z = PV/RT (OPTIMUM)	DENSITY MOLE/CC.10^3	LEAST-SQUARES FIT
186.515	12.8598	.7965	1.2456	M=3 , P0-P5
143.608	9.9014	.8525	0.8961	
107.127	7.3862	.8945	0.63703	
78.125	5.3865	.9253	0.44911	M=2 , P1-P5
56.064	3.8655	.9475	0.31475	
39.783	2.7430	.9633	0.21968	

OPTIMUM COEFFICIENTS		ESTIMATED ERRORS (MAX.)	OPTIMUM FIT
B, CC/MOLE =	-167.93	.60	M=2
C, CC/MOLE^2 =	3718	600	P1-P5
V(A), CC =	359.06	.15	
		Z .0007	

RESULTS OF NON-LINEAR LEAST-SQUARES ANALYSIS

	M=2 P0-P5	M=2 P1-P5	M=3 P0-P5	M=0 P0-P5	M=0 P0-P5	M=0 P0-P5
V(A)	359.14	359.06	359.03			
SD	.06	.08	.21			
A(1)	-167.52	-167.93	-168.31			
SD	.21	.39	1.41			
A(2)	3422	3718	4358			
SD	117	276	1669			
A(3)			-33 .10^4			
SD			59 .10^4			
Z(0)	.79670		.79647			
Z(1)	.85267	.85251	.85244			
Z(2)	.89469	.89453	.89446			
Z(3)	.92547	.92533	.92526			
Z(4)	.94762	.94751	.94744			
Z(5)	.96337	.96329	.96323			

TABLE 4.2
EXPERIMENTAL DATA FOR NITROGEN

RUN 6 291.42 K

PRESSURE LB./SQ.IN.	PRESSURE BAR	Z = PV/RT (OPTIMUM)	DENSITY MOLE/CC.10^3	LEAST-SQUARES FIT
1507.290	103.9241	1.0010	4.2844	M=3 , P0-P5
815.486	56.2258	.9935	2.3357	
445.801	30.7369	.9945	1.2756	
244.215	16.8380	.9964	0.69744	M=2 , P1-P5
133.807	9.2257	.9979	0.38157	
73.304	5.0541	.9988	0.20884	

OPTIMUM COEFFICIENTS		ESTIMATED ERRORS (MAX.)	OPTIMUM FIT
B, CC/MOLE =	-6.20	.30	M=2
C, CC/MOLE =	1458	150	P1-P5
V(A), CC =	361.23	.08	
		Z .0004	

RESULTS OF NON-LINEAR LEAST-SQUARES ANALYSIS

	M=2 P0-P5	M=2 P1-P5	M=3 P0-P5	M=0 P0-P5	M=0 P0-P5	M=0 P0-P5
V(A)	361.112	361.232	361.268			
SD	.059	.015	.010			
A(1)	-6.582	-6.200	-5.987			
SD	.112	.047	.038			
A(2)	1572.1	1457.6	1298.1			
SD	18.4	13.3	17.1			
A(3)			3.6 $.10^4$			
SD			2.3 $.10^4$			
Z(0)	1.00067		1.00106			
Z(1)	.99320	.99347	.99356			
Z(2)	.99416	.99446	.99455			
Z(3)	.99617	.99638	.99647			
Z(4)	.99772	.99785	.99791			
Z(5)	.99869	.99877	.99881			

TABLE 4.2
EXPERIMENTAL DATA FOR NITROGEN

RUN 9 276.94 K

PRESSURE LB./SQ.IN.	PRESSURE BAR	Z = PV/RT (OPTIMUM)	DENSITY MOLE/CC.10^3	LEAST-SQUARES FIT
1180.937	81.4228	.9859	3.5865	M=3 , P0-P5
661.445	45.6050	.9872	2.0062	
371.665	25.6254	.9914	1.1225	
208.715	14.3904	.9947	0.62826	M=2 , P1-P5
117.081	8.0724	.9969	0.35166	
65.629	4.5249	.9982	0.19686	

OPTIMUM COEFFICIENTS		ESTIMATED ERRORS (MAX.)	OPTIMUM FIT
B, CC/MOLE =	-9.38	.25	M=2
C, CC/MOLE =	1496	150	P1-P5
V(A), CC =	360.91	.07	
		Z .0003	

RESULTS OF NON-LINEAR LEAST-SQUARES ANALYSIS

	M=2 P0-P5	M=2 P1-P5	M=3 P0-P5	M=0 P0-P5	M=0 P0-P5	M=0 P0-P5
V(A)	360.869	360.912	360.934			
SD	.037	.050	.079			
A(1)	-9.545	-9.378	-9.247			
SD	.080	.167	.327			
A(2)	1553.5	1495.9	1394.7			
SD	15.6	54.5	169.4			
A(3)			$2.5 \cdot 10^4$			
SD			$2.6 \cdot 10^4$			
Z(0)	.98575		.98592			
Z(1)	.98710	.98721	.98726			
Z(2)	.99124	.99136	.99141			
Z(3)	.99462	.99470	.99475			
Z(4)	.99684	.99689	.99692			
Z(5)	.99818	.99821	.99823			

TABLE 4.2
EXPERIMENTAL DATA FOR NITROGEN

RUN 17 263.08 K

PRESSURE LB./SQ.IN.	PRESSURE BAR	Z = PV/RT (OPTIMUM)	DENSITY MOLE/CC.10^3	LEAST-SQUARES FIT
1497.925	103.2784	.9751	4.8418	M=3 , P0-P6
860.625	59.3381	.9763	2.7787	
496.915	34.2611	.9834	1.5927	
286.383	19.7454	.9895	0.9122	M=2 , P1-P6
164.645	11.3519	.9937	0.52232	
94.481	6.5142	.99627	0.29892	
54.152	3.7336	.99783	0.17106	

OPTIMUM COEFFICIENTS		ESTIMATED ERRORS (MAX.)	OPTIMUM FIT
B, CC/MOLE =	-12.95	.25	M=2
C, CC/MOLE =	1586	150	P1-P6
V(A), CC =	360.59	.06	
		Z .0003	

RESULTS OF NON-LINEAR LEAST-SQUARES ANALYSIS

	M=2 P1-P6	M=2 P2-P6	M=3 P0-P6	M=3 P1-P6	M=4 P0-P6	M=0 P*-P6
V(A)	360.588	360.558	360.614	360.546	360.532	
SD	.013	.007	.033	.008	.007	
A(1)	-12.954	-13.093	-12.803	-13.186	-13.304	
SD	.035	.030	.108	.039	.039	
A(2)	1585.6	1644.2	1480.4	1738.6	1886.9	
SD	8.6	12.0	43.1	25.3	30.5	
A(3)			$2.1 \cdot 10^4$	$-3.0 \cdot 10^4$	$-11 \cdot 10^4$	
SD			$.5 \cdot 10^4$	$.5 \cdot 10^4$	$1 \cdot 10^4$	
A(4)					$13 \cdot 10^6$	
SD					$1 \cdot 10^6$	
Z(0)			.97514		.97492	
Z(1)	.97625		.97631	.97614	.97610	
Z(2)	.98339	.98332	.98345	.98329	.98325	
Z(3)	.98950	.98942	.98957	.98939	.98936	
Z(4)	.99367	.99361	.99371	.99358	.99355	
Z(5)	.99627	.99623	.99631	.99621	.99619	
Z(6)	.99783	.99781	.99785	.99780	.99779	

TABLE 4.2

EXPERIMENTAL DATA FOR NITROGEN

RUN 10 248.54 K

PRESSURE LB./SQ.IN.	PRESSURE BAR	Z = PV/RT (OPTIMUM)	DENSITY MOLE/CC.10^3	LEAST-SQUARES FIT
1169.198	80.6134	.9583	4.0706	M=3 , P0-P6
697.018	48.0577	.9688	2.4005	
414.461	28.5761	.9794	1.4119	
245.298	16.9127	.9871	0.82909	M=2 , P1-P6
144.635	9.9722	.99217	0.48636	
85.065	5.8650	.99532	0.28514	
49.949	3.4439	.99722	0.16712	

OPTIMUM COEFFICIENTS		ESTIMATED ERRORS (MAX.)	OPTIMUM FIT
B, CC/MOLE =	-16.88	.20	M=2
C, CC/MOLE =	1608	100	P1-P6
V(A), CC =	360.38	.05	
		Z .0002	

RESULTS OF NON-LINEAR LEAST-SQUARES ANALYSIS

	M=2 P1-P6	M=2 P2-P6	M=3 P0-P6	M=3 P1-P6	M=4 P0-P6	M=0 P0-P6
V(A)	360.379	360.400	360.400	360.407	360.409	
SD	.008	.021	.004	.003	.005	
A(1)	-16.879	-16.778	-16.756	-16.711	-16.698	
SD	.024	.062	.014	.013	.029	
A(2)	1608.3	1560.9	1517.8	1484.0	1464.8	
SD	6.8	20.1	6.2	9.7	25.3	
A(3)			$2.0 \cdot 10^4$	$2.8 \cdot 10^4$	$3.9 \cdot 10^4$	
SD			$.1 \cdot 10^4$	$.2 \cdot 10^4$	$.9 \cdot 10^4$	
A(4)					$-2.2 \cdot 10^6$	
SD					$1.1 \cdot 10^6$	
Z(0)			.95830		.95832	
Z(1)	.96875		.96880	.96882	.96882	
Z(2)	.97937	.97942	.97943	.97944	.97945	
Z(3)	.98711	.98716	.98716	.98718	.98719	
Z(4)	.99217	.99221	.99221	.99223	.99223	
Z(5)	.99532	.99534	.99535	.99536	.99536	
Z(6)	.99722	.99724	.99724	.99725	.99725	

TABLE 4.2
EXPERIMENTAL DATA FOR NITROGEN

RUN 11 248.54 K

PRESSURE LB./SQ.IN.	PRESSURE BAR	Z = PV/RT (OPTIMUM)	DENSITY MOLE/CC.10^3	LEAST-SQUARES FIT
1457.613	100.4989	.9566	5.0836	M=3 , P0-P7
867.175	59.7896	.9637	3.0021	
516.530	35.6135	.9751	1.7674	
306.289	21.1179	.9841	1.0384	
180.852	12.4693	.99025	0.60933	M=2 , P1-P7
106.461	7.3402	.99414	0.35729	
62.544	4.3123	.99651	0.20941	
36.700	2.5304	.99794	0.12270	

OPTIMUM COEFFICIENTS		ESTIMATED ERRORS (MAX.)	OPTIMUM FIT
B, CC/MOLE =	-17.00	.20	M=2
C, CC/MOLE =	1637	100	P1-P7
V(A), CC =	360.32	.05	
		Z .0003	

RESULTS OF NON-LINEAR LEAST-SQUARES ANALYSIS

	M=2 P1-P7	M=2 P2-P7	M=3 P0-P7	M=3 P1-P7	M=4 P0-P7	M=0 P0-P7
V(A)	360.322	360.299	360.349	360.293	360.283	
SD	.014	.014	.030	.021	.032	
A(1)	-16.998	-17.100	-16.837	-17.154	-17.242	
SD	.033	.053	.094	.102	.174	
A(2)	1636.8	1677.8	1530.6	1735.3	1847.3	
SD	7.8	20.1	36.1	61.8	130.5	
A(3)			$2.0 \cdot 10^4$	$-1.8 \cdot 10^4$	$-7.4 \cdot 10^4$	
SD			$.4 \cdot 10^4$	$1.1 \cdot 10^4$	$3.8 \cdot 10^4$	
A(4)					$9.0 \cdot 10^6$	
SD					$3.7 \cdot 10^6$	
Z(0)			.95661		.95644	
Z(1)	.96372		.96379	.96365	.96362	
Z(2)	.97507	.97502	.97514	.97500	.97498	
Z(3)	.98411	.98405	.98419	.98404	.98401	
Z(4)	.99025	.99020	.99031	.99019	.99016	
Z(5)	.99414	.99410	.99418	.99409	.99407	
Z(6)	.99651	.99649	.99654	.99648	.99647	
Z(7)	.99794	.99793	.99796	.99792	.99791	

TABLE 4.2

EXPERIMENTAL DATA FOR NITROGEN

RUN 12 234.05 K

PRESSURE LB./SQ.IN.	PRESSURE BAR	Z = PV/RT (OPTIMUM)	DENSITY MOLE/CC.10^3	LEAST-SQUARES FIT
1198.314	82.6209	.9373	4.5294	M=3 , P0-P6
740.589	51.0618	.9534	2.7521	
455.110	31.3788	.9688	1.6644	
277.610	19.1405	.9801	1.0036	
168.348	11.6072	.9876	0.60394	M=2 , P1-P6
101.688	7.0112	.99239	0.36305	
61.265	4.2241	.99538	0.21807	

OPTIMUM COEFFICIENTS		ESTIMATED ERRORS (MAX.)	OPTIMUM FIT
B, CC/MOLE =	-21.57	.25	M=2
C, CC/MOLE =	1685	150	P1-P6
V(A), CC =	360.13	.06	
		Z .0003	

RESULTS OF NON-LINEAR LEAST-SQUARES ANALYSIS

	M=2 P1-P6	M=2 P2-P6	M=3 P0-P6	M=3 P1-P6	M=4 P0-P6	M=0 P0-P6
V(A)	360.131	360.167	360.164	360.175	360.172	
SD	.023	.030	.030	.053	.090	
A(1)	-21.573	-21.425	-21.407	-21.352	-21.364	
SD	.057	.110	.094	.244	.464	
A(2)	1685.2	1626.2	1581.0	1545.5	1546.8	
SD	14.0	41.7	38.1	150.6	354.7	
A(3)			$2.0 \cdot 10^4$	$2.7 \cdot 10^4$	$3. \cdot 10^4$	
SD			$.5 \cdot 10^4$	$2.9 \cdot 10^4$	$11 \cdot 10^4$	
A(4)					$-1 \cdot 10^6$	
SD					$11 \cdot 10^6$	
Z(0)			.93732		.93734	
Z(1)	.95339		.95348	.95350	.95350	
Z(2)	.96876	.96885	.96884	.96887	.96886	
Z(3)	.98005	.98014	.98013	.98016	.98015	
Z(4)	.98759	.98765	.98765	.98767	.98767	
Z(5)	.99239	.99244	.99244	.99245	.99245	
Z(6)	.99538	.99541	.99541	.99542	.99542	

TABLE 4.2
EXPERIMENTAL DATA FOR NITROGEN

RUN 13 218.88 K

PRESSURE LB./SQ.IN.	PRESSURE BAR	Z = PV/RT (OPTIMUM)	DENSITY MOLE/CC.10^3	LEAST-SQUARES FIT
1402.587	96.7050	.9022	5.8896	M=4 , P0-P8
904.710	62.3776	.92338	3.7119	M=3 , P1-P8
579.825	39.9776	.94630	2.3213	
367.468	25.3361	.96433	1.4437	
230.686	15.9053	.97702	0.89451	M=2 , P2-P8
143.832	9.9169	.98546	0.55295	
89.267	6.1548	.99089	0.34130	
55.239	3.8086	.99433	0.21047	
34.119	2.3524	.99649	0.12971	

OPTIMUM COEFFICIENTS		ESTIMATED ERRORS (MAX.)	OPTIMUM FIT
B, CC/MOLE =	-27.30	.10	M=2
C, CC/MOLE =	1794	50	P2-P8
V(A), CC =	359.88	.03	
		Z .0001	

RESULTS OF NON-LINEAR LEAST-SQUARES ANALYSIS

	M=2 P1-P8	M=2 P2-P8	M=2 P3-P8	M=3 P1-P8	M=3 P2-P8	M=4 P0-P8
V(A)	359.882	359.881	359.889	359.882	359.895	359.871
SD	.005	.007	.009	.009	.012	.016
A(1)	-27.294	-27.298	-27.260	-27.294	-27.210	-27.379
SD	.009	.019	.038	.034	.064	.070
A(2)	1792.4	1793.6	1775.3	1792.1	1726.6	1876.9
SD	1.8	5.5	17.1	16.6	47.2	43.3
A(3)				$.00 \cdot 10^4$	$1.5 \cdot 10^4$	$-3.3 \cdot 10^4$
SD				$.24 \cdot 10^4$	$1.1 \cdot 10^4$	$1.0 \cdot 10^4$
A(4)						$4.2 \cdot 10^6$
SD						$0.8 \cdot 10^6$
Z(0)						.90221
Z(1)	.92338			.92338		.92335
Z(2)	.94630	.94630		.94630	.94633	.94627
Z(3)	.96433	.96433	.96435	.96433	.96436	.96431
Z(4)	.97702	.97702	.97704	.97702	.97705	.97699
Z(5)	.98546	.98545	.98547	.98546	.98549	.98543
Z(6)	.99089	.99089	.99090	.99089	.99092	.99087
Z(7)	.99433	.99433	.99434	.99433	.99435	.99432
Z(8)	.99649	.99649	.99649	.99649	.99650	.99648

TABLE 4.2
EXPERIMENTAL DATA FOR NITROGEN

RUN 14 218.88 K

PRESSURE LB./SQ.IN.	PRESSURE BAR	Z = PV/RT (OPTIMUM)	DENSITY MOLE/CC.10^3	LEAST-SQUARES FIT
1147.732	79.1334	.9107	4.7737	M=4 , P0-P7
739.234	50.9684	.9343	2.9972	M=3 , P1-P7
471.346	32.4982	.95525	1.8693	
297.324	20.4998	.97074	1.1604	
186.008	12.8248	.98131	0.71811	M=2 , P2-P7
115.705	7.9776	.98824	0.44357	
71.701	4.9436	.99266	0.27365	
44.327	3.0562	.99544	0.16870	

OPTIMUM COEFFICIENTS		ESTIMATED ERRORS (MAX.)	OPTIMUM FIT
B, CC/MOLE =	-27.32	.15	M=2
C, CC/MOLE =	1810	75	P2-P7
V(A), CC =	359.87	.04	
		Z .0002	

RESULTS OF NON-LINEAR LEAST-SQUARES ANALYSIS

	M=2 P1-P7	M=2 P2-P7	M=2 P3-P7	M=3 P0-P7	M=3 P1-P7	M=4 P0-P7
V(A)	359.896	359.874	359.855	359.916	359.863	359.850
SD	.019	.024	.041	.034	.035	.050
A(1)	-27.234	-27.321	-27.426	-27.124	-27.392	-27.498
SD	.042	.081	.199	.100	.151	.250
A(2)	1777.5	1810.0	1868.1	1706.5	1872.7	1991.1
SD	9.8	28.3	105.1	39.2	88.3	183.2
A(3)				$1.3 \cdot 10^4$	$-1.7 \cdot 10^4$	$-7.1 \cdot 10^4$
SD				$0.5 \cdot 10^4$	$1.6 \cdot 10^4$	$5.3 \cdot 10^4$
A(4)						$8.2 \cdot 10^6$
SD						$5.2 \cdot 10^6$
Z(0)				.91085		.91069
Z(1)	.93434			.93439	.93426	.93423
Z(2)	.95530	.95525		.95535	.95523	.95519
Z(3)	.97079	.97074	.97069	.97085	.97071	.97068
Z(4)	.98136	.98131	.98127	.98141	.98129	.98126
Z(5)	.98827	.98824	.98820	.98831	.98822	.98819
Z(6)	.99268	.99266	.99263	.99271	.99264	.99262
Z(7)	.99546	.99544	.99543	.99547	.99543	.99542

TABLE 4.2
EXPERIMENTAL DATA FOR NITROGEN

RUN 15 204.61 K

PRESSURE LB./SQ.IN.	PRESSURE BAR	Z = PV/RT (OPTIMUM)	DENSITY MOLE/CC.10^3	LEAST-SQUARES FIT
1143.456	78.8386	.8758	5.2911	M=4 , P0-P6
769.595	53.0617	.9071	3.4384	M=3 , P1-P6
510.754	35.2153	.93510	2.2136	
334.052	23.0321	.95638	1.4156	
215.985	14.8916	.97136	0.90115	M=2 , P2-P6
138.513	9.5501	.98147	0.57196	
88.339	6.0907	.98812	0.36232	

OPTIMUM COEFFICIENTS		ESTIMATED ERRORS (MAX.)	OPTIMUM FIT
B, CC/MOLE =	-33.47	.15	M=2
C, CC/MOLE =	1874	75	P2-P6
V(A), CC =	359.69	.04	
		Z .0002	

RESULTS OF NON-LINEAR LEAST-SQUARES ANALYSIS

	M=2 P1-P6	M=2 P2-P6	M=3 P0-P6	M=3 P1-P6	M=4 P0-P6	M=0 P0-P6
V(A)	359.676	359.685	359.737	359.685	359.662	
SD	.011	.018	.030	.033	.051	
A(1)	-33.493	-33.465	-33.275	-33.460	-33.573	
SD	.020	.045	.071	.108	.192	
A(2)	1882.0	1873.7	1774.3	1865.7	1957.1	
SD	4.1	13.2	23.7	51.2	114.8	
A(3)			$1.6 \cdot 10^4$	$0.2 \cdot 10^4$	$-2.9 \cdot 10^4$	
SD			$.2 \cdot 10^4$	$0.7 \cdot 10^4$	$2.8 \cdot 10^4$	
A(4)					$3.8 \cdot 10^6$	
SD					$2.3 \cdot 10^6$	
Z(0)			.87602		.87584	
Z(1)	.90708		.90723	.90711	.90705	
Z(2)	.93508	.93510	.93522	.93510	.93505	
Z(3)	.95636	.95638	.95650	.95638	.95633	
Z(4)	.97135	.97136	.97147	.97136	.97132	
Z(5)	.98146	.98147	.98155	.98147	.98143	
Z(6)	.98811	.98812	.98818	.98812	.98809	

TABLE 4.2
EXPERIMENTAL DATA FOR NITROGEN

RUN 16 — 204.61 K

PRESSURE LB./SQ.IN.	PRESSURE BAR	Z = PV/RT (OPTIMUM)	DENSITY MOLE/CC.10^3	LEAST-SQUARES FIT
1448.508	99.8711	.8606	6.8211	M=4 , P0-P8
978.034	67.4331	.88807	4.4633	M=3 , P1-P8
654.996	45.1604	.91884	2.8890	
432.062	29.7896	.94427	1.8544	
281.187	19.3872	.96292	1.1835	
181.147	12.4896	.97581	0.75236	M=2 , P2-P8
115.883	7.9898	.98441	0.47709	
73.786	5.0873	.99003	0.30205	
46.837	3.2293	.99366	0.19103	

OPTIMUM COEFFICIENTS		ESTIMATED ERRORS (MAX.)	OPTIMUM FIT
B, CC/MOLE =	-33.57	.15	M=2
C, CC/MOLE =	1898	75	P2-P8
V(A), CC =	359.64	.04	
		Z .0002	

RESULTS OF NON-LINEAR LEAST-SQUARES ANALYSIS

	M=2 P1-P8	M=2 P2-P8	M=2 P3-P8	M=3 P0-P8	M=3 P1-P8	M=4 P0-P8
V(A)	359.620	359.638	359.663	359.710	359.655	359.644
SD	.016	.020	.041	.032	.024	.038
A(1)	-33.626	-33.575	-33.507	-33.300	-33.504	-33.573
SD	.026	.044	.093	.067	.072	.134
A(2)	1911.5	1898.1	1891.6	1770.2	1859.8	1919.4
SD	4.2	10.7	31.7	19.0	29.4	69.6
A(3)				$1.75 \cdot 10^4$	$.63 \cdot 10^4$	$-1.3 \cdot 10^4$
SD				$.15 \cdot 10^4$	$.35 \cdot 10^4$	$1.4 \cdot 10^4$
A(4)						$2.1 \cdot 10^6$
SD						$1.0 \cdot 10^6$
Z(0)				.86079		.86064
Z(1)	.88799			.88820	.88807	.88804
Z(2)	.91880	.91884		.91900	.91888	.91886
Z(3)	.94421	.94427	.94433	.94446	.94431	.94428
Z(4)	.96288	.96292	.96299	.96311	.96297	.96294
Z(5)	.97578	.97581	.97586	.97596	.97585	.97582
Z(6)	.98439	.98441	.98444	.98452	.98444	.98442
Z(7)	.99002	.99003	.99005	.99010	.99005	.99003
Z(8)	.99365	.99366	.99367	.99370	.99367	.99366

TABLE 4.2
EXPERIMENTAL DATA FOR NITROGEN

RUN 30 192.64 K

PRESSURE LB./SQ.IN.	PRESSURE BAR	Z = PV/RT (OPTIMUM)	DENSITY MOLE/CC.10^3	LEAST-SQUARES FIT
1185.288	81.7228	.8329	6.1259	M=4 , P0-P8
833.040	57.4361	.8708	4.1179	M=3 , P1-P8
575.880	39.7056	.9066	2.7343	
390.774	26.9429	.9352	1.7986	
261.105	18.0025	.9562	1.1754	
172.479	11.8920	.9709	0.76466	M=2 , P2-P8
113.026	7.7928	.98086	0.49601	
73.671	5.0794	.98750	0.32113	
47.846	3.2989	.99187	0.20765	

OPTIMUM COEFFICIENTS		ESTIMATED ERRORS (MAX.)	OPTIMUM FIT
B, CC/MOLE =	-39.57	.20	M=2
C, CC/MOLE =	1981	100	P2-P8
V(A), CC =	359.49	.05	
		Z .0003	

RESULTS OF NON-LINEAR LEAST-SQUARES ANALYSIS

	M=2 P1-P8	M=2 P2-P8	M=2 P3-P8	M=3 P0-P8	M=3 P1-P8	M=4 P0-P8
V(A)	359.456	359.487	359.531	359.517	359.513	359.519
SD	.021	.021	.019	.017	.025	.033
A(1)	-39.661	-39.573	-39.407	-39.446	-39.462	-39.436
SD	.033	.048	.061	.038	.076	.120
A(2)	2005.0	1981.1	1917.1	1908.9	1916.2	1902.6
SD	5.9	12.2	22.0	11.7	32.7	66.9
A(3)				$1.3 \cdot 10^4$	$1.2 \cdot 10^4$	$1.4 \cdot 10^4$
SD				$.1 \cdot 10^4$	$.4 \cdot 10^4$	$1.5 \cdot 10^4$
A(4)						$-0.1 \cdot 10^6$
SD						$1.1 \cdot 10^6$
Z(0)				.83286		.83286
Z(1)	.87067			.87081	.87080	.87081
Z(2)	.90654	.90661		.90688	.90667	.90668
Z(3)	.93515	.93523	.93533	.93530	.93529	.93530
Z(4)	.95615	.95622	.95634	.95630	.95629	.95630
Z(5)	.97084	.97090	.97099	.97096	.97095	.97096
Z(6)	.98082	.98086	.98093	.98091	.98090	.98091
Z(7)	.98747	.98750	.98754	.98753	.98753	.98753
Z(8)	.99185	.99187	.99190	.99189	.99189	.99189

TABLE 4.2

EXPERIMENTAL DATA FOR NITROGEN

RUN 28 181.86 K

PRESSURE LB./SQ.IN.	PRESSURE BAR	Z = PV/RT (OPTIMUM)	DENSITY MOLE/CC.10^3	LEAST-SQUARES FIT
728.383	50.2202	.8532	3.8928	M=3 , P0-P8
518.513	35.7503	.8932	2.6470	
361.371	24.9157	.92489	1.7815	
247.581	17.0701	.94836	1.1904	
167.480	11.5474	.96501	0.79135	
112.282	7.7415	.97653	0.52427	M=2 , P2-P8
74.811	5.1580	.98436	0.34653	
49.638	3.4224	.98962	0.22870	
32.841	2.2643	.99313	0.15078	

OPTIMUM COEFFICIENTS		ESTIMATED ERRORS (MAX.)	OPTIMUM FIT
B, CC/MOLE =	-45.85	.15	M=2
C, CC/MOLE =	2072	100	P2-P8
V(A), CC =	359.35	.04	
		Z .0002	

RESULTS OF NON-LINEAR LEAST-SQUARES ANALYSIS

	M=2 P1-P8	M=2 P2-P8	M=2 P3-P8	M=3 P0-P8	M=3 P1-P8	M=4 P0-P8
V(A)	359.332	359.350	359.344	359.344	359.357	359.357
SD	.016	.020	.032	.022	.031	.044
A(1)	-45.925	-45.850	-45.879	-45.866	-45.796	-45.784
SD	.038	.067	.147	.071	.138	.231
A(2)	2101.5	2072.2	2088.3	2065.3	2017.8	1995.4
SD	10.2	25.0	76.6	32.3	87.6	189.7
A(3)				$0.7 \cdot 10^4$	$1.6 \cdot 10^4$	$3 \cdot 10^4$
SD				$.4 \cdot 10^4$	$1.7 \cdot 10^4$	$6 \cdot 10^4$
A(4)						$-3 \cdot 10^6$
SD						$7 \cdot 10^6$
Z(0)				.85315		.85318
Z(1)	.89316			.89319	.89322	.89322
Z(2)	.92485	.92489		.92488	.92491	.92491
Z(3)	.94831	.94836	.94835	.94834	.94837	.94837
Z(4)	.96497	.96501	.96500	.96500	.96503	.96503
Z(5)	.97650	.97653	.97652	.97652	.97655	.97655
Z(6)	.98434	.98436	.98435	.98435	.98437	.98438
Z(7)	.98961	.98962	.98962	.98962	.98963	.98963
Z(8)	.99312	.99313	.99313	.99313	.99314	.99314

TABLE 4.2
EXPERIMENTAL DATA FOR NITROGEN

RUN 29 155.90 K

PRESSURE LB./SQ.IN.	PRESSURE BAR	Z = PV/RT (OPTIMUM)	DENSITY MOLE/CC.10^3	LEAST-SQUARES FIT
884.558	60.9881	.6592	7.1368	M=4 , P0-P10
727.119	50.1331	.7189	5.3794	
581.659	40.1040	.77795	3.9770	M=3 , P2-P10
451.467	31.1276	.83056	2.8913	
340.820	23.4988	.87413	2.0739	
251.430	17.3355	.90840	1.4723	
182.180	12.5609	.93432	1.0372	
130.239	8.9747	.95342	0.72662	M=2 , P4-P10
92.200	6.3570	.96721	0.50705	
64.811	4.4685	.97704	0.35284	
45.330	3.1254	.98399	0.24504	

OPTIMUM COEFFICIENTS		ESTIMATED ERRORS (MAX.)	OPTIMUM FIT
B, CC/MOLE =	-65.96	.20	M=2
C, CC/MOLE =	2540	100	P4-P10
V(A), CC =	358.95	.05	
		Z .0003	

RESULTS OF NON-LINEAR LEAST-SQUARES ANALYSIS

	M=2 P2-P10	M=2 P3-P10	M=2 P4-P10	M=2 P5-P10	M=3 P0-P10	M=3 P1-P10
V(A)	358.917	358.946	358.945	358.903	358.894	358.939
SD	.017	.014	.020	.024	.028	.020
A(1)	-66.025	-65.955	-65.958	-66.121	-66.081	-65.958
SD	.024	.028	.052	.082	.044	.042
A(2)	2558.1	2539.1	2540.2	2614.2	2575.4	2529.7
SD	4.6	6.9	17.0	35.1	12.0	14.4
A(3)					$-0.1 \cdot 10^4$	$.35 \cdot 10^4$
SD					$.1 \cdot 10^4$	$.14 \cdot 10^4$
Z(0)					.65908	
Z(1)					.71882	.71891
Z(2)	.77786				.77782	.77790
Z(3)	.83047	.83052			.83041	.83052
Z(4)	.87406	.87414	.87413		.87400	.87412
Z(5)	.90833	.90840	.90840	.90831	.90828	.90838
Z(6)	.93427	.93433	.93432	.93423	.93423	.93431
Z(7)	.95337	.95342	.95342	.95333	.95334	.95341
Z(8)	.96718	.96721	.96721	.96714	.96715	.96721
Z(9)	.97702	.97704	.97704	.97700	.97700	.97704
Z(0)	.98397	.98399	.98399	.98395	.98396	.98399

TABLE 4.2

RUN 29 155.90 K (CONTINUED)

RESULTS OF NON-LINEAR LEAST-SQUARES ANALYSIS

	M=3 P2-P10	M=3 P3-P10	M=4 P0-P10	M=4 P1-P10	M=5 P0-P10
V(A)	358.963	358.930	358.966	358.965	358.953
SD	.024	.030	.026	.036	.048
A(1)	-65.881	-66.019	-65.853	-65.861	-65.913
SD	.066	.109	.068	.123	.186
A(2)	2493.1	2576.2	2465.8	2470.4	2509.1
SD	28.8	61.7	31.1	71.3	128.9
A(3)	$.84\ .10^4$	$-.6\ .10^4$	$1.8\ .10^4$	$1.7\ .10^4$	$.5\ .10^4$
SD	$.36\ .10^4$	$1.0\ .10^4$	$.5\ .10^4$	$1.6\ .10^4$	$3.9\ .10^4$
A(4)			$-1.2\ .10^6$	$-1.1\ .10^6$	$.7\ .10^6$
SD			$.3\ .10^6$	$1.3\ .10^6$	$5.4\ .10^6$
A(5)					$-1.0\ .10^8$
SD					$.3\ .10^8$
Z(0)			.65921		.65919
Z(1)			.71896	.71896	.71894
Z(2)	.77795		.77796	.77795	.77793
Z(3)	.83056	.83049	.83057	.83057	.83054
Z(4)	.87417	.87410	.87418	.87417	.87415
Z(5)	.90844	.90836	.90845	.90844	.90842
Z(6)	.93436	.93429	.93437	.93437	.93434
Z(7)	.95345	.95339	.95346	.95346	.95343
Z(8)	.96724	.96719	.96725	.96724	.96723
Z(9)	.97707	.97703	.97707	.97707	.97706
Z(0)	.98401	.98398	.98401	.98401	.98400

TABLE 4.3
EXPERIMENTAL DATA FOR MIX.A(CH4-48.4, N2-51.6 MOLE%)

RUN 25 291.40 K

PRESSURE LB./SQ.IN.	PRESSURE BAR	Z = PV/RT (OPTIMUM)	DENSITY MOLE/CC.10^3	LEAST-SQUARES FIT
1398.179	96.4011	.9395	4.2346	M=3 , P0-P6
775.037	53.4369	.9586	2.3008	
429.775	29.6320	.9750	1.2544	
237.333	16.3635	.98560	0.68523	M=2 , P1-P6
130.613	9.0055	.99191	0.37472	
71.723	4.9451	.99551	0.20502	
39.336	2.7122	.99752	0.11221	

OPTIMUM COEFFICIENTS		ESTIMATED ERRORS (MAX.)	OPTIMUM FIT
B, CC/MOLE =	-22.28	.25	M=2
C, CC/MOLE =	1853	150	P1-P6
V(A), CC =	361.15	.06	
		Z .0003	

RESULTS OF NON-LINEAR LEAST-SQUARES ANALYSIS

	M=2 P1-P6	M=2 P2-P6	M=3 P0-P6	M=3 P1-P6	M=4 P0-P6	M=0 P0-P6
V(A)	361.152	361.132	361.170	361.132	361.130	
SD	.025	.041	.039	.062	.091	
A(1)	-22.279	-22.400	-22.145	-22.417	-22.451	
SD	.079	.213	.152	.394	.694	
A(2)	1852.7	1918.2	1737.4	1968.0	2045.2	
SD	24.2	111.0	72.8	320.5	678.3	
A(3)			$2.9 \cdot 10^4$	$-2.8 \cdot 10^4$	$-8.7 \cdot 10^4$	
SD			$1.0 \cdot 10^4$	$7.7 \cdot 10^4$	$2.5 \cdot 10^4$	
A(4)					$14 \cdot 10^6$	
SD					$31 \cdot 10^6$	
Z(0)			.93955		.93945	
Z(1)	.95855		.95859	.95850	.95849	
Z(2)	.97497	.97491	.97501	.97492	.97491	
Z(3)	.98560	.98555	.98565	.98555	.98555	
Z(4)	.99191	.99188	.99195	.99187	.99187	
Z(5)	.99551	.99549	.99553	.99549	.99548	
Z(6)	.99752	.99751	.99754	.99751	.99751	

TABLE 4.3

EXPERIMENTAL DATA FOR MIX. A (CH4-48.4, N2-51.6 MOLE %)

RUN 26 248.53 K

PRESSURE LB./SQ.IN.	PRESSURE BAR	Z = PV/RT (OPTIMUM)	DENSITY MOLE/CC.10^3	LEAST-SQUARES FIT
1396.714	96.3001	.8630	5.4001	M=3 , P0-P7
869.023	59.9170	.9030	3.2109	
553.229	36.7648	.93733	1.8981	
322.080	22.2066	.96126	1.1179	
192.312	13.2594	.97660	0.65704	M=2 , P2-P7
113.967	7.8578	.98604	0.38564	
67.232	4.6355	.99174	0.22619	
39.550	2.7269	.99513	0.13261	

OPTIMUM COEFFICIENTS		ESTIMATED ERRORS (MAX.)	OPTIMUM FIT
B, CC/MOLE =	-37.00	.20	M=2
C, CC/MOLE =	2097	100	P2-P7
V(A), CC =	360.55	.05	
		Z .0002	

RESULTS OF NON-LINEAR LEAST-SQUARES ANALYSIS

	M=2 P1-P7	M=2 P2-P7	M=3 P0-P7	M=3 P1-P7	M=4 P0-P7	M=0 P0-P7
V(A)	360.514	360.548	360.554	360.565	360.570	
SD	.023	.026	.023	.034	.046	
A(1)	-37.138	-37.000	-36.942	-36.884	-36.850	
SD	.050	.091	.063	.148	.227	
A(2)	2149.9	2096.9	2032.9	1997.1	1963.7	
SD	11.4	32.6	23.4	86.0	163.2	
A(3)			$2.0 \cdot 10^4$	$2.6 \cdot 10^4$	$3.9 \cdot 10^4$	
SD			$.3 \cdot 10^4$	$1.5 \cdot 10^4$	$4.5 \cdot 10^4$	
A(4)					$-1.7 \cdot 10^6$	
SD					$4.3 \cdot 10^6$	
Z(0)			.86295		.86298	
Z(1)	.90291		.90301	.90303	.90304	
Z(2)	.93725	.93733	.93734	.93737	.93738	
Z(3)	.96117	.96126	.96127	.96130	.96131	
Z(4)	.97652	.97660	.97661	.97664	.97665	
Z(5)	.98600	.98604	.98606	.98608	.98608	
Z(6)	.99171	.99174	.99175	.99176	.99177	
Z(7)	.99511	.99513	.99514	.99514	.99515	

TABLE 4.3
EXPERIMENTAL DATA FOR MIX.A (CH4-48.4, N2-51.6 MOLE%)

RUN 27 218.86 K

PRESSURE LB./SQ.IN.	PRESSURE BAR	Z = PV/RT (OPTIMUM)	DENSITY MOLE/CC.10^3	LEAST-SQUARES FIT
1359.582	93.7399	.7643	6.7400	M=4 , P0-P8
942.690	64.9962	.8216	4.3471	M=3 , P1-P8
637.958	43.9857	.87581	2.7598	
419.630	28.9325	.91761	1.7327	
269.903	18.6092	.94689	1.0800	
170.896	11.7829	.96637	0.67002	M=2 , P2-P8
107.100	7.3843	.97893	0.41452	
66.679	4.5974	.98689	0.25599	
41.341	2.8504	.99187	0.15792	

OPTIMUM COEFFICIENTS		ESTIMATED ERRORS (MAX.)	OPTIMUM FIT
B, CC/MOLE =	-51.86	.20	M=2
C, CC/MOLE =	2486	100	P2-P8
V(A), CC =	359.95	.05	
		Z .0003	

RESULTS OF NON-LINEAR LEAST-SQUARES ANALYSIS

	M=2 P1-P8	M=2 P2-P8	M=2 P3-P8	M=3 P0-P8	M=3 P1-P8	M=4 P0-P8
V(A)	359.935	359.947	360.009	359.983	359.961	359.961
SD	.021	.029	.024	.028	.038	.051
A(1)	-51.893	-51.858	-51.605	-51.717	-51.799	-51.808
SD	.032	.066	.083	.059	.116	.184
A(2)	2495.5	2485.7	2381.3	2414.9	2453.0	2467.5
SD	5.8	17.4	32.3	17.5	50.3	101.5
A(3)				$1.03 \cdot 10^4$	$0.5 \cdot 10^4$	$-0.1 \cdot 10^4$
SD				$.15 \cdot 10^4$	$0.6 \cdot 10^4$	$2.1 \cdot 10^4$
A(4)						$0.8 \cdot 10^6$
SD						$1.5 \cdot 10^6$
Z(0)				.76430		.76425
Z(1)	.82157			.82167	.82162	.82162
Z(2)	.87579	.87581		.87589	.87584	.87584
Z(3)	.91758	.91761	.91775	.91770	.91764	.91765
Z(4)	.94687	.94689	.94705	.94698	.94693	.94693
Z(5)	.96635	.96637	.96650	.96643	.96640	.96640
Z(6)	.97892	.97893	.97902	.97898	.97895	.97895
Z(7)	.98688	.98689	.98695	.98692	.98690	.98690
Z(8)	.99187	.99187	.99191	.99189	.99188	.99188

TABLE 4.3

EXPERIMENTAL DATA FOR MIX. A (CH4-48.4, N2-51.6 MOLE%)

RUN 31 192.64 K

PRESSURE LB./SQ.IN.	PRESSURE BAR	Z = PV/RT (OPTIMUM)	DENSITY MOLE/CC.10^3	LEAST-SQUARES FIT
981.677	67.6843	.6811	6.2042	M=4 , P0-P9
754.823	52.0433	.7545	4.3062	M=3 , P1-P9
557.830	38.4610	.8215	2.9229	
396.793	27.3579	.87539	1.9511	
273.777	18.8763	.91537	1.2874	
184.757	12.7386	.94354	0.84287	
122.792	8.4662	.96277	0.54900	M=2 , P3-P9
80.773	5.5691	.97564	0.35637	
52.775	3.6387	.98414	0.23083	
34.327	2.3667	.98971	0.14930	

OPTIMUM COEFFICIENTS		ESTIMATED ERRORS (MAX.)	OPTIMUM FIT
B, CC/MOLE =	-69.37	.30	M=2
C, CC/MOLE =	2819	200	P3-P9
V(A), CC =	359.55	.07	
		Z .0004	

RESULTS OF NON-LINEAR LEAST-SQUARES ANALYSIS

	M=2 P2-P9	M=2 P3-P9	M=2 P4-P9	M=3 P1-P9	M=3 P2-P9	M=4 P0-P9
V(A)	359.481	359.551	359.519	359.519	359.581	359.547
SD	.033	.025	.034	.038	.041	.045
A(1)	-69.621	-69.366	-69.524	-69.460	-69.161	-69.315
SD	.068	.073	.147	.109	.166	.155
A(2)	2916.9	2819.3	2903.7	2823.0	2630.2	2711.4
SD	17.5	26.2	74.0	47.3	99.9	87.4
A(3)				$1.6 \cdot 10^4$	$5.1 \cdot 10^4$	$4.9 \cdot 10^4$
SD				$.6 \cdot 10^4$	$1.8 \cdot 10^4$	$1.8 \cdot 10^4$
A(4)						$-3.3 \cdot 10^6$
SD						$1.3 \cdot 10^6$
Z(0)						.68106
Z(1)				.75451		.75456
Z(2)	.82141			.82149	.82163	.82155
Z(3)	.87525	.87539		.87534	.87546	.87540
Z(4)	.91518	.91537	.91530	.91528	.91544	.91535
Z(5)	.94338	.94354	.94346	.94347	.94361	.94353
Z(6)	.96265	.96277	.96270	.96272	.96283	.96277
Z(7)	.97556	.97564	.97559	.97561	.97569	.97564
Z(8)	.98408	.98414	.98411	.98412	.98418	.98415
Z(9)	.98967	.98971	.98968	.98969	.98973	.98971

TABLE 4.3

EXPERIMENTAL DATA FOR MIX.A (CH4-48.4, N2-51.6 MOLE %)

RUN 32 181.87 K

PRESSURE LB./SQ.IN.	PRESSURE BAR	Z = PV/RT (OPTIMUM)	DENSITY MOLE/CC.10^3	LEAST-SQUARES FIT
881.856	60.8018	.6239	6.4444	M=4 , P0-P9
715.467	49.3297	.7019	4.6479	M=3 , P1-P9
556.061	38.3391	.7759	3.2674	
413.925	28.5391	.83838	2.2512	
297.256	20.4951	.88681	1.5284	
207.745	14.3236	.92232	1.0270	
142.394	9.8177	.94744	0.68528	M=2 , P3-P9
96.297	6.6395	.96476	0.45512	
64.527	4.4490	.97653	0.30129	
42.975	2.9630	.98443	0.19905	

OPTIMUM COEFFICIENTS		ESTIMATED ERRORS (MAX.)	OPTIMUM FIT
B, CC/MOLE =	-78.85	.20	M=2
C, CC/MOLE =	3136	100	P3-P9
V(A), CC =	359.31	.05	
		Z .0003	

RESULTS OF NON-LINEAR LEAST-SQUARES ANALYSIS

	M=2 P2-P9	M=2 P3-P9	M=2 P4-P9	M=3 P1-P9	M=3 P2-P9	M=4 P0-P9
V(A)	359.258	359.311	359.301	359.299	359.341	359.327
SD	.028	.023	.035	.031	.036	.037
A(1)	-79.016	-78.854	-78.895	-78.867	-78.694	-78.737
SD	.048	.057	.122	.076	.125	.113
A(2)	3190.5	3135.5	3154.0	3111.0	3011.6	3018.8
SD	11.4	18.2	53.1	30.6	67.2	60.0
A(3)				$1.21 \cdot 10^4$	$2.8 \cdot 10^4$	$3.7 \cdot 10^4$
SD				$.34 \cdot 10^4$	$1.0 \cdot 10^4$	$1.2 \cdot 10^4$
A(4)						$-2.3 \cdot 10^6$
SD						$.8 \cdot 10^6$
Z(0)						.62390
Z(1)				.70186		.70191
Z(2)	.77586			.77594	.77603	.77600
Z(3)	.83827	.83838		.83836	.83844	.83842
Z(4)	.88667	.88681	.88679	.88677	.88687	.88684
Z(5)	.92221	.92232	.92230	.92230	.92239	.92236
Z(6)	.94734	.94744	.94741	.94742	.94750	.94747
Z(7)	.96470	.96476	.96475	.96475	.96481	.96480
Z(8)	.97648	.97653	.97651	.97652	.97657	.97655
Z(9)	.98440	.98443	.98442	.98442	.98446	.98445

TABLE 4.3
EXPERIMENTAL DATA FOR MIX.A (CH4-48.4, N2-51.6 MOLE %)

RUN 37 155.88 K

PRESSURE LB./SQ.IN.	PRESSURE BAR	Z = PV/RT (OPTIMUM)	DENSITY MOLE/CC.10^3	LEAST-SQUARES FIT
411.793	28.3921	.6975	3.1407	M=3 , P0-P8
335.550	23.1354	.7693	2.3204	
262.220	18.0794	.8286	1.6834	
198.196	13.6651	.8753	1.2046	
146.058	10.0704	.9106	0.8533	
105.653	7.2845	.9366	0.60012	M=2 , P2-P8
75.405	5.1990	.9553	0.41988	
53.306	3.6753	.9687	0.29272	
37.432	2.5809	.9782	0.20357	

OPTIMUM COEFFICIENTS		ESTIMATED ERRORS (MAX.)	OPTIMUM FIT
B, CC/MOLE =	-107.91	.40	M=2
C, CC/MOLE =	3624	250	P2-P8
V(A), CC =	358.98	.08	
		Z .0003	

RESULTS OF NON-LINEAR LEAST-SQUARES ANALYSIS

	M=2 P1-P8	M=2 P2-P8	M=2 P3-P8	M=3 P0-P8	M=3 P1-P8	M=4 P0-P8
V(A)	358.906	358.982	358.940	359.003	359.034	359.039
SD	.048	.047	.070	.057	.082	.142
A(1)	-108.187	-107.912	-108.106	-107.739	-107.585	-107.517
SD	.105	.141	.281	.182	.345	.660
A(2)	3745.3	3624.3	3733.7	3423.2	3306.7	3209.0
SD	34.5	58.7	150.6	101.2	245.0	619.0
A(3)				$6.7 \cdot 10^4$	$9.2 \cdot 10^4$	$15 \cdot 10^4$
SD				$1.6 \cdot 10^4$	$5.0 \cdot 10^4$	$23 \cdot 10^4$
A(4)						$-10 \cdot 10^6$
SD						$30 \cdot 10^6$
Z(0)				.69746		.69753
Z(1)	.76908			.76927	.76934	.76935
Z(2)	.82846	.82861		.82866	.82872	.82874
Z(3)	.87509	.87527	.87518	.87531	.87538	.87540
Z(4)	.91040	.91056	.91046	.91061	.91067	.91069
Z(5)	.93642	.93655	.93646	.93659	.93665	.93667
Z(6)	.95523	.95533	.95526	.95537	.95542	.95544
Z(7)	.96865	.96872	.96867	.96876	.96880	.96881
Z(8)	.97813	.97818	.97815	.97821	.97824	.97825

TABLE 4.4

EXPERIMENTAL DATA FOR MIX.B (CH4-71.9, N2-28.1 MOLE%)

RUN 40 291.40 K

PRESSURE LB./SQ.IN.	PRESSURE BAR	Z = PV/RT (OPTIMUM)	DENSITY MOLE/CC.10^3	LEAST-SQUARES FIT
1394.088	96.1190	.9000	4.4081	M=3 , P0-P6
785.078	54.1292	.9353	2.3885	
439.521	30.3039	.9618	1.3005	
244.026	16.8250	.9782	0.7099	M=2 , P1-P6
134.703	9.2875	.9878	0.38805	
74.091	5.1084	.99326	0.21227	
40.669	2.8041	.99629	0.11617	

OPTIMUM COEFFICIENTS		ESTIMATED ERRORS (MAX.)	OPTIMUM FIT
B, CC/MOLE =	-32.19	.25	M=2
C, CC/MOLE =	2135	150	P1-P6
V(A), CC =	361.13	.07	
		Z .0003	

RESULTS OF NON-LINEAR LEAST-SQUARES ANALYSIS

	M=2 P0-P6	M=2 P1-P6	M=2 P2-P6	M=3 P0-P6	M=0 P0-P6	M=0 P0-P6
V(A)	361.092	361.133	361.088	361.140		
SD	.024	.018	.041	.031		
A(1)	-32.339	-32.188	-32.443	-32.128		
SD	.043	.055	.123	.115		
A(2)	2183.1	2135.3	2270.8	2081.0		
SD	7.5	16.5	53.9	53.8		
A(3)				$1.36 \cdot 10^4$		
SD				$.71 \cdot 10^4$		
Z(0)	.89986			.89998		
Z(1)	.93521	.93530		.93532		
Z(2)	.96163	.96175	.96165	.96177		
Z(3)	.97814	.97823	.97811	.97825		
Z(4)	.98778	.98783	.98775	.98785		
Z(5)	.99323	.99326	.99322	.99327		
Z(6)	.99627	.99629	.99626	.99630		

TABLE 4.4
EXPERIMENTAL DATA FOR MIX.B (CH4-71.9, N2-28.1 MOLE%)

RUN 38 248.54 K

PRESSURE LB./SQ.IN.	PRESSURE BAR	Z = PV/RT (OPTIMUM)	DENSITY MOLE/CC.10^3	LEAST-SQUARES FIT
1332.360	91.8630	.8028	5.5369	M=4 , P0-P6
856.556	59.0575	.8635	3.3093	M=3 , P1-P6
536.614	36.9983	.91258	1.9618	
328.207	22.6291	.94615	1.1573	
197.427	13.6121	.96753	0.68080	M=2 , P2-P6
117.520	8.1027	.98066	0.39982	
69.505	4.7922	.98856	0.23458	

OPTIMUM COEFFICIENTS		ESTIMATED ERRORS (MAX.)	OPTIMUM FIT
B, CC/MOLE =	-49.36	.20	M=2
C, CC/MOLE =	2446	100	P2-P6
V(A), CC =	360.61	.05	
		Z .0002	

RESULTS OF NON-LINEAR LEAST-SQUARES ANALYSIS

	M=2 P1-P6	M=2 P2-P6	M=3 P0-P6	M=3 P1-P6	M=4 P0-P6	M=0 P0-P6
V(A)	360.582	360.605	360.626	360.609	360.603	
SD	.015	.021	.021	.035	.051	
A(1)	-49.439	-49.359	-49.252	-49.323	-49.365	
SD	.031	.064	.054	.137	.246	
A(2)	2474.7	2446.0	2369.1	2409.5	2447.0	
SD	6.8	21.8	19.4	75.4	166.4	
A(3)			1.73 $.10^4$	1.1 $.10^4$	-0.3 $.10^4$	
SD			.20 $.10^4$	1.2 $.10^4$	4.3 $.10^4$	
A(4)					1.8 $.10^6$	
SD					3.7 $.10^6$	
Z(0)			.80287		.80282	
Z(1)	.86349		.86359	.86355	.86353	
Z(2)	.91253	.91258	.91263	.91259	.91257	
Z(3)	.94609	.94615	.94620	.94616	.94614	
Z(4)	.96749	.96753	.96757	.96754	.96753	
Z(5)	.98063	.98066	.98069	.98067	.98065	
Z(6)	.98854	.98856	.98858	.98856	.98855	

TABLE 4.4

EXPERIMENTAL DATA FOR MIX.B (CH4-71.9, N2-28.1 MOLE%)

RUN 39 218.86 K

PRESSURE LB./SQ.IN.	PRESSURE BAR	Z = PV/RT (OPTIMUM)	DENSITY MOLE/CC.10^3	LEAST-SQUARES FIT
1296.867	89.4159	.6675	7.361	M=4 , P0-P8
953.523	65.7431	.7451	4.8485	M=3 , P1-P8
675.457	46.5711	.8201	3.1204	
458.653	31.6230	.8796	1.9756	
301.191	20.7664	.92197	1.2377	
193.250	13.3241	.95041	0.77039	M=2 , P3-P8
122.113	8.4194	.96886	0.47753	
76.421	5.2690	.98060	0.29527	
47.538	3.2776	.98796	0.18231	

OPTIMUM COEFFICIENTS		ESTIMATED ERRORS (MAX.)	OPTIMUM FIT
B, CC/MOLE =	-66.55	.25	M=2
C, CC/MOLE =	2839.	150	P3-P8
V(A), CC =	360.06	.06	
		Z .0004	

RESULTS OF NON-LINEAR LEAST-SQUARES ANALYSIS

	M=2 P1-P8	M=2 P2-P8	M=2 P3-P8	M=3 P0-P8	M=3 P1-P8	M=4 P0-P8
V(A)	359.955	360.010	360.063	359.975	360.045	360.071
SD	.037	.038	.049	.048	.046	.056
A(1)	-66.881	-66.744	-66.554	-66.831	-66.599	-66.472
SD	.048	.076	.149	.086	.124	.177
A(2)	2945.4	2910.0	2839.3	2927.9	2828.2	2736.7
SD	8.1	18.4	51.2	24.0	49.6	89.9
A(3)				$0.17 \cdot 10^4$	$1.33 \cdot 10^4$	$3.8 \cdot 10^4$
SD				$.26 \cdot 10^4$	$.55 \cdot 10^4$	$1.7 \cdot 10^4$
A(4)						$-2.3 \cdot 10^6$
SD						$1.1 \cdot 10^6$
Z(0)				.66735		.66752
Z(1)	.74492			.74496	.74510	.74515
Z(2)	.81995	.82005		.82000	.82013	.82018
Z(3)	.87933	.87948	.87959	.87938	.87956	.87962
Z(4)	.92171	.92184	.92197	.92175	.92192	.92199
Z(5)	.95021	.95030	.95041	.95024	.95038	.95043
Z(6)	.96873	.96879	.96886	.96875	.96884	.96889
Z(7)	.98051	.98054	.98060	.98052	.98058	.98061
Z(8)	.98790	.98793	.98796	.98791	.98795	.98797

TABLE 4.4
EXPERIMENTAL DATA FOR MIX.B (CH4-71.9, N2-28.1 MOLE %)

RUN 41 192.65 K

PRESSURE LB./SQ.IN.	PRESSURE BAR	Z = PV/RT (OPTIMUM)	DENSITY MOLE/CC.10^3	LEAST-SQUARES FIT
806.233	55.5878	.6166	5.628	M=4 , P0-P8
650.516	44.8515	.7064	3.9638	M=3 , P1-P8
496.451	34.2291	.7869	2.7156	
360.621	24.8639	.8512	1.8236	
252.213	17.3895	.89888	0.12077	
171.695	11.8380	.93251	0.79252	M=2 , P3-P8
114.752	7.9119	.95549	0.51695	
75.755	5.2231	.97087	0.33586	
49.609	3.4204	.98103	0.21766	

OPTIMUM COEFFICIENTS		ESTIMATED ERRORS (MAX.)	OPTIMUM FIT
B, CC/MOLE =	-87.89	.25	M=2
C, CC/MOLE =	3453	150	P3-P8
V(A), CC =	359.49	.06	
		Z .0004	

RESULTS OF NON-LINEAR LEAST-SQUARES ANALYSIS

	M=2 P2-P8	M=2 P3-P8	M=3 P1-P8	M=3 P3-P8	M=4 P0-P8	M=4 P1-P8
V(A)	359.457	359.488	359.508	359.499	359.531	359.489
SD	.020	.024	.025	.040	.040	.057
A(1)	-88.003	-87.894	-87.778	-87.819	-87.651	-87.877
SD	.041	.071	.072	.160	.138	.269
A(2)	3496.3	3452.5	3349.2	3376.4	3238.2	3431.9
SD	11.5	27.1	33.7	101.5	83.8	218.8
A(3)				$2.2 \cdot 10^4$	$6.4 \cdot 10^4$	$0.1 \cdot 10^4$
SD				$1.9 \cdot 10^4$	$1.9 \cdot 10^4$	$6.9 \cdot 10^4$
A(4)					$-4.1 \cdot 10^6$	$2.9 \cdot 10^6$
SD					$1.5 \cdot 10^6$	$7.6 \cdot 10^6$
Z(0)					.61662	
Z(1)			.70641		.70645	.70637
Z(2)	.78678		.78688	.78686	.78693	.78684
Z(3)	.85113	.85120	.85124	.85122	.85129	.85120
Z(4)	.89881	.89888	.89893	.89891	.89898	.89888
Z(5)	.93245	.93251	.93255	.93253	.93261	.93251
Z(6)	.95544	.95549	.95552	.95551	.95557	.95549
Z(7)	.97084	.97087	.97090	.97089	.97093	.97087
Z(8)	.98101	.98103	.98105	.98105	.98108	.98104

TABLE 4.4
EXPERIMENTAL DATA FOR MIX.B (CH4-71.9, N2-28.1 MOLE%)

RUN 43 181.86 K

PRESSURE LB./SQ.IN.	PRESSURE BAR	Z = PV/RT (OPTIMUM)	DENSITY MOLE/CC.10^3	LEAST-SQUARES FIT
641.575	44.2351	.6155	4.753	M=4 , P0-P8
528.897	36.4662	.7059	3.4166	M=3 , P1-P8
411.588	28.3780	.7849	2.3913	
305.094	21.0355	.8478	1.6410	
217.945	15.0268	.8948	1.1106	
151.620	10.4538	.9285	0.7446	M=2 , P3-P8
103.554	7.1398	.9519	0.49607	
69.860	4.8166	.96790	0.32913	
46.733	3.2221	.97868	0.21775	

OPTIMUM COEFFICIENTS		ESTIMATED ERRORS (MAX.)	OPTIMUM FIT
B, CC/MOLE =	-98.73	.30	M=2
C, CC/MOLE =	3636	200	P3-P8
V(A), CC =	359.38	.08	
		Z .0004	

RESULTS OF NON-LINEAR LEAST-SQUARES ANALYSIS

	M=2 P1-P8	M=2 P2-P8	M=2 P3-P8	M=3 P0-P8	M=3 P1-P8	M=4 P0-P8
V(A)	359.212	359.319	359.378	359.355	359.403	359.431
SD	.070	.068	.098	.068	.094	.135
A(1)	-99.241	-98.947	-98.725	-98.741	-98.562	-98.412
SD	.109	.152	.309	.152	.293	.519
A(2)	3831.2	3733.5	3636.0	3562.6	3461.5	3327.9
SD	26.3	47.7	129.5	60.6	154.2	359.4
A(3)				$4.0 \cdot 10^4$	$5.6 \cdot 10^4$	$10.2 \cdot 10^4$
SD				$6.2 \cdot 10^4$	$2.2 \cdot 10^4$	$9.4 \cdot 10^4$
A(4)						$-5.5 \cdot 10^6$
SD						$8.7 \cdot 10^6$
Z(0)				.61543		.61554
Z(1)	.70553			.70579	.70588	.70593
Z(2)	.78451	.78470		.78478	.78487	.78492
Z(3)	.84739	.84766	.84778	.84772	.84783	.84789
Z(4)	.89446	.89470	.89484	.89478	.89489	.89495
Z(5)	.92820	.92838	.92850	.92846	.92855	.92861
Z(6)	.95170	.95183	.95192	.95190	.95197	.95202
Z(7)	.96775	.96784	.96790	.96789	.96794	.96798
Z(8)	.97857	.97863	.97868	.97867	.97870	.97873

TABLE 4.4
EXPERIMENTAL DATA FOR MIX.B (CH4-71.9, N2-28.1 MOLE%)

RUN 42 155.89 K

PRESSURE LB./SQ.IN.	PRESSURE BAR	Z = PV/RT (OPTIMUM)	DENSITY MOLE/CC.10^3	LEAST-SQUARES FIT
225.273	15.5320	.8112	1.477	M=2 , P0-P5
171.928	11.8540	.8628	1.060	
127.537	8.7934	.9017	0.7523	
92.653	6.3882	.9303	0.5298	
66.325	4.5729	.9510	0.3710	
46.981	3.2393	.9657	0.2588	

OPTIMUM COEFFICIENTS		ESTIMATED ERRORS (MAX.)	OPTIMUM FIT
B, CC/MOLE =	-133.6	.80	M=2
C, CC/MOLE =	3950	700	P0-P5
V(A), CC =	358.93	.15	
		Z .0008	

RESULTS OF NON-LINEAR LEAST-SQUARES ANALYSIS

	M=2 P0-P5	M=2 P1-P5	M=3 P0-P5	M=0 P0-P5	M=0 P0-P5	M=0 P0-P5
V(A)	358.93	359.03	359.06			
SD	.11	.18	.44			
A(1)	-133.62	-133.14	-132.84			
SD	.34	.72	2.52			
A(2)	3947	3652	3164			
SD	160	431	2510			
A(3)			24 $.10^4$			
SD			75 $.10^4$			
Z(0)	.8112		.8115			
Z(1)	.8628	.8630	.8631			
Z(2)	.9017	.9019	.9020			
Z(3)	.9303	.9305	.9306			
Z(4)	.9510	.9511	.9512			
Z(5)	.9657	.9658	.9658			

TABLE 4.5

EXPERIMENTAL DATA FOR MIXTURE C (CH4/N2/C2H6)

RUN 46 273.02 K

PRESSURE LB./SQ.IN.	PRESSURE BAR	Z = PV/RT (OPTIMUM)	DENSITY MOLE/CC.10^3	LEAST-SQUARES FIT
1441.41	99.382	.7945	5.510	M=3 , P0-P6
882.13	60.821	.8630	3.1046	
527.53	36.372	.9161	1.7490	
308.37	21.261	.9506	0.9853	M=2 , P1-P6
177.54	12.241	.9715	0.5551	
101.28	6.983	.9837	0.3127	
57.47	3.962	.9908	0.17615	

OPTIMUM COEFFICIENTS		ESTIMATED ERRORS (MAX.)	OPTIMUM FIT
B, CC/MOLE =	-52.90	.50	M=2
C, CC/MOLE =	2826	300	P1-P6
V(A), CC =	360.85	.10	
		Z .0007	

RESULTS OF NON-LINEAR LEAST-SQUARES ANALYSIS

	M=2 P1-P6	M=3 P0-P6	M=0 P0-P6	M=0 P0-P6	M=0 P0-P6	M=0 P0-P6
V(A)	360.848	360.871				
SD	.052	.086				
A(1)	-52.901	-52.750				
SD	.101	.212				
A(2)	2825.9	2773.4				
SD	52.8	156.5				
A(3)		0.56 $.10^4$				
SD		0.53 $.10^4$				
Z(0)		.79448				
Z(1)	.86300	.86314				
Z(2)	.91612	.91625				
Z(3)	.95062	.95070				
Z(4)	.97151	.97156				
Z(5)	.98373	.98375				
Z(6)	.99077	.99078				

TABLE 4.6
EXPERIMENTAL DATA FOR MIXTURE C (CH4/N2/C2H6)

RUN 47 248.55 K

PRESSURE LB./SQ.IN.	PRESSURE BAR	Z = PV/RT (OPTIMUM)	DENSITY MOLE/CC.10^3	LEAST-SQUARES FIT
1394.07	96.118	.7008	6.6367	M=4 , P0-P7
946.58	65.264	.7852	4.0219	M=3 , P1-P7
618.87	42.670	.8593	2.4028	
389.22	26.836	.9122	1.4235	
238.17	16.421	.9467	0.8393	M=2 , P2-P7
143.23	9.875	.9681	0.4936	
85.24	5.877	.9811	0.28986	
50.41	3.475	.9889	0.17004	

OPTIMUM COEFFICIENTS		ESTIMATED ERRORS (MAX.)	OPTIMUM FIT
B, CC/MOLE =	-66.11	.30	M=2
C, CC/MOLE =	3137	150	P2-P7
V(A), CC =	360.42	.07	
		Z .0005	

RESULTS OF NON-LINEAR LEAST-SQUARES ANALYSIS

	M=2 P2-P7	M=3 P1-P7	M=4 P0-P7	M=0 P0-P7	M=0 P0-P7	M=0 P0-P7
V(A)	360.422	360.438	360.391			
SD	.040	.057	.071			
A(1)	-66.113	-66.068	-66.159			
SD	.062	.105	.131			
A(2)	3137.4	3063.4	3154.1			
SD	20.8	46.9	88.2			
A(3)		$2.1 \cdot 10^4$	$-1.4 \cdot 10^4$			
SD		$0.5 \cdot 10^4$	$1.0 \cdot 10^4$			
A(4)			$2.6 \cdot 10^6$			
SD			$2.2 \cdot 10^6$			
Z(0)			.70082			
Z(1)		.78520	.78526			
Z(2)	.85926	.85923	.85931			
Z(3)	.91224	.91220	.91229			
Z(4)	.94672	.94668	.94676			
Z(5)	.96813	.96810	.96816			
Z(6)	.98110	.98109	.98112			
Z(7)	.98885	.98885	.98886			

TABLE 4.5

EXPERIMENTAL DATA FOR MIXTURE C ($CH_4/N_2/C_2H_6$)

RUN 48 218.86 K

PRESSURE LB./SQ.IN.	PRESSURE BAR	Z = PV/RT (OPTIMUM)	DENSITY MOLE/CC.10^3	LEAST-SQUARES FIT
1061.83	73.211	.5721	7.033	M=4 , P0-P8
838.87	57.838	.6696	4.748	M=3 , P1-P8
625.80	43.147	.7646	3.1016	
439.88	30.329	.8411	1.9817	
295.32	20.362	.8964	1.2484	
192.12	13.246	.9339	0.7795	M=2 , P2-P8
122.45	8.443	.9584	0.4841	
77.04	5.312	.9741	0.2997	
48.08	3.315	.9839	0.1852	

OPTIMUM COEFFICIENTS		ESTIMATED ERRORS (MAX.)	OPTIMUM FIT
B, CC/MOLE =	-87.71	.30	M=2
C, CC/MOLE =	3806	150	P2-P8
V(A), CC =	360.00	.08	
		Z .0005	

RESULTS OF NON-LINEAR LEAST-SQUARES ANALYSIS

	M=2 P1-P8	M=2 P2-P8	M=2 P3-P8	M=3 P0-P8	M=3 P1-P8	M=4 P0-P8
V(A)	359.934	359.999	360.007	359.920	360.004	360.076
SD	.044	.044	.055	.071	.056	.072
A(1)	-87.860	-87.705	-87.754	-87.923	-87.545	-87.355
SD	.053	.083	.157	.121	.144	.220
A(2)	3846.9	3805.6	3869.1	3879.4	3711.3	3565.1
SD	14.7	21.2	57.0	35.8	59.6	115.8
A(3)				$-.42 \cdot 10^4$	$1.57 \cdot 10^4$	$5.7 \cdot 10^4$
SD				$.27 \cdot 10^4$	$.66 \cdot 10^4$	$2.2 \cdot 10^4$
A(4)						$-3.9 \cdot 10^6$
SD						$1.4 \cdot 10^6$
Z(0)				.57200		.57214
Z(1)	.66959			.66955	.66964	.66984
Z(2)	.76447	.76458		.76445	.76466	.76474
Z(3)	.84096	.84114	.84120	.84093	.84122	.84130
Z(4)	.89630	.89644	.89648	.89626	.89654	.89663
Z(5)	.93384	.93395	.93395	.93381	.93403	.93411
Z(6)	.95836	.95843	.95842	.95834	.95849	.95856
Z(7)	.97401	.97405	.97404	.97399	.97409	.97414
Z(8)	.98386	.98389	.98388	.98385	.98392	.98395

TABLE 4.6

EXPERIMENTAL DATA FOR NATURAL GAS NO.1

RUN 44 291.39 K

PRESSURE LB./SQ.IN.	PRESSURE BAR	Z = PV/RT (OPTIMUM)	DENSITY MOLE/CC.10^3	LEAST-SQUARES FIT
1016.04	70.053	.8595	3.364	M=3 , P0-P5
586.14	40.413	.9163	1.8205	M=2 , P1-P5
331.58	22.862	.9523	0.9909	
185.03	12.757	.9733	0.5410	
102.42	7.061	.9852	0.29584	
56.43	3.891	.9918	0.16192	

OPTIMUM COEFFICIENTS		ESTIMATED ERRORS (MAX.)	OPTIMUM FIT
B, CC/MOLE =	-50.76	.50	M=2
C, CC/MOLE =	2613	300	P1-P5
V(A), CC =	361.66	.10	
		Z .0007	

RESULTS OF NON-LINEAR LEAST-SQUARES ANALYSIS

	M=2 P0-P5	M=2 P1-P5	M=3 P0-P5	M=0 P0-P5	M=0 P0-P5	M=0 P0-P5
V(A)	361.557	361.656	361.689			
SD	.054	.033	.043			
A(1)	-51.168	-50.759	-50.521			
SD	.115	.119	.189			
A(2)	2775.3	2612.5	2382.8			
SD	26.2	45.4	112.0			
A(3)			$1.5 \cdot 10^4$			
SD			$1.0 \cdot 10^4$			
Z(0)	.85924		.85955			
Z(1)	.91603	.91625	.91633			
Z(2)	.95201	.95227	.95234			
Z(3)	.97313	.97330	.97338			
Z(4)	.98510	.98521	.98527			
Z(5)	.99179	.99185	.99188			

TABLE 4.6
EXPERIMENTAL DATA FOR NATURAL GAS NO.1

RUN 45 273.76 K

PRESSURE LB./SQ.IN.	PRESSURE BAR	Z = PV/RT (OPTIMUM)	DENSITY MOLE/CC.10^3	LEAST-SQUARES FIT
987.11	68.058	.8236	3.630	M=3 , P0-P5
600.76	41.421	.8913	2.6416	M=2 , P1-P5
354.93	24.471	.9359	1.1487	
205.54	14.172	.9630	0.6465	
117.61	8.109	.9789	0.3639	
66.84	4.608	.9880	0.2049	

OPTIMUM COEFFICIENTS		ESTIMATED ERRORS (MAX.)	OPTIMUM FIT
B, CC/MOLE =	-59.05	.50	M=2
C, CC/MOLE =	2844	300	P1-P5
V(A), CC =	361.57	.10	
		Z .0007	

RESULTS OF NON-LINEAR LEAST-SQUARES ANALYSIS

	M=2 P0-P5	M=2 P1-P5	M=3 P0-P5	M=0 P0-P5	M=0 P0-P5	M=0 P0-P5
V(A)	361.487	361.573	361.604			
SD	.045	.102	.076			
A(1)	-59.354	-59.051	-58.861			
SD	.083	.211	.129			
A(2)	2951.8	2843.5	2680.6			
SD	37.7	67.7	45.8			
A(3)			2.1 $.10^4$			
SD			0.8 $.10^4$			
Z(0)	.82340		.82365			
Z(1)	.89111	.89129	.89136			
Z(2)	.93570	.93592	.93599			
Z(3)	.96286	.96301	.96308			
Z(4)	.97879	.97889	.97894			
Z(5)	.98796	.98802	.98805			

TABLE 4.7
EXPERIMENTAL DATA FOR NATURAL GAS NO.2

RUN 49 294.12 K

PRESSURE LB./SQ.IN.	PRESSURE BAR	Z = PV/RT (OPTIMUM)	DENSITY MOLE/CC.10^3	LEAST-SQUARES FIT
1479.04	101.977	.8232	5.065	M=3 , P0-P6
851.84	58.732	.8884	2.7033	M=2 , P1-P6
483.53	33.338	.9350	1.4580	
270.16	18.627	.9633	0.7906	
149.39	10.300	.9796	0.4299	
82.11	5.661	.9888	0.2341	
44.97	3.101	.9939	0.1276	

OPTIMUM COEFFICIENTS		ESTIMATED ERRORS (MAX.)	OPTIMUM FIT
B, CC/MOLE =	-48.49	.50	M=2
C, CC/MOLE =	2661	300	P1-P6
V(A), CC =	361.52	.10	
		Z .0007	

RESULTS OF NON-LINEAR LEAST-SQUARES ANALYSIS

	M=2 P1-P6	M=2 P2-P6	M=3 P0-P6	M=0 P0-P6	M=0 P0-P6	M=0 P0-P6
V(A)	361.516	361.468	361.528			
SD	.020	.062	.035			
A(1)	-48.494	-48.739	-48.417			
SD	.052	.268	.113			
A(2)	2660.7	2779.9	2598.9			
SD	14.3	78.8	48.1			
A(3)			1.36 $.10^4$			
SD			.56 $.10^4$			
Z(0)			.82320			
Z(1)	.88835		.88838			
Z(2)	.93495	.93484	.93497			
Z(3)	.96332	.96320	.96335			
Z(4)	.97964	.97956	.97967			
Z(5)	.98879	.98874	.98881			
Z(6)	.99386	.99383	.99387			

TABLE 4.7

EXPERIMENTAL DATA FOR NATURAL GAS NO.2

RUN 50 273.16 K

PRESSURE LB./SQ.IN.	PRESSURE BAR	Z = PV/RT (OPTIMUM)	DENSITY MOLE/CC.10^3	LEAST-SQUARES FIT
1468.13	101.224	.7606	5.860	M=3 , P0-P7
912.48	62.913	.8407	3.295	
551.30	38.011	.9027	1.8539	
324.18	22.351	.9428	1.0438	
187.26	12.911	.9670	0.5879	M=2 , P1-P7
107.03	7.380	.9812	0.3312	
60.81	4.193	.9893	0.1866	
34.43	2.374	.9940	0.1052	

OPTIMUM COEFFICIENTS		ESTIMATED ERRORS (MAX.)	OPTIMUM FIT
B, CC/MOLE =	-57.75	.80	M=2
C, CC/MOLE =	2852	500	P1-P7
V(A), CC =	361.38	.15	
		Z .0010	

RESULTS OF NON-LINEAR LEAST-SQUARES ANALYSIS

	M=2 P1-P7	M=2 P2-P7	M=3 P0-P7	M=0 P0-P7	M=0 P0-P7	M=0 P0-P7
V(A)	361.384	361.493	361.427			
SD	.049	.092	.050			
A(1)	-57.749	-57.282	-57.546			
SD	.104	.341	.137			
A(2)	2851.8	2663.1	2732.8			
SD	24.4	132.4	50.6			
A(3)			1.97 $.10^4$			
SD			.50 $.10^4$			
Z(0)			.76059			
Z(1)	.84068		.84077			
Z(2)	.90274	.90298	.90284			
Z(3)	.94283	.94313	.94294			
Z(4)	.96704	.96725	.96712			
Z(5)	.98119	.98133	.98124			
Z(6)	.98932	.98941	.98936			
Z(7)	.99396	.99401	.99398			

TABLE 4.8

Experimental Virial Coefficients

Methane

Temperature, K.	B, $cm^3.mole^{-1}$	C, $cm^6.mole^{-2}$
291.41	-45.50 ± .15	2489 ± 100
263.08	-58.34 ± .07	2788 ± 50
248.54	-66.48 ± .10	3015 ± 75
234.05	-75.89 ± .15	3299 ± 100
218.87	-87.16 ± .30	3551 ± 200
204.60	-100.14 ± .25	3928 ± 150
192.64	-112.83 ± .25	4227 ± 150
181.86	-125.71 ± .30	4256 ± 200
167.67	-146.54 ± .40	4187 ± 300
155.89	-167.93 ± .60	3718 ± 600

Nitrogen

Temperature, K.	B, $cm^3.mole^{-1}$	C, $cm^6.mole^{-2}$
291.42	-6.20 ± .30	1458 ± 150
276.94	-9.38 ± .25	1496 ± 150
263.08	-12.95 ± .25	1586 ± 150
248.54 (run 10)	-16.88 ± .20	1608 ± 100
248.54 (run 11)	-17.00 ± .20	1637 ± 100
234.05	-21.57 ± .25	1685 ± 150
218.88 (run 13)	-27.30 ± .10	1794 ± 50
218.88 (run 14)	-27.32 ± .15	1810 ± 75
204.61 (run 15)	-33.47 ± .15	1874 ± 75
204.61 (run 16)	-33.57 ± .15	1898 ± 75
192.64	-39.57 ± .20	1981 ± 100
181.86	-45.85 ± .15	2072 ± 75
155.90	-65.96 ± .20	2540 ± 100

TABLE 4.9

Experimental Virial Coefficients

Methane/Nitrogen : Mixture A — Mole fractions CH_4: .4840 N_2: .5160

Temperature, K	B, $cm^3.mole^{-1}$	C, $cm^6.mole^{-2}$
291.40	-22.28 ± .25	1853 ± 150
248.53	-37.00 ± .20	2097 ± 100
218.86	-51.86 ± .20	2486 ± 100
192.64	-69.37 ± .30	2819 ± 200
181.87	-78.85 ± .20	3136 ± 100
155.88	-107.91 ± .30	3624 ± 200

Methane/Nitrogen : Mixture B — Mole fractions CH_4: .7190 N_2: .2810

Temperature, K	B, $cm^3.mole^{-1}$	C, $cm^6.mole^{-2}$
291.40	-32.19 ± .25	2135 ± 150
248.54	-49.36 ± .20	2446 ± 100
218.86	-66.55 ± .25	2839 ± 150
192.65	-87.89 ± .25	3453 ± 150
181.86	-98.73 ± .30	3636 ± 200
155.89	-133.6 ± .80	3950 ± 600

Methane/Nitrogen. Interactional Virial Coefficients
(subscript 1 refers to methane, subscript 2 refers to nitrogen)

	B_{12}, $cm^3.mole^{-1}$		
Temperature, K	Mix A	Mix B	Mean
291.40	-20.0 ± .4	-20.2 ± .4	-20.1 ± .4
248.53	-33.8 ± .5	-33.8 ± .4	-33.8 ± .4
218.86	-48.4 ± .5	-47.8 ± .6	-48.1 ± .6
192.64	-64.9 ± .7	-65.4 ± .7	-65.2 ± .7
181.87	-74.5 ± .8	-74.5 ± .8	-74.5 ± .8
155.88	-102.1 ± 1.0	-102.9 ± 1.7	-102.3 ± 1.0

Temperature, K	C_{112}, $cm^6.mole^{-2}$	C_{221}, $cm^6.mole^{-2}$
291.40	2080 ± 500	1590 ± 500
248.53	2230 ± 300	1880 ± 300
218.86	2430 ± 500	2480 ± 500
192.64	3320 ± 600	2300 ± 600
181.87	3520 ± 600	2850 ± 600
155.88	4540 ± 1000	3130 ± 800

TABLE 4.10

Coefficients in 0 °C Equation of State

$$Z = 1 + a_1\rho + a_2\rho^2 + a_3\rho^3 + a_4\rho^4$$

	a_1	a_2	a_3	a_4
Methane	-53.35	2620.0	7000	-
Nitrogen	-10.25	1500.0	6000	-
Mixture A	-27.87	1920.0	16000	-400,000
Mixture B	-38.70	2250.0	5000	-100,000
Mixture C	-52.85	2824.0	5600	-
Natural Gas 1	-59.28	2850.0	20000	-
Natural Gas 2	-57.55	2734	20000	-

TABLE 4.11

	Temperature, K				
	291.4	248.5	218.9	181.9	155.9
$\partial B(T)/\partial B^{o}$	.37	.34	.33	.25	.20
$\partial B(T)/\partial C^{o}$	.00005	.00004	.00004	.00003	.00002
$\partial C(T)/\partial B^{o}$	13	31	56	68	78
$\partial C(T)/\partial C^{o}$	.19	.15	.08	.10	.13
δB CH_4	.04	.04	.03	.03	.02
δB N_2	.08	.07	.07	.05	.04
cc/mole CH_4/N_2	.16	.14	.13	.10	.08
δC CH_4	15	14	12	14	18
δC N_2	33	28	23	29	36
$(cc/mole)^2$ CH_4/N_2	50	45	40	50	60

TABLE 4.12

Estimated Max. Errors in Z(T) due to Uncertainty in Z^{o}.

$\delta Z \cdot 10^4$

Temperature, K	CH_4	N_2	CH_4/N_2	Multi-component Mixtures
291.4	1.0	1.6	3.0	5.0
263.1	1.0	1.5	-	
248.5	1.1	1.5	3.0	4.0
234.0	0.9	1.3	-	
218.9	1.1	1.5	3.0	4.0
204.6	0.9	1.6	-	
192.6	0.6	1.4	2.5	
181.9	0.4	1.0	2.0	
167.7.	0.2	-		
155.9	0.1	1.0	1.0	

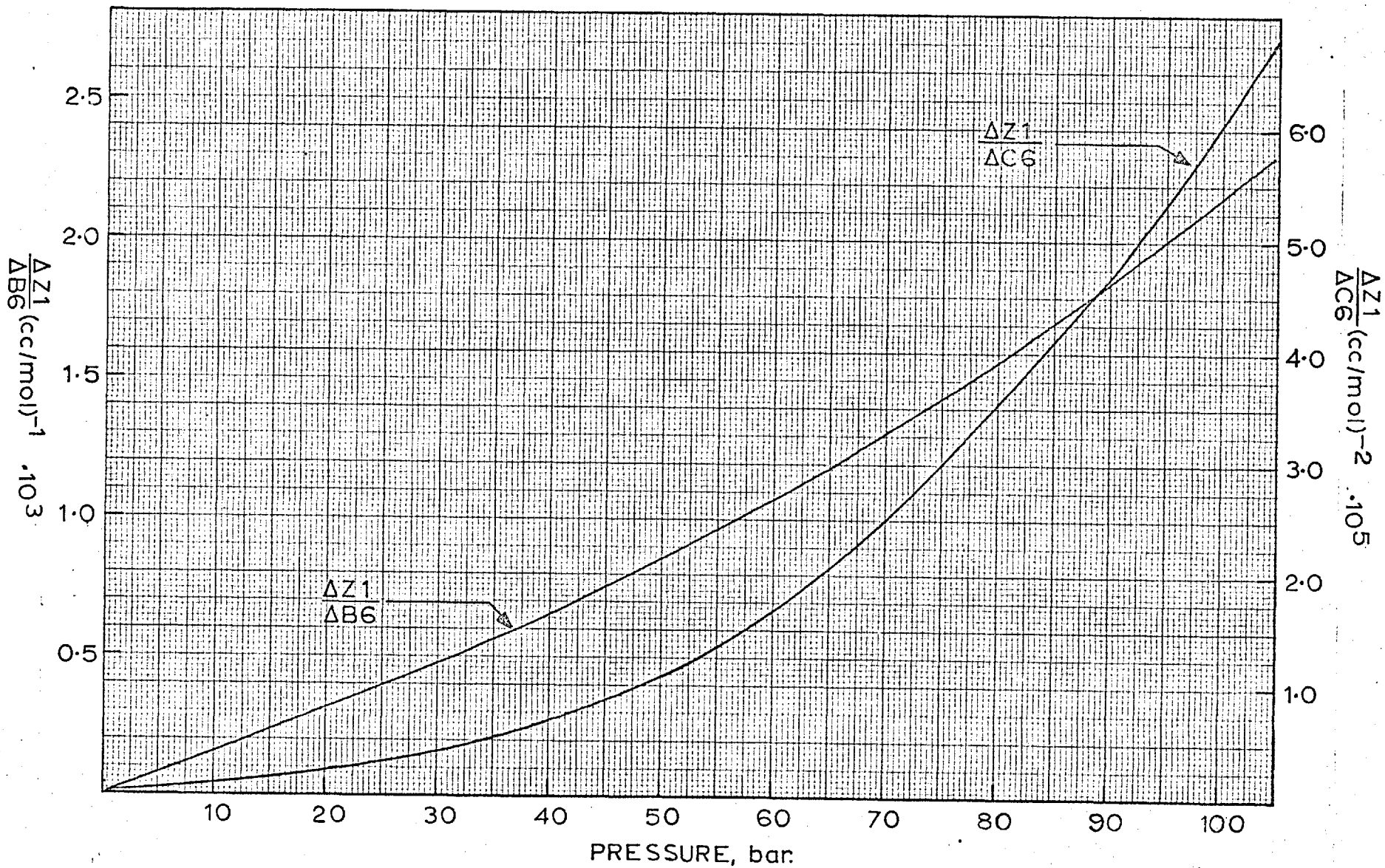

FIG. 4.1. EFFECT OF ERRORS IN 273.15K VIRIAL COEFFICIENTS ON EXPERIMENTAL COMPRESSIBILITY FACTORS.

FIGURE 4.2

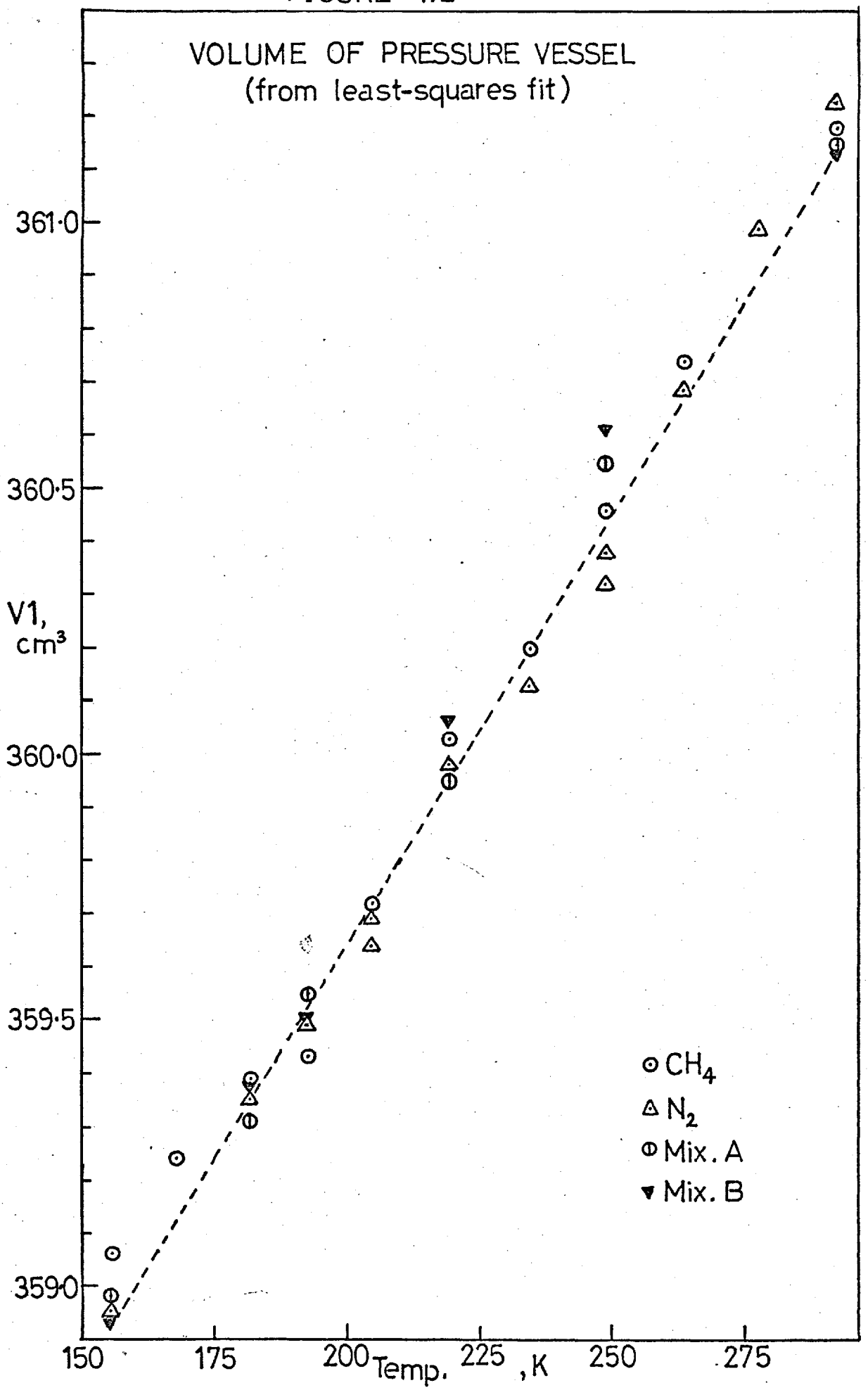
VOLUME OF PRESSURE VESSEL
(from least-squares fit)
361·0
360·5
360·0
359·5
359·0
V1, cm³
150
175
200
225
250
275
Temp. , K
CH4
N2
Mix. A
Mix. B

4.4 Experimental Data of Other Workers

(a) Experimental Methods

There are a variety of available experimental methods for determination of PVT data and virial coefficients of gases. They have recently been reviewed in detail by Mason and Spurling (1). The methods fall into four basic categories,

1) The constant-volume, normal-volume apparatus. The pressure is measured of a gas confined by mercury in a fixed volume at constant temperature. The quantity of gas in the apparatus is determined by an expansion into a known volume at N.T.P.; the mass of the gas is calculated from the normal volume, which, if not known with sufficient accuracy, must be measured independently. Alternatively, the gas may be confined by a diaphragm differential-pressure cell, enabling low temperature measurements to be made.

2) The free-compression apparatus. A weighed sample of gas is confined by mercury in a volume which can be varied by withdrawing or injecting mercury.

3) The Burnett-type of apparatus and similar expansion methods.

4) Comparative methods. These are usually confined to low-pressure measurements of the second virial coefficient. The volumetric behaviour of the gas under study is compared with that of a reference gas, usually helium, for which the second virial coefficient is known accurately.

(b) Extraction of Virial Coefficients from PVT Data

From the virial equation of state, equation (1.3),

$$\frac{Z - 1}{\rho} = B + C\rho + D\rho^2 + \ldots\ldots \qquad (4.4\text{-}1)$$

$$\therefore B = \lim_{\rho \to 0} \left(\frac{Z - 1}{\rho}\right) \qquad (4.4\text{-}2)$$

$$\text{and } C = \lim_{\rho \to 0} \frac{\partial}{\partial \rho} \left(\frac{Z - 1}{\rho}\right) \qquad (4.4\text{-}3)$$

For the published data given in terms of experimental compressibility factors and densities, $(Z - 1)/\rho$ was plotted against density, ρ, and B obtained from the intercept at zero density and C from the limiting slope at zero density. When the data was given in terms of pressure and density, it was first converted into compressibility factors only if the temperature was measured with sufficient accuracy. Older published compressibility factors were corrected, if necessary, using the correct thermodynamic temperature (IPTS '68 scale) and value of the gas constant, R. These corrections were usually small.

Many of the results from apparatuses of category (1) are given in amagat units of density, which is defined as the volume of a given mass of gas at N.T.P. divided by the actual volume at the experimental temperature and pressure. These densities may be converted to units of $mole.cm^{-3}$ if the normal volume is known accurately from independent measurements, as is the case with methane, nitrogen and argon. When the temperature was measured with sufficient accuracy, as in most of the work of Michels et al, e.g. (36, 37), the data was converted into compressibility factors and treated

graphically to obtain virial coefficients.

The precision with which second and third virial coefficients may be obtained by this graphical extrapolation depends on the precision of the measurements, the lowest density to which they extend, and the curvature of the graphical plot. The absolute accuracy is very difficult to assess as it depends also on the absolute accuracy of the original data which is often not estimated by the original experimentalists.

This method is preferred to that of curve-fitting in this instance because any systematic error at low density is shown up as a departure from linearity of the plot, and because it offers a convenient comparison of different data on the same isotherm. It is easier also to find and discard 'rogue' points. When the virial coefficients obtained by re-analysing the data did not differ significantly from those obtained by the experimentalists themselves, the latter values were used.

In dealing with the calculation of virial coefficients from experimental data, Mason and Spurling (1) argue that the accurate determination of virial coefficients requires measurements down to at least 1 or 2 atm pressure. They cite as an example the results of Michels et al (38) for carbon dioxide, where the values of B differ by as much as 3 $cm^3.mole^{-1}$ from those obtained by Butcher and Dadson (39), whose measurements extend down to 2 atmospheres. However, the $(Z - 1)/\rho$ plots for Michels data are linear at low density and extrapolate with precision to zero density. A difference of 3 $cm^3.mole^{-1}$ cannot be attributed to the error in

extrapolation of Michels' data and must be due to systematic errors in one, or both, sets of measurements.

The literature contains many examples of different sets of 'high pressure' measurements (> 10 atmospheres) which show good agreement at the same temperature on $(Z - 1)/\rho$ plots, e.g. methane above 0 ^{o}C (section 4.4(c)), and for which $(Z - 1)/\rho$ is linear at low density. In these cases confidence can be placed in the value of B obtained by extrapolation as it is unlikely that two or more sets of data would exhibit identical systematic errors over a large range, particularly when obtained on different types of apparatus.

At the present 'state of the art' in PVT measurements it appears that, at least for the gases considered here, estimates of B from recent precise 'high-pressure' measurements in general tend to be more accurate than those from 'low-pressure' measurements (below 2 atmospheres). For the latter type of measurements the non-ideality of the gas (i.e. the deviation of Z from 1) is very small and a much higher relative accuracy is required from the pressure measurement, usually with a precision mercury manometer. It is only at low reduced temperatures ($T < T_c$), where the isotherm curvature is high and the maximum pressure is limited by the saturation line, that 'low-pressure' measurements appear more reliable.

(c) Methane

Since the review by Tester (40) in 1961 there appears to be no satisfactory complete review of the PVT data of methane, so it will be treated here in some detail.

(i) Michels and Nederbragt (41)

Using a constant-volume, normal-volume type of apparatus measurements were obtained from 273 to 423 K at pressures from 20 to 380 atmospheres. The results are believed accurate to within 0.1%.

(ii) Schamp, Mason, Richardson and Altman (42)

These workers used an apparatus of the same type as that used by Michels and Nederbragt and the results covered the same temperature range at pressures up to 230 atmospheres. Their results differed by a small amount (about 0.1%) which they attributed to a small quantity of ethane impurity in the methane used by Michels. The second and third virial coefficients, derived by graphical treatment of the data, are given in Table 4.13.

(iii) Douslin, Harrison, Moore and McCulloch (43)

Using an apparatus of the free-compression type, isochoric measurements were obtained from 273 to 623 K and densities from 0.75 to 12.5 mole.litre^{-1} (15 to 400 atmospheres). The results are of high precision and are universally regarded as of high accuracy. The compressibility factors differ by less than .0003 from those of Schamp at densities up to 5 mole.litre^{-1}, which is excellent agreement. Second and third virial coefficients were obtained by Douslin using a method of graphical extrapolation; these values are given in Table 4.13. The small differences between these values and those of Schamp are mainly due to the difference in the method of extraction of the virial coefficients, as retreatment of the data of Douslin by the

TABLE 4.13

Methane: Experimental Virial Coefficients of Other Workers (In units of cc/mole).

(ii) Schamp (42)*

T,K	B	C
273.15	-53.37	2635
298.15	-42.90	2430
323.15	-34.38	2280
348.15	-27.32	2170
373.15	-21.35	2060
398.15	-16.02	1900
423.15	-11.55	1810

(iv) Deffet (44)*

T,K	B	C
323.78	-34.30	2250
374.49	-21.35	2080
425.03	-11.30	1800

(v) Olds (45)*

T,K	B	C
294.26	-44.90	2520
310.93	-38.93	2500
327.59	-33.80	2400
344.26	-28.95	2290
360.93	-24.40	2100
377.59	-20.57	2070
⁎427.59	-8.00	1750
477.59	-3.75	1700
510.93	0.0	1650

(viii) Mueller (49)*

T,K	B	C
199.83	-104.6	3920
⁎227.60	-79.6	3250
⁎255.38	-62.3	2750
283.16	-48.6	2490

(iii) Douslin (43)

T,K	B	C
273.15	-53.35	2620
298.15	-42.82	2370
303.15	-40.91	2320
323.15	-34.23	2150
348.15	-27.06	1975
373.15	-21.00	1834
398.15	-15.87	1727
423.15	-11.40	1640
448.15	-7.56	1585
473.15	-4.16	1514
498.15	-1.16	1465
523.15	+1.49	1420
548.15	+3.89	1385
573.15	+5.98	1360
598.15	+7.88	1345
623.15	+9.66	1330

(vii) Kvalnes (48)*

T,K	B	C
203.15	-99.7	3700
223.15	-82.5	3320
248.15	-66.4	3000
273.15	-53.7	2660

(xi) Thomaes (53)

T,K	B
108.5	-363.0
125.2	-268.5
149.1	-187.8
186.4	-126.2
223.6	-82.7
249.3	-68.5

* Re-treated data

⁎ large scatter on isotherm

TABLE 4.13 (continued)

(xii) Brewer (54)

T,K	B
123.15	-264.3
148.15	-185.9
173.15	-138.7
198.15	-106.5
223.15	-83.6

(xiii) Byrne (55)

T,K	B
110.83	-330.1
112.43	-319.9
114.45	-307.8
116.79	-295.5
121.25	-274.5
128.84	-244.3
136.75	-218.9
148.28	-187.7
162.29	-158.4
178.41	-132.2
202.49	-103.4
221.10	-85.8
243.80	-70.3
273.17	-53.7

method of 4.4(b) leads to values in even closer agreement.

(iv) Deffet, Liliane and Fick (44)

Using an apparatus of the free-compression type, results were obtained at three temperatures, 328.8 K, 374.5 K and 425.0 K at pressures from 10 to 253 bars. Plots of $(Z - 1)/\rho$ vs. ρ were smooth and B and C could be obtained with precision; these values are shown in Table 4.13. They are in close agreement with those of Douslin and Schamp.

(v) Olds, Reamer, Sage and Lacey (45)

Measurements were obtained on a free-compression type of apparatus at temperatures from 294 to 511 K and at pressures from 13 to 670 bars. The results are of lower accuracy than those of Douslin et al and were pre-smoothed prior to publication. The second and third virial coefficients obtained by graphical retreatment are shown in Table 4.13.

(vi) Keyes and Burks (46), Freeth and Verschoyle (47)

These early measurements above 0 ^{o}C have been superseded by the later, more accurate and extensive data already mentioned, and therefore were not considered here.

(vii) Kvalnes and Gaddy (48)

These early low-temperature measurements (203 to 473 K) at pressures from 20 to 1000 atmospheres were obtained on an early form of constant-volume, normal-volume apparatus. An accuracy no better than 0.1 to 0.2% is expected. Above 273 K the $(Z - 1)/\rho$ plots showed considerably more scatter than those of Douslin and the higher temperature isotherms

were rejected in favour of Douslin's. Below 273 K the data appear to show less scatter and the virial coefficients given in Table 4.13 were obtained by graphical retreatment. The lowest pressure on each isotherm is quite high and the points are not closely spaced, leading to an estimated error in B of about $\pm$ 1 $cm^3.mole^{-1}$ caused by the extrapolation alone.

(viii) Mueller, Leland and Kobayashi (49)

These workers obtained results at six temperatures from 144 to 283 K at pressures up to 500 bar using a Burnett apparatus. The experimental compressibility factors had been derived from the actual Burnett measurements by a graphical method of data treatment and then interpolated to evenly-spaced values of pressure. Plots of $(Z - 1)/\rho$ vs ρ show considerable scatter on two isotherms (227.6 and 255.4 K) and for the two lowest temperatures insufficient points (3 or 4) are given to enable virial coefficients to be extracted. The derived values of B and C for the other isotherms are given in Table 4.13.

(ix) Hoover, Nagata, Leland and Kobayashi (50)

A Burnett apparatus capable of very high precision was used in this work and second and third virial coefficients were obtained at 131.9 K and 191.1 - 273.2 K. The maximum pressure was 40 atmospheres. However, the compressibility factors from Hoover (51) show considerable scatter on a Z vs. P plot (e.g. as much as .2 to .5% at 240 K), which is completely incompatible with the high precision claimed for the virial coefficients. In view of this serious, unexplained

discrepancy these data were rejected as a source of virial coefficients.

(x) Vennix, Leland and Kobayashi (52)

A constant-volume apparatus was used, the cell being charged with a known mass of methane from a weighed cylinder. The volume of the cell was determined by a procedure involving Burnett expansions of helium into a cylinder of known internal volume. Isochoric measurements were obtained between .0025 and .225 mole.cm^{-3} at temperatures from 130 to 273 K and at pressures up to 690 bars. The data, which were estimated as accurate to 0.05%, were also presented as interpolated to even values of temperature. There are too few low density points to enable the virial coefficients to be extracted. At 0 ^{o}C the data are in excellent agreement with those of Douslin and of Schamp.

(xi) Thomaes and van Steenwinkel (53)

These authors measured the second virial coefficient at low pressure (below 1 atmosphere) and low temperatures (108 to 249 K). The volumetric expansion was compared with that of hydrogen. The values obtained are shown in Table 4.13; no corrections were applied for the effect of higher virial coefficients, which could be significant at the lowest temperature.

(xii) Brewer (54)

The second virial coefficients between 123 and 223 K were determined in a low-pressure apparatus by measurement of the pressure difference between two constant, equal volumes

of methane and helium. The second virial coefficient at 0 °C was taken as - 53.75 $cm^3.mole^{-1}$ and corrections were applied for the effect of the third virial coefficient. The results are given in Table 4.13; they are estimated as accurate to .5%.

(xiii) Byrne, Jones and Staveley (55)

The apparatus used was similar in principle to that of Brewer, the pressure difference between methane and helium being measured with a precision differential manometer. The second virial coefficient was measured at temperatures from 111 to 273 K. The value of 42.96 $cm^3.mole^{-1}$ was assumed for the second virial coefficient at 25 °C. Small corrections to the results were applied for the effect of adsorption, but none for the third virial coefficient. The results are given in Table 4.13.

(xiv) McMath and Edmister (56), Lee and Edmister (57)

Measurements were obtained by Lee at 298, 323 and 348 K with a Burnett apparatus. McMath obtained isochoric measurements at 264.3, 277.6 and 288.7 K in a constant-volume apparatus, the density of the gas being taken from the isotherm of Lee at 298 K. Unfortunately the methane used was only of 99% purity and the results were not of sufficient accuracy to justify their inclusion here.

(xv) Pavlovich and Timrot (58)

These results covered a wide range of temperature (103 to 333 K), but were found by Douslin et al (iii) to be of very low accuracy and were therefore discarded.

(xvi) Robertson and Babb (59)

Very high-pressure measurements (up to 10 k bar) were determined from 273 to 473 K.

(xvii) Jansoone, Gielen, Boelpaep and Verbeke (60)

Measurements were obtained in the immediate vicinity of the critical point, giving accurate estimates of the critical constants:

$$T^c = 190.50 \text{ K}$$
$$\rho^c = 0.010148 \text{ mole.cm}^{-3}$$

(d) Nitrogen

Recent reviews of the PVT data on nitrogen have been published by Vasserman and Rabinovich (61), Wood et al (27), and Coleman and Stewart (62). All of the available data are not considered here, but only those results not rejected by these reviewers.

(i) Holborn and Otto (63)

This early work used a constant-volume, normal-volume apparatus to obtain measurements at temperatures from 143 to 673 K and at pressures from 20 to 100 atmospheres. The second and third virial coefficients given in Table 4.14 are those obtained by Saville (64) from a curve-fit to the data after applying necessary corrections to the original figures. B is estimated as accurate to $\pm$ 1 $\text{cm}^3.\text{mole}^{-1}$.

(ii) Onnes and van Urk (65)

These early measurements were obtained at Leiden with a glass capillary free-compression apparatus at temperatures

TABLE 4.14

Nitrogen: Experimental Virial Coefficients of Other Workers (in units of $cm^3.mole^{-1}$)

(i) Holborn (63)*

T,K	B	C
143.15	-79.38	2814
173.15	-52.73	2313
223.15	-26.28	1784
273.15	-10.31	1546
323.15	-0.83	1450
373.15	+6.05	1425
423.15	+11.58	1174
473.15	+15.53	1068
573.15	+20.44	1068
673.15	+23.77	1085

(ii) Onnes (65)*

T,K	B	C
⁎126.83	-102.2	3482
128.69	-99.5	3488
131.62	-94.5	3232
141.88	-81.16	2992
151.96	-69.63	2586
170.90	-52.38	2022
⁎192.05	-39.48	1929
⁎222.89	-24.8	1360
⁎249.53	-16.8	1552
⁎273.15	-8.96	868
⁎293.15	-5.69	1228

(iii) Michels (33),(66)*

T,K	B	C
273.15	-10.25	1500
298.48	-4.78	1405
322.92	-0.52	1400
347.91	+3.00	1385
372.88	+6.31	1260
398.22	+9.20	1185
423.04	+11.90	1040

(iv) Canfield (67)*

T,K	B	C
133.15	-92.27	3305
143.14	-79.51	2975
158.15	-64.08	2596
183.15	-45.17	2162
223.13	-25.35	1741
273.15	-10.06	1441

(v) Crain (34)

T,K	B	C
143.16	-79.45	2889
163.16	-59.42	2392
203.16	-33.85	1837
273.15	-10.26	1517

(vi) Saurel (68)*

T,K	B	C
423.15	+11.25	1320
473.15	+15.05	1265
573.15	+20.30	1200
673.15	+23.80	1140
773.15	+26.10	1120
873.15	+28.00	1040
973.15	+29.25	1050
1073.15	+30.10	1040

* Re-treated data

⁎ Large scatter on isotherm

TABLE 4.14 (continued)

(vii) Friedman (70)

T,K	B
80	-251
90	-200.5
100	-162.1
110	-131.8
120	-114.6
125.2	-106.9
150	-71.2
175	-49.4
200	-34.33
250	-16.19
273.15	-9.50
300	-3.54

(viii) Pool (71)

T,K	B
90	-201

(ix) Witonsky (72)

T,K	B
448.15	+14.28
523.15	+18.34
598.15	+20.83
673.15	+23.40
748.15	+24.75

(x) Pfefferle (73)

T,K	B	C
303.16	-4.17	1485

from 124 to 293 K and at pressures from 30 to 50 atmospheres. The second and third virial coefficients as determined by Saville (64) are shown in Table 4.14. Although of lower accuracy than those of Holborn and Otto, the results are useful at low temperature, where there is a scarcity of experimental third virial coefficients.

(iii) Michels, Wouters and de Boer (33), Otto, Michels and Wouters (66)

With a constant-volume, normal-volume apparatus measurements believed accurate to .05% were obtained at temperatures from 273 to 423 K and at pressures from 20 to 410 atmospheres. Second and third virial coefficients obtained by graphical treatment of the data are shown in Table 4.14. B is estimated as accurate to $\pm$ .5 $cm^3.mole^{-1}$.

(iv) Canfield, Leland and Kobayashi (67)

Canfield used a Burnett apparatus in conjunction with the graphical method of data reduction to obtain compressibility factors at temperatures from 133 to 273 K and pressures up to 500 atmospheres. There are apparently systematic errors at low pressure and the virial coefficients obtained by Wood et al (27) from a graphical treatment of the data are preferred. These are shown in Table 4.14.

(v) Crain and Sonntag (34)

These authors also used a Burnett apparatus, obtaining results at four temperatures from 143 to 273 K and pressures up to 500 atmospheres. The data are in excellent agreement with those of Canfield, within .05% except at very high

pressure. The virial coefficients given in (34) are shown in Table 4.14.

(vi) Saurel (68)

These results obtained with a modified free-compression type of apparatus are important as they extend to high temperatures (423 to 1073 K); the pressure range is from 10 to 900 atmospheres. The plots of $(Z - 1)/\rho$ vs ρ are quite smooth, enabling B and C to be extracted with high precision; these values are shown in Table 4.14.

(vii) Friedman (69)

These results were obtained with a constant-volume gas thermometer, and extend to very low temperatures (from 80 to 300 K) and pressures up to 200 atmospheres. The data have, unaccountably, not been published in the standard scientific literature but the experimental virial coefficients have been published elsewhere (70): the values of B are shown in Table 4.14. The overall precision in Z has been estimated as $\pm$ 0.1%, but this is still not sufficiently precise to enable meaningful third virial coefficients to be obtained at very low temperatures.

(viii) Pool, Saville, Herrington, Shields and Staveley (71)

One second virial coefficient, at 90 K, was obtained by expansion from a calibrated piezometer into a series of calibrated bulbs at 25 ^{o}C. The accuracy was estimated as $\pm$ 2 $cm^3.mole^{-1}$.

(ix) Witonsky and Miller (72)

The results of these high-temperature Burnett measurements

(448 to 748 K) were given in terms of the 'pressure' virial coefficient, B',

where $Z = 1 + B'P + \ldots$

These values were converted to volume virial coefficients by means of the approximate relation, $B = B'.RT$. The results are given in Table 4.14.

(x) Pfefferle, Goff and Miller (73)

The same Burnett method was used as in (ix) but results were obtained at only one temperature, 303 K. The values of B and C are shown in Table 4.14.

(xi) Hall and Canfield (74)

A low-temperature Burnett apparatus was used to study the helium/nitrogen system. Only two isotherms were determined for pure nitrogen, at 113 and 103 K, where the maximum pressure was very low (16 bar and 9 bar respectively), and the problems with the data treatment are large: these results were not used.

(e) Methane/Nitrogen Mixtures

(i) Keyes and Burks (75)

These early measurements (1928) were obtained with a free-compression type of apparatus at temperatures from 273 to 373 K and at pressures from 30 to 240 bars. Two compositions were studied; the data were re-treated graphically to obtain the second and third virial coefficients shown in Table 4.15. The $(Z - 1)/\rho$ plots were quite smooth, indicating a reasonable degree of precision. Values of B_{12} were obtained for each mixture using the pure component virial coefficients of Douslin et al (32) (Table 4.13) and of Michels et al (33)

(Table 4.14). It can be seen that there are systematic differences between the values for different mixtures. The mean of the two values was used for purposes of data comparison.

Estimates of C_{112} and C_{221} were obtained from the experimental third virial coefficients, by solving the equations,

$$C = x_1^3 C_{111} + 3x_1^2 x_2 C_{112} + 3x_1 x_2^2 C_{221} + x_2^3 C_{222}$$

where x_1 is the mole fraction of methane and x_2 the mole fraction of nitrogen.

These values, shown in Table 4.15, are unlikely to be more accurate than $\pm$ 500 $cm^6.mole^{-2}$ because of the systematic differences between the mixtures.

(ii) Brewer (54)

By measurement of the pressure change on mixing at constant volume, the quantity E was obtained,

where $E = B_{12} - \frac{1}{2}(B_{11} + B_{22})$

Only one measurement, at 0 ^oC, appears to have been carried out; B_{12} was re-calculated using the pure component virial coefficients of Douslin et al and of Crain and Sonntag. The result, believed accurate to about 1 $cm^3.mole^{-1}$, is given in Table 4.15.

(iii) Krichevskii and Levchenko (76)

The minimum pressure measured in this work was 100 atmospheres and so virial coefficients cannot be extracted. Plots of $(Z - 1)/\rho$ vs ρ for a few isotherms showed large scatter and the data were discarded.

TABLE 4.15

Methane/Nitrogen: Virial Coefficients of Other Workers
(in units of $cm^3.mole^{-1}$)

(i) Keyes (75)*

(1) X_{CH_4} = 0.4332

T,K	B	C
273.15	-25.55	1995
323.15	-12.15	1710
373.15	-3.05	1670

(2) X_{CH_4} = 0.80531

T,K	B	C
273.15	-42.35	2295
323.15	-25.28	1990
373.15	-13.57	1835

T,K	$B_{12}(1)$	$B_{12}(2)$	C_{112}	C_{221}
273.15	-24.9	-23.4	1890	2170
323.15	-11.2	-9.4	1780	1690
373.15	-2.19	-0.6	1780	1710

(ii) Brewer (54)*

T,K	B_{12}
273.15	-25.54

* Re-treated data.

(iv) Bloomer, Eakin, Ellington and Gami (77)

Results on mixtures at low temperatures and high pressure have been obtained but unfortunately the actual data remain unpublished. Tables of compressibility factors are presented which are the result of a fit of the Benedict-Webb-Rubin equation of state to the data. These tables represent the data to within 0.5%, but these authors presented no estimate of the accuracy of the original measurements.

(v) Blake, Bretton and Dodge (78)

Measurements were obtained at one temperature only (299.5 K) and at high pressures (300 to 5000 atmospheres), for two mixtures in a modified constant-volume type of apparatus. The results were pre-smoothed and presented at fixed intervals of pressure.

4.5 Comparison with other workers

A detailed comparison of the second virial coefficients can be made by presenting graphically the differences between the experimental values and those calculated from an arbitrary smooth function of temperature. That chosen was the function

$$B_{ref}(T) = a_1 + a_2/T + a_3/T^3 + a_4/T^4 \qquad (4.5\text{-}1)$$

This equation was fitted to the experimental virial coefficients using the general non-linear least-squares procedure. The resultant coefficients are presented in Chapter 5, Table 5.2.

The deviations, $B_{exp}(T) - B_{ref}(T)$, are shown in

figure 4.3 for methane and figure 4.5 for nitrogen. The third virial coefficients are compared with the previously published results in figure 4.4 for methane and figure 4.6 for nitrogen. The interactional virial coefficients are compared directly: B_{12} in figure 4.7 and C_{112}, C_{221} in figure 4.8.

(a) Methane

It can be seen that the second virial coefficients of this work at the higher temperatures of our range are in excellent agreement, within experimental error, with those of Douslin and of Schamp. (The results of Michels are very close to these latter sets of values and for the sake of clarity are not shown.) At lower temperatures our results are in good agreement with the low-pressure results of Brewer, within experimental error, but some 1 to 3 $cm^3.mole^{-1}$ less negative than those of Byrne. The results of Mueller are in reasonable agreement with our values considering the scatter inherent in some isotherms, but the results of Kvalnes are some 1 to 1.5 $cm^3.mole^{-1}$ less negative. The results of Thomaes show considerable scatter.

For the intermolecular potential study of chapter 5, the following second virial coefficients given in Table 4.13 were not used:-

(i) Michels (41), and Deffet (44), because they are duplicated by the results of Douslin (32) and Schamp (42), with which they are in close agreement.

(ii) Thomaes and van Steenwinkel (53).

(iii) Kvalnes and Gaddy (48).

(iv) Mueller (49) (at 283 K).

(v) Olds (45).

FIGURE 4.3

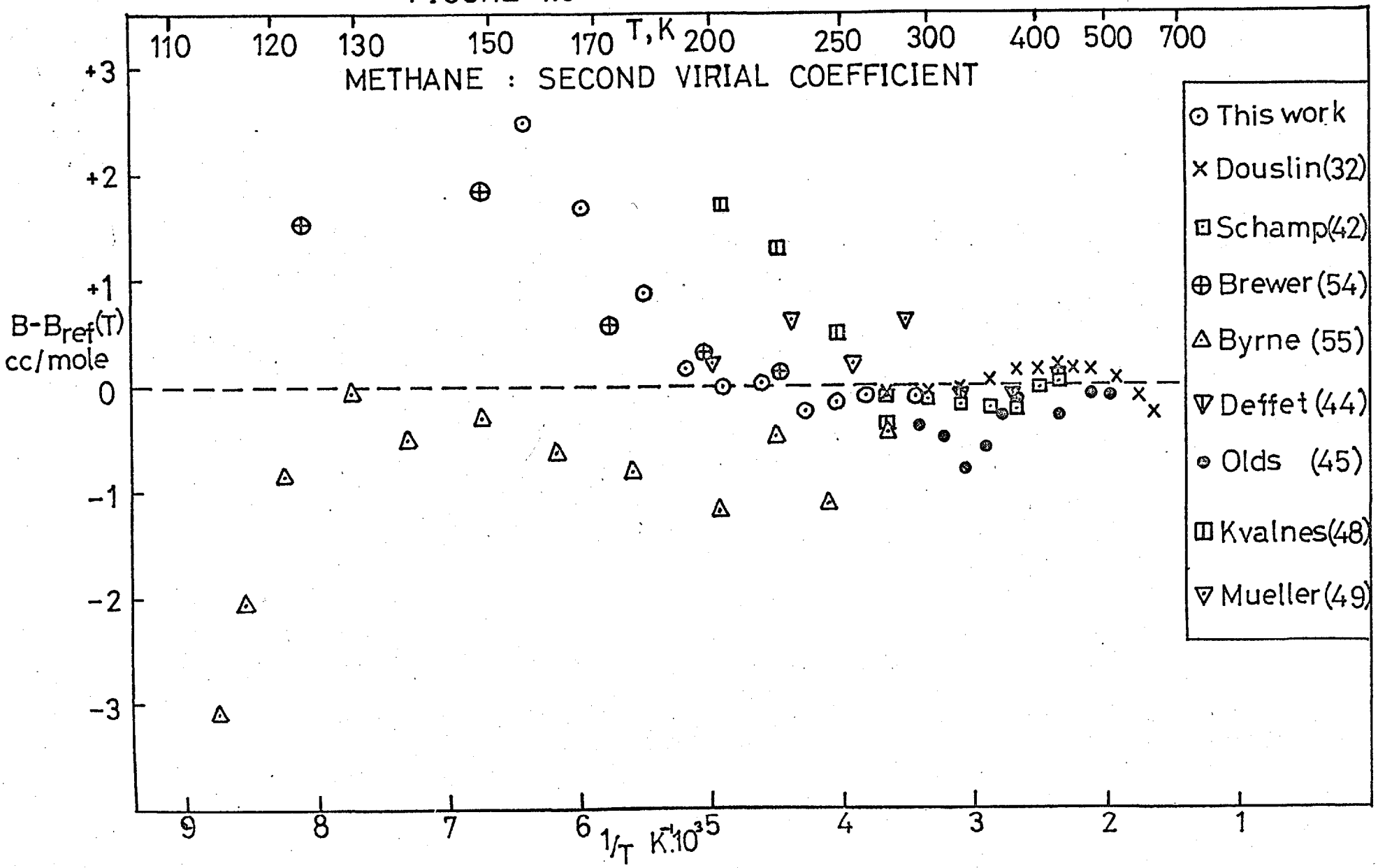
METHANE : SECOND VIRIAL COEFFICIENT
T, K
110
120
130
150
170
200
250
300
400
500
700
+3
+2
+1
0
−1
−2
−3
B-Bref(T)
cc/mole
9
8
7
6
5
4
3
2
1
1/T K.10³
This work
Douslin(32)
Schamp(42)
Brewer(54)
Byrne (55)
Deffet (44)
Olds (45)
Kvalnes(48)
Mueller(49)

FIGURE 4.4

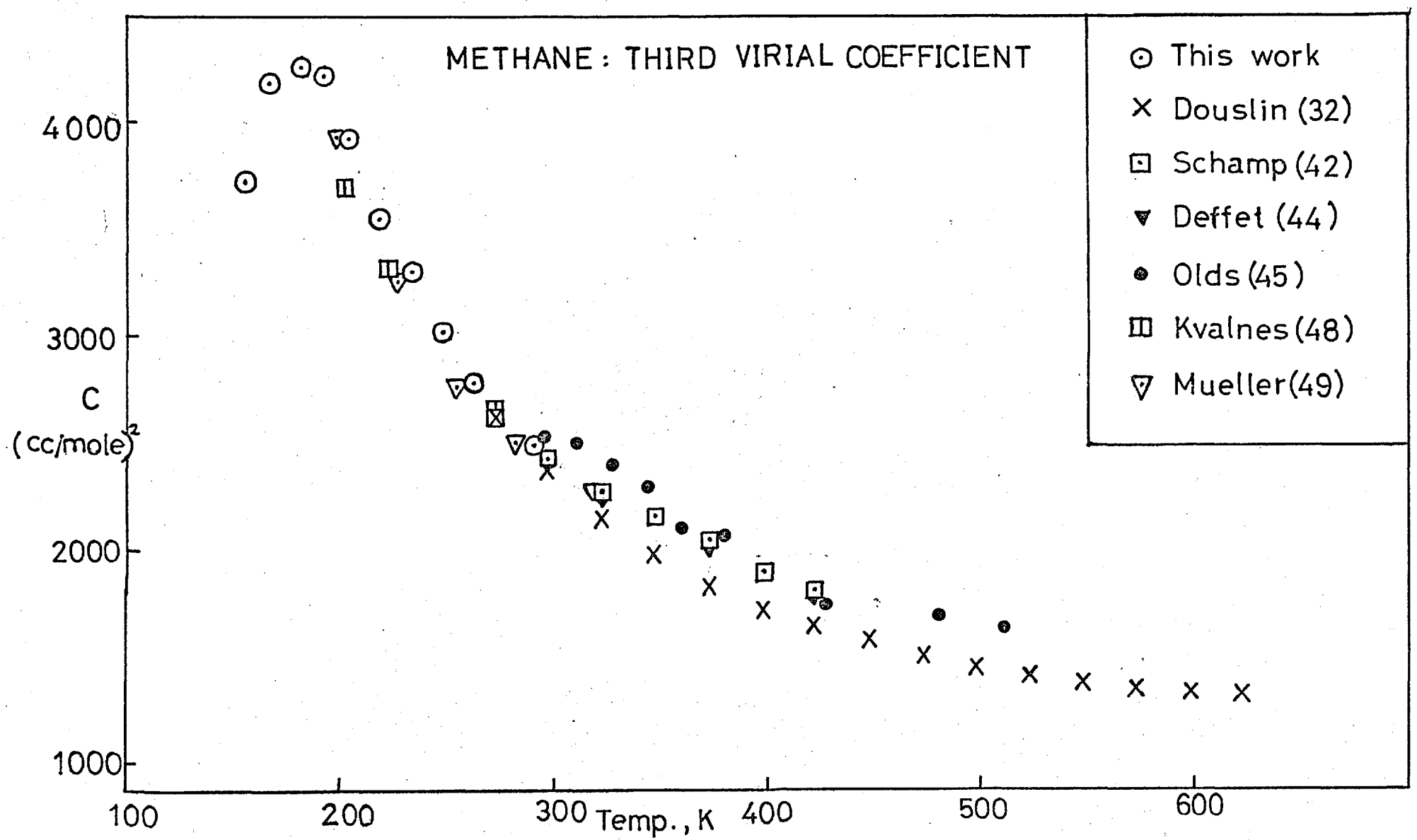
METHANE : THIRD VIRIAL COEFFICIENT
This work
Douslin (32)
Schamp (42)
Deffet (44)
Olds (45)
Kvalnes (48)
Mueller (49)
4000
3000
2000
1000
C
(cc/mole)²
100
200
300
400
500
600
Temp., K

FIGURE 4.5

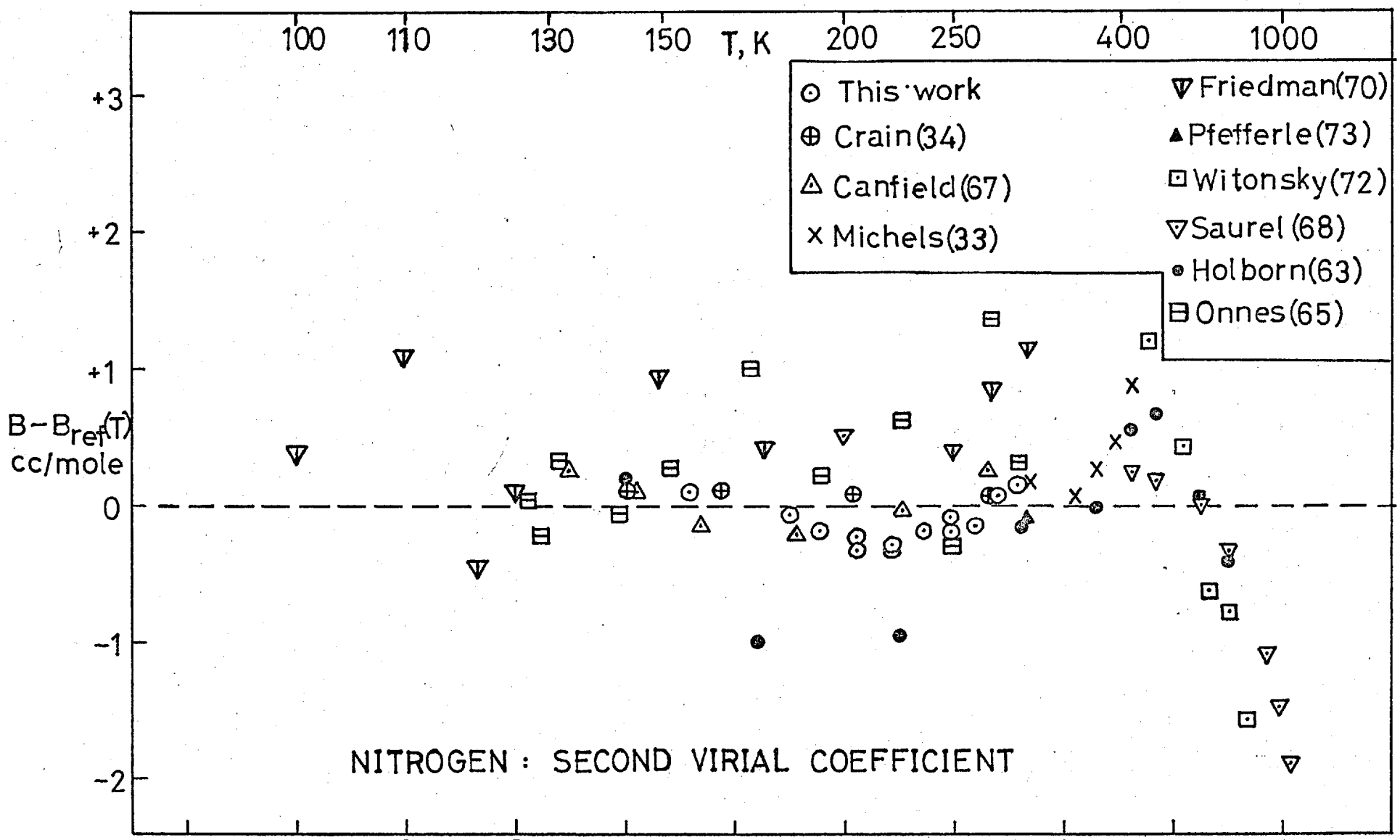
100
110
130
150
T, K
200
250
400
1000
+3
+2
+1
0
-1
-2
B-B_ref(T)
cc/mole
This work
Crain(34)
Canfield(67)
Michels(33)
Friedman(70)
Pfefferle(73)
Witonsky(72)
Saurel(68)
Holborn(63)
Onnes(65)
NITROGEN : SECOND VIRIAL COEFFICIENT
11
10
9
8
7
6
5
4
3
2
1
1/T, K⁻¹.10³

FIGURE 4.6

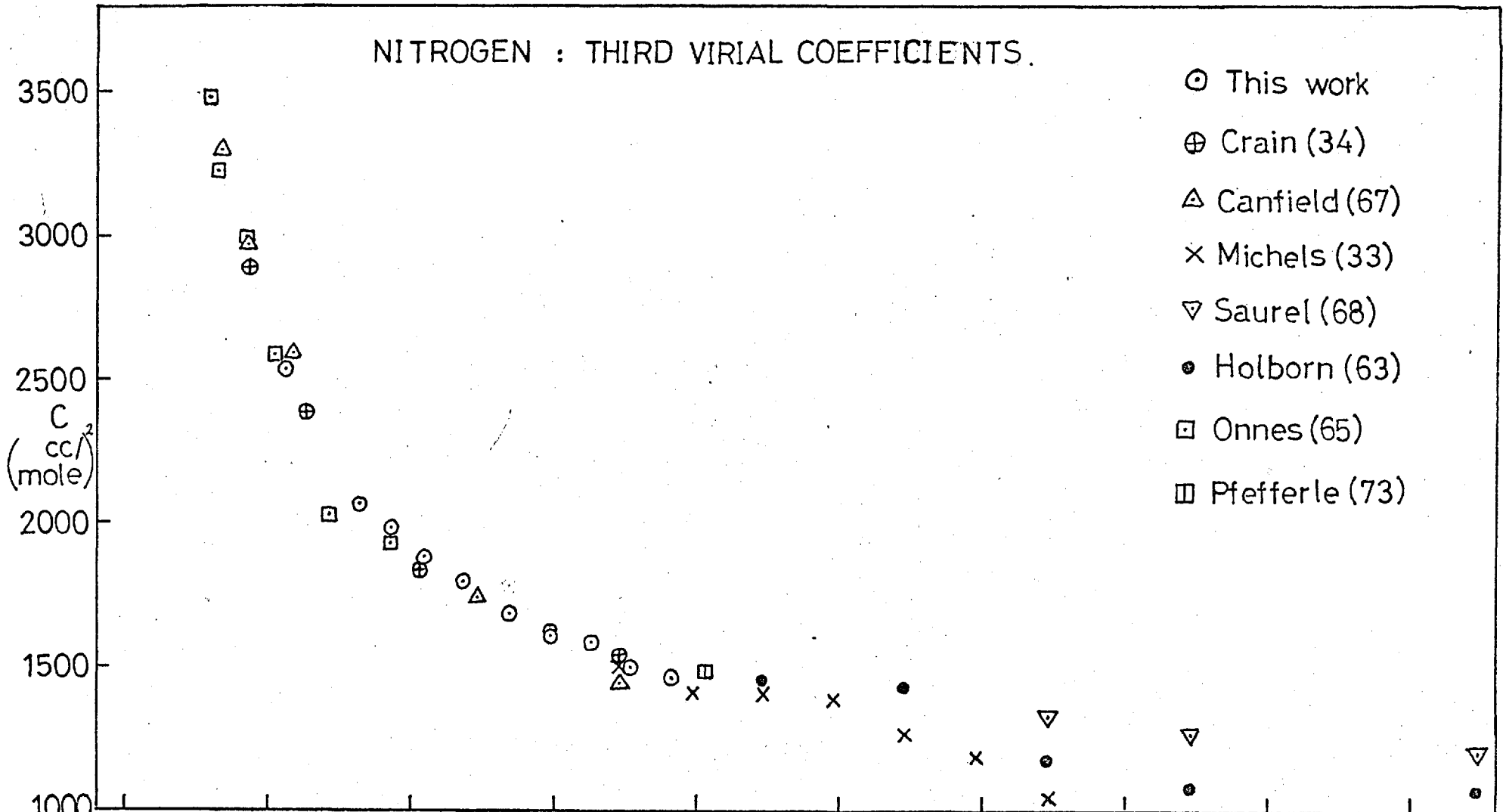
NITROGEN : THIRD VIRIAL COEFFICIENTS.
This work
Crain (34)
Canfield (67)
Michels (33)
Saurel (68)
Holborn (63)
Onnes (65)
Pfefferle (73)
C (cc/mole)²
3500
3000
2500
2000
1500
1000
100
150
200
250
300
350
400
450
500
550
Temp. , K

FIG. 4.7

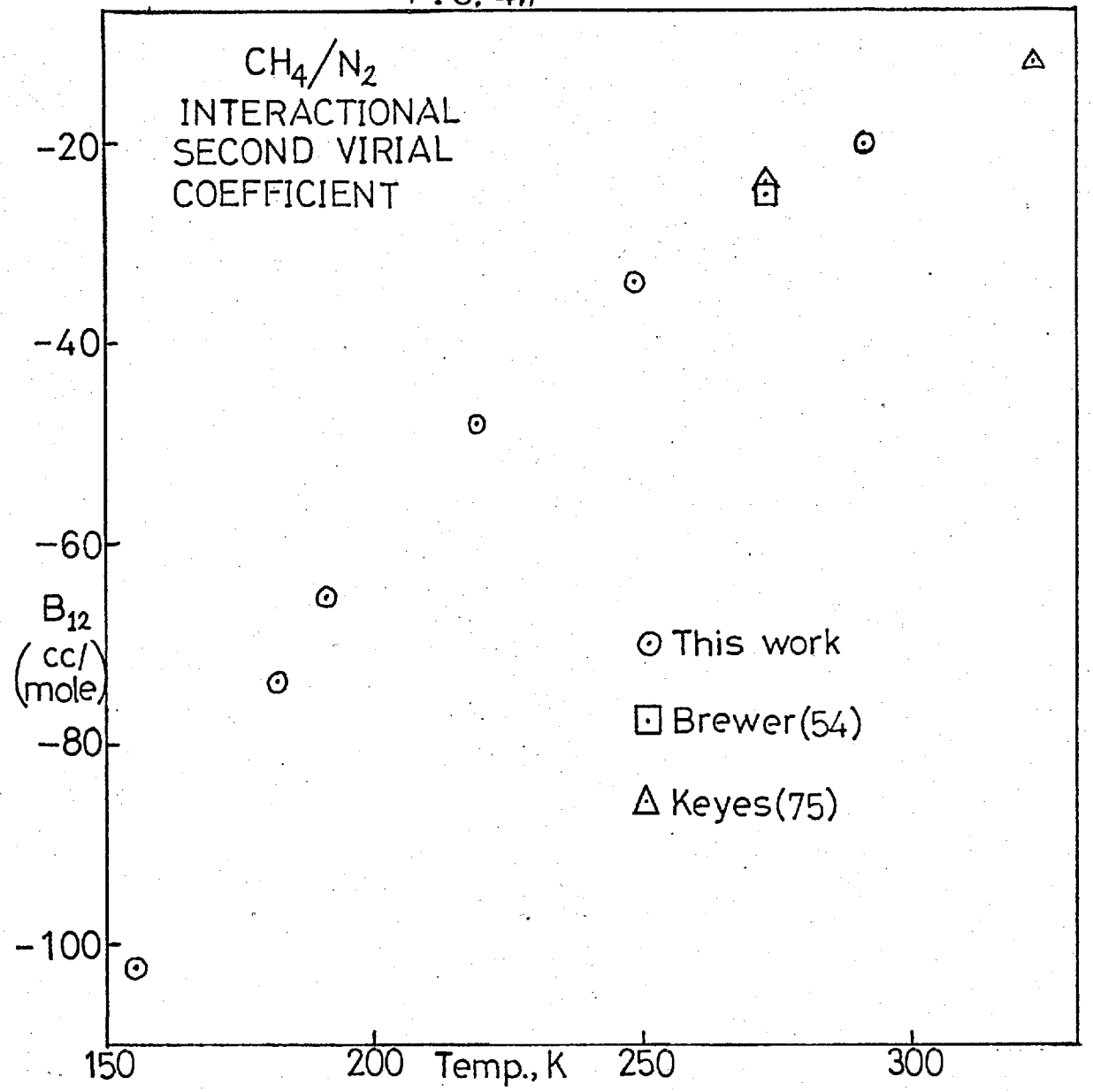
CH_4/N_2
INTERACTIONAL
SECOND VIRIAL
COEFFICIENT
-20
-40
-60
-80
-100
B_{12}
(cc/mole)
⊙ This work
⊡ Brewer(54)
△ Keyes(75)
150
200
Temp., K
250
300

FIG. 4.8

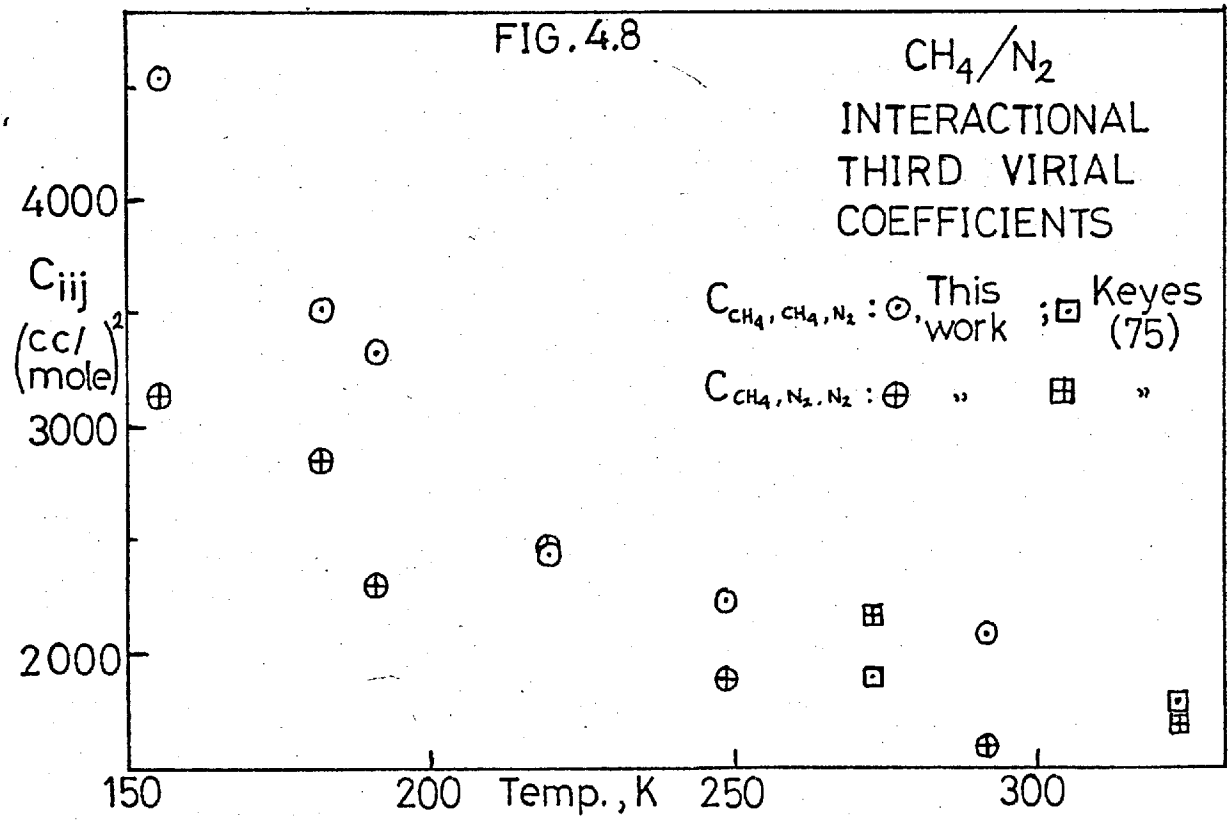
CH_4/N_2
INTERACTIONAL
THIRD VIRIAL
COEFFICIENTS
C_{CH_4, CH_4, N_2} : ⊙, This work ; ⊡ Keyes (75)
C_{CH_4, N_2, N_2} : ⊕ " ⊞ "
4000
3000
2000
C_{iij}
$(cc/mole)^2$
150
200
Temp., K
250
300

Each of the remaining experimental B values was assigned a weighting factor, ω, for use in the curve-fitting of chapter 5,

$$\text{where } \omega = \frac{1}{\sigma^2} \qquad (4.5\text{-}2)$$

σ is the probable error in the experimental value, estimated by consideration of both the quoted experimental errors and the deviation from a smooth curve through the data. For methane the data sets were weighted in the following order, those at the beginning being most highly weighted:- Douslin; Schamp; this work; Brewer; Mueller; Byrne.

The third virial coefficients of this work (figure 4.4) are also in excellent agreement with those of Douslin and of Schamp at the upper end of our temperature range. Below 0 ^{o}C there are no other measurements of equivalent accuracy, but there is fair agreement with the results of Mueller and of Kvalnes, which show greater scatter.

(b) Nitrogen

It can be seen from figure 4.5 that the second virial coefficients of this work are in good agreement (within 0.2 to 0.3 $cm^3.mole^{-1}$) with those of Crain, of Canfield, and of Michels. The results of Holborn, of Onnes, and of Friedman all show greater scatter but the differences are probably within their experimental error. The high temperature results of Saurel are in good agreement with those of Holborn but show a small difference of 0.6 $cm^3.mole^{-1}$ from the result of Michels at 423 K. The results of Witonsky are also in reasonable agreement with those of Saurel, but show a little more scatter.

On the whole there are no serious discrepancies between

the results of different experimentalists and in the intermediate temperature range good agreement exists between our results and those of Crain and of Canfield. For the intermolecular potential study the following values of Table 4.14 were not used,

(i) Onnes and van Urk (65) (B only).

(ii) Holborn and Otto (63) (below 300 K).

(iii) Hall and Canfield (74).

The remaining sets of data were weighted for use in curve-fitting in the following order of decreasing importance: Crain, Michels and this work; Canfield; Saurel; Witonsky; Pfefferle; Holborn; Friedman; Pool.

Our third virial coefficients, figure 4.6, also agree within experimental error with the results of Crain and of Canfield, and, at the upper end of our temperature range, with the results of Michels. It can be seen that accurate measurements are still needed at lower temperatures, around the maximum of the third virial coefficient.

(c) Methane/Nitrogen

Our values of B_{12}, figure 4.7, show scatter of less than 1 $cm^3.mole^{-1}$ about a smooth curve through the data, which is within the estimated maximum limits of experimental error. The one point of Brewer at 273 K is in good agreement. If our results are extrapolated to higher temperatures, the curve lies some 2 $cm^3.mole^{-1}$ below the results of Keyes and Burks, which is within the estimated experimental error of these early measurements.

The scatter shown about a smooth curve through our interactional third virial coefficients, figure 4.8, is also

within experimental error.

4.6 Comparison of Compressibility Factors

As many of the experimental isotherms extended beyond the region where only second and third virial coefficients were important, it is necessary to compare the higher-pressure compressibility factors with the results of other workers. The results for the mixtures will be discussed in chapter 6.

(a) Methane

To facilitate the comparison of compressibility factor data an equation of state was employed; the differences between the calculated and experimental values may then be readily interpolated between temperatures and pressures (or densities). The equation of state used was that of Vennix and Kobayashi (79), as described in more detail in section 6.

In figure 4.9 Z(experimental) - Z(calculated) is plotted against density for the 218.9 K, 204.6 K and 192.6 K isotherms of Table 4.1, and for the experimental isotherms in this temperature range of Vennix (52), of Mueller (49), and of Kvalnes (48).

For the 218.9 K and 204.6 K isotherms our results are in good agreement with those of Vennix, the largest discrepancy being about + .001 (.2%) at a density of about .008 mole.cm^{-3} on the 204.6 K isotherm. The data of Mueller show fairly large scatter but apart from one or two points they lie within .5% of our values. The compressibility factors of Kvalnes and Gaddy, however, show a systematic deviation which increases with density, reaching a maximum of .026 (7%) at 203.1 K and .0107 mole.cm^{-3}.

FIGURE 4.9

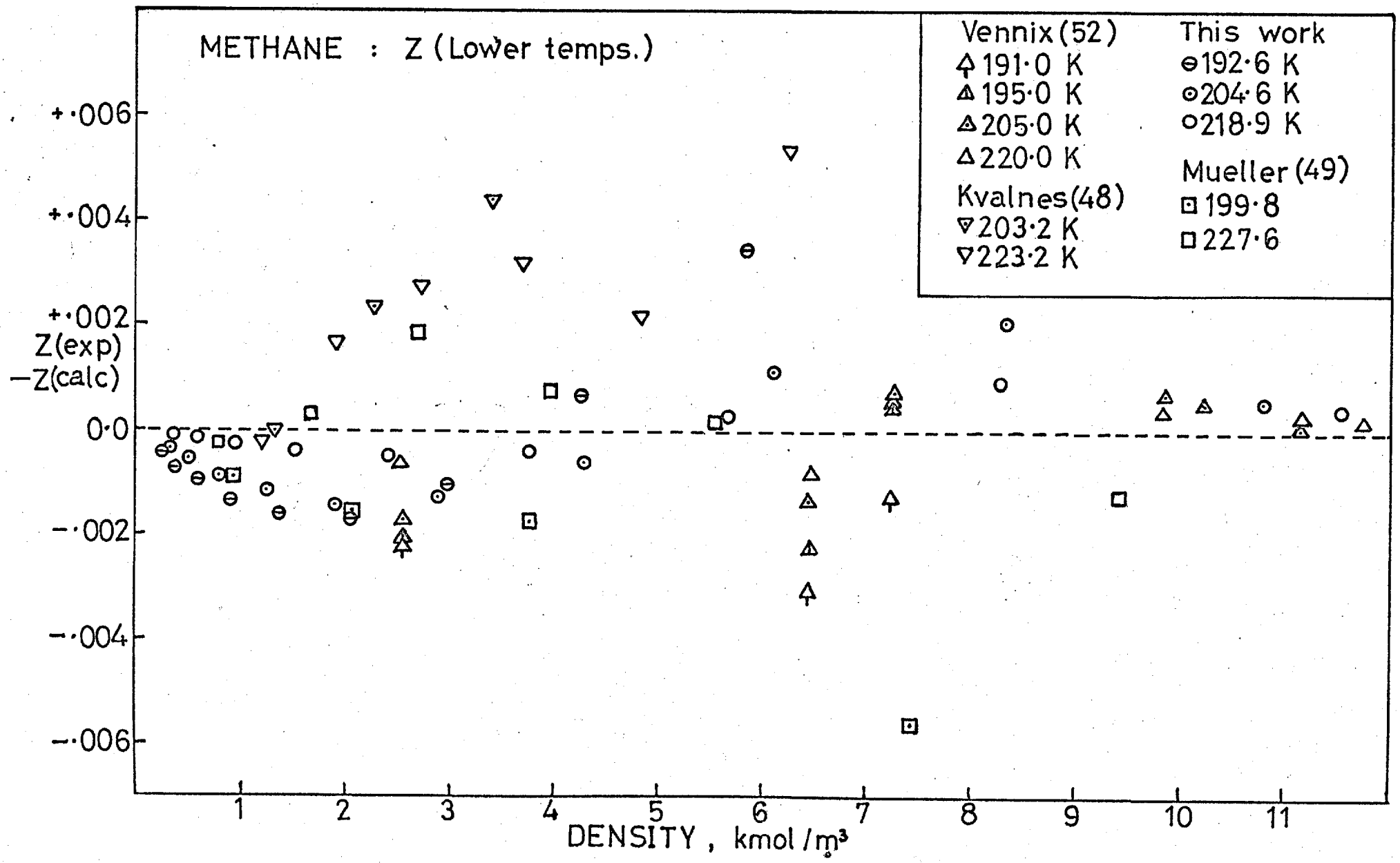
METHANE : Z (Lower temps.)
Vennix (52)
191·0 K
195·0 K
205·0 K
220·0 K
Kvalnes (48)
203·2 K
223·2 K
This work
192·6 K
204·6 K
218·9 K
Mueller (49)
199·8
227·6
+·006
+·004
+·002
Z(exp) −Z(calc)
0·0
−·002
−·004
−·006
1
2
3
4
5
6
7
8
9
10
11
DENSITY , kmol /m³

FIGURE 4.10

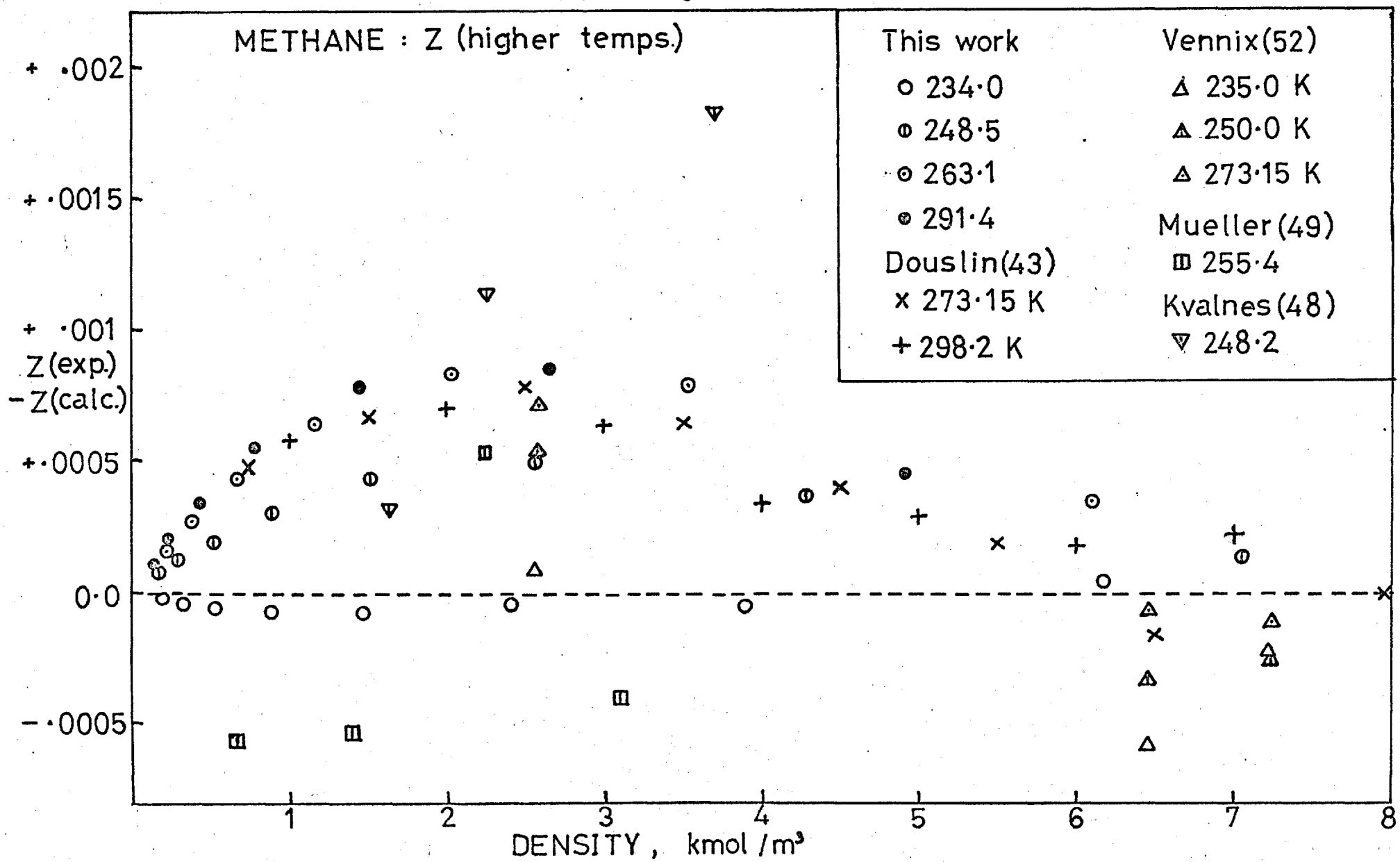
METHANE : Z (higher temps.)
This work
234·0
248·5
263·1
291·4
Douslin(43)
273·15 K
298·2 K
Vennix(52)
235·0 K
250·0 K
273·15 K
Mueller(49)
255·4
Kvalnes(48)
248·2
+ ·002
+ ·0015
+ ·001
Z(exp.) − Z(calc.)
+·0005
0·0
−·0005
1
2
3
4
5
6
7
8
DENSITY , kmol /m³

At lower temperatures the only measurements of Vennix that fall within the density range of our results are at a density of .00255 mole.cm^{-3}. At 192.6 K our value of Z at this density, after interpolation, is greater by about .0008 (.1%) than that of Vennix. The corresponding difference at 181.9 K is about .0013 (.2%). It appears that at our maximum density, .0058 mole.cm^{-3}, on the 192.6 K isotherm the value of Z is larger still than that value interpolated from Vennix, the difference being about .005 (1%).

In figure 4.10 Z(experimental) - Z(calculated) is plotted for our higher temperature isotherms at 234.0 K, 248.5 K, 263.1 K and 291.4 K, and for the experimental isotherms in this range of Douslin (43), of Mueller (49), of Kvalnes (48), and of Vennix (52). It appears that our values of Z at the higher densities on the 291.4 K and 263.1 K isotherms are within .0003 (.04%) of the results of Douslin, after interpolation; this is within the limits of experimental error. There is again fairly good agreement with the low-density measurements of Vennix, and the systematic deviation from the data of Kvalnes is apparent. The results of Mueller exhibit fairly large scatter.

It is to be noted that the deviation of the data from the Vennix-Kobayashi equation of state passes through a maximum at a density of about .002 cm^3.mole^{-1}. This deviation shows a maximum of .0008 at about 260-280 K then passes through zero with decreasing temperature and rises to -.0017 at 192.6 K. This behaviour arises because the equation of state was fitted below 0 ^{o}C to the data of Vennix (52), which does not really extend to sufficiently low densities.

In developing an improved equation of state for methane it should be constrained to give the correct B and C, or, preferably, it should be fitted to low density data, such as that presented in Table 4.1.

(b) Nitrogen

For the corresponding comparisons in the case of nitrogen, the thirteen constant equation of state of Wood et al (27) was employed. This equation had been fitted at low temperatures to the data of Canfield (67).

In figure 4.11 are plotted values of Z(experimental) - Z(calculated) for the lower temperature isotherms of Table 4.2: 204.6 K, 192.6 K, 181.9 K and 155.9 K, which are compared with the results of Crain and Sonntag at 203.2 K, 163.2 K, and 143.2 K, and with those of Canfield at 183.2 K, 158.2 K and 143.2 K.

Agreement at 204.6 K with the results of Crain and Sonntag, after interpolation, is fairly good: within .0004 (.05%). At 181.9 K our results are within .0004 (.05%) of those of Canfield, after interpolation. The 183.15 K isotherm of Canfield shows a small systematic deviation at low density, as does the 158.15 K isotherm. Our results are in good agreement at 155.9 K with those of Crain and Sonntag, although the interpolation is not easy, and within about .0003 (.04%) with those of Canfield. It can be seen that the results of Canfield and of Crain and Sonntag on the 143.15 isotherm are in excellent agreement.

In Figure 4.12 the equivalent comparisons are shown for the higher temperature isotherms of this work: 218.9 K, 234.0 K, 248.5 K, 263.1 K, 276.9 K and 291.4 K; with the 223.2 K and 273.2 K isotherms of Canfield; the 273.2 K and

FIGURE 4.11

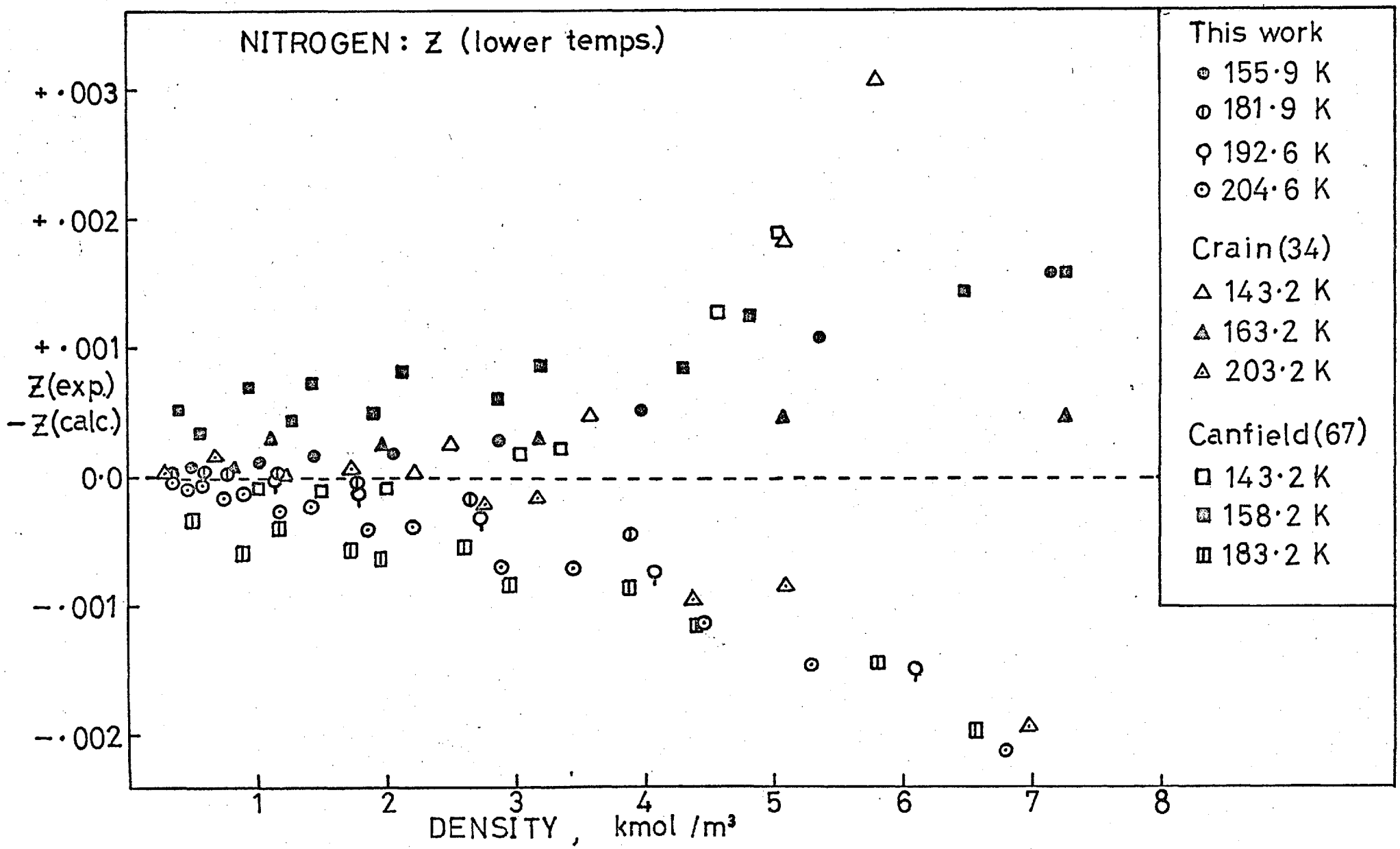
NITROGEN : Z (lower temps.)
+ · 003
+ · 002
+ · 001
Z(exp.)
−Z(calc.)
0·0
− · 001
− · 002
1
2
3
4
5
6
7
8
DENSITY , kmol /m³
This work
155·9 K
181·9 K
192·6 K
204·6 K
Crain (34)
143·2 K
163·2 K
203·2 K
Canfield (67)
143·2 K
158·2 K
183·2 K

FIGURE 4.12

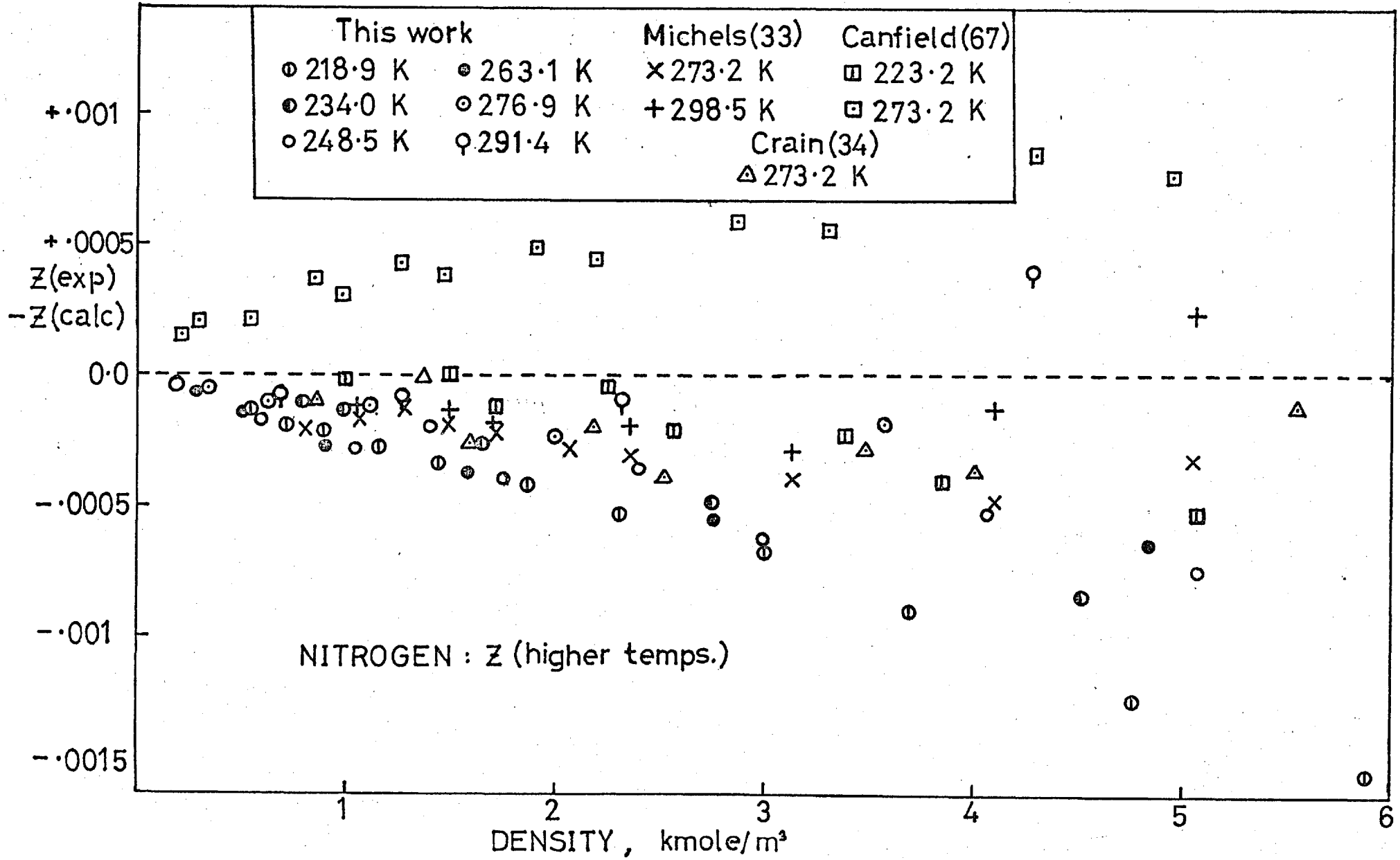
This work
218·9 K
234·0 K
248·5 K
263·1 K
276·9 K
291·4 K
Michels(33)
273·2 K
298·5 K
Canfield(67)
223·2 K
273·2 K
Crain(34)
273·2 K
+·001
+·0005
Z(exp)
−Z(calc)
0·0
−·0005
−·001
−·0015
NITROGEN : Z (higher temps.)
1
2
3
4
5
6
DENSITY , kmole/m³

298.5 K isotherms of Michels et al; and the 273.2 K isotherm of Canfield.

It is immediately apparent that the 273.2 K isotherm of Canfield differs by up to .001 in Z (.1%) from the other results at this temperature. Otherwise the agreement of our results, after interpolation, with other workers is good. Similarly, the results of Canfield at 223.2 K are up to .0008 (.1%) more positive than the values interpolated from our 218.9 K and 234.0 K isotherms. On the whole, however, the agreement is very good between these sets of low-density nitrogen compressibility factor data.

4.7 Experimental Results for Other Gases and Binary Mixtures

Apart from methane, nitrogen and the methane/nitrogen system the gases considered in the intermolecular potential study, chapter 5, were argon, ethane and the methane/argon, nitrogen/argon and methane/ethane systems. In addition, propane and n-butane were included in the test of virial coefficient correlations, chapter 6.

In collating the data much use was made of the compilations of Dymond and Smith (80) and of Mason and Spurling (1). The sources of the more accurate second and third virial coefficients are listed here, but only those values obtained by retreating the data are given in the Tables. Otherwise, the values used were as given in the original references.

(a) Argon

(i) Michels, Levelt and De Graaf (81), Michels, Wijker and Wijker (82): re-treated graphically (Table 4.16).

(ii) Crain and Sonntag (34).

(iii) Provine and Canfield (83); re-treated graphically (Table 4.16).

(iv) Whalley and Schneider (84) re-analysed by Saville (64) (Table 4.16).

(v) Holborn and Otto (85); re-analysed by Saville (64) (Table 4.16).

(vi) Byrne, Jones and Staveley (55).

(vii) Weir, Wynn-Jones, Rowlinson and Saville (18).

(viii) Fender and Halsey (86).

(ix) Pool, Saville, Herrington, Shields and Staveley (71).

(b) Ethane

(i) Michels, van Straaten and Dawson (87); re-treated graphically (Table 4.17).

(ii) Reamer, Olds, Sage and Lacey (88); re-treated graphically.

(iii) Hoover, Nagata, Leland and Kobayashi (50).

(c) Methane/Argon

(i) Byrne, Jones and Staveley (55).

(ii) Thomaes and van Steenwinkel (89).

(d) Nitrogen/Argon

(i) Crain and Sonntag (34).

(ii) Brewer and Vaughn (90). B_{12} was re-calculated using more accurate values of B_{11} and B_{22} (Table 4.18).

(iii) Zandbergen and Beenakker (91). B_{12} was re-calculated using more accurate values of B_{11} and B_{22} (Table 4.18).

(iv) Knobler, Beenakker and Knapp (92). One point at 90 K, which was not utilized here because of the uncertainties in B for nitrogen and argon at this temperature.

(e) Methane/Ethane

(i) Michels and Nederbragt (93); re-treated graphically (Table 4.19).

(ii) Dantzler, Knobler and Windsor (94). B_{12} was re-calculated using more accurate values of B_{11} and B_{22}.

(iii) Hoover, Nagata, Leland and Kobayashi (50).

(f) Propane

(i) Cherney, Marchman and York (95); re-treated graphically (Table 4.20).

(ii) Beattie, Kay and Kaminsky (96); re-treated graphically (Table 4.20).

(iii) McGlashan and Potter (97).

(iv) Kapallo, Lund and Schafer (98).

(g) n-Butane

(i) Connally (99). Presented in Table 4.21.

(ii) Beattie, Simard and Su (100); re-treated graphically (Table 4.21).

(iii) Jones and Kay (101).

(iv) Bottomley and Spurling (102).

TABLE 4.16

Argon: Experimental Virial Coefficients (Retreated)
(in units of $cm^3.mole^{-1}$)

(i) Michels (81), (82)

T,K	B	C
128.15	-115.3	2000
133.15	-107.8	2275
138.15	-100.8	2370
143.15	-94.4	2410
150.65	-85.6	2290
163.15	-73.20	2060
173.15	-65.10	1950
188.15	-54.70	1690
203.15	-46.25	1580
223.15	-37.26	1440
248.15	-28.4	1320
273.15	-21.35	1200
298.15	-15.68	1100
323.15	-11.16	1080
348.15	-7.20	1000
373.15	-3.96	984
398.15	-1.14	950
423.15	+1.32	920

(iii) Provine (83)

T,K	B	C
143.15	-94.0	2335
158.15	-77.9	2180
*183.15	-56.6	1560

(iv) Whalley (84)

T,K	B	C
273.16	-21.88	1298
323.16	-11.04	1096
373.16	-4.34	1078
423.16	+1.01	1014
473.16	+5.28	912
573.16	+10.77	818
673.16	+15.74	-
773.16	+17.76	-
873.16	+19.48	-

(v) Holborn (85)

T,K	B	C
173.15	-65.28	2000
223.15	-37.31	1463
273.15	-21.23	1195
323.15	-10.66	1003
373.15	-4.06	1046
423.15	+1.53	872
473.15	+4.98	966
*573.15	+11.34	-
*673.15	+15.58	-

* Large scatter on isotherm

TABLE 4.17

Ethane: Experimental Virial Coefficients (Re-treated)
(in units of $cm^3.mole^{-1}$)

(i) Michels (87)

T,K	B	C
273.15	-221.6	10,700
298.15	-185.5	10,680
322.76	-156.6	9,750
347.66	-132.9	8,600
372.53	-113.8	7,800
397.85	-97.6	7,030
422.71	-83.65	6,400

(ii) Reamer (88)

T,K	B	C
⁎310.94	-164.4	7,500
344.27	-134.4	8,200
⁎377.60	-110.0	7,400
410.94	-90.0	6,700
444.27	-73.3	6,150
477.60	-59.0	5,450
⁎510.94	-47.0	4,800

TABLE 4.18

Nitrogen/Argon: Experimental Virial Coefficients (Re-treated)

(ii) Brewer (90)

T,K	B_{12}
148.15	-81.7
173.15	-59.3
198.15	-43.4
223.15	-32.2
248.15	-23.4
273.15	-16.3
298.15	-10.82
323.15	-6.19

(iii) Zandbergen (91)

T,K	B_{12}
170.5	
231.7	
292.6	

(iv) Knobler (92)

T,K	B_{12}
90	-216

⁎ Large scatter on isotherm

TABLE 4.19

Methane/Ethane : Experimental Virial Coefficients (Re-treated)
(in units of $cm^3.mole^{-1}$)

(i) Michels (93)

T,K	B_{12}	C_{112}	C_{221}
273.15	-112.9	4500	9400
298.50	-92.1	4500	7000
322.99	-77.4	4000	6500

(ii) Dantzler (94)

T,K	B_{12}
298.15	-93.4
323.15	-78.6
348.15	-67.0
373.15	-55.5

TABLE 4.20

Propane : Experimental Virial Coefficients (Re-treated)
(in units of $cm^3.mole^{-1}$)

(i) Cherney (95)

T,K	B	C
323.15	-328	20,250
373.15	-239.8	19,200
398.15	-207.5	17,500

(ii) Beattie (96)

T,K	B	C
398.15	-209.3	18,400
423.15	-181.2	16,150
448.15	-158.6	14,400
473.15	-138.2	13,300
498.15	-120.6	12,000

TABLE 4.21

n-Butane : Experimental Virial Coefficients (Re-treated)

(i) Connally (99)**

T,K	B	C
344.26	-517.0	25,000
360.93	-464.7	40,000
377.59	-418.6	40,000
394.26	-381.3	39,500
406.85	-356.1	39,000
410.93	-348.6	38,500
444.26	-289.8	34,000

(ii) Beattie (100)

T,K	B	C
423.16	-326.6	37,250
448.16	-284.5	32,750
473.16	-250.5	29,500
498.16	-221.0	26,500
523.16	-196.5	24,900
548.16	-174.0	22,500
573.16	-154.5	21,350

** Not re-treated

CHAPTER FIVE

INTERMOLECULAR POTENTIALS

5.1 Introduction

(a) The form of the intermolecular potential

The potential energy of interaction, U(r), between two spherical non-polar molecules is a function of the intermolecular separation, r, having the general form shown in figure 5.1. At ~~large~~ small r the ~~long~~ short-range repulsive forces predominate. The latter are essentially due to the overlap of the electron clouds. The maximum energy of attraction is ϵ, the potential well-depth.

The most important long-range attraction between non-polar molecules is caused by the dispersion (or London) forces, which may be described (1) as originating from the mutual interaction of instantaneous induced dipoles and multipoles. The potential energy due to dispersion forces is a series in inverse powers of r,

$$U(\text{dispersion}) = -\frac{C_6}{r^6} - \frac{C_8}{r^8} - \ldots\ldots \qquad (5.1\text{-}1)$$

At large r, as U(r) tends to zero, the leading term in (5.1-1) predominates. In general, calculations of the short-range forces, which are highly complex, do not lead to any equivalent simple functional dependence on r, although an exponential dependence is a fair approximation.

There are several means of obtaining information on the shape or size of the potential curve, or at least part of the curve (103), one of the most useful methods being through

FIGURE 5.1

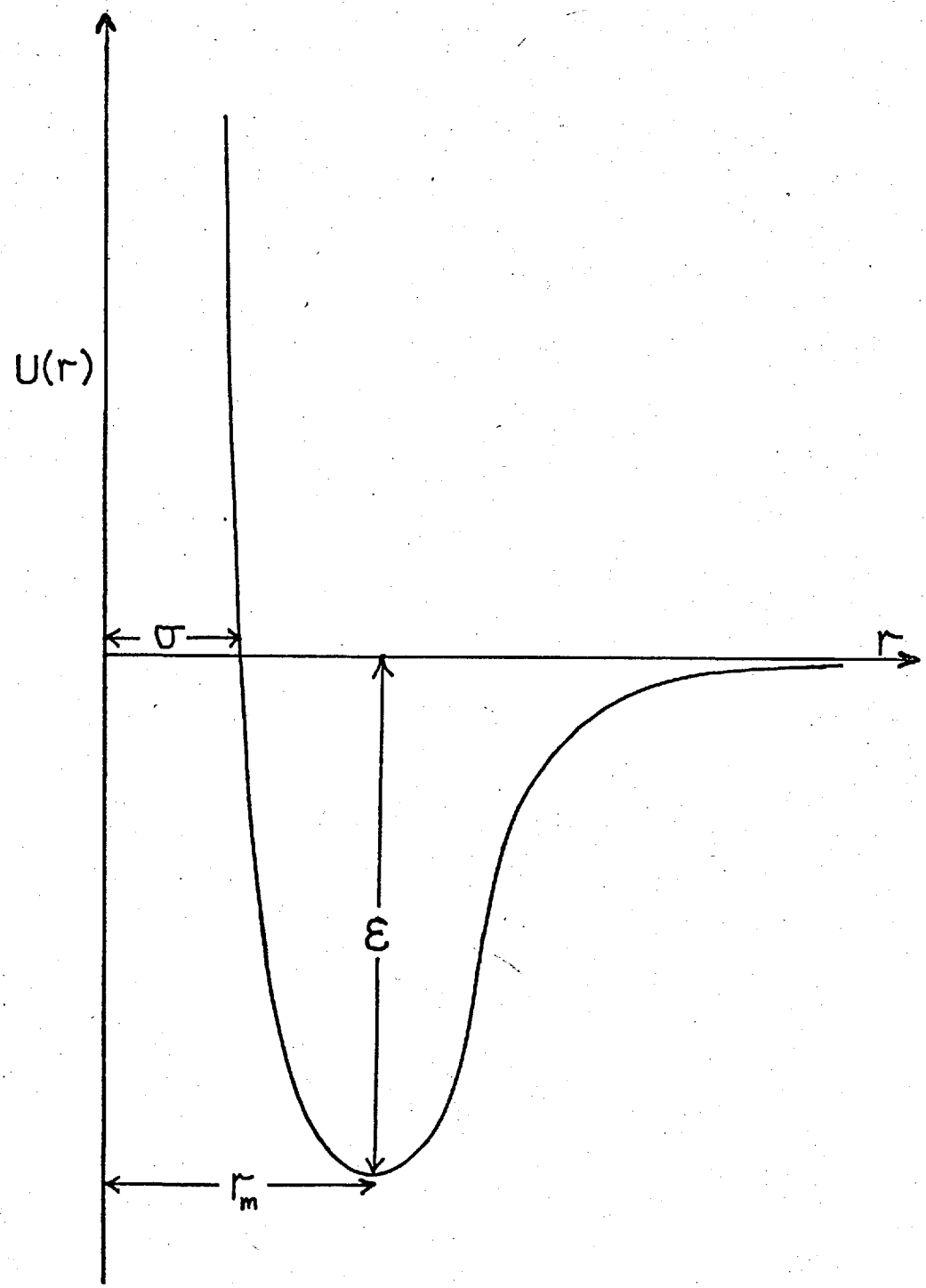

INTERMOLECULAR POTENTIAL
(QUALITATIVE)

experimental second virial coefficients. There follows a brief outline of the statistical-mechanical derivation of the dependence of B(T) on U(r).

(b) The Intermolecular potential and the virial expansion

The partition function for the grand canonical ensemble is

$$\Xi = \sum_{N \geq 0} e^{\mu N / kT} Z_N \qquad (5.1\text{-}2)$$

where Z_N is the partition function for a canonical ensemble of N molecules with chemical potential μ.

$$Z_N = \sum_{i=0}^{\infty} e^{-E_i / kT} \qquad (5.1\text{-}3)$$

where E_i is the energy of the ith. quantum state of the system.

As $E_o = 0$ when $N = 0$,

$$\Xi = 1 + \sum_{N \geq 1} e^{\frac{\mu N}{kT}} Z_N \qquad (5.1\text{-}3)$$

Equation (5.1-3) is a power series expansion in $e^{\mu/kT}$.

Now as the pressure of the system is related to Ξ through the equation,

$$PV = kT \ln \Xi$$

then,

$$\frac{PV}{kT} = \ln \left\{ 1 + \sum_{N \geq 1} e^{\mu N / kT} Z_N \right\} \qquad (5.1\text{-}4)$$

The right-hand side of (5.1-4) may be expanded as an infinite series in $e^{\mu/kT}$. It may be shown that this can be converted to a series in powers of density by use of the relationship,

$$N_o \rho = \frac{\bar{N}}{V} = \frac{kT}{V}\left(\frac{\partial \ln \Xi}{\partial \mu}\right)_{T,V} \qquad (5.1\text{-}5)$$

where N_o is Avogadro's number.

By equating coefficients of the resultant series with those of the virial series,

$$P = NkT\rho\left(1 + B\rho + C\rho^2 + \cdots\cdots\cdots\right) \qquad (5.1\text{-}6)$$

we have

$$B(T) = -V\left(\frac{2Z_2}{Z_1^2} - \frac{1}{2}\right)N_o \qquad (5.1\text{-}7)$$

$$C(T) = -V^2\left(\frac{12Z_3}{Z_1^3} + \frac{16Z_2^2}{Z_1^4} + \frac{2Z_2}{Z_1^2} - \frac{5}{12}\right)N_o \qquad (5.1\text{-}8)$$

These equations are valid for quantum-mechanical systems and require no assumptions other than that Boltzmann statistics are applicable and that the expansion of $\ln \Xi$ in powers of density exists, i.e. that the virial series is convergent.

In the classical limit the canonical ensemble partition function for a monatomic gas of N atoms is,

$$Z_N = \Lambda^{3N} Q_N \qquad (5.1\text{-}9)$$

where $$\Lambda = \left(\frac{2\pi mkT}{h}\right)^{\frac{1}{2}} \qquad (5.1\text{-}10)$$

where Q_N is the configurational integral,

$$Q_N = \frac{1}{N!}\int\cdots\int e^{-U(\underline{r}_1 \ldots\ldots \underline{r}_N)/kT}\, d\underline{r}_1 \ldots\ldots d\underline{r}_N \qquad (5.1\text{-}11)$$

where U is the molecular potential energy of the N molecules.

Assuming that the potential between molecules is independent of the angular orientation,

$$Q_1 = \int d\underline{r}_1 = V \qquad (5.1\text{-}12)$$

$$Q_2 = \iint e^{-U(r_{12})}\, d\underline{r}_1\, d\underline{r}_2 \qquad (5.1\text{-}13)$$

From equations (5.1-9), (5.1-12) and (5.1-13), on substitution into (5.1-7), we have

$$B(T) = -\frac{N_o}{2V}\int_V\int\left(1 - e^{-U(r_{12})/kT}\right) d\underline{r}_1\, d\underline{r}_2 \qquad (5.1\text{-}14)$$

On changing variables from $\underline{r}_1$ and $\underline{r}_2$ to $\underline{r}_1$ and $\underline{r}_{12}$, integration over $\underline{r}_{12}$ leads to

$$B(T) = 2\pi N_o \int_0^\infty \left(1 - e^{-U(r)/kT}\right) r^2\, dr \qquad (5.1\text{-}15)$$

where r is the intermolecular separation.

Thus the second virial coefficient is directly related to U(r) and information on the potential is often obtained from experimental measurements of B over a range of temperatures, as considered in the following section.

The equivalent expression to (5.1-14) for the third

virial coefficient is not so useful as a means of obtaining information on U(r), for two reasons. Firstly, experimental third virial coefficients are much less accurate, and secondly an assumption must be made concerning the contribution to $U(\overline{r}_1 \ldots \overline{r}_N)$ of non-additive forces. The total potential is given by,

$$U(r_1 \ldots r_N) = \sum_i \sum_j U(r_{ij}) + \sum_i \sum_j \sum_k U(r_{ij}, r_{jk}, r_{ik}) + \ldots \quad (5.1\text{-}16)$$

i.e. it is the sum of two-body terms (pairwise-additive) plus three-body, four-body ... N-body terms (pairwise non-additive). The second term in (5.1-16) is the contribution from three-body forces and must be included in Q_3 and hence in C(T). The third virial coefficient is considered further in section 5.5.

Equation (5.1-14) was derived for the classical-mechanical second virial coefficient, B_{cl}, and corrections must be applied for quantum effects. At normal temperatures these corrections are given by a power series expansion in Planck's constant, h(2),

$$B(T) = B_{cl}(T) + \left(\frac{h^2}{m}\right) B_I(T) + \left(\frac{h^2}{m}\right)^2 B_{II}(T) + \ldots\ldots \quad (5.1\text{-}17)$$

where m = molecular mass

B_I = first quantum correction

B_{II} = second quantum correction.

There is also a small correction for non-classical statistics that is negligible in the intermediate temperature range. The first quantum correction may be shown (2) to be,

$$B_I(T) = \frac{N_o}{24\pi^2 k^2 T^3} \int_0^\infty e^{-U(r)/kT} \left(\frac{dU(r)}{dr}\right)^2 r^2\, dr \qquad (5.1\text{-}18)$$

(c) Inverse Laplace Transform of B(T)

If the potential curve is considered as divided at the minimum into left and right branches, $U(r_L)$ and $U(r_R)$ respectively, then a new variable Δr^3 may be defined as

$$\Delta r^3 = r_L^3 - r_R^3 \quad \text{for } -\epsilon \leqslant U \leqslant 0$$

$$= r_L^3 \qquad\qquad 0 < U < \infty$$

Then by defining

$$\psi = U + \epsilon$$

and taking ψ as the independent variable it may be shown (104) from equation (5.1-14) that

$$\frac{3}{2\pi N_o \beta} e^{-\beta\epsilon} B(\beta) = \int_o^\infty \Delta r^3(\psi)\, e^{-\beta\psi}\, d\psi \qquad (5.1\text{-}19)$$

where $\beta = \frac{1}{kT}$

This is a Laplace transform for which there exists an inversion. By inversion,

$$\Delta r^3(\psi) = \frac{3}{2\pi N_o} \mathcal{L}^{-1}\left(\frac{B(\beta)\, e^{-\beta\epsilon}}{\beta}\right) \qquad (5.1\text{-}20)$$

Thus no matter how accurate the data, U(r) cannot be obtained as an explicit function of r from second virial coefficients. Equation (5.1-20) shows that the width of the potential bowl can be obtained only as a function of the

well-depth, ϵ . At present, the use of the inverse Laplace transform is limited by the lack of independent estimates of the well-depth, ϵ ; when an independent estimate is available, as for argon (see section 5.3), the method should give information on the shape of the potential bowl (105). It would be necessary first to determine the effect of experimental errors in B on the result of the inverse Laplace transform.

5.2 Pair Potential Models

The usual procedure for obtaining information on the potential energy curve from second virial coefficients is to assume a model for the form of the potential. The model has two or more adjustable parameters which are determined from a comparison between the calculated and experimental second virial coefficients. The usefulness of the model as an approximation to the true pair potential may then be tested by considering its performance in the prediction of other thermodynamic and transport properties of the substance. Ideally, the model should be compatible with known theories of intermolecular forces.

In this work, two three-parameter potential models were considered; firstly, the Lennard-Jones (n-6),

$$U(r) = \frac{\left(\frac{6}{n}\right)^{\frac{-6/n}{(1-6/n)}}}{(1-6/n)} \cdot \epsilon \left[\left(\frac{\sigma}{r}\right)^n - \left(\frac{\sigma}{r}\right)^6\right] \qquad (5.2\text{-}1)$$

where the parameters are ϵ , σ , and n.

Secondly, the Kihara spherical-core potential (106),

$$U(r) = 4.\epsilon \left[\left(\frac{\sigma-a}{r-a}\right)^{12} - \left(\frac{\sigma-a}{r-a}\right)^6\right] \qquad (5.2\text{-}2)$$

The Kihara potential includes in the model a hard core of the molecule, radius a, inside which U(r) is infinite. By defining $\gamma = a/\sigma$, (5.2-2) can be written,

$$U(r) = 4\epsilon\left[\left(\frac{1-\gamma}{r/\sigma-\gamma}\right)^{12} - \left(\frac{1-\gamma}{r/\sigma-\gamma}\right)^{6}\right] \qquad (5.2\text{-}3)$$

where the parameters are now ϵ, σ, and γ.

Both the Lennard-Jones (n-6) and the Kihara potential contain the leading r^{-6} term in (5.1-1), but only the Kihara possesses the higher terms in r^{-8}, etc., as well as spurious terms in r^{-7}, r^{-9}, etc.

It is usual for a fixed value to be chosen for the repulsive exponent, n, in (5.2-1). When n = 12, (5.2-1) becomes the familiar two-parameter Lennard-Jones (12-6) potential (107)

$$U(r) = 4\epsilon\left[\left(\frac{\sigma}{r}\right)^{12} - \left(\frac{\sigma}{r}\right)^{6}\right] \qquad (5.2\text{-}4)$$

When n = 18, the Lennard-Jones (18-6) potential is obtained,

$$U(r) = \frac{3^{3}}{2}\cdot\epsilon\left[\left(\frac{\sigma}{r}\right)^{18} - \left(\frac{\sigma}{r}\right)^{6}\right] \qquad (5.2\text{-}5)$$

Many other two and three-parameter potential functions have been proposed (2), differing essentially in the manner of representation of the form of the repulsive potential energy. It has been demonstrated by Hanley and Klein (108) that, among those three-parameter potentials that they studied, if the third parameter was fixed, e.g. n = 18 in the L-J(n-6) potential, then another three-parameter potential could be found, e.g. Kihara spherical-

core with $\gamma = 0.1$, that fitted the data in the same manner. Because of the equivalence of three-parameter potential models in this respect, further examples were not considered here.

(a) The Lennard-Jones (n-6) potential

The classical second virial coefficient has been calculated by analytical integration after first expanding the exponential term in (5.2-1) as an infinite series (109). The result is an infinite series in $^1/_T$, involving gamma functions, that is rapidly converging except at very low temperatures,

$$B_{cl}(T) = \frac{2}{3}\pi N_o \sigma^3 \sum_{j=0}^{\infty} -\left(\frac{n}{6}\right)^{\frac{[(n-6)j+3]}{(n-6)}} \cdot \frac{3}{n.j!} \cdot \left(\frac{6}{(n-6)T^*}\right)^{\frac{[(n-6)j+3]}{n}} \cdot \Gamma\left(\frac{6j-3}{n}\right) \qquad (5.2\text{-}6)$$

where $T^* = kT/\epsilon$

The same technique has been used by De Boer and Michels (110) to obtain the first and second quantum corrections. The corresponding expressions are given in full by Pollard (13).

Calculation of B for the (12-6) and (18-6) potentials is simplified by use of the equality

$$\Gamma(a) = a^{-1}\Gamma(a+1) \qquad (5.2\text{-}7)$$

This mathematical convenience is one of the reasons for the choice of n = 12 in the first applications of this potential by Lennard-Jones. It has long been realised that a higher value of n is necessary to provide a good fit to

experimental second virial coefficients at low temperatures (86), and this fact has led to the use of the (18-6) potential (111) and the three-parameter (n-6) potential (108).

(b) The Kihara Spherical-Core Potential

The Kihara spherical-core potential is a special case of the general Kihara potential (106) for a convex core with superimposed L-J (12-6) potential. (The expression for the series expansion for this general potential is given by Pollard (13)).

$B_{Cl}(T)$ for the spherical core potential, (5.2-3) is given by

$$B_{cl}(T) = \frac{2}{3}\pi N_o \sigma^3 (1-\gamma)^3 \left\{ \left(\frac{\gamma}{1-\gamma}\right)^3 + 3.2^{1/6}\left(\frac{\gamma}{1-\gamma}\right)^2 F_1(T^*) + 3.2^{1/3}\left(\frac{\gamma}{1-\gamma}\right) F_2(T^*) + 2^{1/2} F_3(T^*) \right\} \qquad (5.2\text{-}8)$$

where

$$F_s(T^*) = -\frac{s}{12} \sum_{j=0}^{\infty} \frac{2^j}{j!} \cdot \left(\frac{1}{T^*}\right)^{\frac{6j+s}{12}} \cdot \Gamma\left(\frac{6j-s}{12}\right) \qquad (5.2\text{-}9)$$

The corresponding first and second quantum corrections have been calculated by Weir (112).

(c) Calculation of Potential Parameters

The second virial coefficients for the L-J (n-6) and Kihara spherical-core potentials were calculated as described in sections 5.2(a) and 5.2(b), to an accuracy of 0.01 cc/mole at each temperature. The general non-linear least-squares procedure (section 3.2(a)) was used to determine the parameters σ to .00001 nm, and ϵ/k to 0.01 K. For the

L-J (n-6) potential the third parameter was n and for the Kihara potential it was γ. All derivatives, e.g. $\partial B(T)/\partial\sigma$ and $\partial B(T)/\partial(\epsilon/k)$ were determined numerically. The objective function that was minimized in the least-squares procedure was

$$S = \sum_{i=1}^{N} \omega_i \left(B(\text{exp.})_i - B(\text{calc.})_i \right)^2 \qquad (5.2\text{-}10)$$

The experimental second virial coefficients with their associated weighting factors were those given in Chapter 4.

The second quantum correction for the Lennard-Jones (12-6) potential was found to be less than .07 cc/mole for methane at 110 K. This is negligible compared with the experimental error and so the second quantum corrections were not included for the other potentials. However, first quantum corrections were included as they are by no means negligible, e.g. for methane at 110.8 K, the total correction to B is 7.41 cc/mole for L-J (18-6) potential and at 273.2 K it is 0.75 cc/mole.

The parameters obtained for the Lennard-Jones (12-6), (18-6) and (n-6) potentials and for the Kihara potential are given in Table 5.1 for argon, methane, nitrogen and ethane. Column 4 gives the root mean square deviation,

$$\text{RMS} = \sqrt{S/N} \qquad (5.2\text{-}11)$$

It was shown by Hanley and Klein (108) that the second virial coefficient is insensitive to the form of the potential function in the range,

$$2 < T^*_{12\text{-}6} < 10 \qquad (5.2\text{-}12)$$

TABLE 5.1

Pair-Potential Parameters

Argon

	σ,nm	ϵ/k,K	γ or n
Lennard-Jones (12-6)	.3458	118.6	
Lennard-Jones (18-6)	.3264	160.3	
Lennard-Jones (n-6)	.3240	166.4	19.1
Kihara	.3259	160.8	.153

Methane

	σ,nm	ϵ/k,K	γ or n
Lennard-Jones (12-6)	.3820	148.6	
Lennard-Jones (18-6)	.3640	199.6	
Lennard-Jones (n-6)	.3561	228.0	22.9
Kihara	.3614	209.2	.177

Nitrogen

	σ,nm	ϵ/k,K	γ or n
Lennard-Jones (12-6)	.3742	95.3	
Lennard-Jones (18-6)	.3571	127.8	
Lennard-Jones (n-6)	.3449	159.9	27.9
Kihara	.3528	139.4	.197

Ethane

	σ,nm	ϵ/k,K	γ or n
Lennard-Jones (12-6)	.4911	202.4	
Lennard-Jones (18-6)	.4605	277.1	
Lennard-Jones (n-6)	.4375	347.1	26.6
Kihara	.4427	319.8	.211

where

$$T^*_{12-6} = \frac{kT}{\varepsilon_{12-6}} \qquad (5.2\text{-}13)$$

They recommend using experimental second virial coefficients that fall only outside this range. However, Ahlert et al (113) found that by using methane data only in the range

$$0{\cdot}8 < T^*_{12-6} < 2 \qquad (5.2\text{-}14)$$

it was possible to obtain more than one minimum in the objective function, (5.2-10). A necessary condition for uniqueness in the potential parameters was the use of experimental data that covered a broad temperature range. This was confirmed by Lin and Robinson (114) in a systematic study of the effect of the temperature range and number of data points on the uncertainties in the derived parameters. In general it is best to use experimental B values down to the lowest available temperature, and when the minimum value of T^*_{12-6} is from 0.5 to 1.0, it is preferable to use data up to about $T^*_{12-6} = 10.0$ to obtain minimum uncertainty in the parameters. All of the available data used in the present study falls within this wide temperature range. It is stressed that the preceding discussions refer to parameter uncertainty with respect to the particular potential model, and not with respect to the ε/k and σ of the true pair potential.

To show the performances of the pair potentials in fitting the experimental data, the differences $B - B_{ref}(T)$ for each gas are shown in figures 5.2 - 5.5, where the base line refers to the equation

$$B_{ref}(T) = a_1 + a_2/T + a_3/T^3 + a_4/T^4 \qquad (5.2\text{-}15)$$

The coefficients were obtained by fitting this equation to experimental data; they are given in Table 5.2. Use of this type of plot enables the differences between the calculated and experimental second virial coefficients to be conveniently presented.

It is immediately apparent that the L-J (12-6) potential is a poor approximation, especially at low temperatures, for all the gases studied. There is little difference between the results for the flexible three-parameter L-J (n-6) and Kihara potentials, both of which give a good fit to the experimental data. The two-parameter L-J (18-6) potential does very well, but tends to give less negative values of B at low temperatures. On the basis of the goodness of fit to the experimental second virial coefficients, only the L-J (12-6) potential must be rejected as an approximation to the true pair potential.

In Table 5.3 the parameters obtained in this work are compared with those of other investigators, omitting the L-J (12-6) potential parameters. All of these values were obtained via second virial coefficients only. Others have often been derived from a joint fit to both second virial coefficient and viscosity data but these are not included here as many of these investigations used high-temperature viscosity data now known to be erroneous (115).

It can be seen from Table 5.3 that there is in general good agreement between the different sets of parameters for a given potential, the small differences reflecting the different sets of data used. There are one or two exceptions, notably the results of Tee et al. (116) for the Kihara

FIGURE 5.2

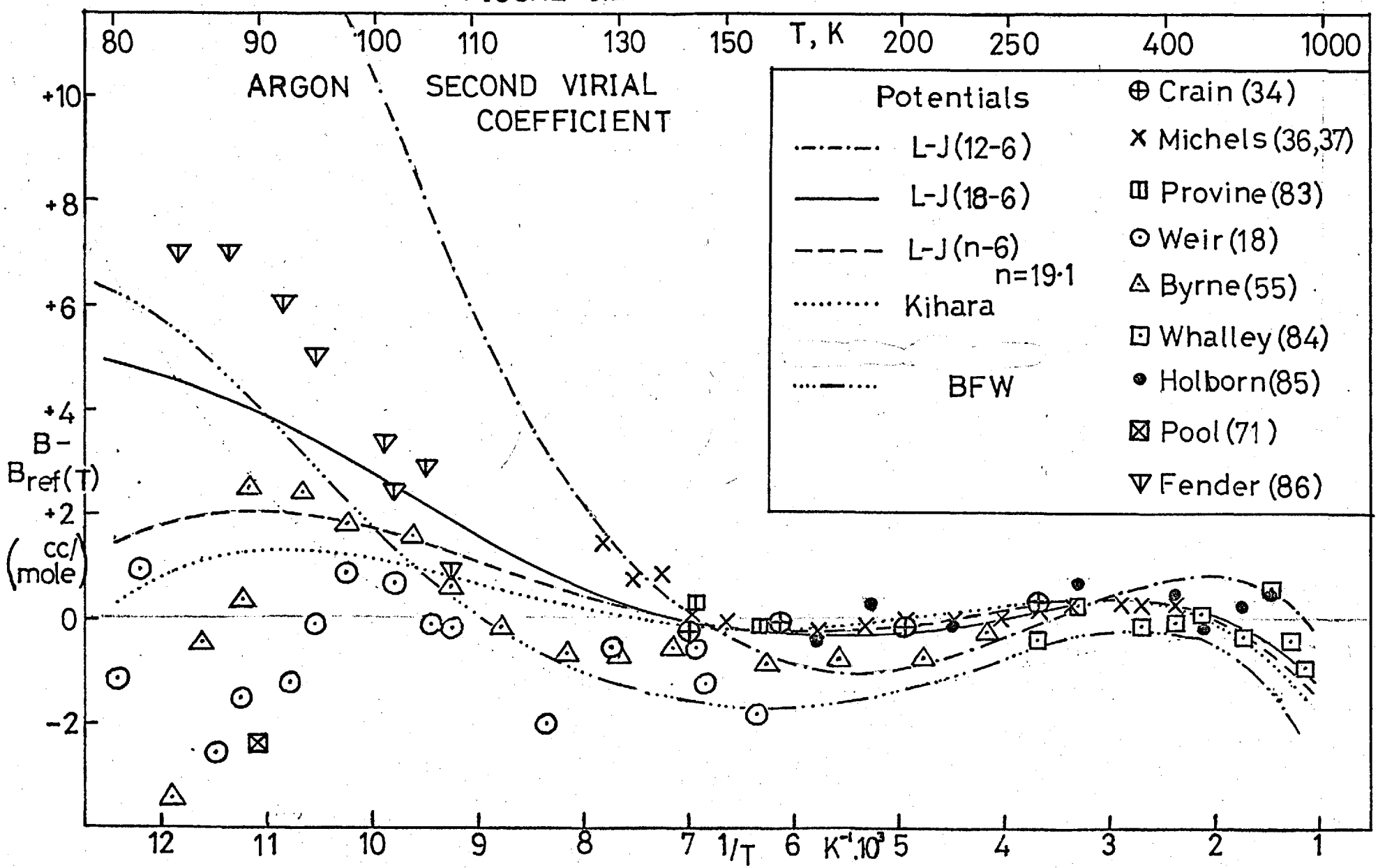
80
90
100
110
130
150
T, K
200
250
400
1000
ARGON SECOND VIRIAL COEFFICIENT
Potentials
L-J(12-6)
L-J(18-6)
L-J(n-6) n=19·1
Kihara
BFW
Crain (34)
Michels (36,37)
Provine (83)
Weir (18)
Byrne (55)
Whalley (84)
Holborn (85)
Pool (71)
Fender (86)
+10
+8
+6
+4
+2
0
-2
B - Bref(T) (cc/mole)
12
11
10
9
8
7
1/T
6
K⁻¹.10³
5
4
3
2
1

FIGURE 5.3

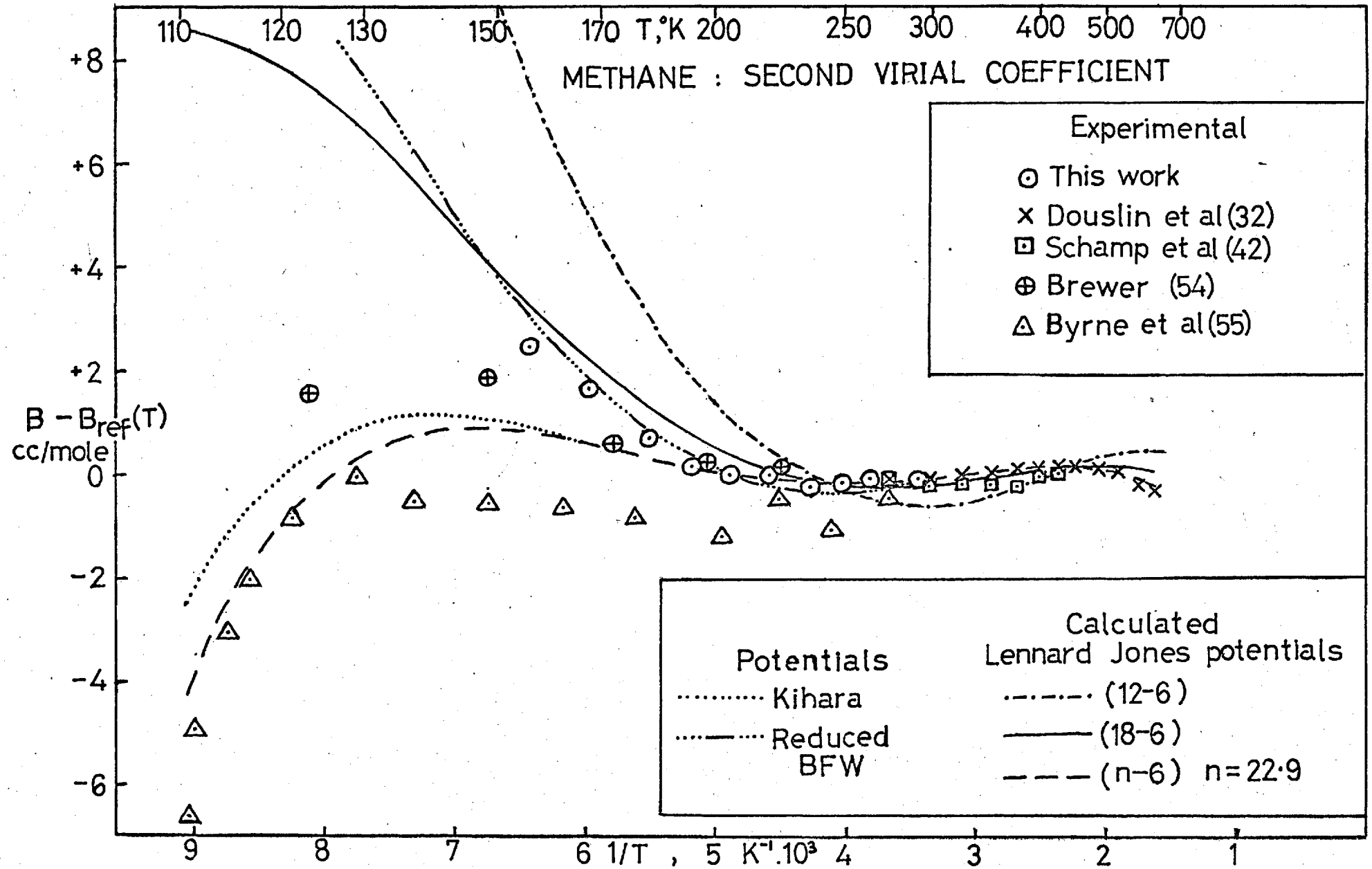
110 120 130 150 170 T,°K 200 250 300 400 500 700
METHANE : SECOND VIRIAL COEFFICIENT
+8
+6
+4
+2
0
-2
-4
-6
B − Bref(T)
cc/mole
9 8 7 6 1/T , 5 K⁻¹.10³ 4 3 2 1
Experimental
This work
Douslin et al (32)
Schamp et al (42)
Brewer (54)
Byrne et al (55)
Potentials
Kihara
Reduced BFW
Calculated
Lennard Jones potentials
(12-6)
(18-6)
(n-6) n=22·9

FIGURE 5.4

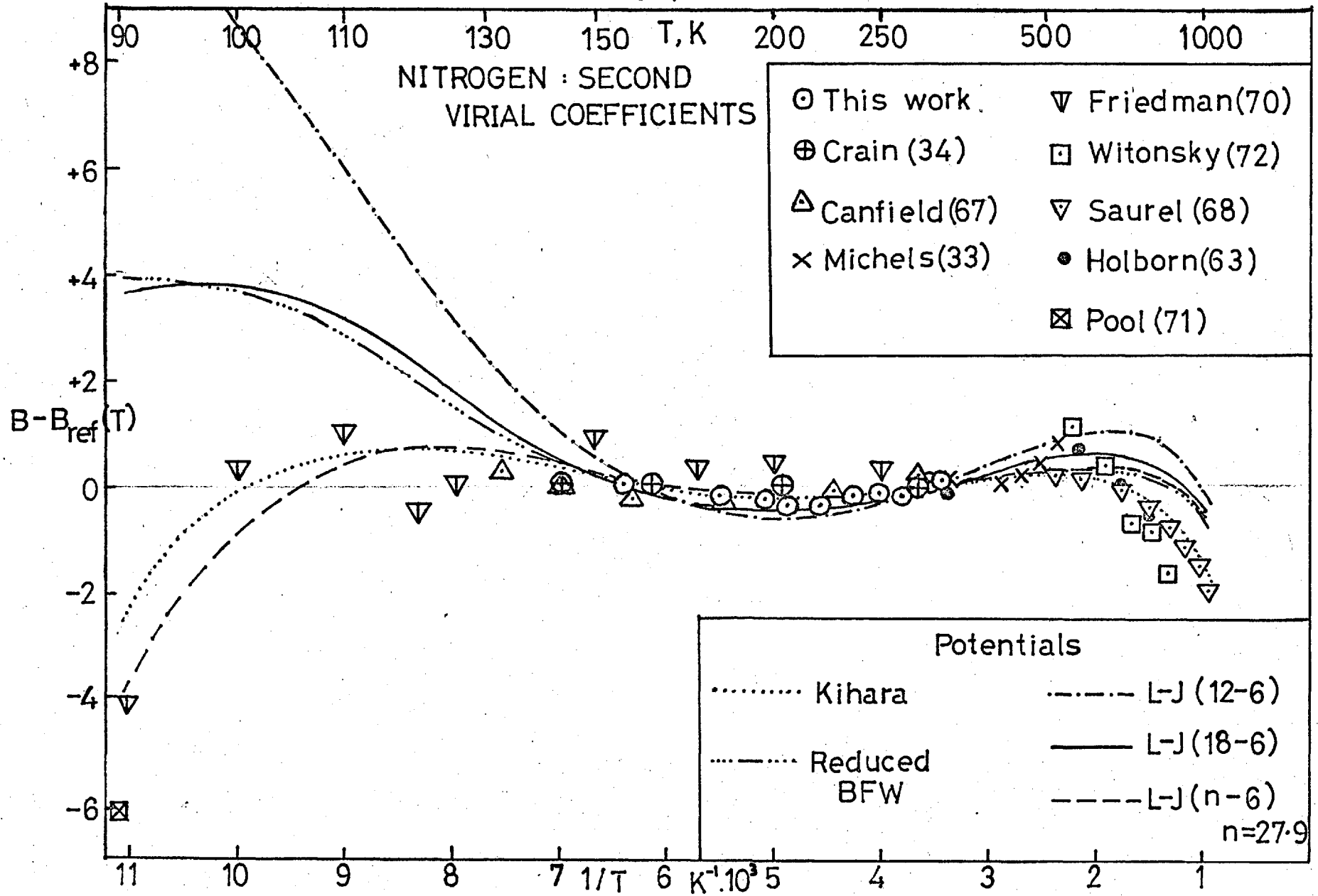
NITROGEN : SECOND VIRIAL COEFFICIENTS
T, K
90
100
110
130
150
200
250
500
1000
+8
+6
+4
+2
0
-2
-4
-6
B-B_ref (T)
1/T K^-1.10^3
11
10
9
8
7
6
5
4
3
2
1
This work
Crain (34)
Canfield (67)
Michels (33)
Friedman (70)
Witonsky (72)
Saurel (68)
Holborn (63)
Pool (71)
Potentials
Kihara
Reduced BFW
L-J (12-6)
L-J (18-6)
L-J (n-6)
n=27·9

FIGURE 5.5

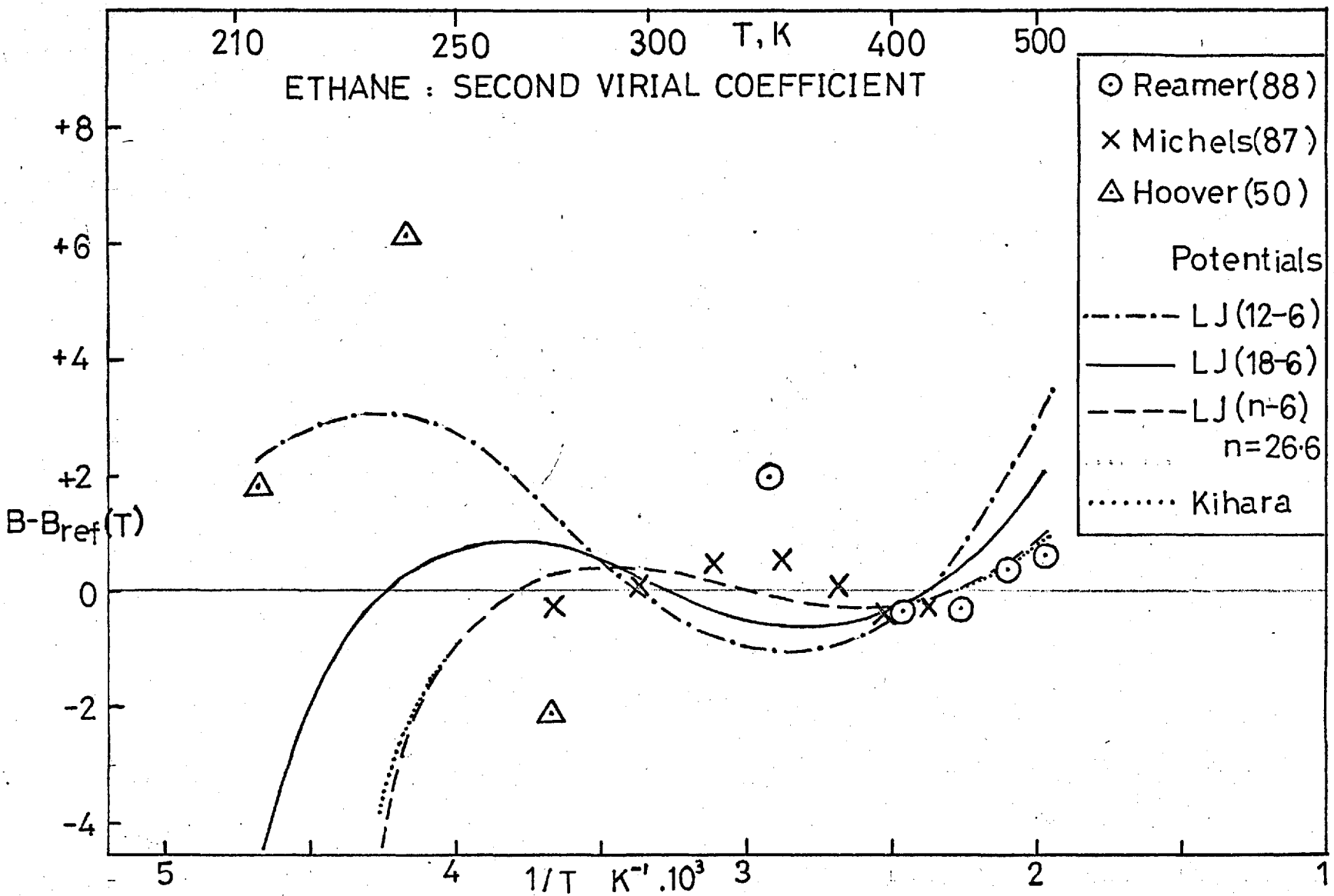
210
250
300
T, K
400
500
ETHANE : SECOND VIRIAL COEFFICIENT
Reamer(88)
Michels(87)
Hoover(50)
Potentials
LJ(12-6)
LJ(18-6)
LJ(n-6)
n=26·6
Kihara
+8
+6
+4
+2
0
-2
-4
B-Bref(T)
5
4
1/T K⁻¹.10³
3
2
1

TABLE 5.2

Coefficients of Equation fitted to Experimental Second Virial Coefficients

$$B = A_1 + A_2/T + A_3/T^3 + A_4/T^4$$

	A_1	A_2	A_3	A_4
Methane	51.40118	-25.1267	-0.298517	-0.0107310
Nitrogen	45.04587	-13.8035	-0.115836	-0.0047443
Argon	37.8635	-15.0738	-0.0911234	0.00170569
Ethane	72.8718	-50.2603	-3.87578	0.445202
Propane	98.9303	-86.7161	-6.17915	0.266462
n-Butane	240.617	-225.079	4.89262	-3.15465

TABLE 5.3

Comparison of Pair-Potential Parameters

ARGON	L-J 18-6		L-J n-6			Kihara		
	ϵ/k, K	σ, nm	ϵ/k, K	σ, nm	n	ϵ/k, K	σ, nm	γ
This work	160.3	.3264	166.4	.3240	19.1	160.8	.3259	.153
						(144.4	.3332	0.1)
Hanley and Klein (108)	161.2		147.5		16	140.8		0.1
Dymond, Rigby and Smith (111)	160.3	.3277						
Lin and Robinson (114)						161.7	.3259	.155
Tee, Gotoh & Stewart (116)						146.5	.3317	
Rossi and Danon (117)						140.4	.3101	.089
Barker, Fock & Smith (118)						142.9	.3363	.1
Sherwood and Prausnitz (119)						147.2	.3314	.125
Calvin and Reed (120)			169.8	.3225	20.0			
Weir et al. (18)						163.7	.315	.164
METHANE								
This work	199.6	.3640	228.1	.3561	22.9	209.2	.3614	.177
Ahlert, Biguria & Gaston (121)			218.0	.3568	21.0			
Sherwood & Prausnitz (119)						204.3	.3620	
Tee, Gotoh & Stewart (116)						227.1	.3565	
Hoover (50)						207.5	.3633	
NITROGEN								
This work	127.8	.3571	159.9	.3449	27.9	139.4	.3528	.197
Calvin and Reed (120)			133.4	.3532	19.3			
Sherwood and Prausnitz (119)						139.2	.3526	
Tee, Gotoh & Stewart (116)						96.3	.3694	0.0

TABLE 5.3 (continued)

ETHANE	L-J 18-6	L-J n-6	Kihara
	ϵ/k, K σ, nm	ϵ/k, K σ, nm n	ϵ/k σ, nm γ
This work	227.1 .4605	347.1 .4375 27.9	319.8 .4427 .211
Hoover (50)			352.0 .4116
Tee, Gotoh & Stewart (116)			496.7 .3504

potential parameters of nitrogen and methane, and the results of Hanley and Klein (108) for the L-J (n-6) potential parameters of argon. With the three-parameter potentials a wider spread of values of $\epsilon/_k$ and σ are obtained because of the greater flexibility introduced into the model by the extra parameter. It is noticeable that the sets of Kihara potential parameters for argon are of two types; one with $\gamma \approx 0.1$, one with $\gamma \approx 0.15$. Setting $\gamma = 0.1$ and repeating the least-squares fit, varying the other two parameters, gives a very similar result to that shown in figure 5.2. If the low-temperature argon data of Weir et al (18) and Byrne et al (55) are not included then a much lower value of $\epsilon/_k$ results (about 150 K for the L-J (18-6) potential).

The larger differences in the case of ethane are mainly due to the lack of accurate low-temperature virial coefficients.

5.3 Multiparameter Pair Potentials

There have been several attempts to determine the true pair potential of a gas by use of multi-parameter potential models or non-analytic forms of the potential. Nearly all of this work has been confined to argon, and the most successful of the recent investigations appear to be those of Barker and co-workers (122- 125).

Barker and Pompe (122) chose the following form for the potential,

$$U(R) = \epsilon \left\{ e^{\alpha(1-r)} \sum_{i=0}^{L} A_i (r-1)^i - \sum_{i=0}^{2} C_{2i+6} / (\delta + r^{2i+6}) \right\} \qquad (5.3\text{-}1)$$

where $r = R/R_m$ $\qquad$ R = molecular separation

$L = 3$ $\qquad$ R_m = value of R at minimum of U(R)

δ was taken as very small and was included to prevent a spurious maximum in U(R) at small separations. The values of C_6, C_8 and C_{10} were found from the theoretical values of the dispersion energy coefficients. High energy molecular beam measurements, which give information on the potential at small values of R, and second virial coefficient data were then used to obtain the remaining parameters. Several sets of parameters were obtained, and one chosen on the basis of a comparison between experimental and calculated static lattice energy and zero-point energy of the crystal at 0 ^{o}K. These calculations required an assumption about the significance of non-pairwise additive forces (three-body and n-body forces), which is discussed in section 5.3 in the section on third virial coefficients.

The potential of Barker and Pompe was later modified by Barker and Bobetic (123) to also give excellent agreement with the experimental specific heat and thermal expansion of crystalline argon below 12 ^{o}K. The same potential was found to predict closely the transport properties of gaseous argon (124), i.e. viscosity, thermal conductivity, self-diffusion coefficients and thermal-diffusion. To obtain good agreement between calculated and experimental thermodynamic properties of liquid argon, Barker, Fisher and Watts (125) derived a new potential which is a linear combination of the Barker-Pompe and Barker-Bobetic potentials. This third potential (BFW) also agreed with the spectroscopic data on the Ar_2 molecule (127), which gives information on the magnitude of the well-depth, ϵ, and it also gave unchanged or sometimes improved agreement with the properties of the gaseous and solid states.

(a) The Reduced Barker-Fisher-Watts Potential

Argon, methane and nitrogen are known to obey fairly closely the principle of corresponding states (3), which is discussed in more detail in Chapter 6. To conform to the principle of corresponding states the pair potential of each substance must be of the form,

$$U_\alpha(R) = f_\alpha U_o(R/g_\alpha) \qquad (5.3\text{-}2)$$

where $U_o(R)$ is the pair potential of a reference substance (in this case taken to be argon), and f_α and g_α are the scale factors for substance α,

$$f_\alpha = \frac{\epsilon_\alpha}{\epsilon_o} \qquad g_\alpha = \frac{\sigma_\alpha}{\sigma_o} \qquad (5.3\text{-}3)$$

The second virial coefficient is then given by

$$B_\alpha(T) = g_\alpha^3 \cdot B_o(T/f_\alpha) \qquad (5.3\text{-}4)$$

The applicability of the BFW potential to methane and nitrogen was investigated through the assumption of the principle of corresponding states, i.e. that (5.3-4) is valid.

The Barker-Pompe (BP) and Barker-Bobetic (BB) potentials for argon are both of the form given in (5.3-1), with constants given in Table 5.4. The BFW potential is,

$$U_{BFW} = .75\, U_{BB} + .25\, U_{BP} \qquad (5.3\text{-}5)$$

The resultant parameters are,

$$\begin{aligned} \epsilon/_k &= 142.095 \text{ K} \\ R_m &= 3.7612 \text{ Å} \\ R_o &= 3.3605 \text{ Å} \end{aligned} \qquad (5.3\text{-}6)$$

TABLE 5.4

The Barker-Fisher-Watts Potential for Argon

Constants of Equation (5.3-1)

	Barker-Pompe	Barker-Bobetic
ϵ/k, K	147.70	140.235
R_m, nm	.37560	.37630
R_o, nm	.33410	.33666
A_o	0.2349	0.29214
A_1	-4.7735	-4.41458
A_2	-10.2194	-7.70182
A_3	-5.2905	-31.9293
A_4	0.0	-136.026
A_5	0.0	-151.0
C_6	1.0698	1.11976
C_8	0.1642	0.171551
C_{10}	0.0132	0.013748
α	12.5	12.5
δ	0.01	0.01

TABLE 5.5

Second Virial Coefficient for the BFW Potential

T,K	B,cc.mole^{-1}	T,K	B,cc.mole^{-1}
75.0	-317.3	223.15	-38.31
84.03	-255.4	248.15	-29.24
89.57	-226.7	273.15	-22.11
97.69	-193.2	323.15	-11.68
102.79	-176.08	373.15	-4.47
113.97	-145.95	423.15	+0.79
128.15	-117.86	473.15	+4.77
143.15	-95.98	573.15	+10.33
163.15	-74.77	673.15	+13.97
183.15	-59.24	773.15	+16.50
203.15	-47.52	873.15	+18.32
		1073.15	+20.72

Unfortunately, the calculated virial coefficients for none of these three potentials have been presented in a usable form. Therefore the second virial coefficient of argon for the BFW potential, with first quantum correction, was calculated by direct numerical integration of equations (5.1-15) and (5.1-18). A standard computer program employing Simpson's Rule integration was used. The range of integration for each temperature was from 0.01 Å to 30.01 Å, giving the classical second virial coefficient to an accuracy of about 0.03 cc/mole from 163.15 K to 1273.15 K, and to an accuracy decreasing at lower temperatures to about 0.2 cc/mole at 75 K. A much smaller range of integration, usually up to 8 Å, was sufficient for the first quantum correction. The values so obtained are presented in Table 5.5, the reduced temperature and second virial coefficient referring to,

$$T^* = \frac{kT}{\epsilon} \qquad B^* = \frac{B}{2/3\pi N_o R_o^3} \tag{5.3-7}$$

In figure 5.2 the deviations from the experimental second virial coefficients are presented. The fit is, on the whole, reasonable, but the calculated values tend to be too negative above 140 K as compared with the majority of the data.

The second virial coefficients of argon for the BFW potential were then fitted to a polynomial in 1/T,

$$B_o = a_1 + \frac{a_2}{T} + \frac{a_3}{T^2} + \frac{a_4}{T^3} + \frac{a_5}{T^4} \tag{5.3-8}$$

which was taken as the reference equation for use in (5.3-4).

This equation can safely be extrapolated to slightly higher temperatures but not to lower temperatures.

The experimental second virial coefficients of methane and nitrogen were then fitted by the equation,

$$B(T) = g^3 \cdot B_o(T/f) \qquad (5.3\text{-}9)$$

The resultant parameters, g^3 and f, are given in Table 5.6, together with the coefficients of equation (5.3-8). The deviations between the calculated and experimental virial coefficients are shown in figures 5.3 and 5.4. The agreement is good except perhaps at low temperatures for methane. Part of this discrepancy is due to the larger quantum corrections for methane; the quantum corrections should not really be included in this corresponding states treatment. However, this introduces only a small error. Most of the discrepancy is due to the fact that the BFW potential gives values that are more negative in the mid-temperature range than the experimental values of argon, but reasonable values at low temperature. When the equation in its reduced form (5.3-9) is fitted to methane data, it gives a good fit to the data of Douslin et al (32) in the mid-temperature range, and hence values of B that are too positive at low temperature. The actual experimental virial coefficients of methane and argon show, in fact, much better agreement with the principle of corresponding states than is apparent from figure 5.3.

To fully test the applicability of the reduced BFW potential, (5.3-9) to methane and nitrogen, it would be necessary to compare experimental and calculated values of

TABLE 5.6

Parameters of Reduced Barker-Fisher-Watts Potential

	Methane	Nitrogen	Argon	Parameters of reference equation	
g^3	1.4060	1.3266	1	a_1	31.84649
f	1.2226	.7836	1	a_2	$-1.000638.10^3$
ϵ/k, K	173.7	111.3	142.1	a_3	$-1.48933\ .10^6$
σ, nm	.3765	.3693	.33605	a_4	$6.76968\ .10^7$
Polarizability, α $(nm)^3$	.00260	.00176	.00163	a_5	$-3.55104\ .10^9$

TABLE 5.7

Dispersion Energy Coefficients

μ, 10^{-79}.J.m^6

	Argon	Methane	Nitrogen
Calculated, (Dalgarno)		143	70
reduced BFW	61.3*	148	84
L-J (12-6)	112.0	255.0	144.5
L-J (18-6)	69.5	166.5	95.0
L-J (n-6)	65.8	139.9	72.1

* Calculated, Leonard (126)

a range of thermodynamic properties as considered by Barker et al. for argon. Here the comparison is confined to the third virial coefficients, presented in section 5.5(b), and the dispersion energy coefficients.

The dispersion energy coefficient, i.e. the coefficient of r^{-6} in the long-range part of the potential, may be calculated by the methods of quantum- mechanics, and recent estimates are believed accurate to within a few per cent. In Table 5.7 the calculations of Dalgarno (128) are compared with those for the reduced Barker-Fisher-Watts potential, the L-J (12-6), L-J (18-6) and L-J (n-6) potentials.

The dispersion energy coefficient for argon from the BFW potential was set equal to the calculated value of Leonard (126),

$$\text{i.e.} \qquad \epsilon \, . \, C_6 \, . \, R_m^6 = 61{\cdot}3 \, . \, 10^{-60} \text{erg.cm}^6 \qquad (5.3\text{-}10)$$

Therefore the coefficient for methane or nitrogen is given by

$$\mu = f_\alpha \, g_\alpha^6 \, . \, 61{\cdot}3 . 10^{-60} \text{erg.cm}^6 \qquad (5.3\text{-}11)$$

The coefficient for the (n-6) potential becomes, from (5.2-1)

$$\mu = \frac{\left(6/n\right)^{\frac{-6/n}{(1-6/n)}}}{(1 - 6/n)} \, . \, \epsilon \, . \, \sigma^6 \qquad (5.3\text{-}12)$$

It can be seen, from Table 5.7, that the (L-J) 12-6 potential gives values that are much too high, and the (18-6) potential gives values that are much nearer the theoretical values, and in the case of argon the agreement is good.

The reduced BFW potential is superior in this respect, giving very good agreement, especially for methane.

Recent new measurements of low-energy molecular beam scattering in the Ar/Ar system (129) and a re-analysis of the vacuum-uv absorption spectra of Ar_2 (130) have both shown that the pair potential of argon appears to be close to that of Barker, Fisher and Watts in both shape and size, e.g. within 0.5% of the value of ϵ/k.

However, all of these potentials give values of the second virial coefficients that tend to be more positive than the experimental values at low temperature (e.g. 7-10 $cm^3.mole^{-1}$ at 100 K): this discrepancy is yet to be explained. It is a possibility that part represents experimental error on the virial coefficients, (18) (55); for methane the results of Byrne et al. (55) appear to be more negative at low temperatures than those of this work and of Brewer (54) (see section 4.5(a)).

5.4 Anisotropic Potential of the Nitrogen Molecule

It has been shown (131) that for a molecule which is non-spherical or anisotropic the intermolecular potential is the sum of an angle-independent term and several terms which depend not only on the separation between the molecules but also on their relative orientation. For a molecule such as nitrogen which possesses zero dipole moment

but a significant quadrupole moment, Q, the intermolecular potential is given by,

$$U = U(\text{spherical}) + U(\text{anisotropic}) + U(q\text{-}q) + U(q\text{-}\mu i) + U(\text{shape}) \qquad (5.4\text{-}1)$$

where U(spherical) is the centrally-symmetric potential.

U(anisotropic) is the effect of anisotropy on the long-range dispersion forces.

U(q-q) is the quadrupole-quadrupole interaction.

U(q-μi) is the quadrupole-induced dipole interaction.

U(shape) is the effect of anisotropy on the short-range exchange forces.

To the first order, the second virial coefficient is given by

$$B = B(\text{spherical}) + B(\text{anisotropic}) + B(q\text{-}q) + B(q\text{-}\mu i) + B(\text{shape}) \qquad (5.4\text{-}2)$$

The largest of the extra terms is usually due to U(q-q), which is proportional to Q^4 and r^{-5}. The above terms have been calculated (132) and applied to the determination of Q from second virial coefficients by Orcutt (133). Unfortunately, the L-J (12-6) potential was assumed for U(spherical) and this gives a poor representation of B(spherical) for the isotropic argon molecule. The potential parameters were determined from viscosity data, which are less sensitive to anisotropic effects, and from the difference between B(experimental) and B(spherical), |Q| was estimated to be $1.90.10^{-26}$ esu.

A much better estimate of Q is obtained from experimental measurements which do not require an assumed form for the

central potential, such as induced birefringence measurements, which give $|Q| = 1.52.10^{-26}$ esu (134). This is much closer to the results of quantum mechanical calculations, which give $|Q| = 1.36.10^{-26}$ esu (135).

Adjusting the results of Orcutt for these new values of Q has the effect of reducing considerably the total contributions to B of the anisotropic terms, which are very sensitive to the magnitude of Q. For instance,

	ΔB	
	T = 123.5 K	T = 274.5 K
Q = 1.90	$-12.1\ cm^3.mole^{-1}$	$-2.7\ cm^3.mole^{-1}$
Q = 1.52	$-6.0\ cm^3.mole^{-1}$	$-1.4\ cm^3.mole^{-1}$
Q = 1.36	$-4.4\ cm^3.mole^{-1}$	$-1.0\ cm^3.mole^{-1}$

These values are still specific to the L-J (12-6) potential but are probably of similar magnitude for the other potentials. The contributions to B are still quite significant but the uncertainties in the calculations and in the magnitude of Q are such that little accuracy is gained in the estimation of the potential parameters of nitrogen if these contributions to B are first subtracted.

5.5 Third Virial Coefficients

The potential energy of interaction between three molecules (the three-body potential) may be written as the sum of pairwise additive terms plus a non-additivity correction,

$$U(r_{12}, r_{23}, r_{31}) = U(r_{12}) + U(r_{23}) + U(r_{31}) + \Delta U(r_{12}, r_{23}, r_{31}) \qquad (5.5\text{-}1)$$

where r_{12}, r_{23} and r_{31} are the lengths of the sides of the triangle bounded by the three molecules.

The total third virial coefficient can be shown by the methods of statistical mechanics (2) to be the sum of a pairwise additive and a pairwise non-additive part,

$$C = C_{add} + \Delta C \qquad (5.5\text{-}2)$$

where, for spherically symmetric potentials,

$$C_{add} = -\frac{8\pi^2 N_o^2}{3} \iiint f_{12}\, f_{23}\, f_{13}\; r_{12}\, r_{23}\, r_{13}\; dr_{12}\, dr_{23}\, dr_{13} \qquad (5.5\text{-}3)$$

$$\Delta C = -\frac{8\pi^2 N_o^2}{3} \iiint \left\{ e^{-\Delta U_{123}/kT} - 1 \right\} e^{-(U_{12}+U_{23}+U_{13})/kT} \cdot r_{12}\, r_{23}\, r_{13}\; dr_{12}\, dr_{23}\, dr_{13} \qquad (5.5\text{-}4)$$

where $f_{12} = e^{-u(r_{12})/kT} - 1$, etc.,
and the integration extends over all values of r_{12}, r_{13}, r_{23} which form the sides of a triangle.

Comparisons of theoretical calculations of the third virial coefficient with experimental values have often been inconclusive because of the uncertainty surrounding the nature of the non-additive contribution. At long-range intermolecular separations the major contribution to non-additivity arises from the Axilrod-Teller (136) triple-dipole, dispersion interaction, which for spherically symmetric potentials is,

$$\Delta U_{123} = \frac{\nu_{123}\left(3\cos\theta_1 \cos\theta_2 \cos\theta_3 + 1\right)}{\left(r_{12}\, r_{23}\, r_{13}\right)^3} \qquad (5.5\text{-}5)$$

where θ_1, θ_2 and θ_3 are the interior angles of the triangle

bounded by r_{12}, r_{13} and r_{23}, and ν_{123} is a non-additive dispersion coefficient, given to a good approximation for a pure gas by

$$\nu_{123} = \frac{3}{4} \alpha \mu \qquad (5.5\text{-}6)$$

where α = polarizability

μ = dispersion energy coefficient of the pair potential.

Sherwood and Prausnitz (137) showed that the non-additive contributions to C due to this interaction are by no means negligible, amounting to almost half of the total third virial coefficient in the vicinity of its maximum.

At small intermolecular separations there is non-additivity due to short-range, three-body exchange forces (or triple-overlap interactions). These are difficult to calculate exactly, but calculations have been made by Sherwood, De Rocco and Mason (138), and by Graben, Present and McCulloch (139) based on the approximate theory of Jansen (140). They concluded that the contributions from three-body exchange forces tend to cancel the contributions from the triple-dipole dispersion forces. However, the theory of Jansen is now believed to greatly over-estimate the magnitude of the three-body exchange forces, a conclusion arrived at by Barker and Pompe (123).

As described in section 5.3, Barker and Pompe obtained a range of two-body potential functions, of the form given by (5.3-1), which were all equally successful in fitting the data for argon on properties dependent on pair-interactions only. The calculated third virial coefficients for all of these potentials agreed within 10% of the

experimental values, which was estimated as just outside the experimental error, when the triple-dipole non-additive contribution was included. It was concluded that the effect of other non-additive interactions on the third virial coefficient must be small, especially as they would be expected to be sensitive to the exact form of the pair potential. On the assumption that all non-additive forces other than the three-body dispersion forces could be neglected, Barker et al. obtained excellent agreement between experimental and calculated values of a wide range of thermodynamic properties of gaseous, liquid and solid argon (see section 5.3). This was support for the validity of the aforementioned assumption.

Dymond and Alder (141) have attempted to calculate the magnitude of the three-body non-additive forces by direct subtraction of Cadd from the experimental third virial coefficients, where the former was calculated for their numerically tabulated pair potential of argon (142). To obtain the experimental values of C, they 'reanalysed' the PVT data of Michels et al (81, 82) by using theoretical values of second, fourth and fifth virial coefficients and calculating C by difference. This method is highly subject to error, however, as a small difference between the calculated and experimental value of B will lead to a large error in C. Their values lie some 100 - 200 cc^3/mole below those given in Chapter 4. Even so, it appears that, except perhaps at very small intermolecular separations, the three-body exchange forces may be neglected. Therefore for the purposes of calculation of the third virial coefficient

for the potentials considered here, no corrections for non-additivity were included other than those for the triple-dipole dispersion interaction.

(a) Third Virial Coefficients for Simple Potential Functions

If the neglect of three-body non-additive interactions other than that given by (5.5-5) is accepted as a valid assumption, then by a comparison of theoretical and experimental third virial coefficients further information may be obtained on the approximation of a simple pair potential function to the true pair potential. This is important for gases such as methane and nitrogen, for which there have been no systematic attempts to determine a true pair potential as there have been for argon.

The models considered here are the Lennard-Jones and the Kihara spherical core potentials. For the L-J (12-6) potential the third cluster integral (5.5-3) has been evaluated by expansion as a series in $(T^*)^{-\frac{1}{2}}$ (143, 144),

$$C^*_{add} = \frac{C_{add}}{(2/3\,\pi N_0 \sigma^3)^2} = \sum_{n=0}^{\infty} c_n \cdot (T^*)^{-\frac{(n+1)}{2}} \qquad (5.5\text{-}7)$$

where $T^* = \frac{kT}{\epsilon}$

For the calculations of this thesis the more recent results of Stogryn (145) have been employed, where the series expansion method was used for evaluation of both C^*_{add} and ΔC^*,

$$\Delta C^* = \nu^* \sum_{n=0}^{\infty} c'_n \, (T^*)^{-\frac{(n+3/2)}{2}} \qquad (5.5\text{-}8)$$

where $$\nu^* = \frac{\alpha}{\sigma^3} \qquad (5.5\text{-}9)$$

c_n(n=1 ... 27) and c'_n(n=1 ... 22) are presented in (145). The results are believed accurate to 0.1% at T* = 0.5 and to higher accuracy at higher temperatures.

Similar calculations have been carried out by Stogryn (146) for the L-J (18-6) potential, the series expansions being,

$$C^*_{add} = \sum_{n=0}^{\infty} c_n (T^*)^{-\frac{(2n+1)}{3}} \qquad (5.5\text{-}10)$$

$$\Delta C^* = \nu^* \sum_{n=0}^{\infty} c'_n (T^*)^{-\frac{(4n+5)}{6}} \qquad (5.5\text{-}11)$$

c_n and c'_n for n=1 to 20 are presented in (146) and the results are believed accurate to about 0.3% at T* = 0.5.

Unfortunately as yet no calculations have been performed for the three-parameter L-J (n-6) potential.

Values of C^*_{add} and $\Delta C^*/\nu^*$ for the Kihara spherical core potential have been tabulated by Sherwood and Prausnitz (119) at discrete values of a* from a* = 0 to 0.85. All calculations were performed by numerical integration.

First quantum corrections to C have been calculated for the L-J (12-6) potential only (147). Values for methane turn out to be 110 cm^6/mole at 150 K and 16 cm^6/mole at 200 K. These are within the present limits of experimental error and so quantum corrections were neglected throughout.

(b) Third Virial Coefficients for the Reduced BFW Potential

The principle of corresponding states requires that

$$C(T)_{add} = g^6 C_o(T/f)_{add} \qquad (5.5\text{-}12)$$

and

$$\Delta C(T) = \frac{\nu^*}{\nu^*_o} g^6 \Delta C_o(T/f) \qquad (5.5\text{-}13)$$

$$\therefore \quad \Delta C(T) = \frac{\alpha}{\alpha_o} g^3 \Delta C_o(T/f) \qquad (5.5\text{-}14)$$

where $C_{add_o}(T)$ and $\Delta C_o(T)$ refer to the additive and non-additive contributions to the third virial coefficient of argon for the Barker-Fisher-Watts potential. These were read to the nearest 50 cm^6 $mole^{-2}$ from figure 7 of (122).

(c) Results of Comparisons

Third virial coefficients calculated according to the methods described in 5.5(a) and (b) are compared with the selected experimental values of Chapter 4, for methane (figure 5.6), nitrogen (figure 5.7) and argon (figure 5.8). The potential parameters used were those obtained by a fit to the second virial coefficients, as listed in Table 5.1. Values of the polarizability, α, were taken from (148) and are given in Table 5.6. For the reduced BFW potential, the values of g^3 and f are those determined in section 5.3(a) and given in Table 5.6.

It is apparent from figures 5.6 - 5.8 that the L-J (12-6) potential, which provides an inadequate fit to second virial coefficients, gives third virial coefficients that are too high for all gases when the triple-dipole non-additive term is included.

The L-J (18-6) potential gives third virial coefficients for argon which are close to those of the Barker-Fisher-Watts potential, and are from 100 to 300 $cm^6.mole^{-2}$ smaller than the experimental values. For methane and nitrogen the results for the reduced BFW potential and the L-J (18-6) potential are also close and in good agreement with experiment.

The Kihara potential generally gives values of C that are higher than those of the L-J (18-6) and BFW potentials,

FIGURE 5.6

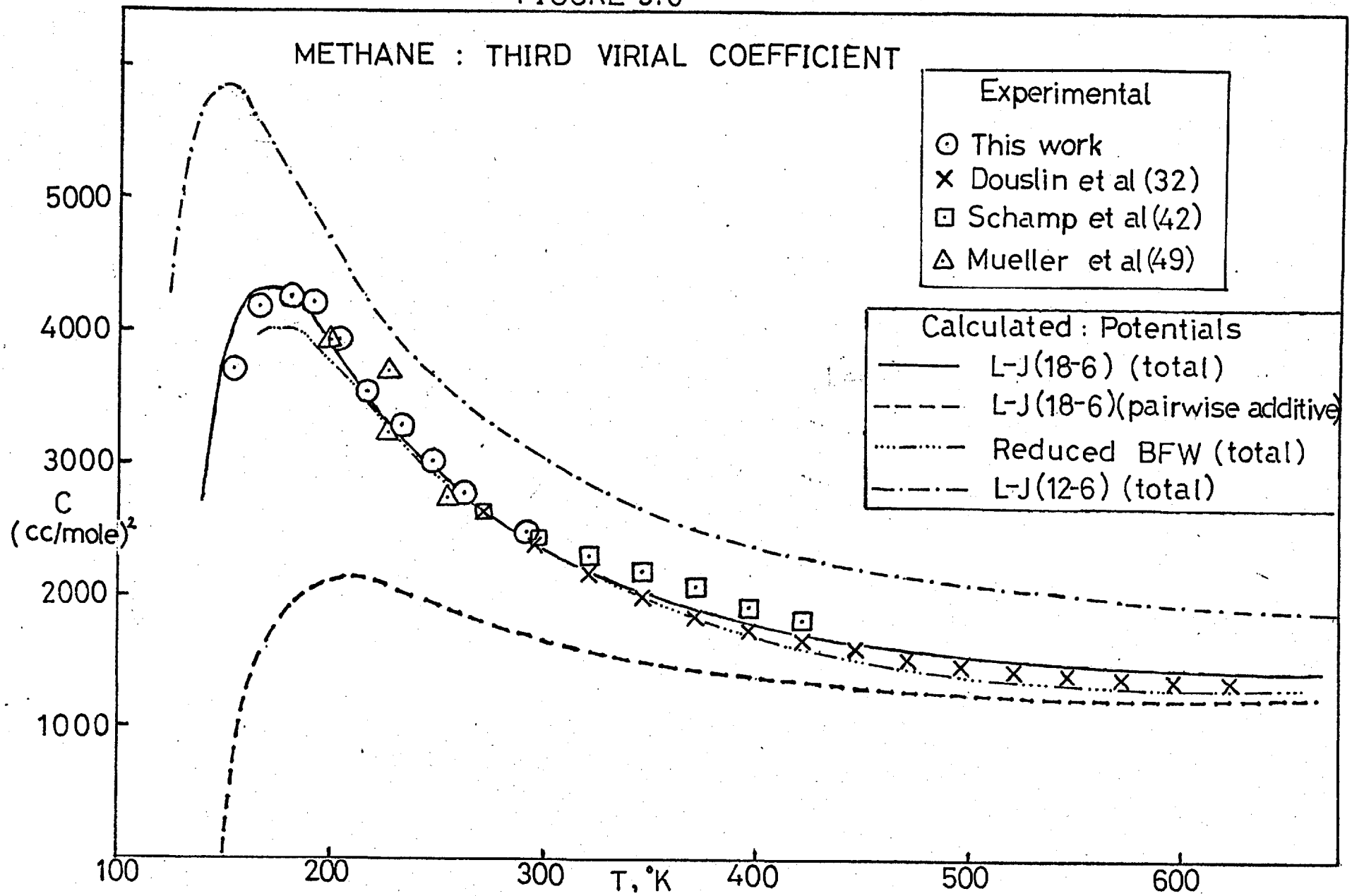
METHANE : THIRD VIRIAL COEFFICIENT
Experimental
This work
Douslin et al (32)
Schamp et al (42)
Mueller et al (49)
Calculated : Potentials
L-J (18-6) (total)
L-J (18-6) (pairwise additive)
Reduced BFW (total)
L-J (12-6) (total)
C
(cc/mole)²
5000
4000
3000
2000
1000
100
200
300
T, °K
400
500
600

FIGURE 5.7

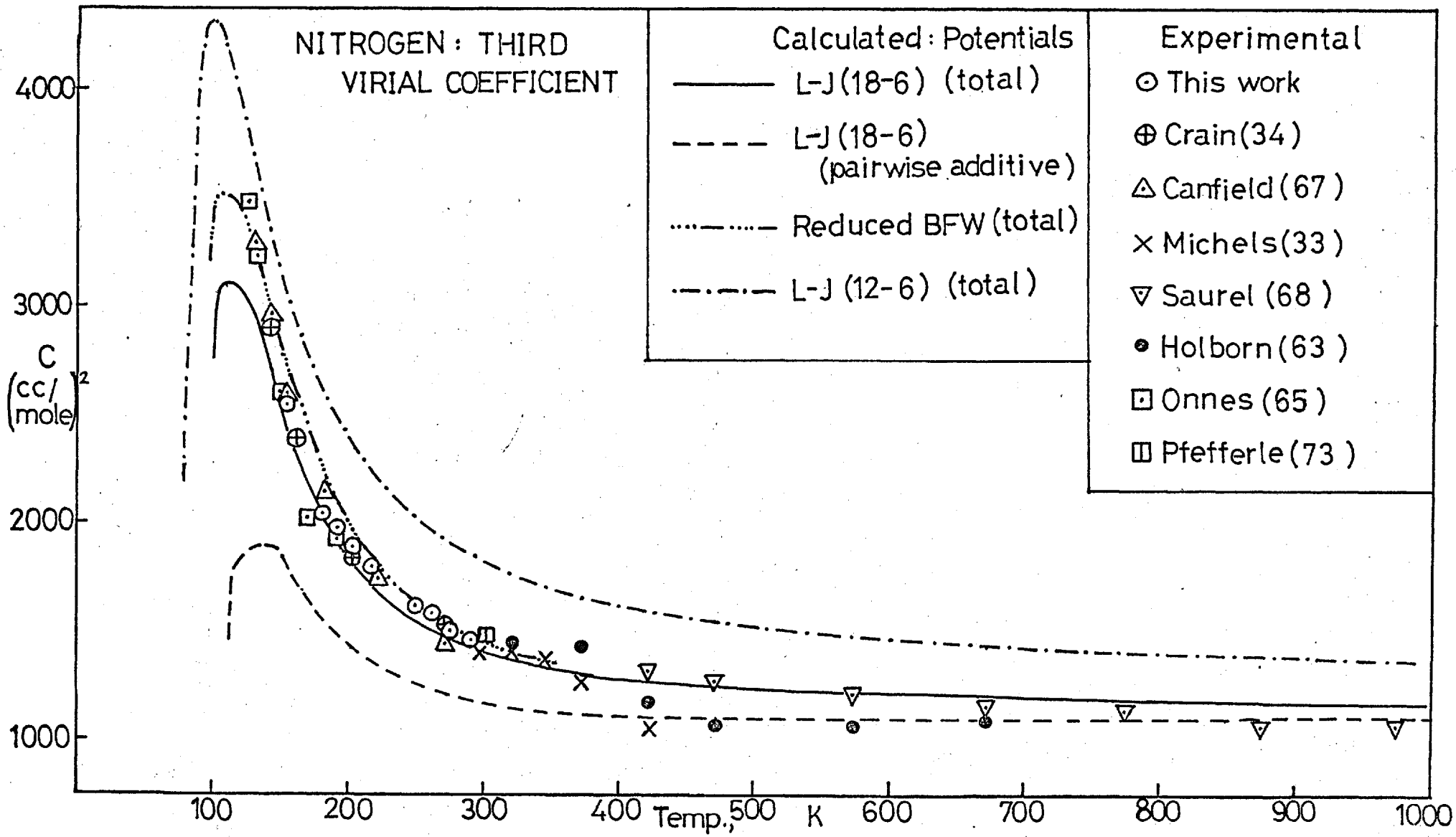
NITROGEN : THIRD VIRIAL COEFFICIENT
Calculated : Potentials
L-J (18-6) (total)
L-J (18-6) (pairwise additive)
Reduced BFW (total)
L-J (12-6) (total)
Experimental
This work
Crain (34)
Canfield (67)
Michels (33)
Saurel (68)
Holborn (63)
Onnes (65)
Pfefferle (73)
C (cc/mole)²
4000
3000
2000
1000
100
200
300
400
500
600
700
800
900
1000
Temp., K

FIGURE 5.8

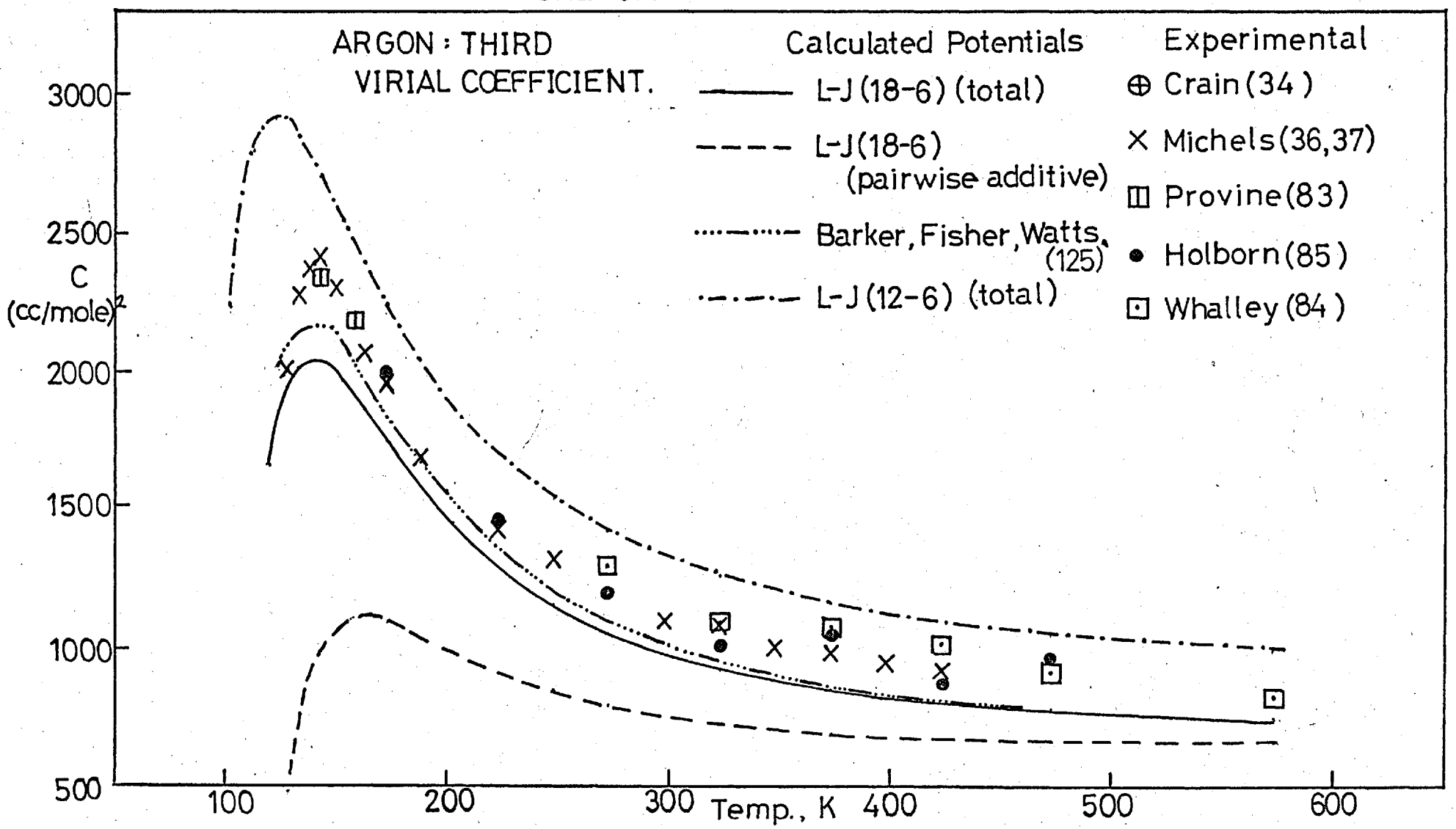
ARGON : THIRD VIRIAL COEFFICIENT.
Calculated Potentials
L-J (18-6) (total)
L-J (18-6) (pairwise additive)
Barker, Fisher, Watts, (125)
L-J (12-6) (total)
Experimental
Crain (34)
Michels (36,37)
Provine (83)
Holborn (85)
Whalley (84)
C (cc/mole)²
3000
2500
2000
1500
1000
500
100
200
300
400
500
600
Temp., K

although in good agreement with experiment for argon and nitrogen, but not for methane. There is some difficulty in calculation of ΔC^* for a potential such as the Kihara that instead of a r^{-6} term has a $(r-a)^{-6}$ term, as mentioned by Sherwood and Prausnitz (119).

(d) Conclusions

It has been shown that the Barker-Fisher-Watts potential (125), which is probably close to the true pair potential of argon, can be applied, in a reduced form, to the successful calculation of third virial coefficients of methane and nitrogen. It must be assumed, as with argon, that non-additive contributions other than those due to triple-dipole dispersion forces are small. This reduced BFW potential also gives good agreement with the theoretical value of the dispersion energy (r^{-6}) coefficient. It would be interesting to investigate further the applicability of this potential by comparison of calculated and experimental values of all the thermodynamic and transport properties of methane and nitrogen that were considered by Barker et al. for argon. This task will not be attempted here.

It has also been shown that a simple analytical form of the pair potential, viz the Lennard-Jones (18-6) potential, is capable of giving good agreement with both second and third virial coefficients of argon, methane and nitrogen. It has been shown elsewhere to give a good fit to the experimental second virial coefficients of krypton and xenon (13). The dispersion energy coefficients are also in reasonable agreement with the theoretical values. Thus it is possible that the L-J (18-6) potential offers a convenient approximation to the

true pair potential for simple spherically-symmetric molecules, at least in the range of intermediate intermolecular separation. This is important because by the use of a pair potential of simple analytical form the calculation of other thermodynamic and transport properties of the fluid is simplified. Although they give a slightly better fit to second virial coefficients, the three-parameter L-J (n-6) and Kihara potentials would offer no advantages over the L-J (18-6) potential in this application.

5.6 Second Virial Coefficients of Mixtures

The interactional second virial coefficient, B_{12}, is given by,

$$B_{12}(T) = 2\pi N_o \int_0^\infty \left(1 - e^{-U(r_{12})/kT}\right) r_{12}^2 \, dr_{12} \qquad (5.6\text{-}1)$$

where $U(r_{12})$ is the intermolecular potential energy of interaction between a molecule of type 1 and a molecule of type 2 separated by a distance r_{12}. B_{12} can be calculated for the potential models of section 5.2, requiring values for the interaction parameters ϵ_{12}, σ_{12} and n_{12} (or γ_{12}). (For the L-J (18-6) potential n_{12} is, of course, equal to 18).

These parameters were obtained for the L-J (18-6), L-J (n-6) and Kihara potentials by a non-linear least-squares fit to the experimental values of B_{12} for the mixtures methane/nitrogen, methane/argon, argon/nitrogen and methane/ethane.

The final parameters are shown in Table 5.8 (columns 1 and 2). The experimental data for these mixtures have been presented in Chapter 4. The L-J (12-6) potential was not

considered because of its inability to fit the second virial coefficients of the pure gases.

For a given potential energy function, the values of σ_{12} and ϵ_{12} required to predict B_{12} are usually estimated from the known like-interaction parameters by means of "combining-rules", the simplest of which is,

$$\sigma_{12} = \tfrac{1}{2}(\sigma_{11} + \sigma_{22}) \tag{5.6-2}$$

$$\text{Rule 1:} \qquad \epsilon_{12} = (\epsilon_{11}\,\epsilon_{22})^{1/2} \tag{5.6-3}$$

(5.6-2) is the Lorentz rule of additive diameters, which is exact for hard spheres, and (5.6-3) is the geometric mean rule of Berthelot.

Many alternatives to the geometric mean rule have been proposed, among which two of the more successful are,

$$\text{Rule 2:} \qquad \epsilon_{12} = 2\epsilon_{11}\epsilon_{22}/(\epsilon_{11} + \epsilon_{22}) \tag{5.6-4}$$

$$\text{Rule 3:} \qquad \epsilon_{12} = (\epsilon_{11}\epsilon_{22})^{1/2}\left[\frac{\sigma_{11}\sigma_{22}}{\sigma_{12}^2}\right]^3\left[\frac{2(I_1 I_2)^{1/2}}{I_1 + I_2}\right] \tag{5.6-5}$$

where I is the ionization potential.

Rule 2, the harmonic-mean rule, was found to be the most successful by Lin and Robinson (149) in the application of the Dymond-Alder potential (142) to rare gas pairs not containing helium. For krypton and xenon Pollard (13) found that none of the rules tested was particularly successful, but that rules 2 and 3 were preferable. Rule 3 is based on the London formula for dispersion forces, and Rule 2 is loosely based on the Kirkwood-Müller formula for the same forces.

Recently it has been shown by Good and Hope (150) that the form of the L-J (n-6) potential function suggests, on theoretical grounds, that the Lorentz rule of additive diameters should be replaced by a geometric mean rule,

$$\sigma_{12} = (\sigma_{11}\,\sigma_{22})^{\frac{1}{2}} \qquad (5.6\text{-}6)$$

On this assumption, Calvin and Reed (120) found the following rules successful in predicting B_{12} of seven mixtures, including methane/ethane and nitrogen/argon, using the L-J (n-6) potential.

$$\text{Rule 4}: \begin{cases} \epsilon_{12} = (\epsilon_{11}\,\epsilon_{22})^{\frac{1}{2}} & (5.6\text{-}7) \\ n_{12} = (n_{11}\,n_{22})^{\frac{1}{2}} & (5.6\text{-}8) \end{cases}$$

For tests of all rules and least-squares fitting using the (n-6) potential, n_{12} was set at the value given by (5.6-8). For the Kihara potential, assumption of the Lorentz rule of additive diameters requires that

$$\gamma_{12} = \frac{\gamma_{11}\sigma_{11} + \gamma_{22}\sigma_{22}}{\sigma_{11} + \sigma_{22}} \qquad (5.6\text{-}9)$$

For all tests and least-squares fitting, γ_{12} was set equal to the value given by (5.6-9).

In Table 5.8 are shown the values of σ_{12} and ϵ_{12} from the full least-squares curve-fitting (columns 1 and 2), and in column 3 the values of n_{12} or γ_{12} given by equations (5.6-8) or (5.6-9). In column 4 the value of σ_{12} given by the rule of additive diameters, (5.6-2), is shown. With σ_{12} fixed at this value, further least-squares fits to the data were carried out, and the resultant parameter ϵ_{12} is shown in column 5. This value of ϵ_{12} was then used to determine the

TABLE 5.8

Potential Parameters for Binary Systems

	σ_{12}	ϵ_{12}/k	n_{12} (or γ_{12})	σ_{12}	ϵ_{12}/k	k_{12}
Methane/Nitrogen	(Full least-squares fit)			(A.M. rule + least-squares fit)		
L-J (18-6)	.3655	152.5		.3605	155.0	.030
L-J (n-6)	.3537	183.7	25.2	.3505	185.6	.028
Kihara	.3600	164.2	.187	.3571	165.8	.029
Methane/Argon						
L-J (18-6)	.3414	181.3		.3457	178.7	.001
L-J (n-6)	.3294	202.9	20.9	.3397	193.7	.006
Kihara	.3350	189.7	.166	.3436	182.5	.005
Argon/Nitrogen						
L-J (18-6)	.3436	143.2		.3418	144.2	-.007
L-J (n-6)	.3353	164.7	23.1	.3343	165.2	-.012
Kihara	.3403	150.6	.176	.3394	151.0	-.009
Methane/Ethane						
L-J (18-6)	.4012	243.5		.4123	234.7	.002
L-J (n-6)	.3841	297.0	25.2	.3947	286.2	-.017
Kihara	.3897	270.9	.196	.4020	259.7	-.004

geometric-mean correction factor, k_{12}, where

$$\epsilon_{12} = (1 - k_{12})(\epsilon_{11}\epsilon_{22})^{1/2} \qquad (5.6\text{-}10)$$

The values of k_{12} are shown in column 6.

In Table 5.9, the values of ϵ_{12} given by Rules 1 - 3 are presented, and, in column 4, the value of ϵ_{12} from the least-squares fit (from column 5 of Table 5.8). It is apparent that for methane/nitrogen and nitrogen/argon σ_{12} given by (5.6-6) is similar to that given by (5.6-2), and Rule 4 is identical to Rule 1. For methane/argon and methane/ethane they are only slightly different.

Because most of the mixture data covers only a limited temperature range, the potential parameters obtained from the least-squares fit are not determined accurately, particularly for the more flexible three-parameter potentials. A more realistic test of the combining rules than a comparison of the values given in Tables 5.8 and 5.9 is the direct comparison of the calculated and experimental values of B_{12}. Any rule must be regarded as acceptable if B_{12} can be predicted within experimental error. These comparisons are shown in Figures 5.~~10~~ 9 - 5.~~13~~ 12.

Figure 5.9 : Methane/Nitrogen.

The results for each rule are virtually independent of the potential model; those for the L-J (18-6) potential are shown. Rule 2 is good, but Rules 1 (and 4) and Rule 3 both give B_{12} values that are too negative.

Figure 5.10: Nitrogen/Argon.

The results for all rules are very similar. Those for

TABLE 5.9

Combining Rules

	ϵ_{12}/k (σ_{12} given by arithmetic mean rule)			
	Rule 1	Rule 2	Rule 3	Least-squares value
Methane/Nitrogen				
L-J (18-6)	159.7	155.8	158.9	155.0
L-J (n-6)	191.0	188.0	190.1	185.6
Kihara	170.8	167.3	170.1	165.8
Methane/Argon				
L-J (18-6)	178.9	177.8	176.5	178.7
L-J (n-6)	194.8	192.4	192.6	193.7
Kihara	183.4	181.8	181.1	182.5
Argon/Nitrogen				
L-J (18-6)	143.1	142.2	142.2	144.2
L-J (n-6)	163.1	163.1	162.6	165.2
Kihara	149.7	149.4	148.9	151.0
Methane/Ethane				
L-J (18-6)	235.1	231.8	-	234.7
L-J (n-6)	281.4	275.3	-	286.2
Kihara	258.7	252.9	-	259.7

FIGURE 5.9

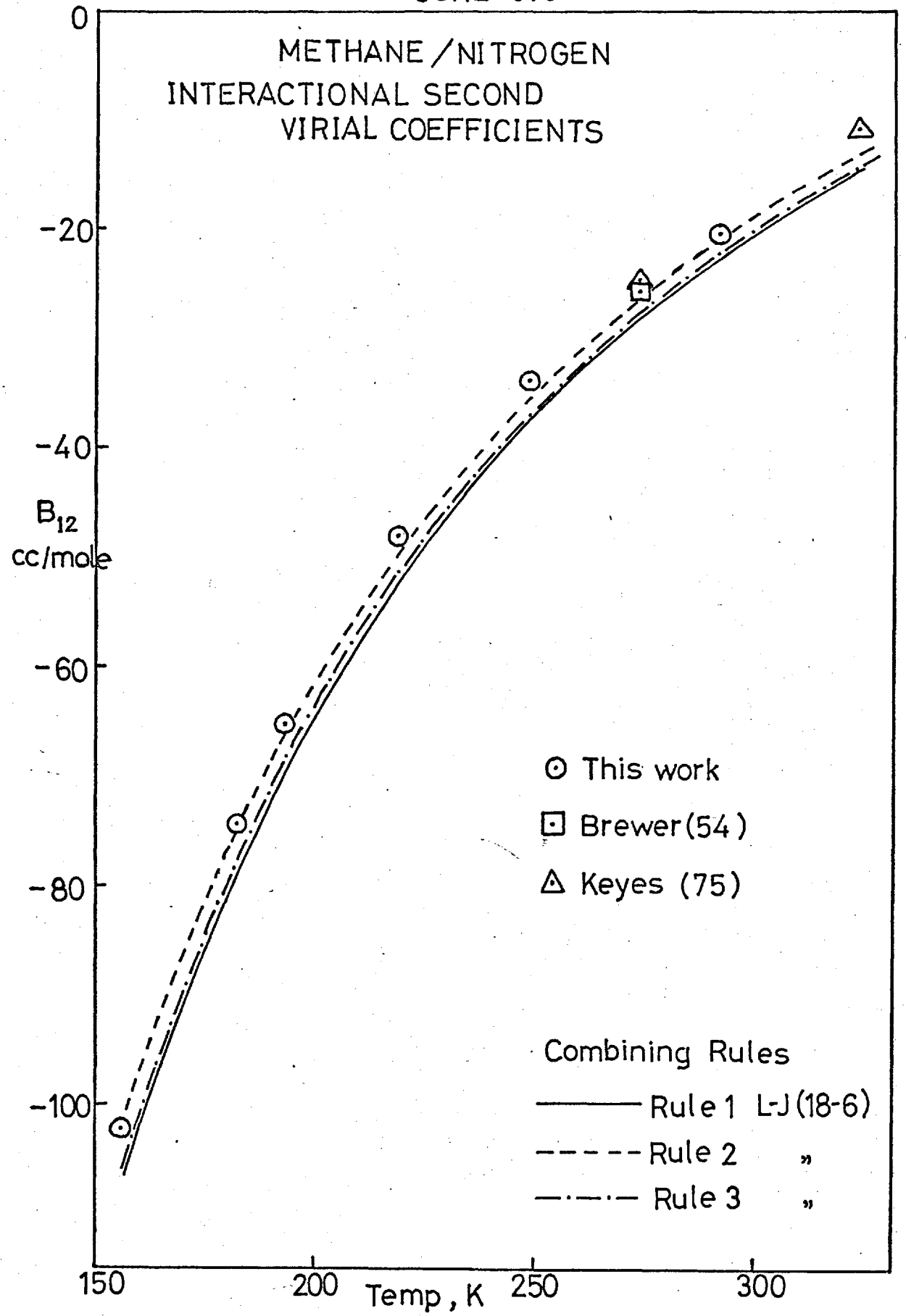
METHANE / NITROGEN
INTERACTIONAL SECOND
VIRIAL COEFFICIENTS
0
-20
-40
-60
-80
-100
B_{12}
cc/mole
150
200
250
300
Temp, K
This work
Brewer (54)
Keyes (75)
Combining Rules
Rule 1 L-J (18-6)
Rule 2 "
Rule 3 "

FIGURE 5.10

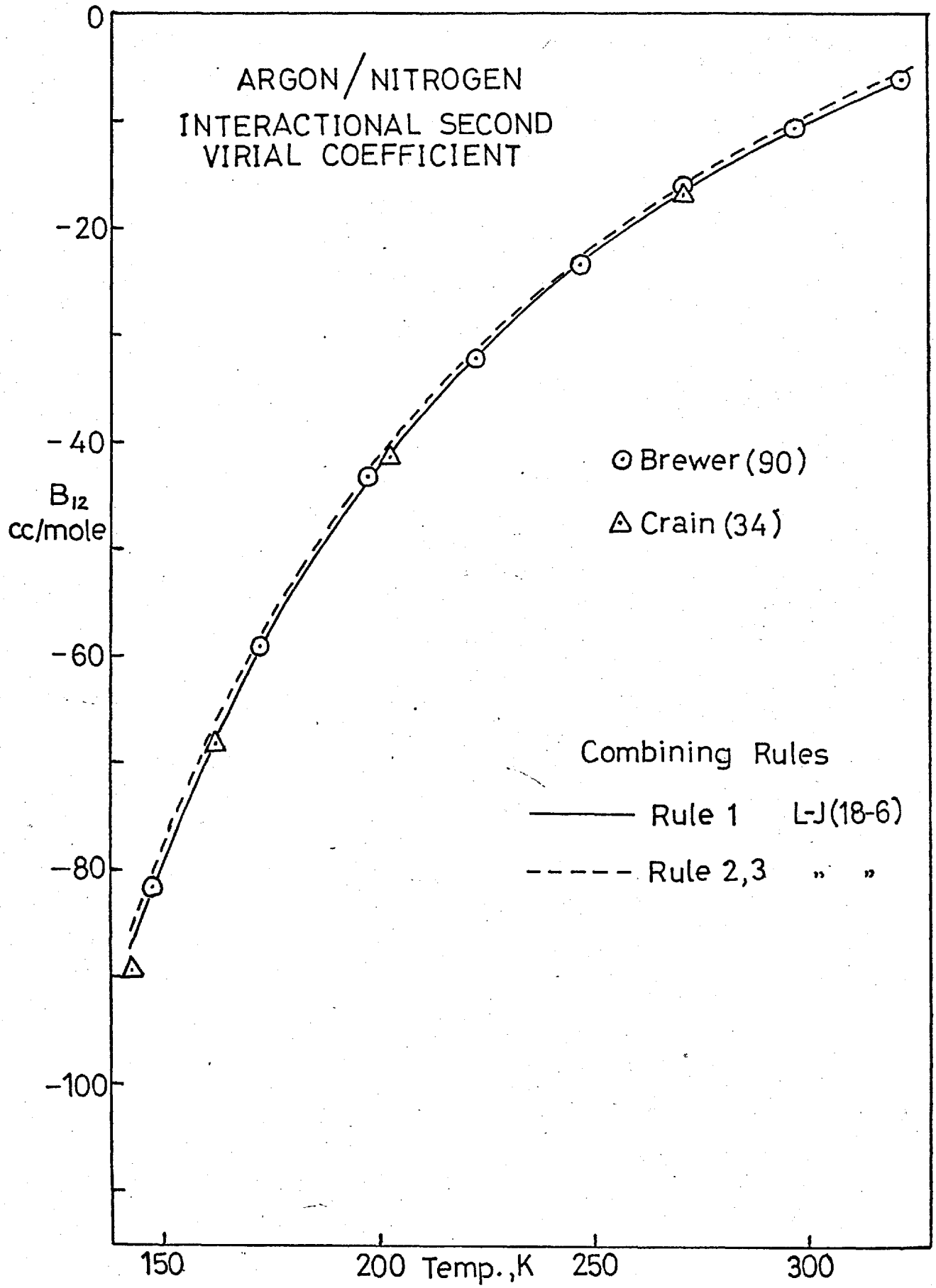
ARGON / NITROGEN
INTERACTIONAL SECOND
VIRIAL COEFFICIENT
0
-20
-40
-60
-80
-100
B_{12}
cc/mole
⊙ Brewer (90)
△ Crain (34)
Combining Rules
Rule 1 L-J(18-6)
Rule 2,3 " "
150
200
Temp.,K
250
300

FIGURE 5.11

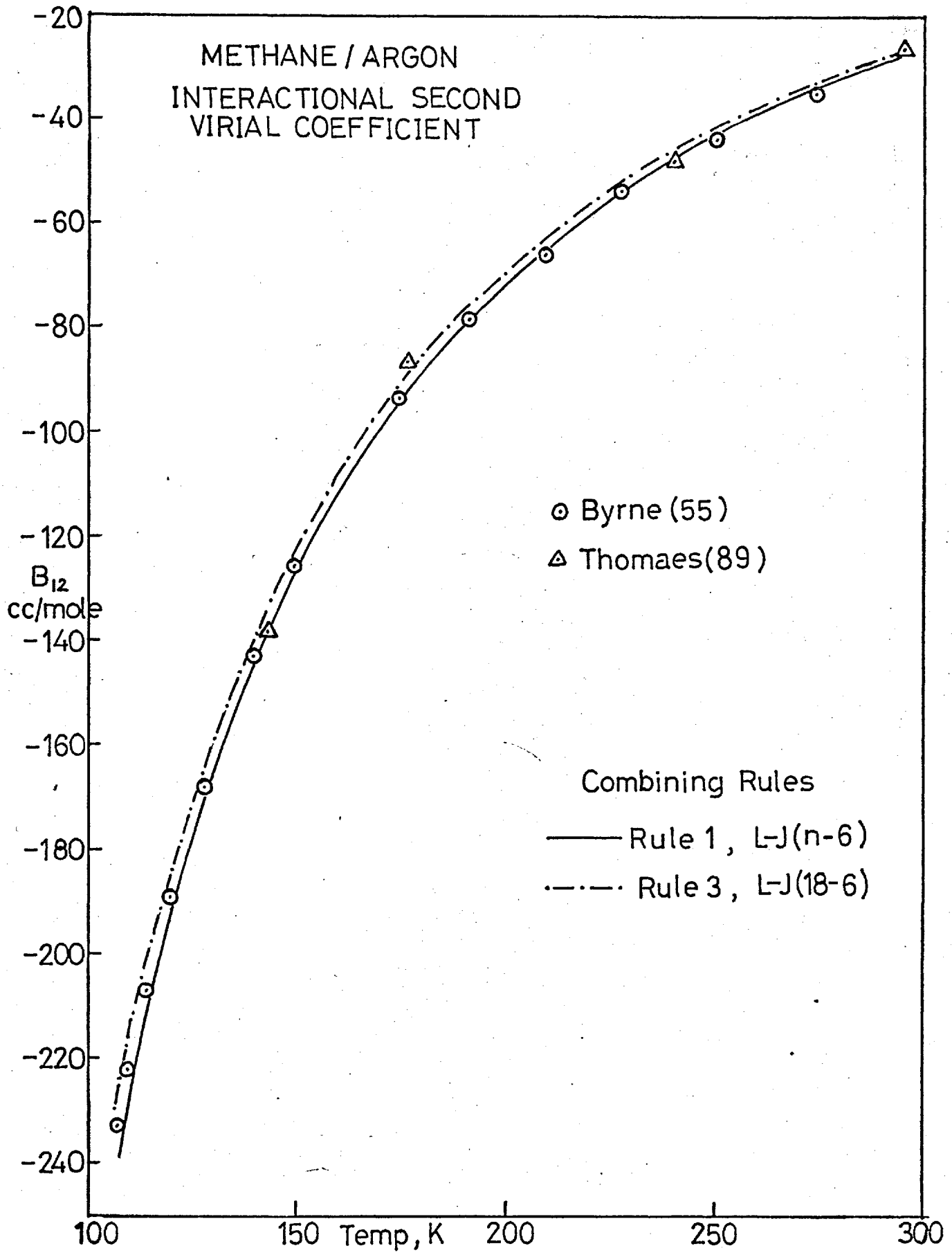
METHANE / ARGON
INTERACTIONAL SECOND
VIRIAL COEFFICIENT
-20
-40
-60
-80
-100
-120
-140
-160
-180
-200
-220
-240
B12
cc/mole
Byrne (55)
Thomaes(89)
Combining Rules
Rule 1, L-J(n-6)
Rule 3, L-J(18-6)
100
150
Temp, K
200
250
300

FIGURE 5.12

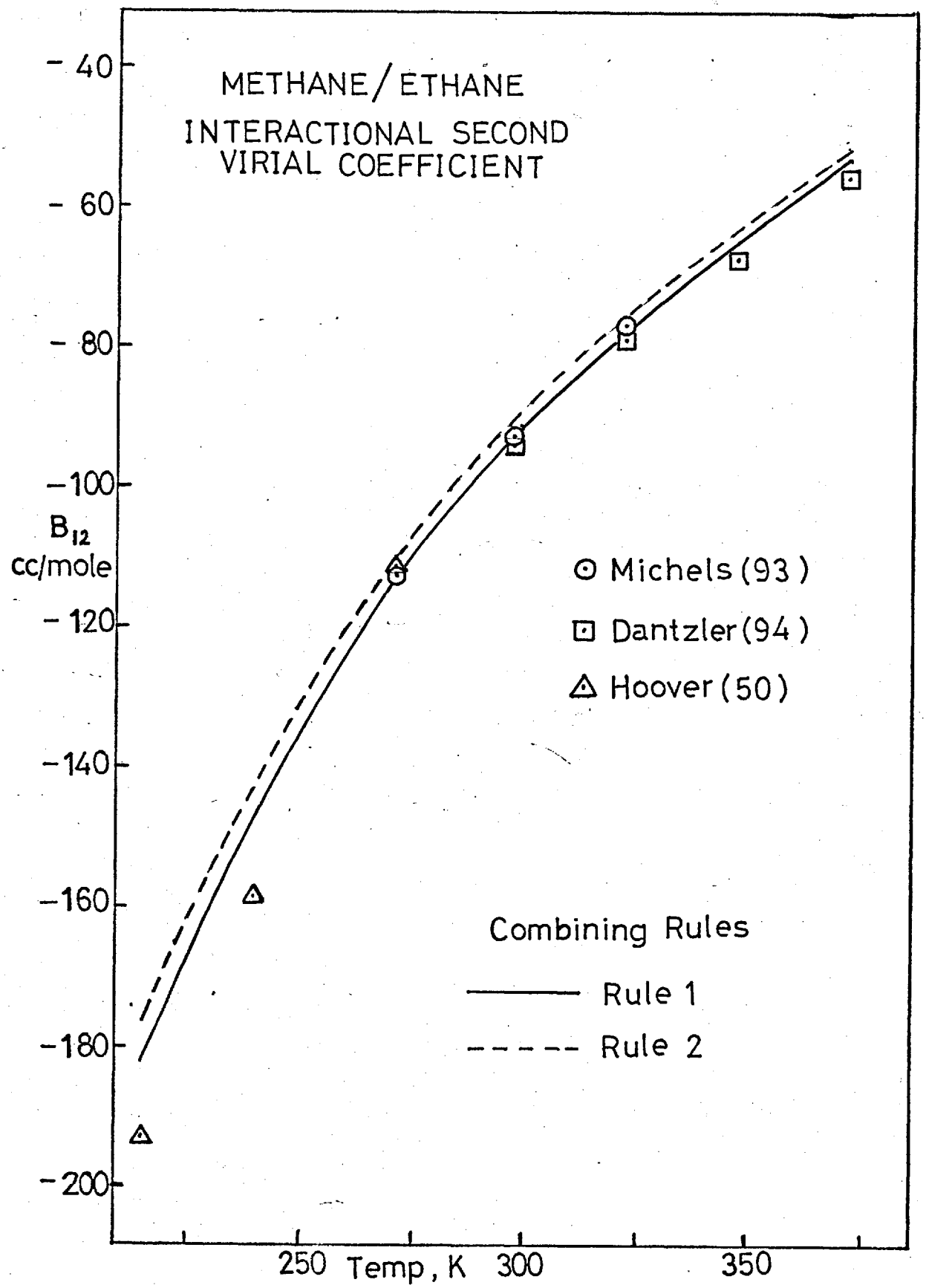
METHANE/ETHANE
INTERACTIONAL SECOND
VIRIAL COEFFICIENT
- 40
- 60
- 80
-100
-120
-140
-160
-180
-200
B_{12}
cc/mole
250
Temp, K
300
350
Michels (93)
Dantzler (94)
Hoover (50)
Combining Rules
Rule 1
Rule 2

Rule 1 and Rules 2 and 3 for the L-J (18-6) potential are shown. The results for the other potentials lie between these two curves. In general, rules 1 and 2 are satisfactory and rule 3 only slightly less so.

Figure 5.11: Methane/Argon.

The results are shown of Rule 1 for the Kihara potential and Rule 3 for the L-J (18-6). All the other results lie between these extremes, Rules 1 and 2 being satisfactory but Rule 3 giving too positive values of B_{12}.

Figure 5.12: Methane/Ethane.

Again, the results for a particular rule tend to be independent of the potential. Those of Rules 1 and 2 for the L-J (18-6) potential are shown. Rule 1 is the most satisfactory and Rule 2 gives values that are slightly too positive. Rules 3 and 4 are generally worse. Conclusions are difficult for this system because of the low experimental acccuracy at low temperatures.

For the systems studied here, Rule 2, the harmonic mean rule is overall the most satisfactory, and Rule 1, the geometric mean rule, almost as good except for the methane/nitrogen system. For these relatively simple systems it is unnecessary to introduce more complex rules such as Rule 3, which involves ionization potentials.

The deviations from Rule 1, the geometric mean rule, are conveniently characterized by the correction factor k_{12}. It can be seen from Table 5.8 that the value of k_{12} for a particular mixture is independent of the potential model. It is estimated that the experimental error in B_{12} sets a

maximum error in k_{12} of about .005.

Estimates of k_{12} have been obtained for a wide range of mixtures by Chueh and Prausnitz (151) from a correlation of gas mixture PVT data with the Redlich-Kwong equation of state. In this case, k_{12} is defined from the critical temperatures,

$$T_{c_{12}} = (1 - k_{12})(T_{c_1} \cdot T_{c_2})^{1/2} \qquad (5.6\text{-}11)$$

These values are in excellent agreement with ours for methane-nitrogen (see Table 5.10) but are up to .02 larger for the other systems; the differences are still fairly small, however. The negative values of k_{12} that we obtain have no real physical significance but are simply the result of fixing σ_{12} to that given by the rule of additive diameters, which is known to be only an approximation for real molecules. A correlation of k_{12} for many mixtures has recently been published (152).

The excess free energy and the excess volume of mixing for liquid mixtures are very sensitive to the value of k_{12} assumed in a theory of liquid mixtures. A value of k_{12} can be found that gives agreement between the theoretical and the experimental excess property, and a comparison with the k_{12} from second virial coefficients is a severe test of the theory of mixing in the liquid state. In Table 5.9 are shown the results from two of the more successful recent theories: the 'van-der-Waals one-fluid' model (153) and the 'van-der-Waals two-fluid'model (154). The relatively close agreement is an indication of the usefulness of these models in the prediction of the thermodynamic properties of natural

TABLE 5.10

Geometric-mean correction factors

	Methane/Nitrogen	Methane/Argon	Nitrogen/Argon	Methane/Ethane
This work (L-J(18-6))	.030	.002	-.007	.002
Chueh and Prausnitz (151)	.03	.02	.00	.01
"Van-der-Waals one-fluid model" (153)		.033	.002	
"Van-der-Waals two-fluid model" (154)	.014	.021	.003	

gas mixtures (see section 6.3).

For systems such as those studied here, where the molecules do not differ greatly in size, k_{12} is relatively small. Systems with large size differences, such as CH_4/C_4F_{10}, however, require values of k_{12} of about 0.1, and there is evidence that this failure of the geometric mean rule is mainly due to differences in size and not effects of asymmetry or of different ionization potentials (152).

When considering the prediction of the PVT properties of mixtures, or of other thermodynamic properties of mixtures, the results are sensitive to the values of k_{12} assumed for each binary interaction. At present it is difficult to pre-determine k_{12} with sufficient accuracy unless there exists accurate data on the binary mixture.

5.7 Third Virial Coefficients of Mixtures

The third virial coefficient of a mixture of N components is given as a function of the mole fractions $x_1, x_2 \ldots$ by

$$C = \sum_i^N \sum_j^N \sum_k^N x_i\, x_j\, x_k\, C_{ijk} \qquad (5.7\text{-}1)$$

where C_{ijk} is given by (5.5-2), (5.5-3) and (5.5-4).

Calculations of C_{ijk} for realistic intermolecular potentials are limited. Stogryn (145) has presented exact results for the Lennard-Jones (12-6) potential plus corrections for the non-additive triple-dipole term. These results were compared with those of the approximations of Rowlinson, Sumner and Sutton (144) and of Orentlicher and Prausnitz((155). These approximations simplify the evaluation of the integrals in the calculation by expressing C_{ijk} as a

function of the reduced third virial coefficient of one pure component and the intermolecular potential parameters. The approximation of Rowlinson et al is,

$$C_{ijk}(T) = \left(2/3\ \pi N_o \sigma_{ijk}^3\right)^2 \cdot C^*(T^*_{ijk}) \qquad (5.7\text{-}2)$$

$$\text{where } C^*(T^*) = C_{iii}(T)/\left(2/3\ \pi N_o \sigma_i^3\right)^2 \qquad (5.7\text{-}3)$$

$$T^*_{ijk} = kT/\epsilon_{ijk} \qquad T^* = kT/\epsilon_i \qquad (5.7\text{-}4)$$

$$\text{and } \epsilon^3_{ijk} = \epsilon_{ij}\,\epsilon_{jk}\epsilon_{ik} \qquad \sigma^3_{ijk} = \sigma_{ij}\,\sigma_{jk}\,\sigma_{ik} \qquad (5.7\text{-}5)$$

The approximation of Orentlicher and Prausnitz is,

$$C_{ijk}(T) = \left(2/3\ \pi N_o \sigma_{ijk}^3\right)^2 \left(C^*_{ij}(T^*_{ij}) \cdot C^*_{ik}(T^*_{ik}) \cdot C^*_{jk}(T^*_{jk}) \right) \qquad (5.7\text{-}6)$$

where $C^*(T)$ is defined as in (5.7-3), σ_{ijk} is defined as in (5.7-5), and $T^*_{ij} = kT/\epsilon_{ij}$ (5.7-7)

Stogryn concluded that neither approximation could be trusted to give accurate results in the vicinity of the maximum of C_{ijk} unless the potential parameters of molecules i, j and k were not too different. At higher temperatures both approximations are usually satisfactory, but that of Rowlinson et al. is overall slightly superior.

Because of the failure of the L-J (12-6) potential to provide a good fit to the second virial coefficients or to predict the third virial coefficient of pure components, comparison with experiment for mixtures will not be given. In a later paper Stogryn (146) has presented results for the L-J (18-6) potential based on the approximation of Rowlinson

et al. ((5.7-2) to (5.7-5)) and a similar approximation for the non-additive triple-dipole contribution. These are given by expansions in powers of T*, (5.5-10) and (5.5-11), where for mixtures,

$$T^*_{ijk} = kT/\epsilon_{ijk} \qquad C^*_{ijk} = C_{ijk}/(2/3\,\pi N_o \sigma^3_{ijk})^2 \tag{5.7-8}$$

and

$$\nu^* = 2^{3/2} \cdot \nu_{ijk} \cdot \epsilon^{1/2}_{ijk} / \left(3^{1/4} (\mu_{ij}\,\mu_{jk}\,\mu_{ik})^{1/2}\right) \tag{5.7-9}$$

where μ_{ij} are the long-range dispersion energy coefficients, i.e.

$$\mu_{ij} = \frac{3^{3/2}}{2} \cdot \epsilon_{ij} \sigma^6_{ij} \tag{5.7-10}$$

and ν_{ijk} is a given function of μ_{ij}, α_i, etc.

C_{112} and C_{221} were calculated for methane/nitrogen and argon/nitrogen, and compared with the selected experimental data (see Chapter 4) in Figures 5.13 and 5.14. The potential parameters were those given by,

$$\sigma_{12} = \tfrac{1}{2}(\sigma_{11} + \sigma_{22}) \tag{5.7-11}$$

$$\epsilon_{12} = (1 - k_{12}) \cdot (\epsilon_{11}\,\epsilon_{22})^{1/2} \tag{5.7-12}$$

These are the values given in columns 4 and 5 of Table 5.8.

For methane/nitrogen the agreement is within the limits of experimental error, and for nitrogen/argon the agreement is fair, the calculated values being too low as in the case of pure argon and nitrogen. However, in view of the probable large experimental errors in C_{112} and C_{221}, the approximation of Rowlinson et al. (144) in conjunction with the L-J (18-6) potential is successful in predicting the third virial coefficients of these two systems.

This is further demonstration of the usefulness of the Lennard-Jones (18-6) potential as a model for the pair potential.

FIGURE 5.13

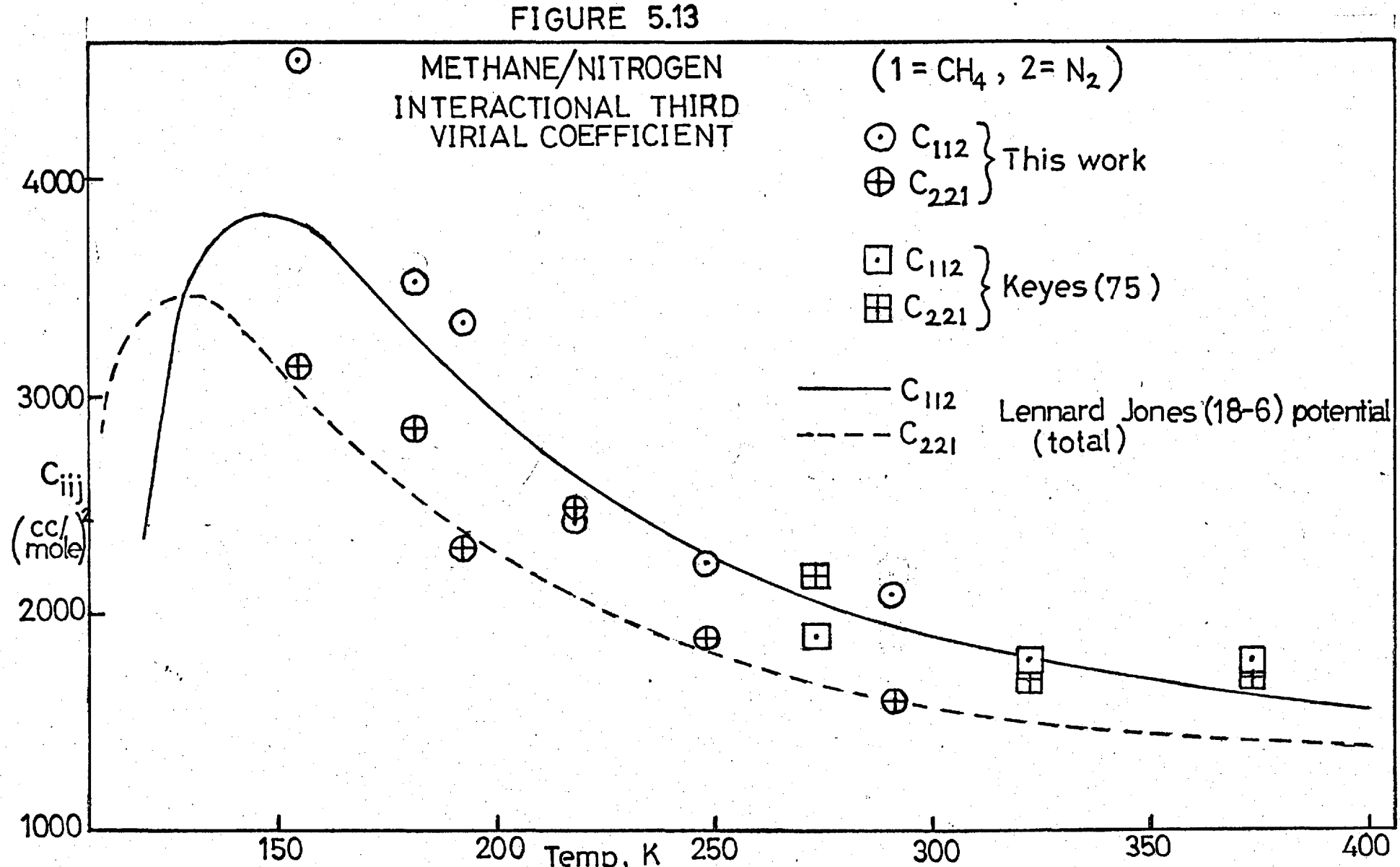
METHANE/NITROGEN
INTERACTIONAL THIRD
VIRIAL COEFFICIENT
(1 = CH4 , 2= N2)
C112
C221
This work
C112
C221
Keyes (75)
C112
C221
Lennard Jones (18-6) potential
(total)
4000
3000
2000
1000
Ciij
(cc/mole)2
150
200
Temp, K
250
300
350
400

FIGURE 5.14

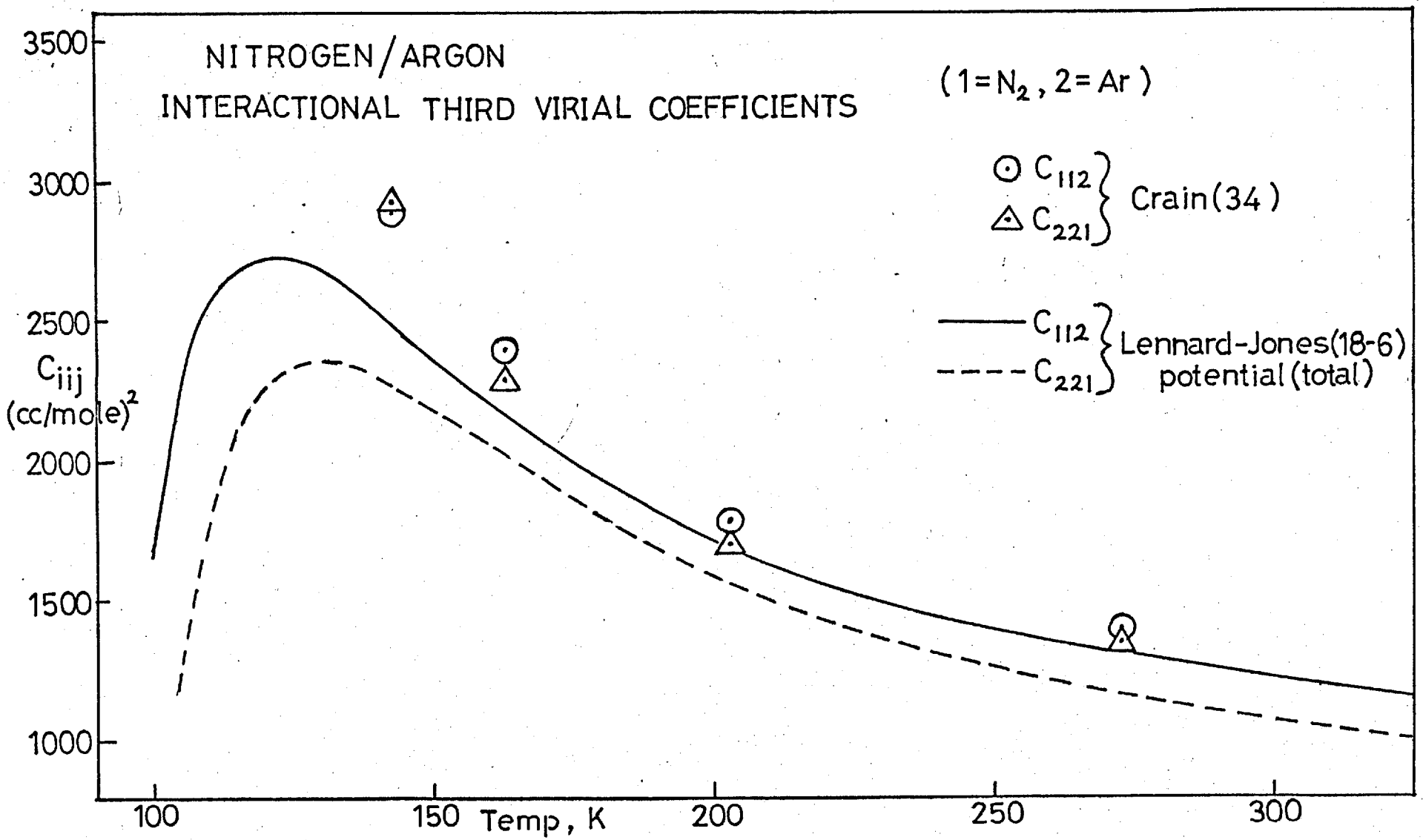
NITROGEN/ARGON
INTERACTIONAL THIRD VIRIAL COEFFICIENTS
(1=N2, 2=Ar)
C112
C221
Crain(34)
C112
C221
Lennard-Jones(18-6) potential (total)
3500
3000
2500
2000
1500
1000
Ciij (cc/mole)2
100
150
Temp, K
200
250
300

CHAPTER SIX

THE PREDICTION OF ACCURATE COMPRESSIBILITY FACTORS OF MULTICOMPONENT GAS MIXTURES

6.1 Introduction

There have been numerous methods proposed in the literature for calculation of the compressibility factor of a multi-component mixture such as a natural gas. A division into two types is possible:

1) Methods which employ the principle of corresponding states combined with the concept of "pseudo-critical" constants for a mixture. These form the basis of the majority of compressibility factor charts in use today and tabulations such as the American Gas Association's comprehensive correlation (156). The principle of corresponding states has been modified and extended by, among others, Pitzer and Curl (157) and Leland and his co-workers(158).

2) Methods which employ an empirical equation of state with a different set of constants for each component of the mixture. The best-known equations are those of Benedict, Webb and Rubin (159) and of Redlich and Kwong (160). These have since been modified and improved, in one way or another, and there are many recent examples of their use.

6.2 The Principle of Corresponding States

The application of the principle of corresponding states to the pair potentials of argon, methane and nitrogen has been considered in section 5.3(a). A substance, α, is said to be conformal with a reference substance, O, if the pair potential of substance α is given by

$$U_\alpha(r) = f_\alpha . U_o(r/g_\alpha) \qquad (6.2\text{-}1)$$

where $U_o(r)$ is the pair potential of the reference substance and f_α and g_α are 'energy' and 'distance' scaling-factors respectively.

All two-parameter pair potentials, such as the Lennard-Jones (18-6) are of the type given by equation (6.2-1).

It follows, through a statistical-mechanical derivation (3), that the equation of state of substance α, assuming pairwise additivity, is

$$\phi_\alpha(P,V,T) = \phi_o\left\{P.\frac{g_\alpha^{\,3}}{f_\alpha} , \frac{V}{g_\alpha^{\,3}} , \frac{T}{f_\alpha}\right\} = 0 \qquad (6.2\text{-}2)$$

where $$\phi_o(P,V,T) = 0 \qquad (6.2\text{-}3)$$

is the equation of state of the reference.

The factors $\frac{f_\alpha}{g_\alpha^{\,3}}$, $g_\alpha^{\,3}$, and f_α are identical to the ratios of the critical constants, $\frac{P_\alpha^{\,c}}{P^c_o}$, $\frac{V_\alpha^{\,c}}{V^c_o}$ and $\frac{T_\alpha^{\,c}}{T^c_o}$, respectively, on the above assumptions.

Equation (6.2-2) may be written,

$$\phi_\alpha\left\{\frac{P}{P^c_\alpha} , \frac{V}{V^c_\alpha} , \frac{T}{T^c_\alpha}\right\} = \phi_o\left\{\frac{P}{P^c_o} , \frac{V}{V^c_o} , \frac{T}{T^c_o}\right\} = 0 \qquad (6.2\text{-}4)$$

$$\text{or} \quad Z_\alpha = Z_o\left(\frac{T}{T^c_\alpha} , \frac{V}{V^c_\alpha}\right) \qquad (6.2\text{-}5)$$

$$\text{i.e.} \quad Z_\alpha = Z_o\left(T^R_\alpha , V^R_\alpha\right) \qquad (6.2\text{-}6)$$

where T^R, V^R are the reduced temperature and volume

respectively. Equations (6.2-4) to (6.2-6) are the standard expressions of the principle of corresponding states.

However, this two-parameter form of the principle of corresponding states is not obeyed exactly by the majority of substances owing to molecular dissimilarities in shape, size, polarity, etc., and because of non-pairwise additivity. Departures from (6.2-6) have often been considered by including a third parameter, ξ ,

$$Z_\alpha = Z_o \ (T^R \ , \ V^R \ , \ \xi \ ) \qquad (6.2\text{-}7)$$

The third parameter may be, among others, the compressibility factor at the critical point, Z^C, or Pitzer's acentric factor, ω (157), which is defined as

$$\omega = - \log \ (P'_R) - 1.0 \qquad (6.2\text{-}8)$$

where P'_R is the reduced vapour pressure at $T^R = 0.7$. Substances which have the same three-parameter pair potential, such as the L-J (n-6) or Kihara spherical core potential, conform to (6.2-7).

Of the methods available for prediction of the compressibility factor or a multi-component mixture, the simplest is that based on the virial equation of state (161). It has the advantage that the mixing rules are exact for each of the virial coefficients. The principle of corresponding states has often been utilized in the correlation of experimental values of the second and third virial coefficients. The most successful of those correlations tested in this investigation were found to be those of

Pitzer and Curl (162),

$$\frac{BP^C}{RT^C} = \frac{BZ^C}{V^C} = (0.1445 + 0.073\omega) \qquad (6.2\text{-}9)$$

$$- \left(\frac{0.33 - 0.46\omega}{T^R}\right) - \left(\frac{0.1385 + 0.5\omega}{(T^R)^2}\right) - \left(\frac{0.0121 + 0.097\omega}{(T^R)^3}\right) - \frac{0.0073\omega}{(T^R)^8}$$

and Chueh and Prausnitz (163),

$$C = (0.232(T^R)^{-0.25} + 0.468(T^R)^{-5})(1 - e^{(1 - 1.89(T^R)^2)}) \qquad (6.2\text{-}10)$$

$$+ d.\exp(-2.49 + 2.30T^R - 2.70(T^R)^2).$$

The fourth parameter, d, effectively accounts for the non-additive contributions to C and is loosely related to the molecular polarizability.

In figure 6.1 are shown the differences between the experimental reduced second virial coefficients and those calculated by the Pitzer-Curl correlation, using the critical constants and acentric factors given by Huff and Reed (164),

$$\text{i.e. } \Delta B^R = \frac{B_{exp}}{V^C} - \frac{B_{calc}}{V^C} \qquad (6.2\text{-}11)$$

The data used are from the sources described in section 4.4. The correlation is good in the range $1 < T^R < 2$, but gives values that are too positive at higher temperatures and too negative at lower temperatures. In figure 6.2 is shown a comparison between the experimental third virial coefficients and those calculated from the Chueh-Prausnitz correlation, using the same critical constants and acentric factors. The values of d used are given also in figure 6.2. This

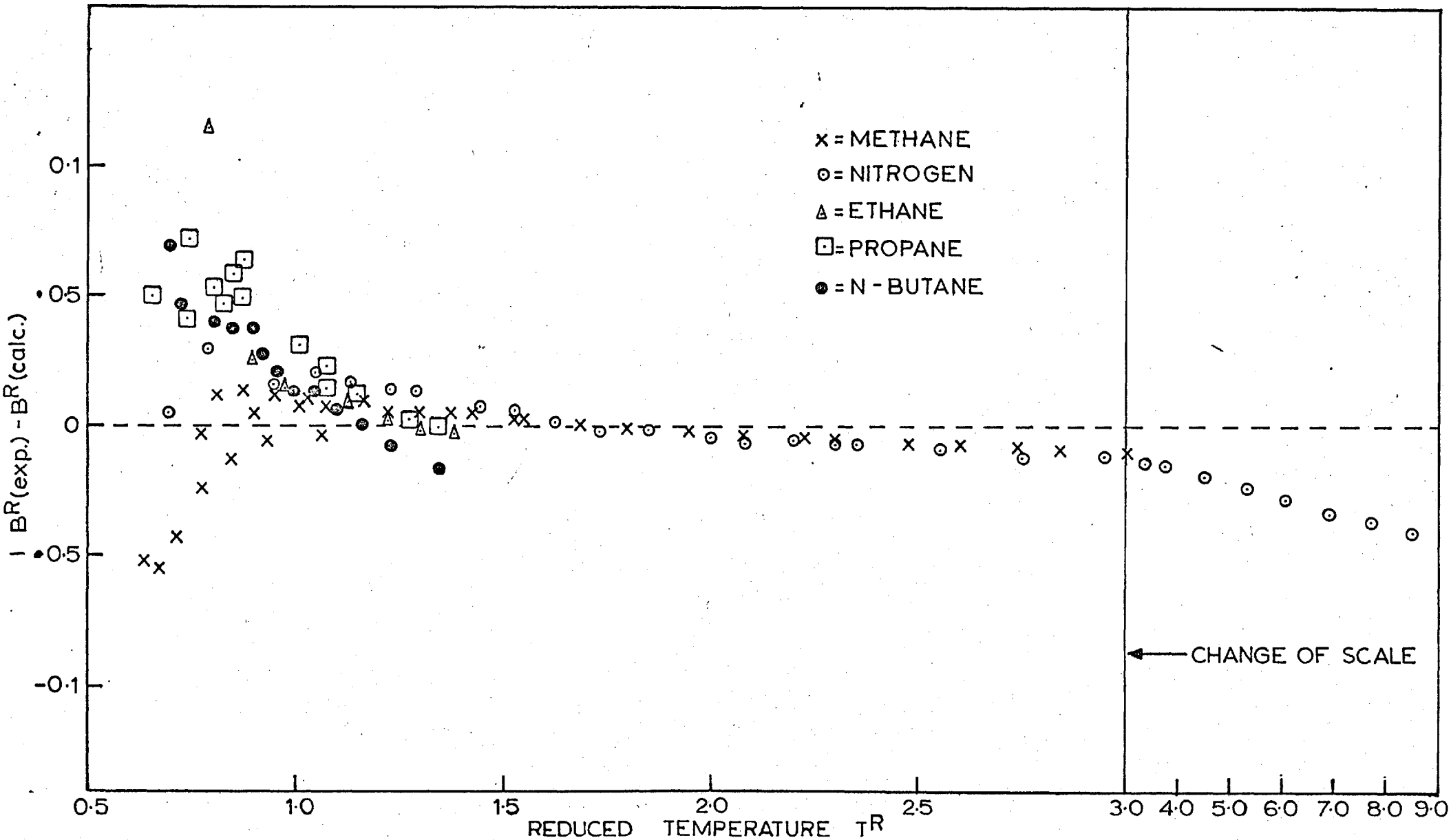

FIG. 6.1. PITZER - CURL CORRELATION OF SECOND VIRIAL COEFFICIENTS.

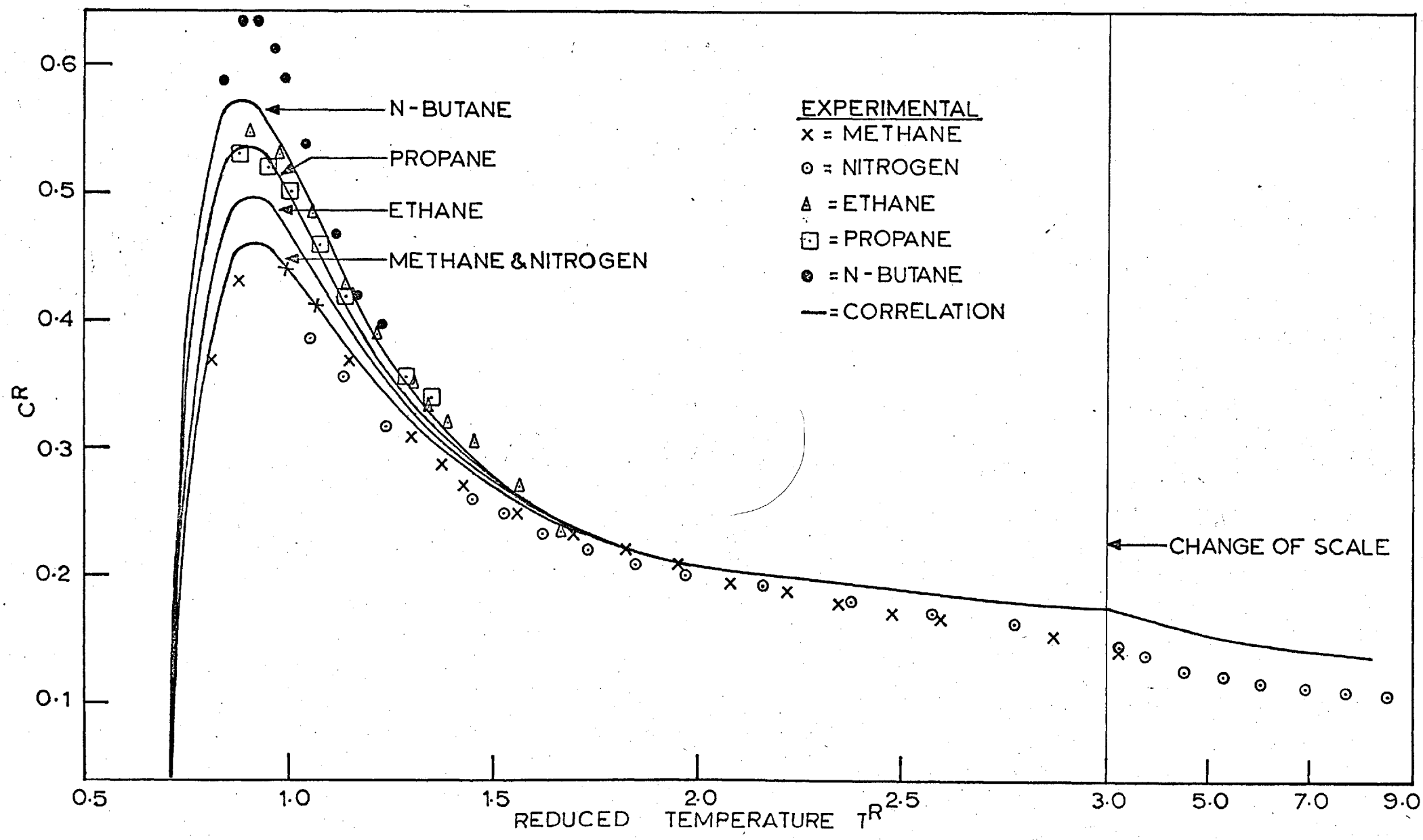

FIG. 6·2 CHUEH - PRAUSNITZ CORRELATION OF THIRD VIRIAL COEFFICIENT

correlation can be seen to be fairly good, except perhaps at high reduced temperatures.

The correlations could be improved, especially the Pitzer-Curl correlation, using accurate recent data. This is a major task if it were extended to include all substances likely to be present in a natural gas mixture. Further investigation along these lines was not attempted here, however, because the virial series approach suffers from two disadvantages in the prediction of the compressibility factor,

1) When only second and third virial coefficients are considered, it is limited to densities (or pressures) below a certain maximum. For example, if a 0.1% accuracy in Z is required, then the maximum pressure is about 80 bar for methane at 273 K, but only about 40 bar at 220 K. At the present time, experimental fourth virial coefficients have not been measured for the majority of gases so that the virial series approach cannot be extended to higher densities.

2) Any correlation of B and C separately is likely to be less accurate than a correlation of Z itself when used to predict Z.

A brief test of the Pitzer-Curl and Chueh-Prausnitz correlations in this application is described later in section 6.3(d).

A predictive method was chosen for use in this investigation that was applicable to high pressures and was also capable of high accuracy; it was taken from the work of Leland et al. (158, 165, 166) and is based on an extension of the principle of corresponding states. A description follows in section 6.3(a) of the use of this method. A

general treatment, giving a more rigorous theoretical derivation, has been presented by Rowlinson and Watson (167). The method has recently been applied successfully to the prediction of vapour-liquid equilibria, enthalpies, etc. by Gunning (168) and of critical behaviour of mixtures by Teja (169).

6.3(a) The Extended Corresponding States Principle

In this method corrections to the two-parameter form of the corresponding-states principle are introduced by the inclusion of additional terms, θ and ϕ, called "shape factors". Methane was chosen as the reference substance; its shape factors are defined as equal to unity, and its compressibility factor, Z_o, is given by its reduced equation of state. The compressibility factor, Z_1, of another substance at a reduced temperature and volume of T_1^R and V_1^R, respectively, is then

$$Z_1 = Z_o \left(\frac{T_1^R}{\theta_1} , \frac{V_1^R}{\phi_1}\right) \qquad (6.3\text{-}1)$$

θ_1 and ϕ_1 are the shape factors relative to methane; they are functions of temperature and volume. They have been evaluated for the higher hydrocarbons by simultaneous solution of (6.3-1) and the corresponding equation for the fugacity-pressure ratio

$$\left(\frac{f}{P}\right)_1 = \left(\frac{f}{P}\right)_0 \left(\frac{T_1^R}{\theta_1} , \frac{V_1^R}{\phi_1}\right) \qquad (6.3\text{-}2)$$

The shape factors were then correlated with Pitzer's acentric factor, ω (157), and the critical point compressibility factor, Z^C, and expressed as functions of reduced temperature

and volume,

$$\theta_1 = g(T_1^R, V_1^R, \omega_1, Z_1^C) \qquad (6.3\text{-}3)$$

$$\phi_1 = h(T_1^R, V_1^R, \omega_1, Z_1^C) \qquad (6.3\text{-}4)$$

These equations are given in full by Leach, Chappelear and Leland (158). They are found to be applicable not only to the higher hydrocarbons, but also to many other non-spherical, non-polar molecules, such as nitrogen and carbon dioxide. It can be seen that their use introduces two extra parameters, ω and Z^C, into the corresponding states principle.

This treatment is readily extended to mixtures through the concept of "pseudo-critical" temperature and volume, $T^C_{m'}$ and $V^C_{m'}$. The formulae given here for the calculation of "pseudo-critical" constants are the consequence of assuming a model for mixtures which is known as the Van der Waals one-fluid model. Reasons for this choice are advanced in a statistical-mechanical analysis by Leland, Rowlinson and Sather (170).

$$V^c_{m'} = \sum_i \sum_j x_i x_j \phi_{ij} V^c_{ij} \qquad (6.3\text{-}5)$$

$$T^c_{m'} V^c_{m'} = \sum_i \sum_j x_i x_j \theta_{ij} T^c_{ij} \phi_{ij} V^c_{ij} \qquad (6.3\text{-}6)$$

The summations are carried out over all components of the mixture. The binary interaction terms, ϕ_{ij}, V^C_{ij}, θ_{ij} and T^C_{ij}, are eliminated by means of the Lorentz-Berthelot combining rules, modified by the inclusion of shape factors,

$$\phi_{ij} V^c_{ij} = \left(\tfrac{1}{2} (\phi_i V^c_i)^{1/3} + \tfrac{1}{2} (\phi_j V^c_j)^{1/3} \right)^3 \qquad (6.3\text{-}7)$$

$$\theta_{ij} T^c_{ij} = (1 - k_{ij}) \, (\theta_i T_i{}^c \theta_j T_j{}^c)^{\frac{1}{2}} \qquad (6.3\text{-}8)$$

The parameter k_{ij}, which has a value specific to each pair of components, is the geometric mean correction factor discussed in section 5.6. Values for the important pairs methane/nitrogen and methane-ethane were taken from Table 5.8 (for the Lennard-Jones (18-6) potential). Others were taken from Chueh and Prausnitz (171).

The pseudo-reduced temperature and volume of the mixture then become,

$$T^R_{m'} = \frac{T_m}{T^c_{m'}} \qquad (6.3\text{-}9)$$

$$V^R_{m'} = \frac{V_m}{V^c_{m'}} \qquad (6.3\text{-}10)$$

Leland et al. show that, in the case of a mixture, it is necessary for thermodynamic consistency to replace T^R and V^R in the shape-factor equations by $\theta_i T^R_{m'}$, and $\phi_i V^R_{m'}$, respectively, so that (6.3-3) and (6.3-4) become, for each component in the mixture,

$$\theta_i = g(\theta_i T^R_{m'}, \; \phi_i V^R_{m'}, \; \omega_i, \; Z^c_i) \qquad (6.3\text{-}11)$$

$$\phi_i = h(\theta_i T^R_{m'}, \; \phi_i V^R_{m'}, \; \omega_i, \; Z^c_i) \qquad (6.3\text{-}12)$$

The compressibility factor of the mixture is given by,

$$Z_m = Z_o \; (T^R_{m'}, \; V^R_{m'}) \qquad (6.3\text{-}13)$$

(b) The Equation of State for Methane

Methane is a convenient reference substance as it is the major component of natural gas mixtures. The equation of state chosen was that of Vennix and Kobayashi (79). It has twenty-five constants, obtained by fitting the equation to the accurate experimental data of Douslin et al. (43) and Vennix et al. (52). It covers the range 130 - 625 K for pressures up to 414 bar (6000 p.s.i.a.), with a maximum density of 0.36 gm./cc. The mean-square percentage deviation in the predicted pressures is 0.07%, including points in the critical and liquid regions. As an independent test of the equation, its predicted compressibility factors were found to agree, to within .001 (.15%), with the experimental results of this work in the range 218.9 - 291.4 K and up to 100 bar. At lower temperatures the agreement is within .3% (see section 4.6(a)).

(c) Computer Program

A computer program in the standard Fortran IV language has been written for use on the University of London CDC 6600 computer. From the known composition of the mixture and the necessary parameters for each component, the shape factors and pseudo-reduced temperature and volume of the mixture are calculated in the program according to (6.3-5) to (6.3-13). It can be seen that these equations require an iteration for their solution; this iteration converges very rapidly. The compressibility factor is then calculated from the reduced Vennix-Kobayashi equation (6.3-13). This is the required answer for a given mixture volume or density; if the answer

is required at a given pressure, then a first trial value of the compressibility factor must be assumed and hence a first approximation to the mixture volume

$$V_m = \frac{RT_m Z_m}{P_m} \qquad (6.3\text{-}14)$$

Equations (6.3-13) and (6.3-14) must be solved by an iterative procedure. Convergence is rapid except in the region of the critical point or at very high pressures (greater than 400 bar).

The average molecular weight of the mixture is computed and hence the density in gm./cc. or lb./cu. ft., obtained.

(d) Test of the Predictive Method

Table 6.1 shows a comparison between the experimental results for the methane/nitrogen mixtures and those predicted by the extended corresponding states principle (C.S.P.). Also shown for Mixture A are the results predicted by the Pitzer-Curl and Chueh-Prausnitz correlations in conjunction with the virial series (Virial). The Lorentz-Berthelot mixing-rules with the geometric mean correction factor were used (equations (6.3-7) and (6.3-8) without the shape factors).

The failure of the virial series method at the higher densities is apparent, the deviation reaching a maximum of - .011 (2%) on the 192.6 K isotherm for mixture A. At 248.5 K the equivalent maximum deviation is - .003 (.35%) but the C.S.P. method has a maximum deviation of only - .0014 (.16%).

For both mixtures the overall agreement between experiment and the predictions of the extended corresponding states

principle is excellent at the higher temperatures ($\geqslant$ 218.9 K) but becomes progressively worse at lower temperatures. The overall maximum deviation is +1.1% for Mixture A on the 155.9 K isotherm and +1.3% for Mixture B on the 181.9 K isotherm. These positive deviations at low temperatures are partly due to the approximations of the mixing-rules as the corresponding deviations for pure methane and pure nitrogen are smaller and largely negative. However, high accuracy is not to be expected below about 190 K as only one or two experimental data points were used in fitting the Vennix equation below this temperature.

In Table 6.2 is shown a comparison between the predicted (C.S.P.) and experimental compressibility factors for Mixture C (methane/nitrogen/ethane) and Natural Gases 1 and 2. The compositions of these mixtures have been given in Table 2.4. A few calculations were performed in order to determine the effect of errors in the composition on the predicted results. For Natural Gases 1 and 2 the only analytical error to have a significant effect is that in the quoted methane percentage (determined by difference). When the methane percentage was increased by 0.5, the estimated maximum uncertainty in the analysis, and the percentage of every other component decreased in proportion, then the resultant changes in Z are about .001 maximum. In view of this fact, the agreement between experimental and calculated results for the Natural gases is excellent.

Agreement for Mixture C is good at 273.0 K, but worsens with decreasing temperature, the deviations $Z_{calc} - Z_{exp}$ becoming more positive, as with methane/nitrogen mixtures, and

TABLE 6.1

COMPARISON OF EXPERIMENTAL AND CALCULATED COMPRESSIBILITY FACTORS
METHANE/NITROGEN MIXTURES

MIXTURE A - 48.4 % CH4

291.40 K

P(BAR)	Z(EXP)	Z(CSP)
96.401	.9345	.9382
53.437	.9586	.9579
29.632	.9750	.9745
16.364	.9856	.9853
9.006	.9919	.9917
4.945	.9955	.9954
2.712	.9975	.9975

248.53 K

P(BAR)	Z(EXP)	Z(CSP)	Z(VIR.)
96.300	.8630	.8616	.8600
59.917	.9030	.9022	.9020
36.765	.9373	.9366	.9368
22.207	.9613	.9606	.9610
13.259	.9766	.9761	.9764
7.858	.9860	.9858	.9859
4.636	.9917	.9916	.9916

218.86 K

P(BAR)	Z(EXP)	Z(CSP)	Z(VIR.)
93.740	.7643	.7635	.7575
64.996	.8216	.8217	.8187
43.986	.8758	.8757	.8744
28.933	.9176	.9174	.9169
18.609	.9469	.9467	.9465
11.783	.9664	.9662	.9660
7.384	.9789	.9788	.9787
4.597	.9869	.9868	.9868
2.850	.9919	.9918	.9918

192.64 K

P(BAR)	Z(EXP)	Z(CSP)	Z(VIR.)
67.684	.6811	.6825	.6704
52.043	.7545	.7565	.7491
38.461	.8215	.8230	.8185
27.358	.8754	.8762	.8737
18.876	.9154	.9158	.9144
12.739	.9435	.9438	.9429
8.466	.9628	.9629	.9623
5.569	.9756	.9757	.9754
3.639	.9841	.9842	.9840

181.87 K

P(BAR)	Z(EXP)	Z(CSP)
60.802	.6239	.6271
49.330	.7019	.7059
38.339	.7759	.7792
28.539	.8384	.8407
20.495	.8868	.8884
14.324	.9223	.9234
9.818	.9474	.9482
6.640	.9648	.9653
4.449	.9765	.9769

155.88 K

P(BAR)	Z(EXP)	Z(CSP)
28.392	.6975	.7052
23.135	.7693	.7748
18.079	.8286	.8327
13.665	.8753	.8783
10.070	.9106	.9127
7.285	.9366	.9381
5.199	.9553	.9565
3.675	.9687	.9695
2.581	.9782	.9788

TABLE 6.1 (CONTINUED)

MIXTURE B - 71.9 % CH4

291.40 K			248.54 K		
P(BAR)	Z(EXP)	Z(CSP)	P(BAR)	Z(EXP)	Z(CSP)
96.119	.9000	.8996	91.863	.8028	.8030
54.129	.9353	.9349	59.058	.8635	.8633
30.304	.9618	.9614	36.998	.9126	.9121
16.825	.9782	.9779	22.629	.9462	.9456
9.288	.9878	.9876	13.612	.9675	.9672
5.108	.9933	.9932	8.103	.9807	.9804
2.804	.9963	.9962	4.792	.9886	.9884

218.86 K			192.65 K		
P(BAR)	Z(EXP)	Z(CSP)	P(BAR)	Z(EXP)	Z(CSP)
89.416	.6675	.6683	55.588	.6166	.6221
65.743	.7451	.7468	44.852	.7064	.7113
46.571	.8201	.8212	34.229	.7869	.7905
31.623	.8796	.8800	24.864	.8512	.8537
20.766	.9220	.9221	17.389	.8989	.9006
13.324	.9504	.9504	11.838	.9325	.9337
8.419	.9689	.9689	7.912	.9555	.9563
5.269	.9806	.9806	5.223	.9709	.9714
3.278	.9880	.9880	3.420	.9810	.9814

181.86 K			155.89 K		
P(BAR)	Z(EXP)	Z(CSP)	P(BAR)	Z(EXP)	Z(CSP)
44.235	.6155	.6236	15.532	.8112	.8149
36.466	.7059	.7120	11.854	.8628	.8656
28.378	.7849	.7893	8.793	.9017	.9039
21.036	.8478	.8510	6.388	.9303	.9319
15.027	.8948	.8970	4.573	.9510	.9522
10.454	.9285	.9300	3.239	.9657	.9665
7.140	.9519	.9530			
4.817	.9679	.9686			
3.222	.9787	.9792			

TABLE 6.2

COMPARISON OF EXPERIMENTAL AND CALCULATED COMPRESSIBILITY FACTORS
MULTICOMPONENT MIXTURES

MIXTURE C - 76.8% CH4, 15.6% N2, 7.2% C2H6, 0.4% O2

273.02 K			248.55 K		
P(BAR)	Z(EXP)	Z(CSP)	P(BAR)	Z(EXP)	Z(CSP)
99.382	.7945	.7955	96.118	.7008	.7023
60.821	.8630	.8639	65.264	.7852	.7876
36.372	.9161	.9165	42.670	.8593	.8609
21.261	.9506	.9507	26.836	.9122	.9131
12.241	.9715	.9715	16.421	.9467	.9472
6.983	.9837	.9837	9.875	.9681	.9684
3.962	.9908	.9908	5.877	.9811	.9813
			3.475	.9889	.9889

218.86 K		
P(BAR)	Z(EXP)	Z(CSP)
73.211	.5721	.5760
57.838	.6696	.6763
43.147	.7646	.7699
30.329	.8411	.8448
20.362	.8964	.8989
13.246	.9339	.9355
8.443	.9584	.9594
5.312	.9741	.9747
3.315	.9839	.9843

NATURAL GAS NO.1

291.39 K			273.76 K		
P(BAR)	Z(EXP)	Z(CSP)	P(BAR)	Z(EXP)	Z(CSP)
70.053	.8595	.8594	68.058	.8236	.8234
40.413	.9163	.9157	41.421	.8913	.8906
22.862	.9523	.9516	24.471	.9359	.9352
12.757	.9733	.9726	14.172	.9630	.9625
7.061	.9852	.9849	8.109	.9789	.9786
3.891	.9918	.9917	4.608	.9880	.9878

NATURAL GAS NO.2

294.12 K			273.16 K		
P(BAR)	Z(EXP)	Z(CSP)	P(BAR)	Z(EXP)	Z(CSP)
101.977	.8232	.8245	101.224	.7606	.7610
58.732	.8884	.8886	62.913	.8407	.8406
33.338	.9350	.9348	38.011	.9027	.9022
18.627	.9633	.9631	22.351	.9428	.9423
10.300	.9796	.9795	12.911	.9670	.9667
5.661	.9888	.9887	7.380	.9812	.9810
3.101	.9939	.9938	4.193	.9893	.9892
			2.374	.9940	.9939

reaching a maximum of .0067 (1%) at 218.9 K. It is difficult to assign this discrepancy at low temperature to one particular cause, as there are no accurate low temperature data on methane/ethane or nitrogen/ethane mixtures with which the method can be compared. There is an obvious need for such data.

6.4 Review of Published Experimental Compressibility Factors of Natural Gases

The literature since 1940 was searched for published compressibility factor data on natural gases and similar multi-component mixtures. The collected references to the experimental data were divided into three classes:

I. Those where the maximum error in compressibility factors claimed by the authors is less than 0.5%.

II. Those where the maximum error in compressibility factors is greater than 0.5%, or where no error estimates are given.

III. Those where no actual figures for compressibility factors are published, but only correlations of the results.

The data from Class I were compared with the predictions of the computer program in order to give an indication of the accuracy of the predictive method for various compositions, pressures and temperatures over a wide range. Differences between calculated and experimental compressibility factors are expressed as the average absolute percentage deviation:

$$\frac{\sum \left| \frac{Z\ (\text{calc.}) - Z\ (\text{exp.})}{Z\ (\text{exp.})} \right|}{\text{No. of points}} \times 100\%$$

(i) Class I

Eilerts, Carlson and Mullens (172) obtained compressibility factors for a typical natural gas and two mixtures of this gas with nitrogen (up to 19%) at pressures from 69 bar to 345 bar (1000 p.s.i.a. to 5000 p.s.i.a.) and from 273 K to 411 K. The authors quote an estimated maximum error in Z of 0.2%. Calculated results were obtained for all three mixtures over the whole range. The average absolute deviation is 0.16% and the maximum deviation is 0.4%. Some comparisons between experimental and calculated results for Mixtures Nos. 1 and 2 are shown in Fig. 6.3. These gases have the following general compositions:

	CH_4 (%)	N_2 (%)	C_2H_6 (%)	C_3-C_8+(%)
No. 1	87.7	0.7	6.5	5.1
No. 2	80.8	8.5	6.0	4.7

Robinson and Jacoby (173) obtained data for nineteen synthetic mixtures of methane, carbon dioxide and hydrogen sulphide with smaller amounts of nitrogen, ethane and propane, at pressure up to 110 bar (1600 p.s.i.a.) from 311 K to 366 K. The authors quote an estimated average uncertainty of 0.05%. Calculated results were obtained for ten multicomponent mixtures, with a total average absolute deviation of 0.08%, and a maximum deviation of 0.2%. Comparisons between experimental and calculated results for four mixtures are shown in Fig. 6.4. These gases have the following general compositions:

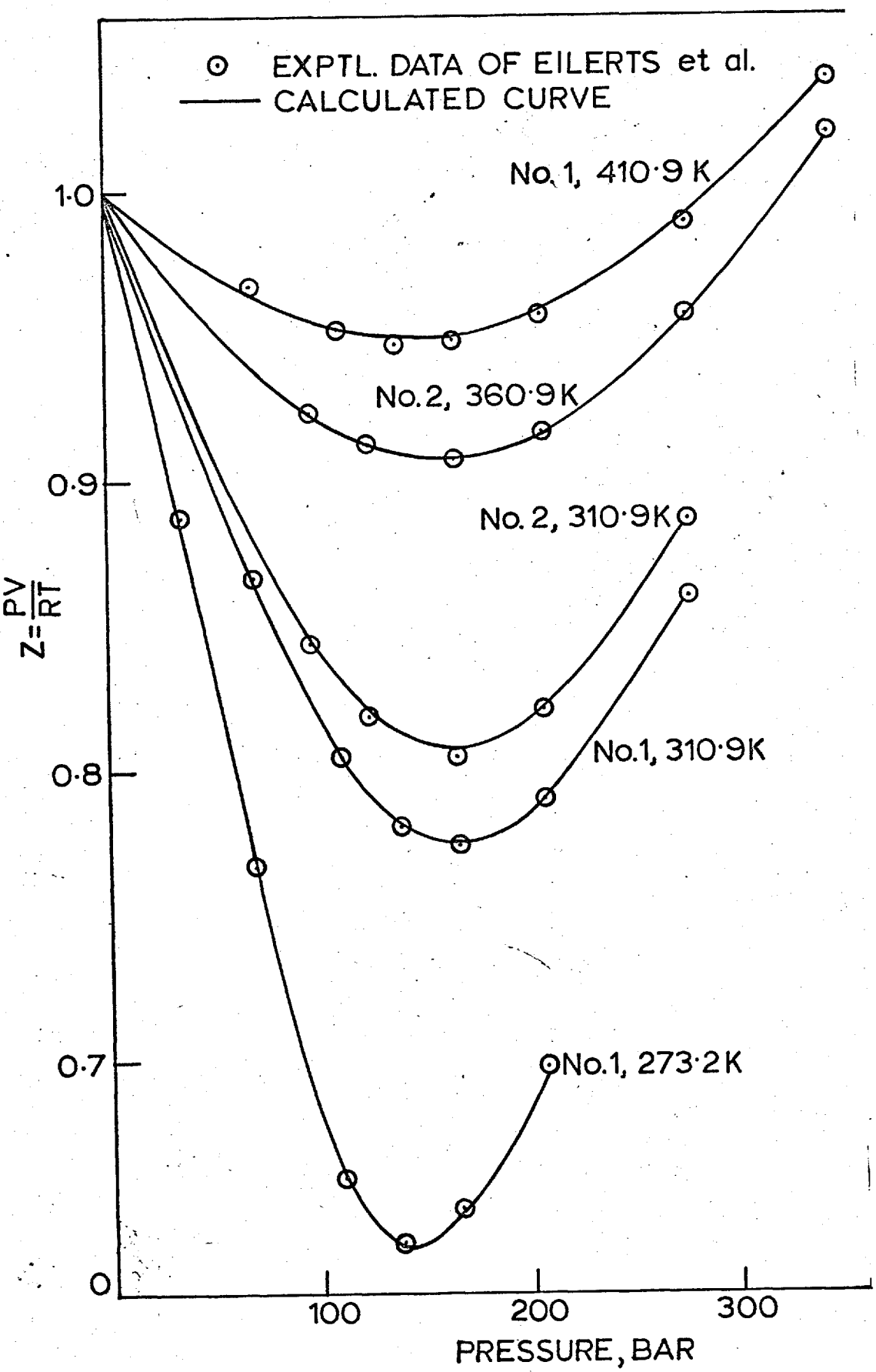

FIG 6.3 COMPRESSIBILITY FACTORS
NATURAL GAS : HIGH PRESSURE

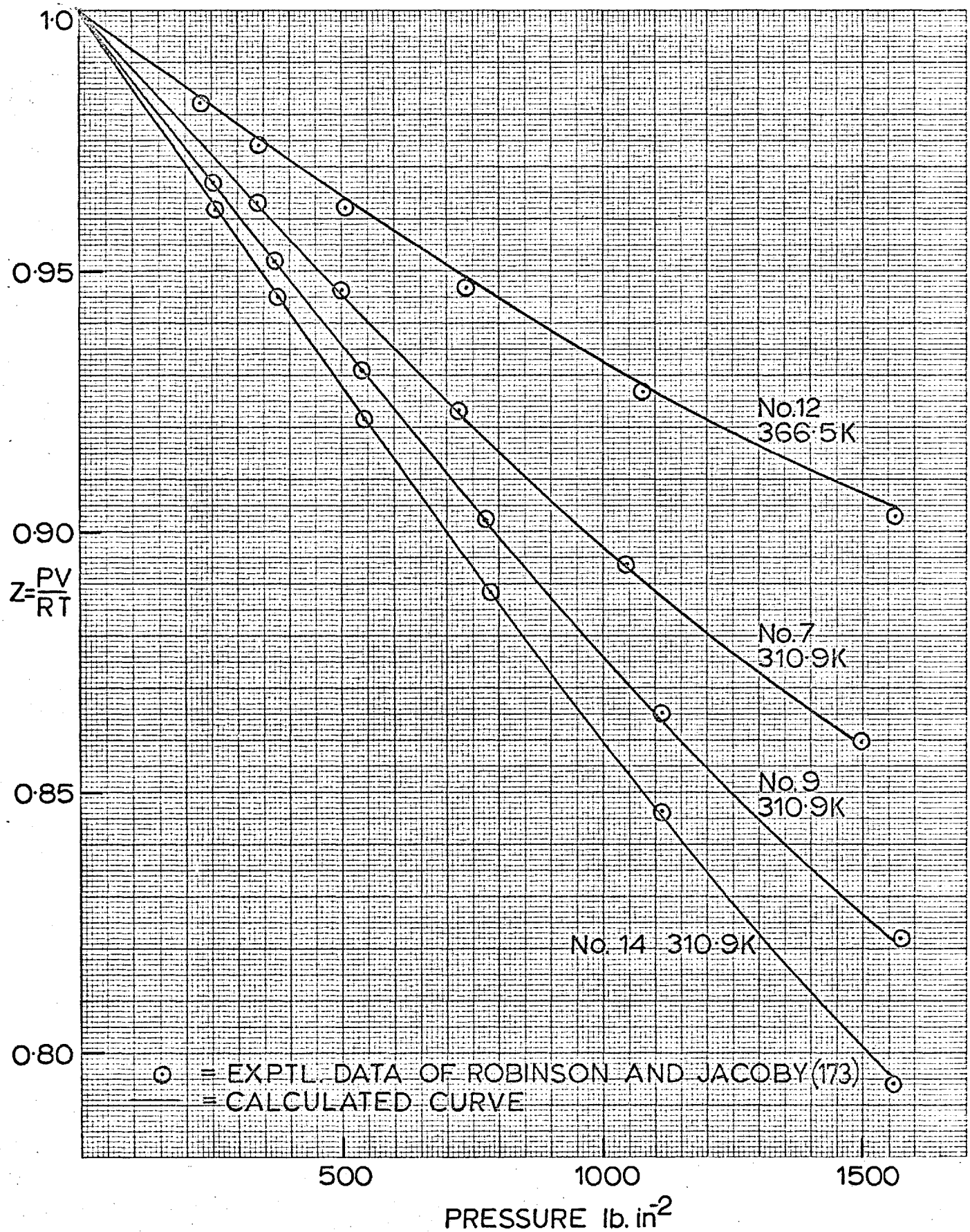
1·0
0·95
0·90
0·85
0·80
Z=PV/RT
No.12
366·5K
No.7
310·9K
No.9
310·9K
No. 14 310·9K
⊙ = EXPTL. DATA OF ROBINSON AND JACOBY (173)
—— = CALCULATED CURVE
500
1000
1500
PRESSURE lb. in⁻²

FIGURE 6.4

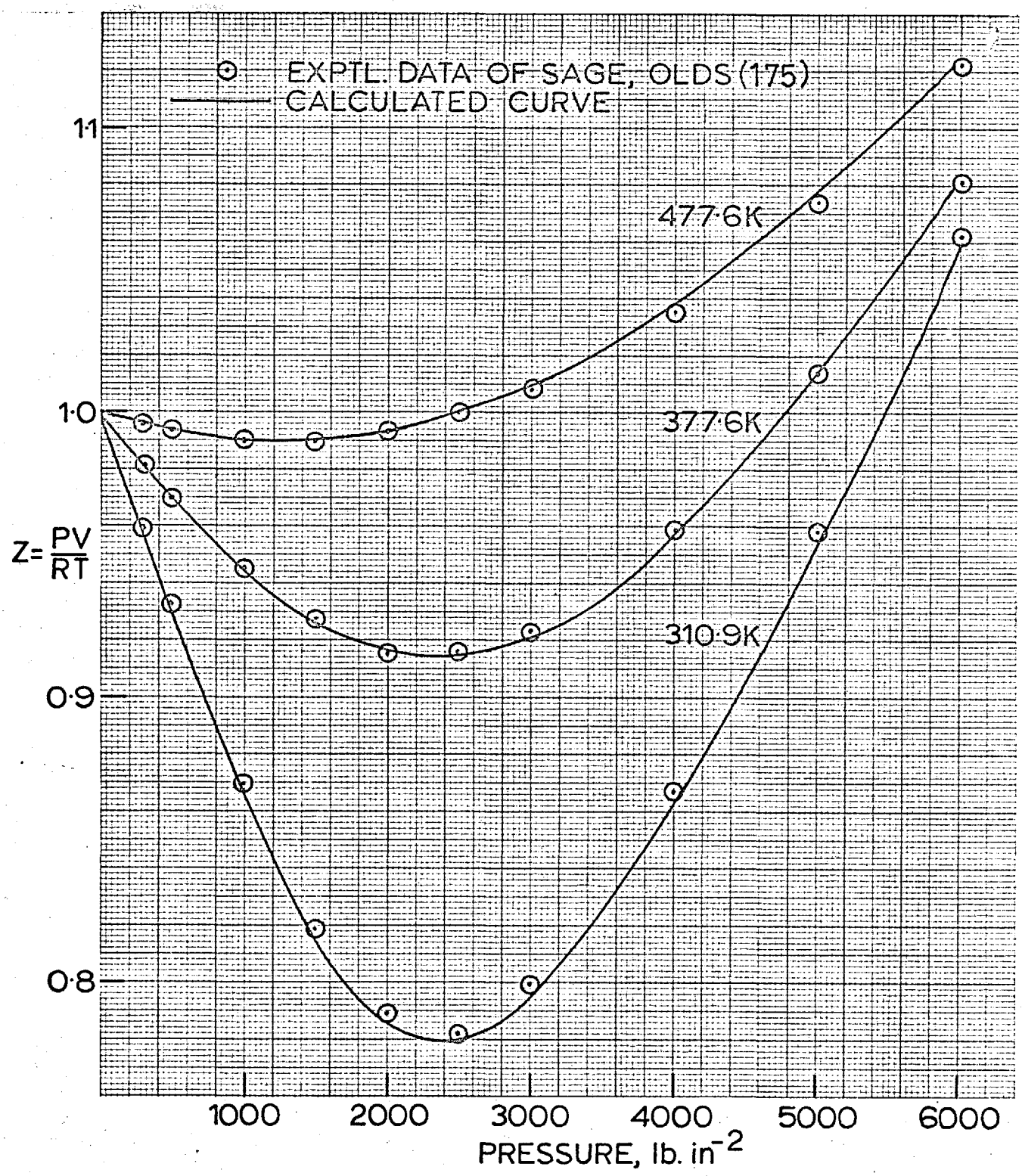
EXPTL. DATA OF SAGE, OLDS (175)
CALCULATED CURVE
477·6K
377·6K
310·9K
1·1
1·0
0·9
0·8
Z= PV/RT
1000
2000
3000
4000
5000
6000
PRESSURE, lb. in⁻²

FIGURE 6·5

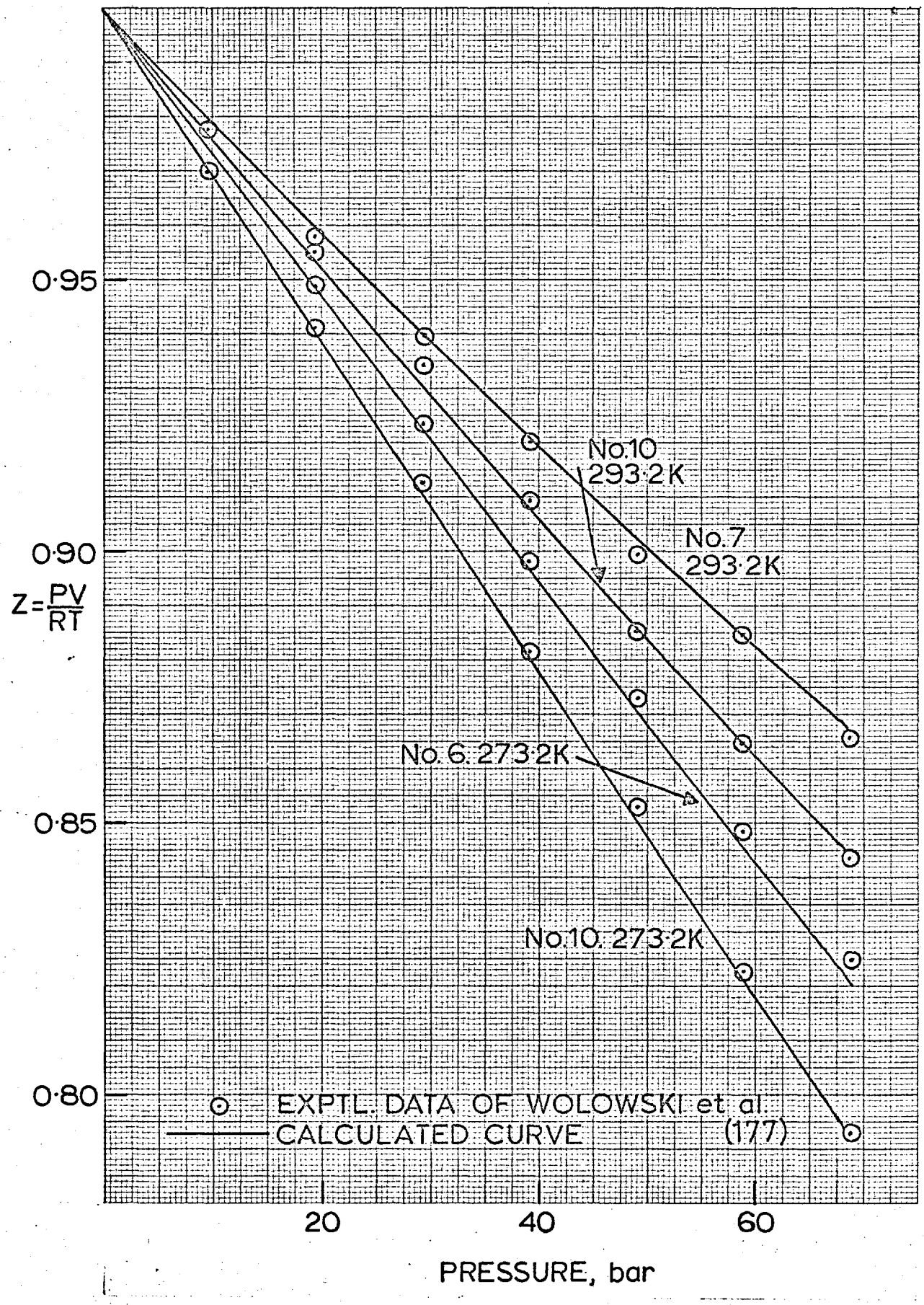
0·95
0·90
0·85
0·80
Z=PV/RT
No.10
293·2K
No.7
293·2K
No.6 273·2K
No.10 273·2K
EXPTL. DATA OF WOLOWSKI et al.
CALCULATED CURVE
(177)
20
40
60
PRESSURE, bar

FIGURE 6.6

	CH_4 (%)	CO_2 (%)	N_2 (%)	C_2-C_3 (%)	H_2S (%)
No. 7	92.2	5.4	0.8	1.6	
No. 9	78.3	19.7	0.6	1.4	
No.12	69.9	28.1	0.8	1.2	
No.14	79.5	1.4	0.8	2.0	16.3

Sage et al. (174 - 176) measured compressibility factors of a series of natural gases as part of a study of vapour-liquid equilibria of reservoir fluids. The estimated maximum error is 0.3%. Data are reported at pressures up to 690 bar (10,000 p.s.i.a.) and from 311 K to 480 K. Calculated results were obtained for two gases, with a total average absolute deviation of 0.2% for pressures up to 276 bar (4000 p.s.i.a.) and a maximum deivation of 0.5%. A comparison between experimental and calculated results for a San Joaquin natural gas (175) is shown in Fig. 6.5. The general composition of this gas is: CH_4 89.5%; CO_2 1.4%; C_2H_6 4.9%; C_3-C_6+4.2%.

Even at 690 bar (10,000 p.s.i.a.), which is, strictly, outside the range of the Vennix-Kobayashi equation, deviations within 1% are obtained.

Wolowski et al. (177, 178) have measured compressibility factors of various synthetic and natural gases (full references are given in (177)), at pressuresup to about 69 bar (1000 p.s.i.a.) and from 273 K to 293 K. The authors quote a maximum experimental error of 0.3%. Data from (32) on eight mixtures of interest were converted to compressibility factors, as defined here, and compared with the predicted values. The average absolute deviation is 0.16% and the maximum deviation is 0.4%. Results for three mixtures are

shown in Fig. 6.6. The general compositions of these mixtures are:

	CH_4 (%)	N_2 (%)	CO_2 (%)	C_2H_6 (%)	C_3-C_6+(%)
No. 6	75.9	7.7	16.0	0.4	-
No. 7	93.4	1.9	-	3.5	1.2
No.10	90.7	0.5	0.2	5.2	3.4

(ii) Class II

Some of the published data in this class are for natural gases similar to North Sea gas and at pressures below 100 bar (1500 p.s.i.a.). It is believed that a comparison of the experimental with the predicted compressibility factors will give an independent assessment of the absolute accuracy of the data. Deviations of up to 1.5% were obtained in the case of Katz et al. (179) who give no estimate of experimental error, and deviations of up to 1% in the case of Verrien (180) who quotes a maximum uncertainty of 0.7%. Subramaniam, Kao and Lee (181) present data for substitute natural gases at temperatures from 163 K to 310 K. However, deviations from calculated values of up to 4% are obtained, even for the most simple gas mixtures at 310 K, and many serious inconsistencies are apparent.

(iii) Class III

An exhaustive study of natural gases using a Burnett apparatus has been carried out by Zimmerman et al. (182, 183) About four hundred experiments were performed at temperatures and pressures usual in gas metering. The actual data are not published, but the results have been extensively correlated in the A.G.A. NX - 19 tables (156), the accuracy of which is

likely to be limited by the overall accuracy of the original data. To give a preliminary indication of the possible usefulness of these tables, the experimental results at 283.2 K for one of the Dutch natural gases, containing 14.3% N_2 (Slochteren, (178)) was compared with the predictions of both the A.G.A. tables (as calculated in (178)) and the extended corresponding-states principle. Both agreed with the data to within the experimental error of 0.2% up to 60 bars. The A.G.A. Tables are therefore of possible high accuracy and worthy of more extensive comparisons with the data of Class I to determine their usefulness as a method of predicting accurate natural gas compressibility factors without recourse to a computer program.

6.5 Conclusions

The results of the predictive method reported here agree, within the estimated maximum experimental error of 0.15%, with the measured compressibility factors of the two typical North Sea gases, Mixtures A and B. The predictive method is thus capable of high accuracy when used to calculate compressibility factors of relatively simple natural gases at low pressures (up to 100 bar) and ambient temperatures. It is stressed that a reasonably accurate analysis must be available before this high accuracy can be attained.

A literature search has revealed that there exist published experimental compressibility factors for various natural gases, some dating back to 1940, which are of sufficiently high accuracy (within 0.3%), to form a basis for comparison with a predictive method. These data, together with more recent experimental results, were compared with the

predictions of the computer program. Agreement, in general, was good.

The comparisons show that the method can be used to predict compressibility factors for the following types of gases within the maximum error limits shown, and over the stated ranges of temperature and pressure:

	Natural Gases		
	Standard (Up to 10% N_2, 5% CO_2, 5% H_2S)	High Nitrogen Content (10 to 20% Nitrogen)	Non-Standard (Up to 20% CO_2, 20% H_2S)
Up to 110 bar 273K to 310K	0.15%	0.3%	0.3%
110 bar to 400 bar 273K to 500K	0.5%	0.5%	-

The results of the program have also been compared with the experimental results for a simple ternary mixture of methane, nitrogen, and ethane, viz. Mixture C. Agreement was excellent at the highest temperature, but deviations of 0.5 to 1.0% are apparent as the critical point of the mixture is approached. It may be concluded that the predictive method is certainly useful at low temperatures, but no general claims as to its accuracy can be made when applied to other multi-component mixtures because of a lack of other accurate low-temperature compressibility factor data. A more stringent test of the extended corresponding-states principle is its ability to predict low-temperature vapour-liquid equilibria (168).

The success of this particular method in the prediction of compressibility factors is a pointer to its usefulness

when extended to the prediction of other thermodynamic properties of natural gases, particularly those properties which are in part derived from the equation of state of the mixture, i.e. enthalpy, entropy, and vapour phase fugacity. (168).

REFERENCES

(1) Mason, E.A. and Spurling, T.H., "The Virial Equation of State", Pergamon Press (1969).

(2) Hirschfelder, J.O., Curtiss, C.F. and Bird, R.B., "Molecular Theory of Gases and Liquids", John Wiley (1954).

(3) Rowlinson, J.S., "Liquids and Liquid Mixtures", 2nd. edition, Butterworth (1969).

(4) Burnett, E.S., J. App. Mech. 58 A-136 (1936).

(5) Eubank, P.T., Personal communication.

(6) Hust, J.G., Cryogenics 9 443 (1969).

(7) Bett, K., Ph.D. Thesis, University of London, (1959).

(8) Cook, A.H. and Hammond, J.A., Metrologia 5 141 (1969).

(9) Kaye, G.W.C. and Laby, T.H., Tables of Physical and Chemical Constants (13th. Ed.), Longmans (1966).

(10) Hayward, A.T.J., J. Inst. Petrol., 56, 12 (1970).

(11) Gould, F.A. and Vickers, T., J. Sci. Inst., 29, 85 (1952).

(12) Bigg, P.H., Brit. J. Appl. Phys., 15, 1111 (1964).

(13) Pollard, C.A., Ph.D. Thesis, University of London (1971).

(14) Bett, K.E. and Newitt, D.M., Chemical Engineering Practice, Vol. 5, Butterworths, (1958).

(15) Woolman, J. and Mottram, R.A., The Mechanical and Physical Properties of the British Standard EN Steels, Vol. 3, BISRA, (1968).

(16) Canfield, F.B., Leland, T.W. and Kobayashi, R., Adv. Cryog. Eng., 8, 146 (1963).

(17) Deming, W.E., Phil. Mag., 11, 146 (1931).

(18) Weir, R.D., Wynn-Jones, I., Rowlinson, J.S. and Saville, G., Trans. Faraday Soc. 63, Part 6, 1320 (1967).

(19) Hall, K.R. and Canfield, F.B., Physica 47 99 (1970).

(20) Barieau, R.E. and Dalton, B.J., U.S. Bur. Mines, Report of Investigation No. 6900 (1967).

(21) Barieau, R.E. and Dalton, B.J., U.S. Bur. Mines, Report of Investigation No. 7020 (1967).

(22) Stanton, R.G., Numerical Methods for Science and Engineering, p. 82, Prentice-Hall, (1961).

(23) Michels, A., Abels, J.C., ten Seldan, C.A. and de Graaff, W. Physica, 26, 381 (1960).

(24) Van Doren, K.R., U.S. Bur. Mines, Information Circular No. 8437 (1969).

(25) Levelt Sengers, J.M.H., 4th Symposium on Thermophysical Properties, A.S.M.E. (1967), p. 37.

(26) Barker, J.A., Leonard, P.J. and Pompe, A., J. Chem. Phys., 44 4206 (1966).

(27) Wood, R.E., Boone, W.J., Marshall, J.D. and Baer, F.W., U.S. Bur. Mines Report of Investigation No. 6896 (1967).

(28) Gyorog, D.A. and Obert, E.F., A.I.Ch.E. Journal 10 , 625 (1964).

(29) Silberberg, I.H., Kobe, K.A. and McKetta, J.J., J. Chem. Eng. Data, 4, 314 (1959).

(30) Waxman, M., Hastings, J.R. and Chen, W.T., Am. Soc. Mech. Engineers: 5th. Symposium on Thermophysical Properties, (1970), 248.

(31) Weir, R., Ph.D. Thesis, University of London, (1966).

(32) Douslin, D.R., 2nd. Symposium on Thermophysical Properties, A.S.M.E., p. 135 (1962).

(33) Michels, A., Wouters, H. and de Boer, J., Physica, 1, 587 (1934).

(34) Crain, R.W. and Sonntag, R.E., Adv. Cryog. Eng., 11, 379 (1966).

(35) Anderson, L.N., Kudchadker, A.P. and Eubank, P.T., J. Chem. Eng. Data, 13, No. 3, 321 (1968).

(36) Michels, A., Wijker, Hub., Wijker, Hk., Physica, 15, 627 (1949).

(37) Michels, A., Levelt, J.M., and de Graaff, W., Physica, 24, 659 (1958).

(38) Michels, A. and Michels, C., Proc. Roy. Soc., A153, 201 (1935).

(39) Butcher, E.G. and Dadson, R.S., Proc. Roy. Soc., A 277 448 (1964).

(40) Tester, H.E., "Thermodynamic Functions of Gases, part 3", ed. Din, F., (Butterworths, London 1961).

(41) Michels, A. and Nederbragt, G.W., Physica, 2, 1000 (1935).

(42) Schamp, H.W., Mason, E.A., Richardson, A.C.B. and Altman, A., Phys. Fluids, 1, 329 (1958).

(43) Douslin, D.R., Harrison, R.H., Moore, R.T. and McCullough, J.P., J. Chem. Eng. Data, 9, 358 (1964).

(44) Deffet, L., Liliane, L. and Fick, F., Ind. chim. belge, 29, 879 (1964).

(45) Olds, R.H., Reamer, H.H., Sage, B.H. and Lacey, W.N., Ind. Eng. Chem., 35, 922 (1943).

(46) Keyes, F.G. and Burks, H.G., J. Am. Chem. Soc., 49, 1403 (1927).

(47) Freeth, F.A. and Verschoyle, T.T.H., Proc. Roy. Soc., A130, 453 (1931).

(48) Kvalnes, H.M. and Gaddy, V.L., J. Am. Chem. Soc., 53, 394 (1931).

(49) Mueller, W.H., Leland, T.W. and Kobayashi, R., A.I.Ch.E. Journal 7, 262 (1961)

(50) Hoover, A.E., Nagata, I., Leland, T.W. and Kobayashi, R., J. Chem. Phys. 48, 2633 (1968).

(51) Hoover, A.E., Ph.D. Thesis, Rice University, (1965).

(52) Vennix, A.J., Leland, T.W. and Kobayashi, R., Adv. Cryog. Eng. 12, 700 (1967).

(53) Thomaes, G. and van Steenwinkel, R., Nature, 187, 229 (1960).

(54) Brewer, J., U.S. Air Force Report AFOSR, no. 67, 2795 (1967).

(55) Byrne, M.A., Jones, M.R. and Staveley, L.A.K., Trans. Faraday Soc. 69, 1747 (1968).

(56) McMath, H.G. and Edmister, W.C., A.I.Ch.E. Journal 15, 370 (1969).

(57) Lee, R.C. and Edmister, W.C., A.I.Ch.E. Journal 16, 1047 (1970).

(58) Pavlovich, N.V. and Timrot, D.L., Teploenergetika, 4, (1958).

(59) Robertson, S.L. and Babb, S.E., J. Chem. Phys. 51, 1357 (1969).

(60) Jansoone, V., Gielen, H., De Boelpaep, J. and Verbeke, O.B., Physica 46, 213 (1970).

(61) Vasserman, A.A. and Rabinovich, V.A., Thermophysical Properties of Air and Its Components, Publishing House for State Standards, Moscow (1966).

(62) Coleman, T.C. and Stewart, R.B., Univ. of Idaho Research Report No. 11 (1970).

(63) Holborn, L. and Otto, J., Z. Phys. 33, 1 (1925).

(64) Saville, G., D. Phil. Thesis, Oxford, (1961).

(65) Kammerlingh Onnes, H. and van Urk, A.T., Commun. phys. Lab., Univ. Leiden, 169d,e (1924).

(66) Otto, J., Michels, A. and Wouters, H., Physica 1, 587 (1934).

(67) Canfield, F.B., Leland, T.W., Kobayashi, R., J. Chem. Eng. Data, 10, No. 2, 92 (1965).

(68) Saurel, J., J. des Recherches des CNRS, 42, 21 (1958).

(69) Friedman, A.S., Ph.D. Thesis, Ohio State Univ. (1950).

(70) Friedman, A.S., Am. Inst. Physics Handbook, part 4, 4 (McGraw-Hill, 1957).

(71) Pool, R.A.H., Saville, G., Herrington, T.M., Shields, B.D.C. and Staveley, L.A.K., Trans. Faraday Soc. 58 , 1692 (1962).

(72) Witonsky, R.J. and Miller, J.G., J. Am. Chem. Soc., 85, 282 (1963).

(73) Pfefferle, W.C., Goff, J.A. and Miller, J.G., J. Chem. Phys. 23, 509 (1955).

(74) Hall, K.R. and Canfield, F.B., Physica, 47, 219 (1970).

(75) Keyes, F.G. and Burks, H.G., J. Amer. Chem. Soc., 50, 1100 (1928).

(76) Krichevskii, I.R. and Levchenko, G.T., Acta phys-chim URSS, 14, 271 (1941).

(77) Bloomer, O.T., Eakin, B.E., Ellington, R.T. and Gami, D.C., I.G.T. Research Bulletin, No. 21 (1955).

(78) Blake, A.G., Bretton, R.H. and Dodge, B.F., Proc. A.I.Ch.E., Inst. Chem. Eng. Joint Meeting, London, 1965, p. 105.

(79) Vennix, A.J. and Kobayashi, R., A.I.Ch.E. Journal 15 926 (1969).

(80) Dymond, J.H. and Smith, E.B., The Virial Coefficients of Gases, Clarendon Press, (1969).

(81) Michels, A., Levelt, J.M. and de Graaff, W., Physica, 24, 659 (1958).

(82) Michels, A., Wijker, Hub., and Wijker, Hk., Physica, 15, 627 (1949).

(83) Provine, J.A. and Canfield, F.B., Physica, 52, 79 (1971).

(84) Whalley, E., Lupien, Y. and Schneider, W.G., Can. J. Chem., 31 722 (1953).

(85) Holborn, L. and Otto, J., Z. Phys. 33, 1 (1925).

(86) Fender, B.E.F. and Halsey, G.D., J. Chem. Phys., 36 1881 (1962).

(87) Michels, A., van Straaten, W., and Dawson, J., Physica, 20, 17 (1954).

(88) Reamer, H.H., Olds, R.H., Sage, B.H. and Lacey, W.N., Ind. Eng. Chem. ind. Edn. 36, 956 (1944).

(89) Thomaes, G., van Steenwinkel, R. and Stone, W., Mol. Phys., 5, 301 (1962).

(90) Brewer, J. and Vaughn, G.W., J. Chem. Phys. 50, 2960 (1969).

(91) Zandbergen, P. and Beenakker, J.J.M., Physica, 33, 343 (1967).

(92) Knobler, C.M., Beenakker, J.J.M. and Knapp, H.F.P., Physica, 25, 909 (1959).

(93) Michels, A. and Nederbragt, G.W., Physica, 6, 656 (1939).

(94) Dantzler, E.M., Knobler, C.M. and Windsor, M.L., J. Phys. Chem., 72, 676 (1968).

(95) Cherney, B.J., Marchman, H. and York, R., Ind. Eng. Chem. 41, 2653 (1949).

(96) Beattie, J.A., Kay, W.C. and Kaminsky, J., J. Am. Chem. Soc., 59, 1589 (1937).

(97) McGlashan, M.L. and Potter, D.J.B., Proc. Roy. Soc., A267, 478 (1962).

(98) Kapallo, W., Lund, N. and Schäfer, K., Z. Phys. Chem. Frankfurt, Ausg. 37, 196 (1963).

(99) Connally, J.F., J. Phys. Chem. 66, 1082 (1962).

(100) Beattie, J.A., Simard, G.L. and Su, G-J., J. Am. Chem. Soc., 39, 26 (1939).

(101) Jones, A.E. and Kay, W.B., A.I.Ch.E. Journal, 13, No. 4, 717.

(102) Bottomley, G.A. and Spurling, T.H., Aust. J. Chem. 17, 501 (1964).

(103) Fitts, D.D., Ann. Review of Phys. Chem., 17, 59 (1966).

(104) Keller, J.B. and Zumino, B., J. Chem. Phys., 30, 1351 (1959).

(105) Saville, G., Personal communication.

(106) Kihara, T., Rev. Mod. Phys. 25, 831 (1953).

(107) Mie, G., Ann. Phys. Lpz., 11, 657 (1903).

(108) Hanley, H.J.M. and Klein, M., Nat. Bur. Std. (U.S.) Tech. Note 360 (1967).

(109) Jones, J.E., Proc. Roy. Soc., A106, 463 (1924).

(110) De Boer, J. and Michels, A., Physica, 5, 945 (1938).

(111) Dymond, J.H., Rigby, M. and Smith, E.B., Phys. Fluids 9, 1222 (1966).

(112) Weir, R.D., Mol. Phys., 11, 97 (1966).

(113) Ahlert, R.C. and Vogl, W.F., J. Phys. Chem., 73, 2304 (1969).

(114) Lin, H-M., and Robinson, R.L., J. Chem. Phys. 52, 3727 (1970).

(115) Hanley, H.J.M. and Childs, G.E., Science, 159, 1114 (1968).

(116) Tee, S.T., Gotoh, S. and Stewart, W.E., Ind. and Eng. Chem. Fundamentals 5, 357 (1966).

(117) Rossi, J.C. and Danon, F., Disc. Faraday Soc., 40, 97 (1965).

(118) Barker, J.A., Fock, W. and Smith, E.B., Phys. Fluids, 7, 899 (1964).

(119) Sherwood, A.E. and Prausnitz, J.M., J. Chem. Phys. 41, 413 (1964).

(120) Calvin, D.W. and Reed, T.M., J. Chem. Phys. 54, 3733 (1971).

(121) Ahlert, R.C., Biguria, C. and Gaston, J.W., J. Phys. Chem. 74, 1639 (1970).

(122) Barker, J.A. and Pompe, A., Aust. J. Chem. 21, 1683 (1968).

(123) Barker, J.A. and Bobetic, M.V., Physical Review B 2, 4169 (1970).

(124) Barker, J.A., Bobetic, M.V. and Pompe, A., Mol. Phys. 20, 347 (1971).

(125) Barker, J.A., Fisher, R.A. and Watts, R.O., Mol. Phys. 21, 657 (1971).

(126) Leonard, P.J., Quoted in ref. (122).

(127) Tanaka, Y. and Yoshino, K., J. Chem. Phys., 53, 2012 (1970).

(128) Dalgarno, A., Adv. Chem. Phys., 12, 329 (1967).

(129) Parson, J.M., Siska, P.E., and Lee, Y.T., J. Chem. Phys. 56, No. 4 1511 (1972).

(130) Maitland, G.C., and Smith, E.B., Mol. Phys., 22, No. 5, 861 (1971).

(131) Buckingham, A.D. and Pople, J.A., Trans. Faraday Soc., 51, 1029 (1955).

(132) Kielitch, S., Physica, 28, 511 (1962).

(133) Orcutt, J., J. Chem. Phys. 39, 605 (1963).

(134) Stogryn, D.E. and Stogryn, A.P., Mol. Phys. 11, 371 (1966).

(135) Karplus, M. and Kolker, H.J., J. Chem. Phys. 38, 1263 (1963).

(136) Axilrod, B.M. and Teller, E., J. Chem. Phys. 11, 299 (1943).

(137) Sherwood, A.E. and Prausnitz, J.M., J. Chem. Phys. 41, 429 (1964).

(138) Sherwood, A.E., De Rocco, A.G., and Mason, E.A., J. Chem. Phys. 44, 2984 (1966).

(139) Graben, H.W., Present, R.D. and McCulloch, R.D., Phys. Rev., 144, 140 (1966).

(140) Jensen, L., Phys. Rev., 125, 1798 (1962).

(141) Dymond, J.H. and Alder, B.J., J. Chem. Phys. 54, 3472 (1971).

(142) Dymond, J.H. and Alder, B.J., J. Chem. Phys. 51, 309 (1969).

(143) Kihara, T., Rev. mod. Phys. 27, 412 (1955).

(144) Rowlinson, J.S., Sumner, F.H. and Sutton, J.R., Trans. Faraday Soc. 50 1 (1954).

(145) Stogryn, D.E., J. Chem. Phys. 48, 4474 (1968).

(146) Stogryn, D.E., J. Chem. Phys. 50, 4967 (1969).

(147) Kim, S. and Henderson, D., Proc. Nat. Academy of Sciences, Washington, 55, 705 (1966).

(148) Pitzer, K.S., Adv. in Chem. Phys., 2, 59 (1959).

(149) Lin, H-M. and Robinson, R.L., J. Chem. Phys., 54, 52 (1971).

(150) Good, R.J. and Hope C.J., J. Chem. Phys. 53, 540 (1970).

(151) Chueh, P.L. and Prausnitz, J.M., Ind. Eng. Chem. Fundamentals, 6, 492 (1967).

(152) Hiza, M.J. and Duncan, A.G., A.I.Ch.E. Jour. 16, 733 (1970).

(153) Rowlinson, J.S. and Watson, I.D., Chem. Eng. Science 24, 1565 (1969).

(154) Leland, T.W., Rowlinson, J.S. and Sather, G.A., Trans. Faraday Soc., 64, 1447 (1968).

(155) Orentlicher, M. and Prausnitz, J.M., Can. J. Chem. 45, 363 (1967).

(156) AGA PAR Research project NX-19 (Manual for the determination of super-compressibility factors for natural gas, American Gas Association, 1962).

(157) Pitzer, K.S. and Curl, R.F., J. Amer. Chem. Soc., 79, 2369 (1957).

(158) Leach, J.W., Chappelear, P.S. and Leland, T.W., A.I.Ch.E. J. 14 No. 4 568 (1968).

(159) Benedict, M., Webb, G.B. and Rubin, L.C., J. Chem. Phys., 8, 334 (1940).

(160) Redlich, O. and Kwong, J.N.S., Chem. Rev. 44 233 (1949).

(161) Zellner, M.G., Claitor, L.C. and Prausnitz, J.M., Ind. Eng. Chem. Fundamentals, 9, No. 4 549 (1970).

(162) Pitzer, K.E. and Curl, R.F., J. Am. Chem. Soc., 77, 3427 (1957).

(163) Chueh, P.L. and Prauznitz, J.M., A.I.Ch.E. Journal, 13 896 (1967).

(164) Huff, J.A. and Reed, T.M., J. Chem. Eng. Data 8, 306 (1963).

(165) Vennix, A.J., Leland, T.W., Chappelear P.S. and Kobayashi, R., Proc. Nat. Gas Proc. Assn., 47, 22 (1968).

(166) Fisher, G.D. and Leland, T.W., Ind. Eng. Chem. Fundamentals, 9, No. 4 537 (1970).

(167) Rowlinson, J.S. and Watson, I.D., Chem. Eng. Science 24 1565 (1969).

(168) Gunning, A., Ph.D. Thesis, University of London (1972).

(169) Teja, A., Ph.D. Thesis, University of London (1972).

(170) Leland, T.W., Rowlinson, J.S. and Sather, G.A., Trans. Faraday Soc. 64 1447 (1968).

(171) Chueh, P.L. and Prausnitz, J.M., Ind. Eng. Chem. Fundamentals 6 492 (1967).

(172) Eilerts, C.K., Carlson, H.A. and Mullens, N.B., World Oil, 128 No. 2 part 1, 129; ibid, 128 No. 3 part 2, 144 (1948).

(173) Robinson, R.L. and Jacoby, R.H., Hydrocarbon Processing 44 No. 4 141 (1965).

(174) Sage, B.H. and Reamer, H.H., Trans. A.I.M.E., 142, 179 (1941).

(175) Sage, B.H. and Olds, R.H., Trans. A.I.M.E. 170 156 (1947).

(176) Reamer, H.H. and Sage, B.H., Trans. A.I.M.E., 189 261 (1950).

(177) Simmler, W. and Wolowski, E., 11th International Gas Conference, Moscow (1970) (IGU/A14-70).

(178) Wolowski, E., Dissertation, Technische Hochschule Aachen (1971).

(179) Katz, D.L., Proc. Nat. Gas. Assn. America, May 1942, 41.

(180) Verrien, J.P., Rev. Inst. Franc.Petrole, 8, 454 (1953).

(181) Subramaniam, T.K., Kao, R.L. and Lee, A.L., Gas Age, 136 No. 8 12A (1969).

(182) Zimmerman, R.H. and Beitler, S.R., Trans. A.S.M.E., 74 945 (1952).

(183) Zimmerman, R.H., Beitler, S.R. and Darrow, R.G., Trans. A.S.M.E., 79 1358 (1957).